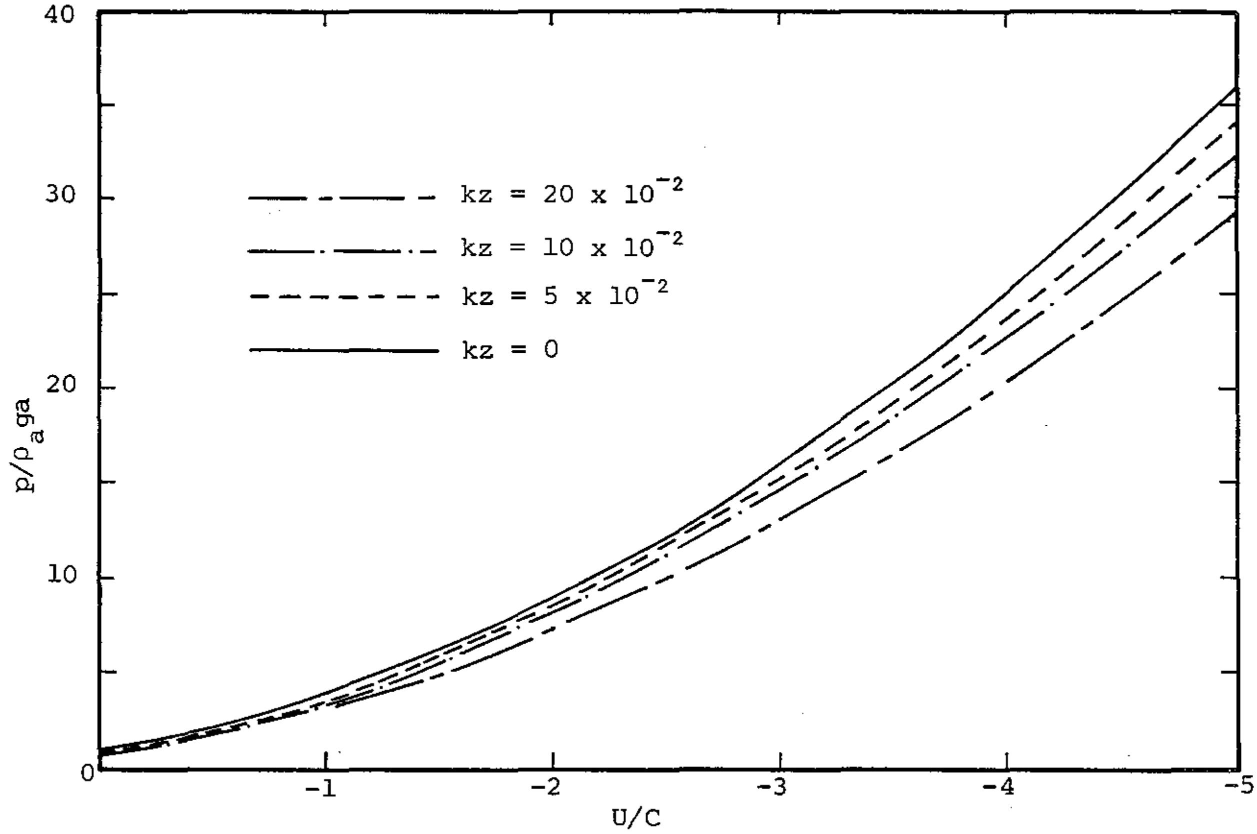

Figure 2.1 The wave-induced pressure in an opposing wind predicted by potential flow theory. kz is the non-dimensional height above the waves

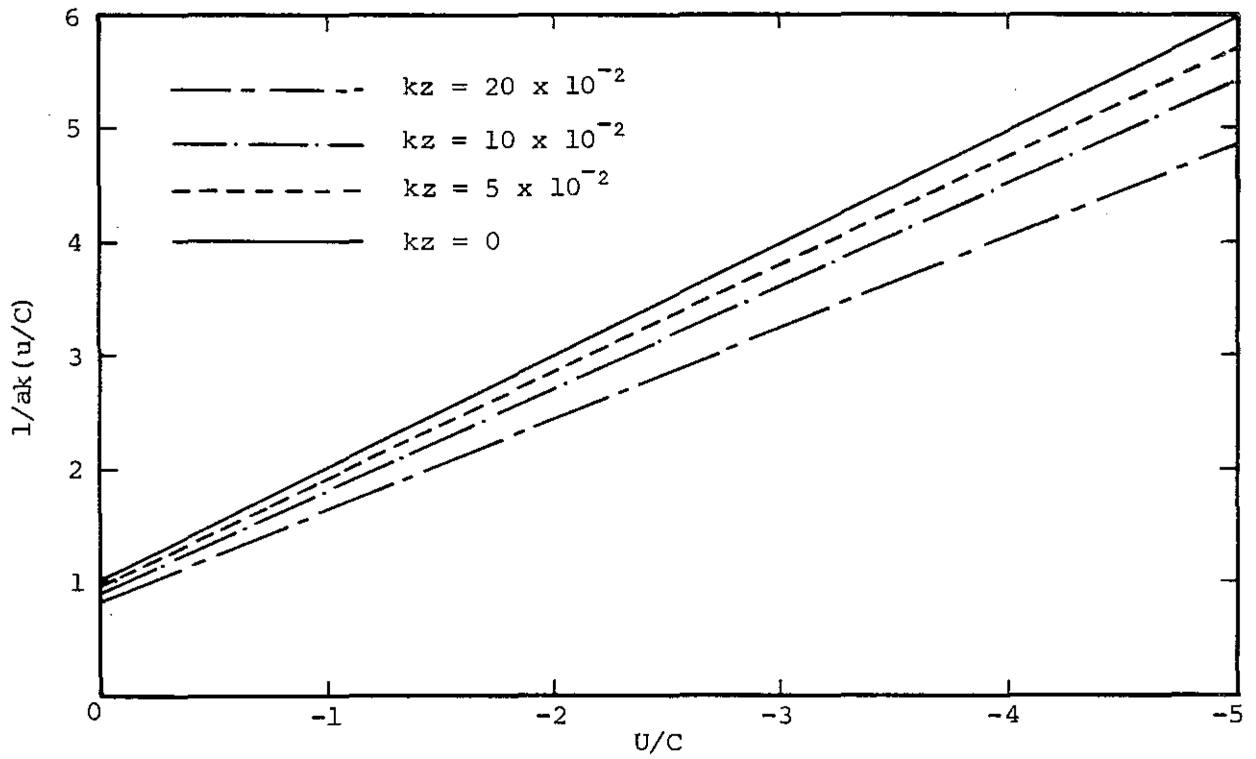

Figure 2.2 The wave-induced velocity in an opposing wind predicted by potential flow theory. kz is the non-dimensional height above the waves

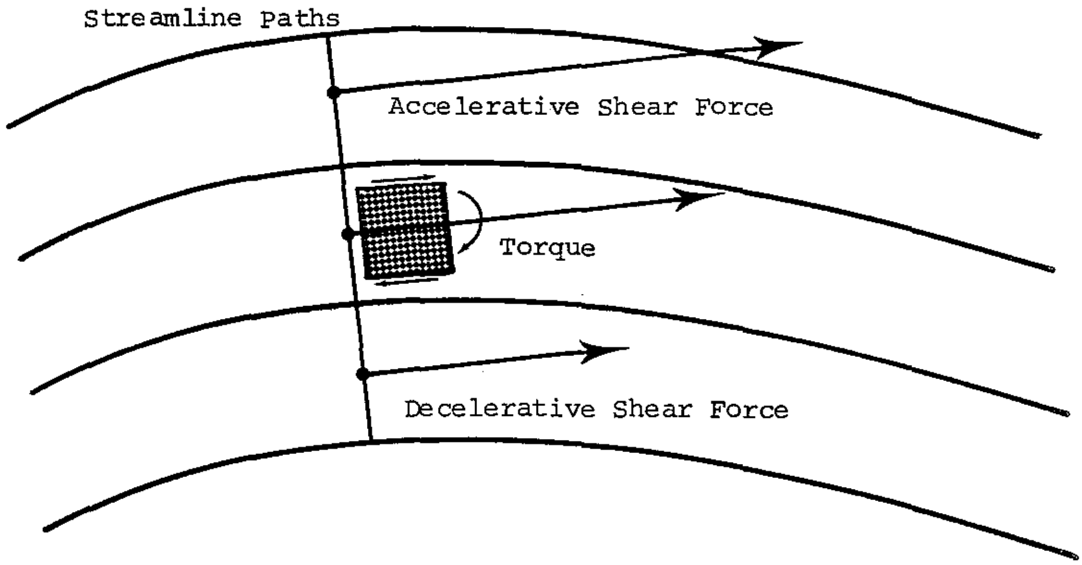

Figure 2.3 The variation of velocity in a direction perpendicular to the flow induces a difference in the direction of the friction forces and a torque resulting in a rotational motion. [After Le Mehaute (67)]

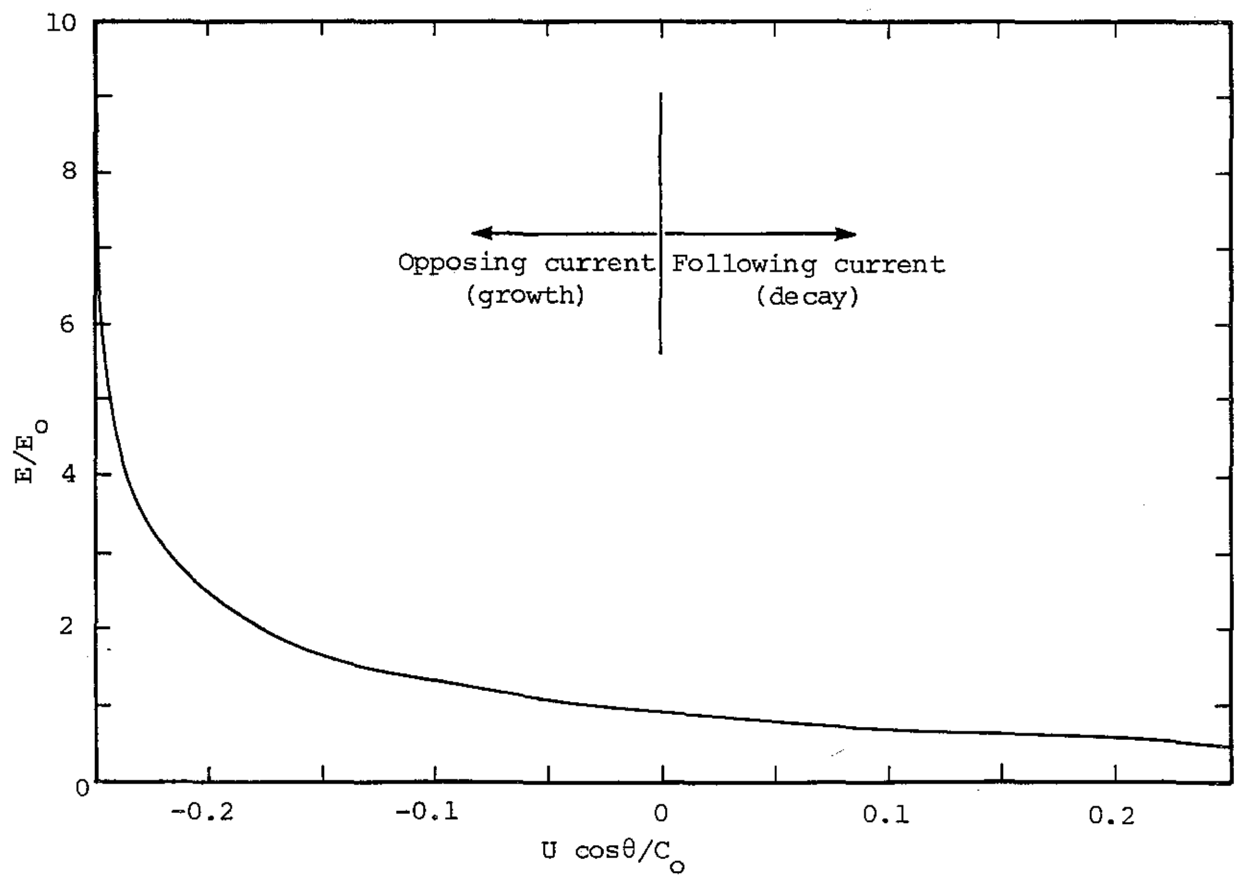

Figure 2.6 Wave growth and decay due to a uniform current as predicted by Eq. 2.62.

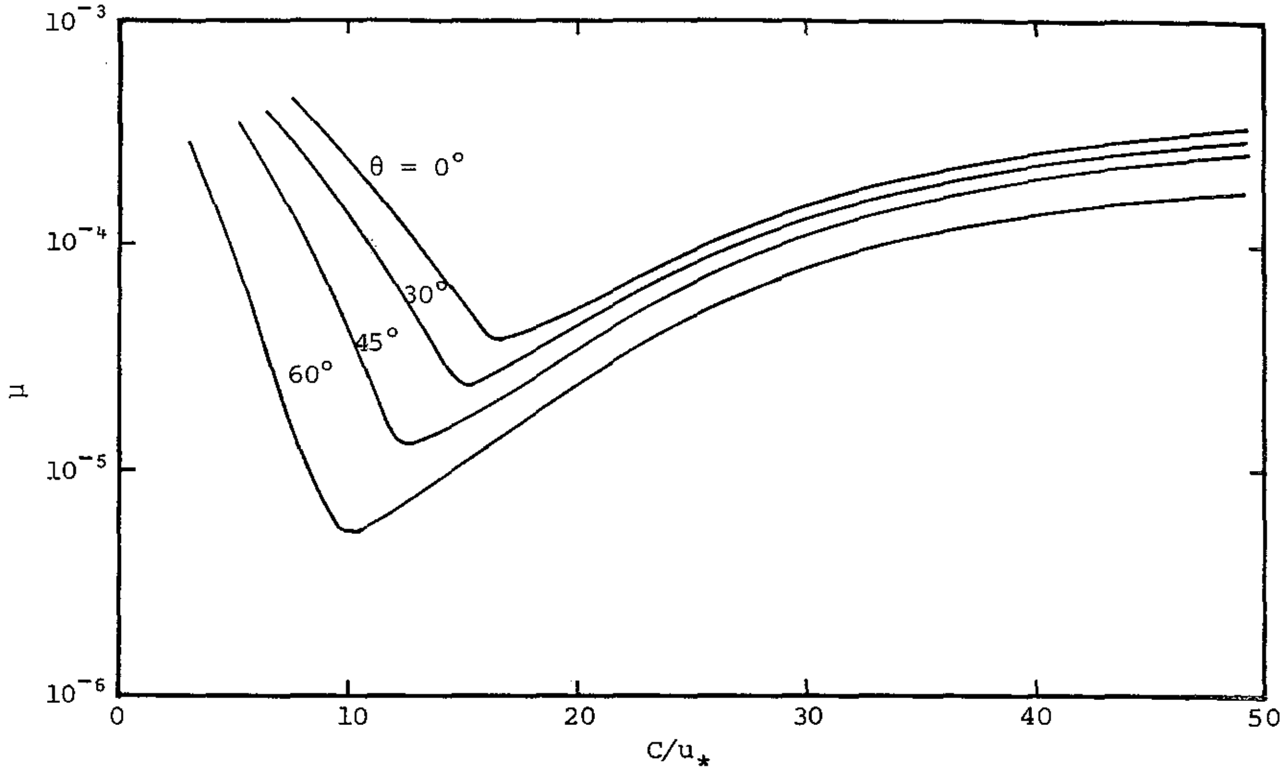

Figure 2.4a The theoretical wave growth coupling coefficient as a function of C/u_*. [after Phillips (93)].

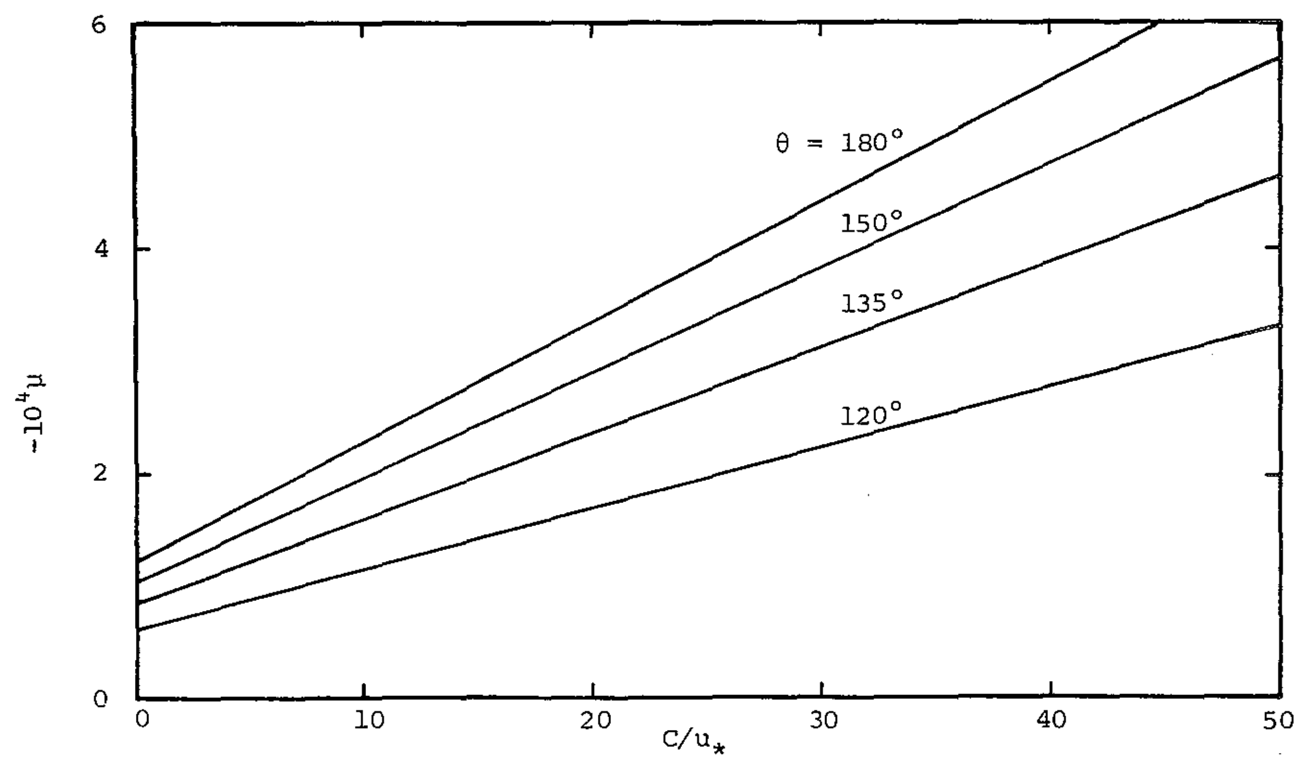

Figure 2.4b The theoretical wave decay coupling coefficient as a function of C/u_*. [after Phillips (93)].

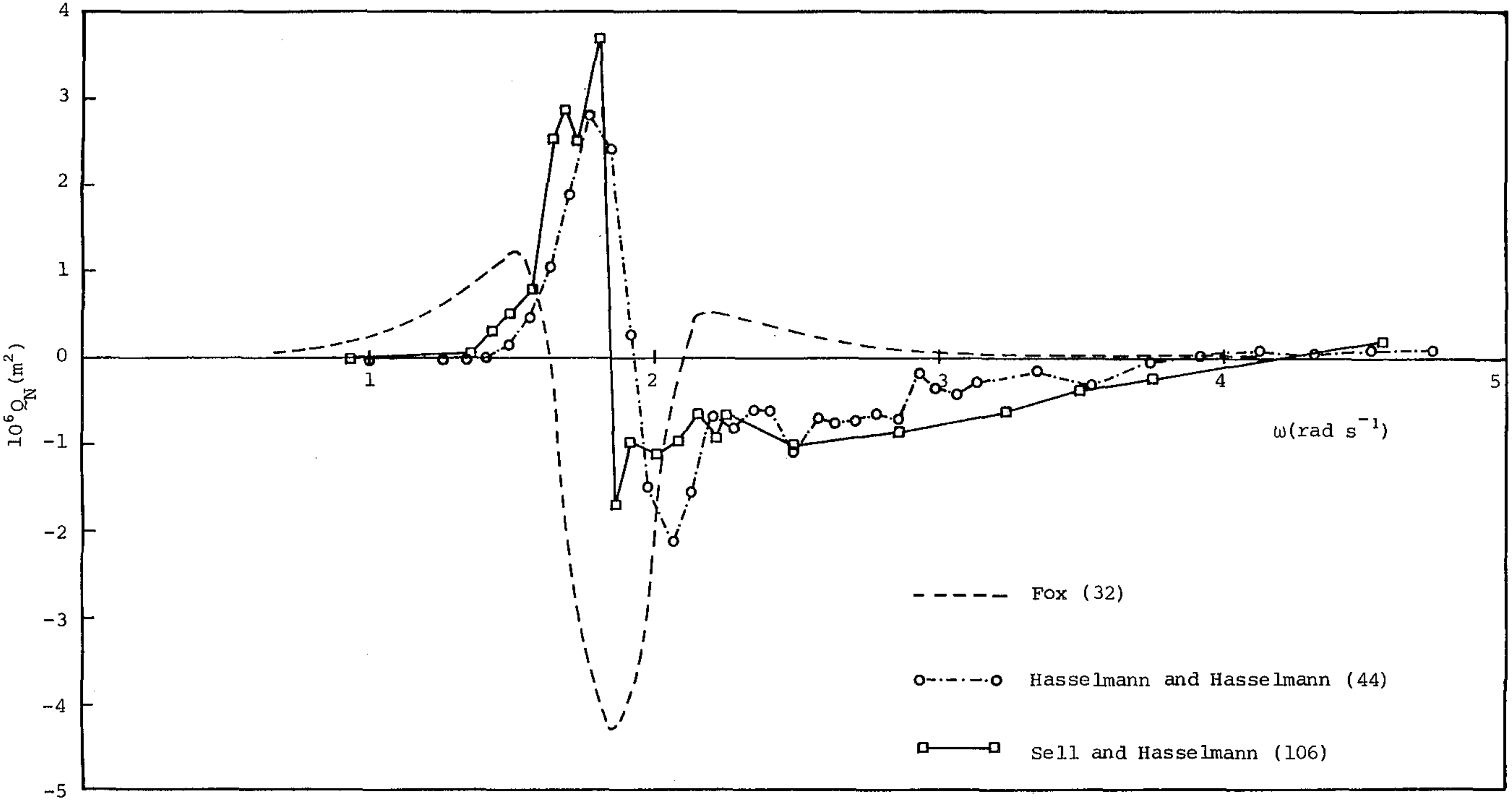

Figure 2.5 Energy transfer due to wave-wave interactions for the mean JONSWAP spectrum.

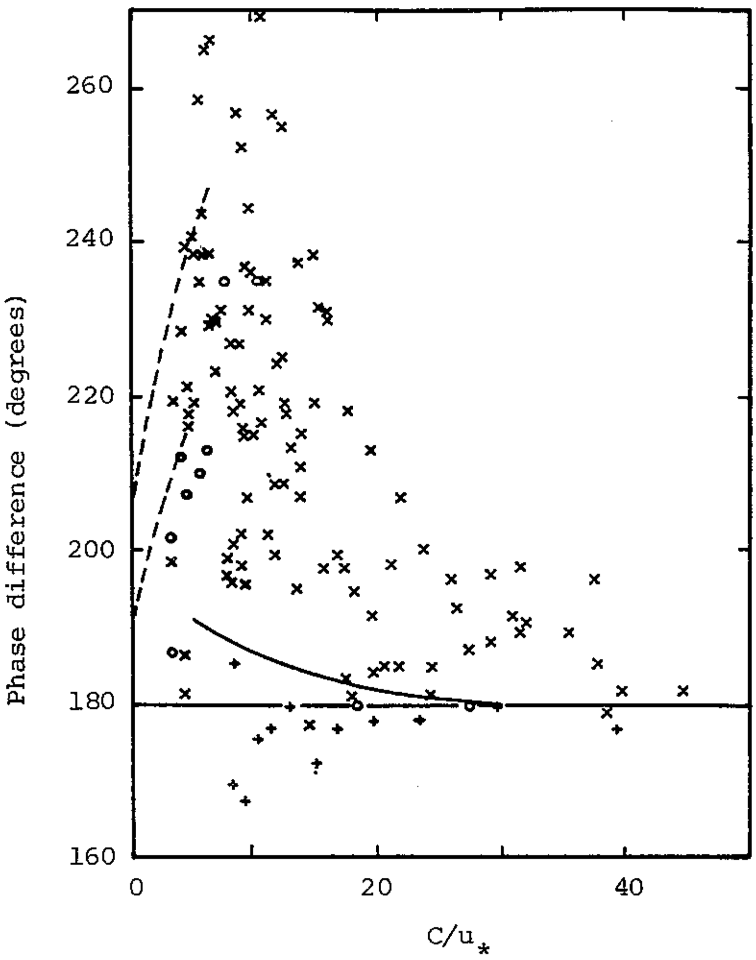

Figure 2.7 The phase angle of the pressure signal relative to the water surface as a function of C/u_*, measured by Longuet-Higgins et al. (74), + ; Shemdin and Hsu (111), o ; and Dobson (26), × . The broken lines indicate the envelope of Kendall's (57) wind tunnel measurements and the continuous curve is calculated from Miles formula (78). [After Phillips 94)]

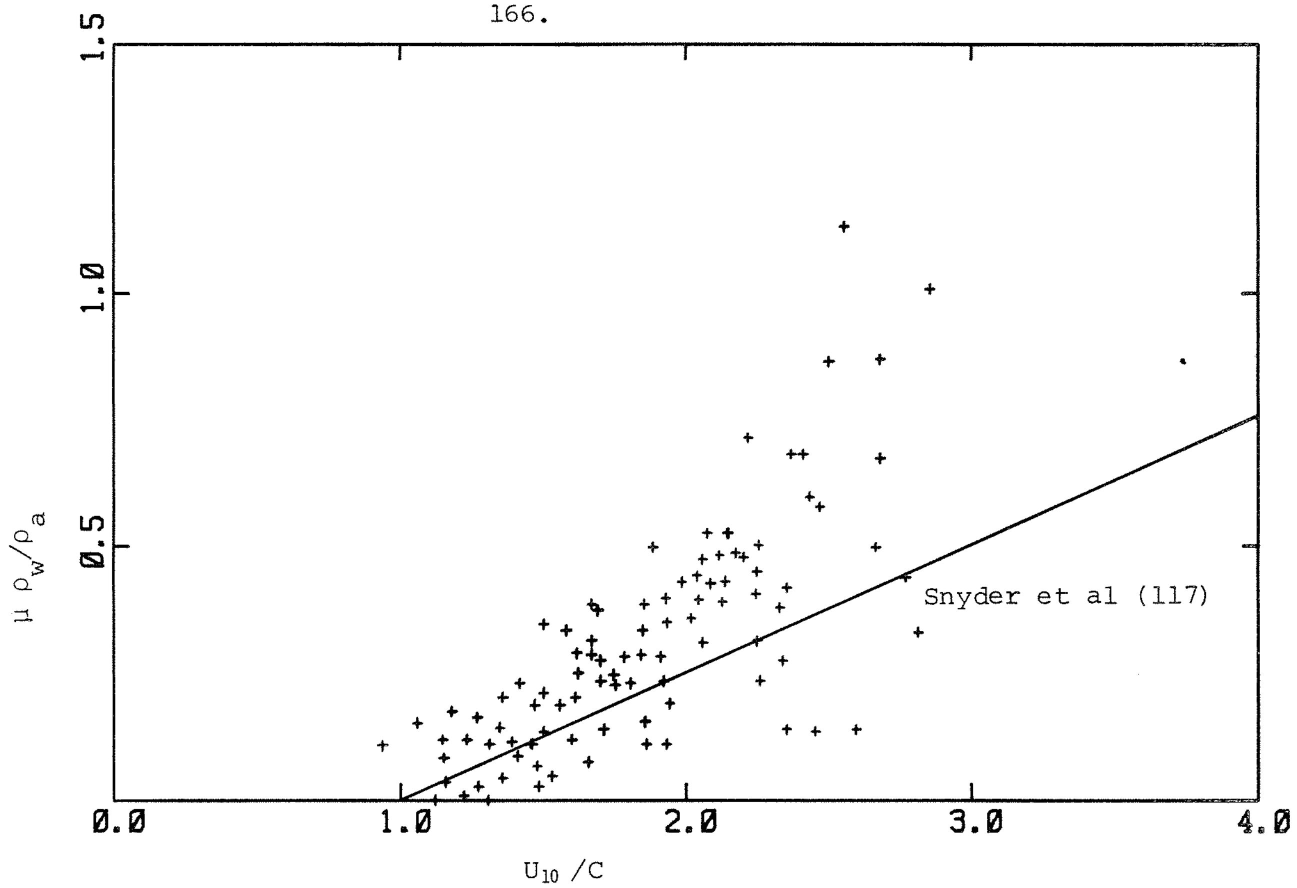

Figure 2.8 Early measurements of the air-sea energy flux in a following wind, (57), (108), (111) and the more recent result of Snyder et al (117).

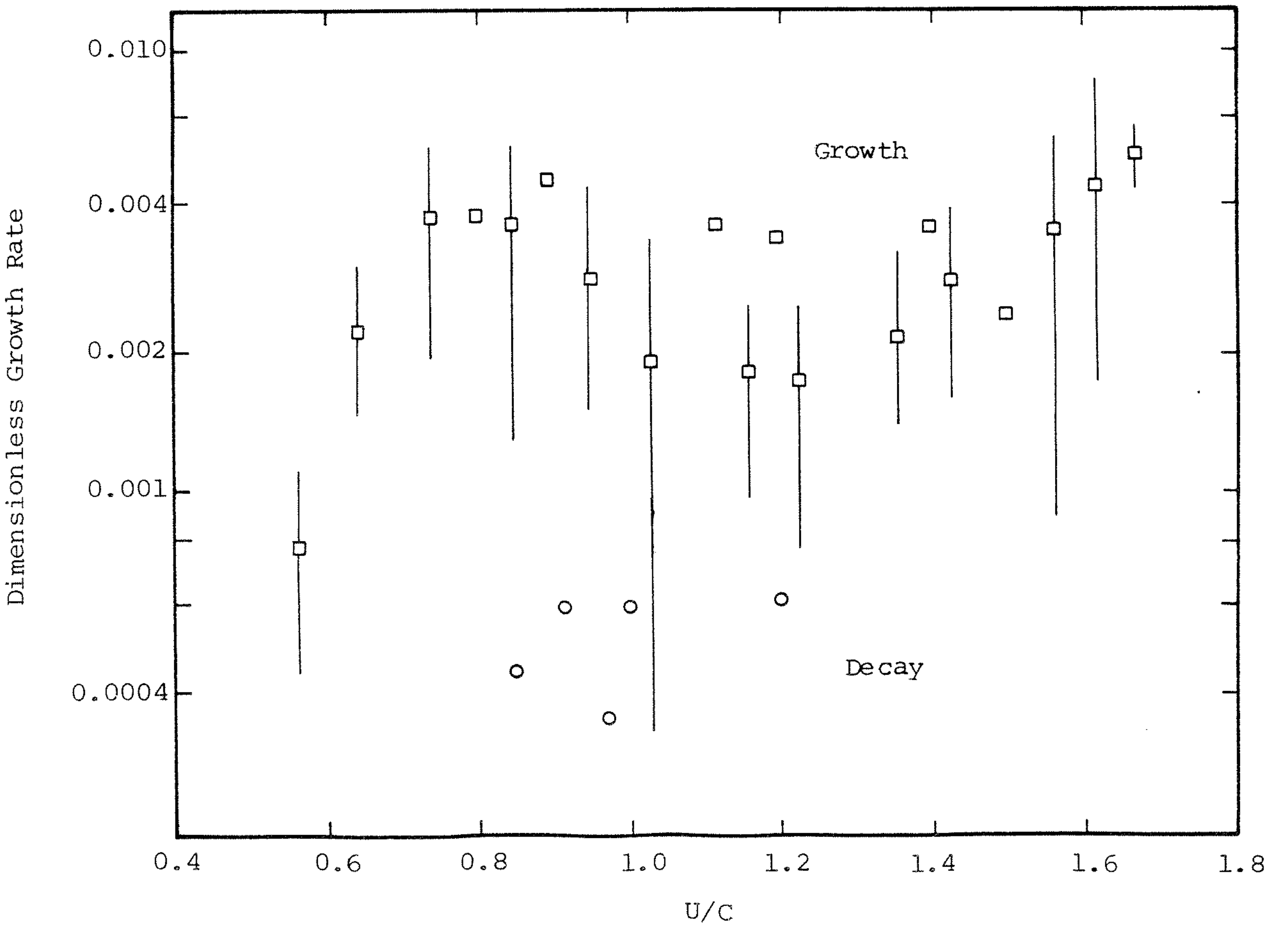

Figure 2.9 Dimensionless growth (or decay) rates as a function of U/C, following wind, opposing wind. [After Stewart and Teague (124)]

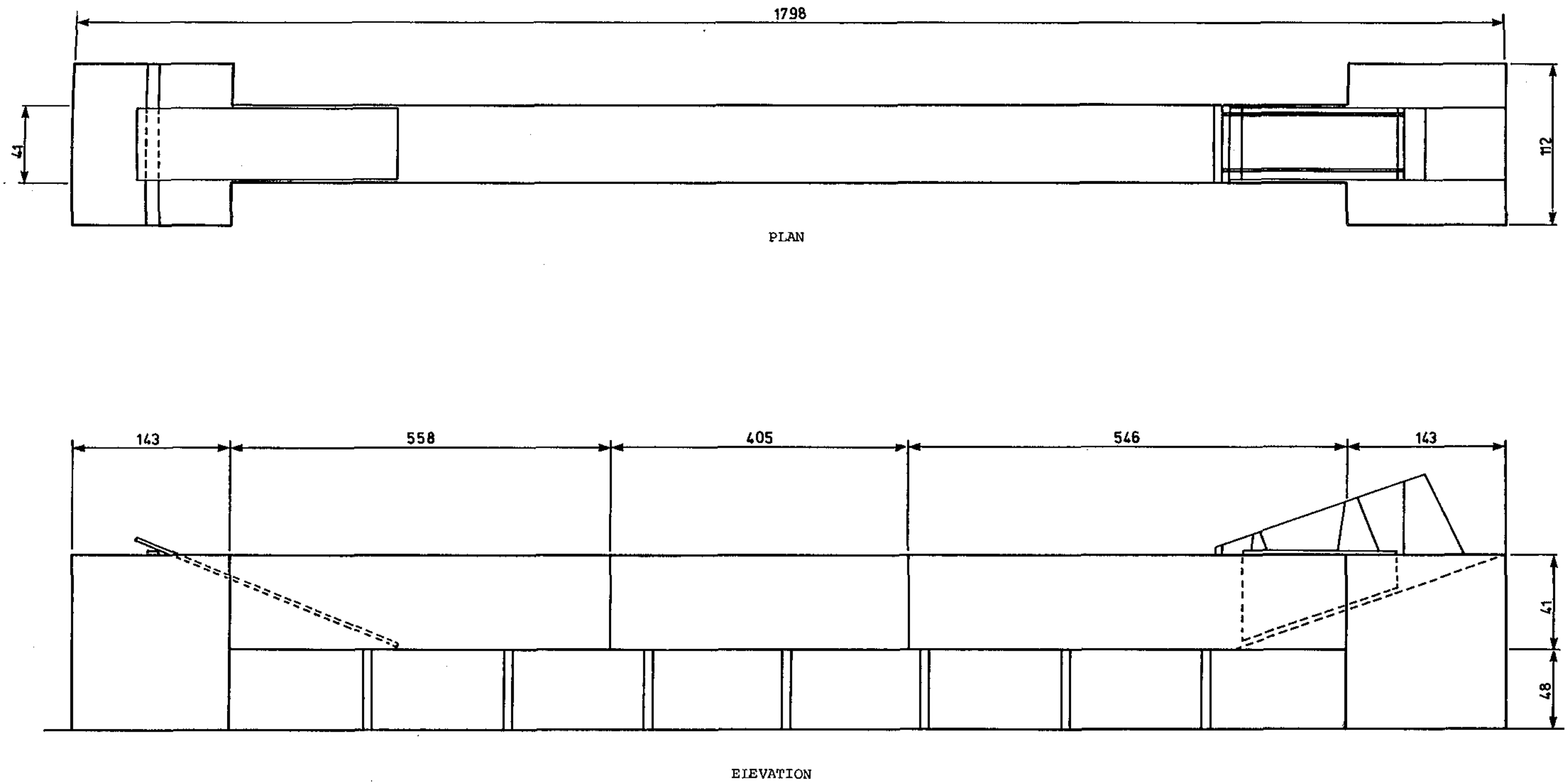

Figure 3.1a Plan and elevation of the existing wave flume (all dimensions in cms).

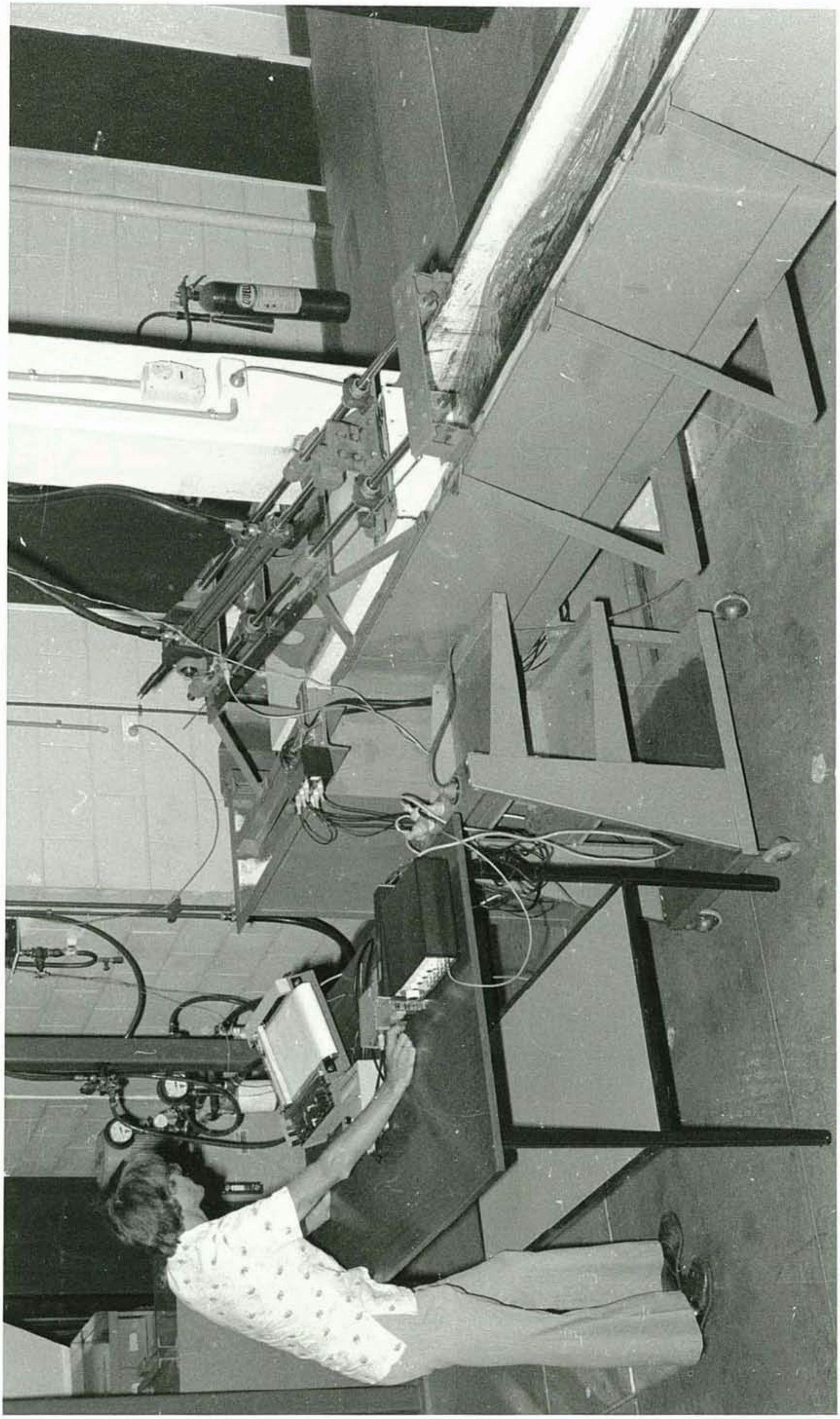

Figure 3.2 Photograph of existing wave flume.

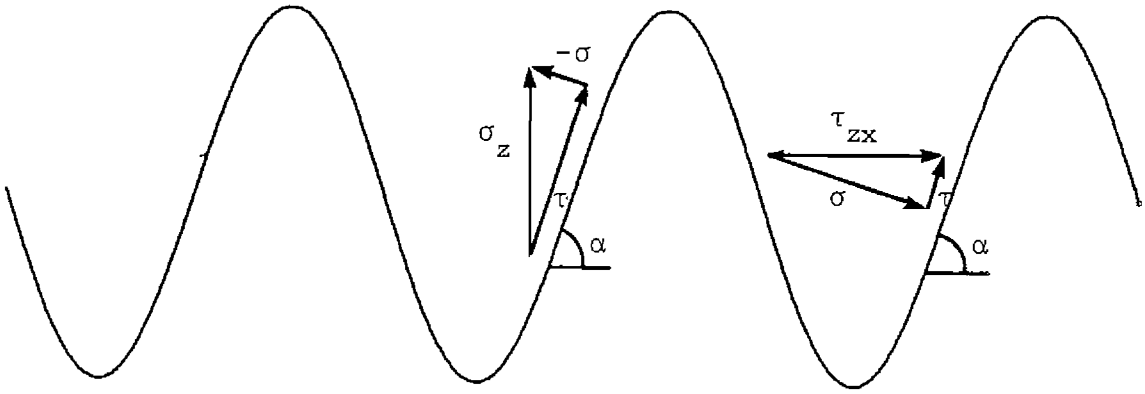

Figure 2.10 Definition sketch of stresses exerted at the water surface

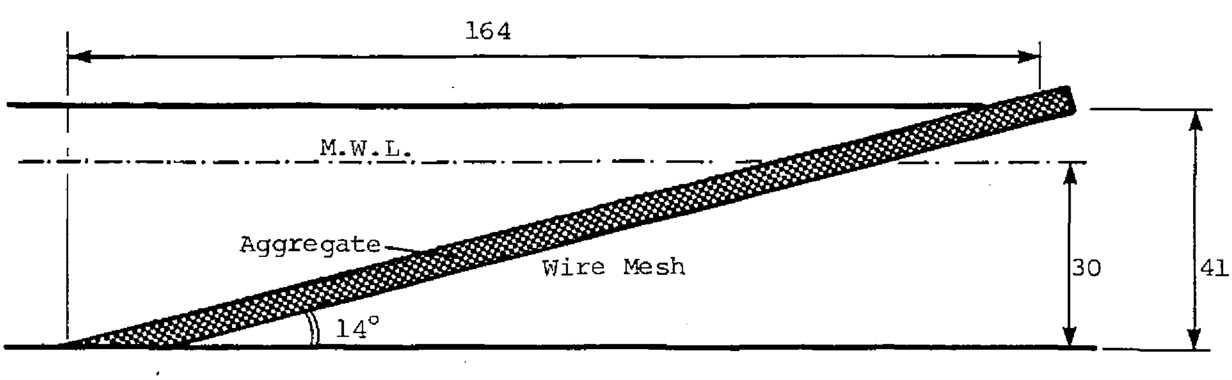

Figure 3.3 Dimensions of wave absorbing beach (all dimensions in cms).

Figure 3.4 Photograph of wedge wave maker.

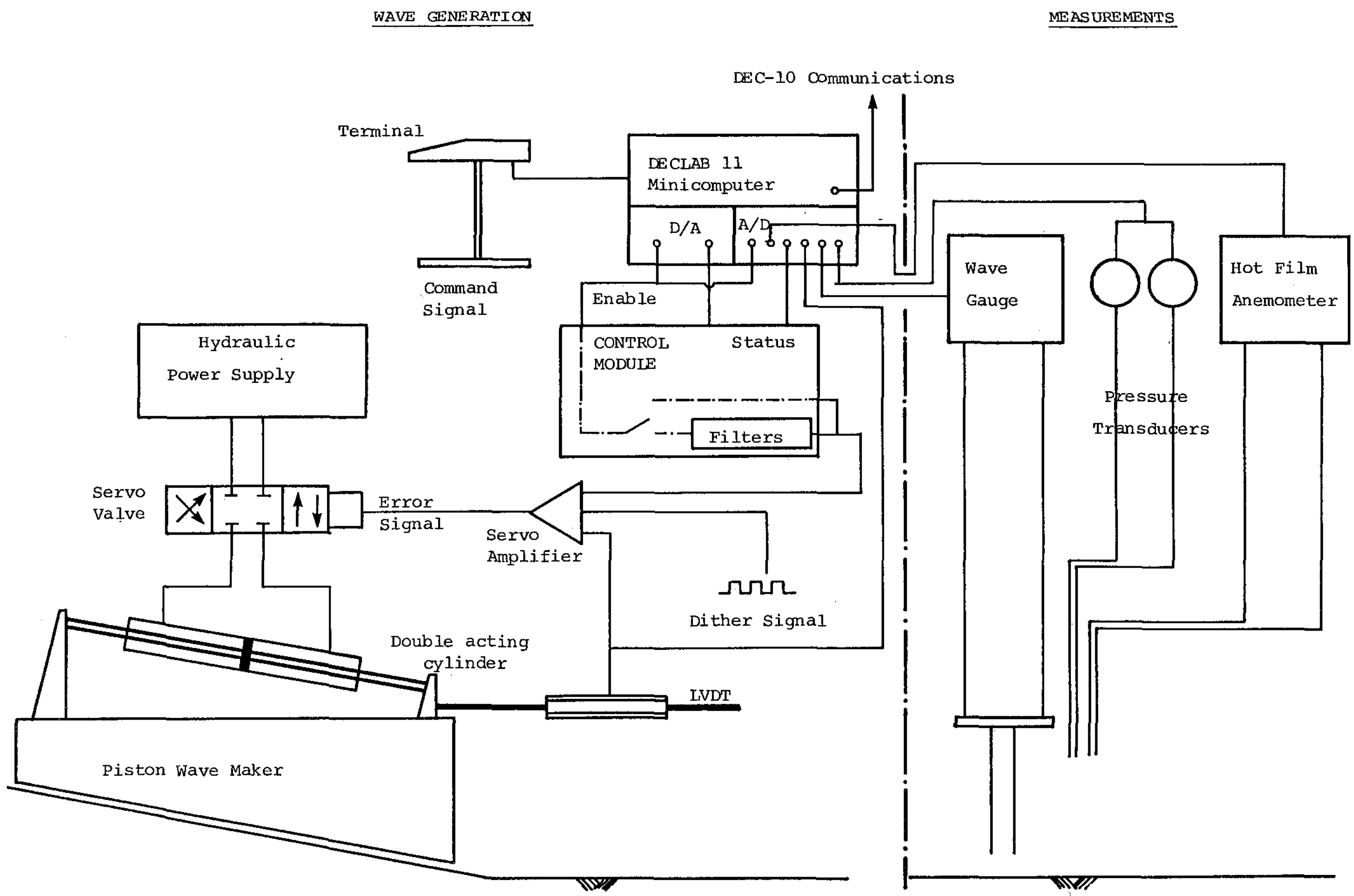

Figure 3.5 Schematic Diagram of Experimental Facility

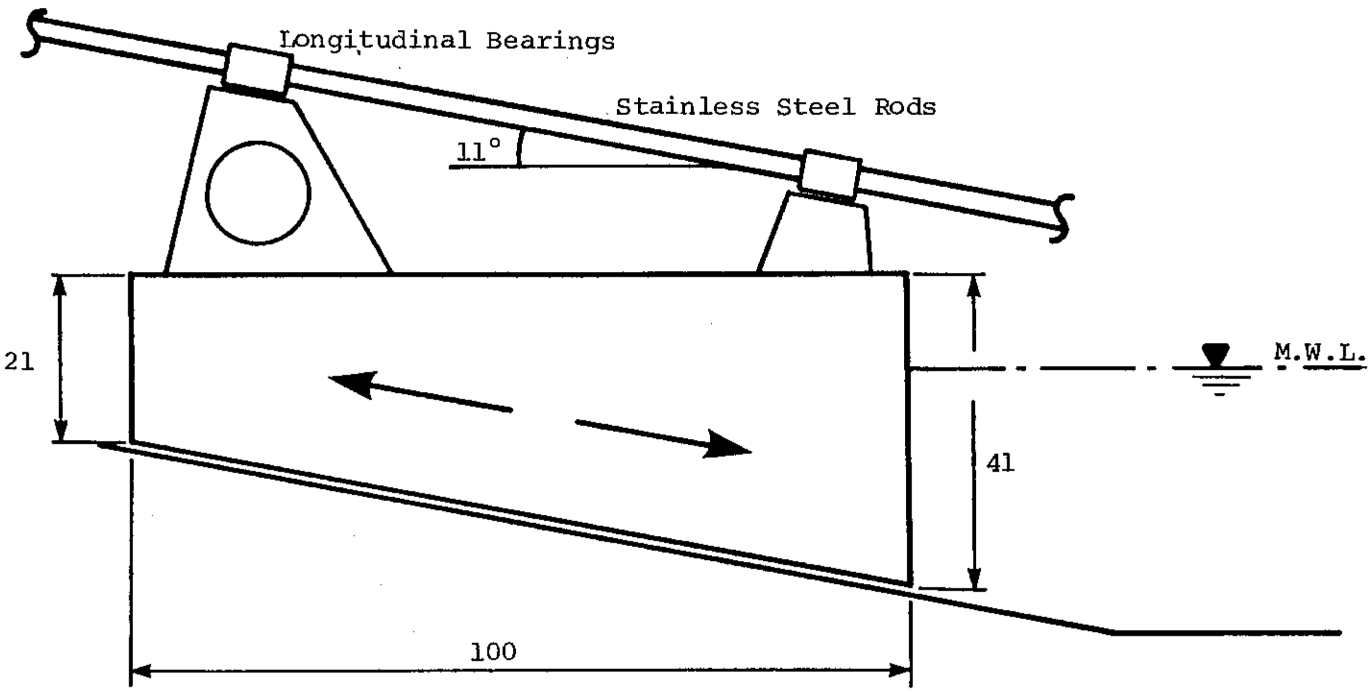

Figure 3.6 Piston Wave Maker Dimensions (all dimensions in cm).

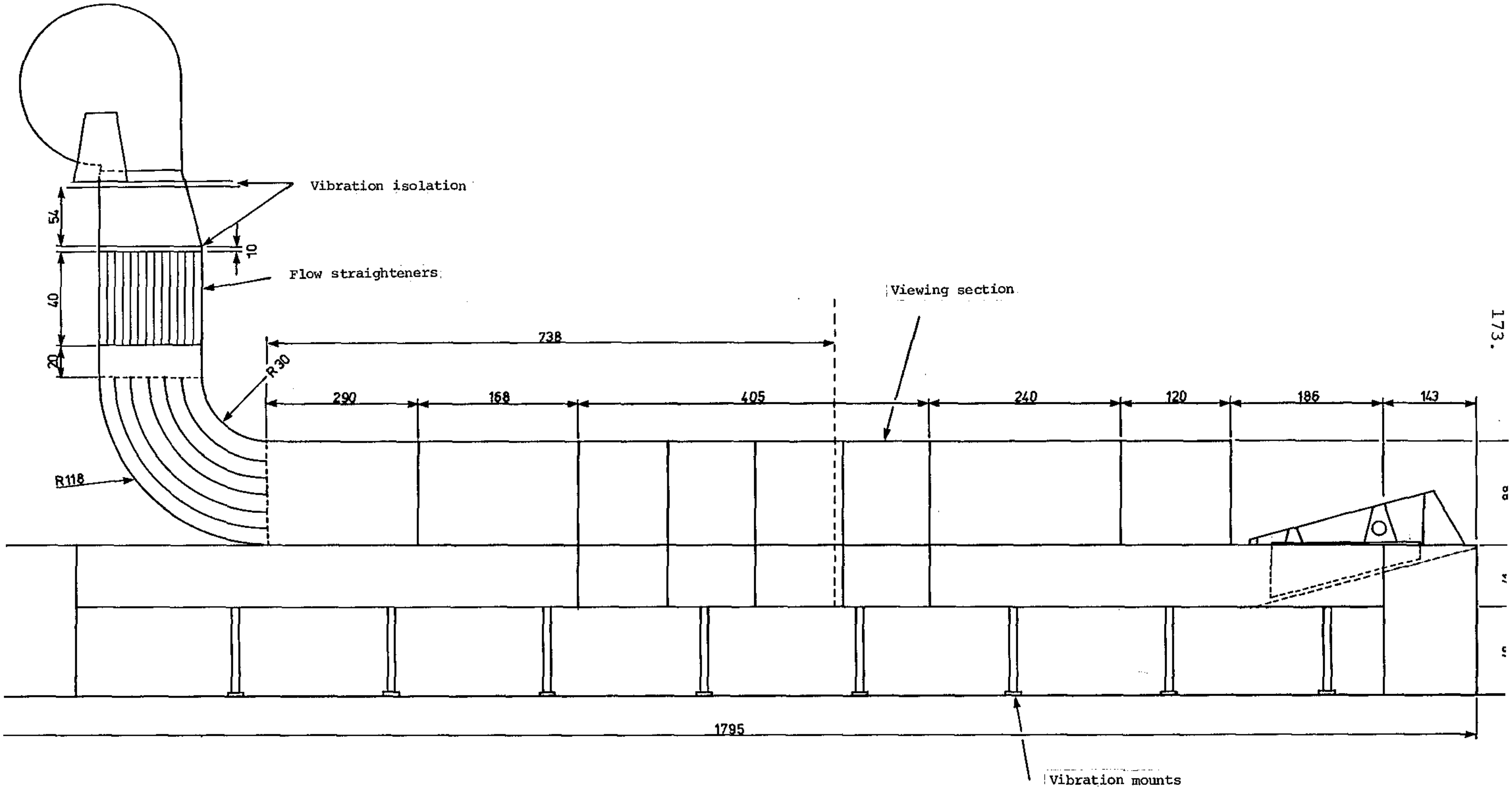

Figure 3.8 The opposing wind-wave research facility (all dimensions in cms).

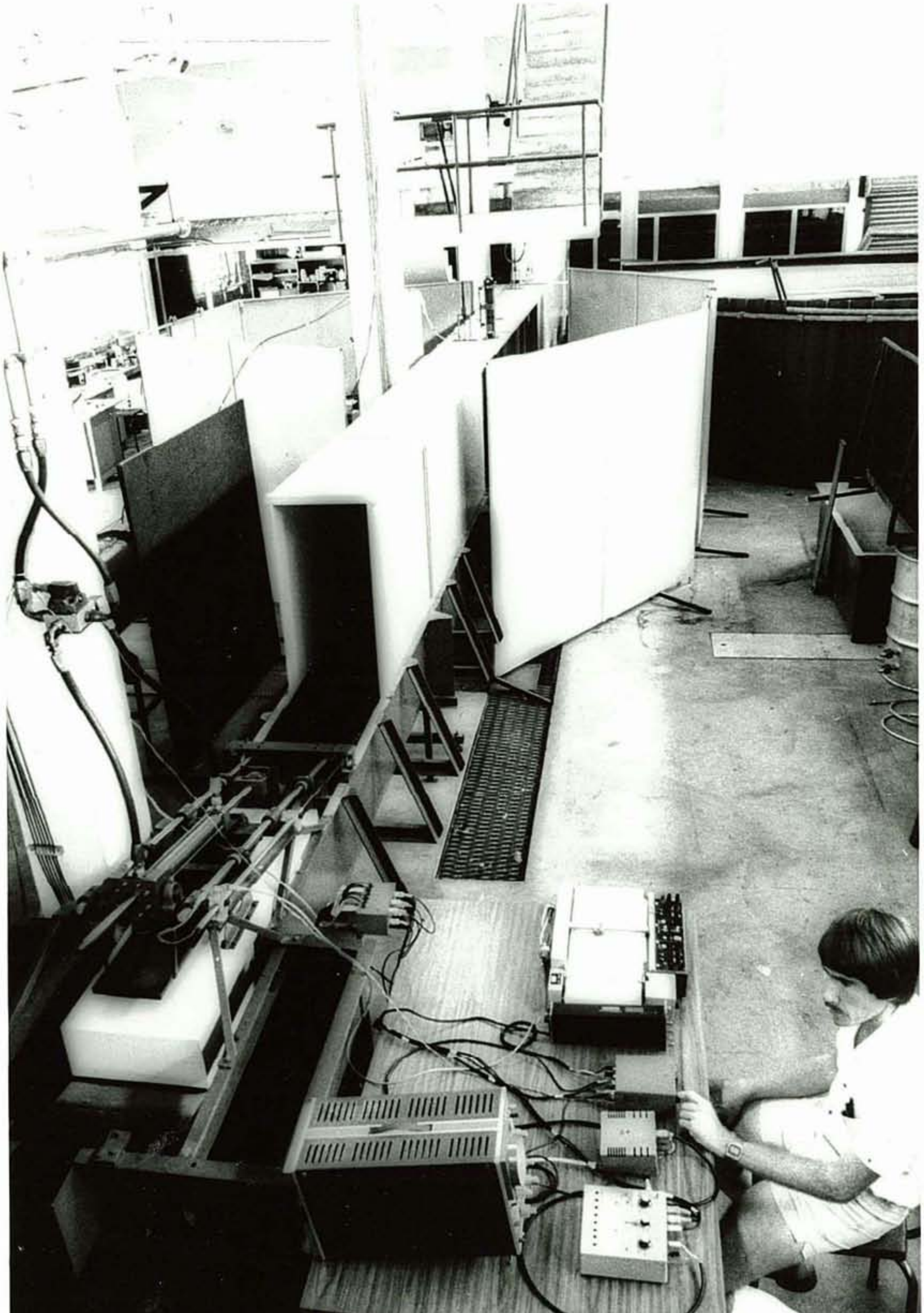

Figure 3.8b Photograph of the complete wind-wave flume.

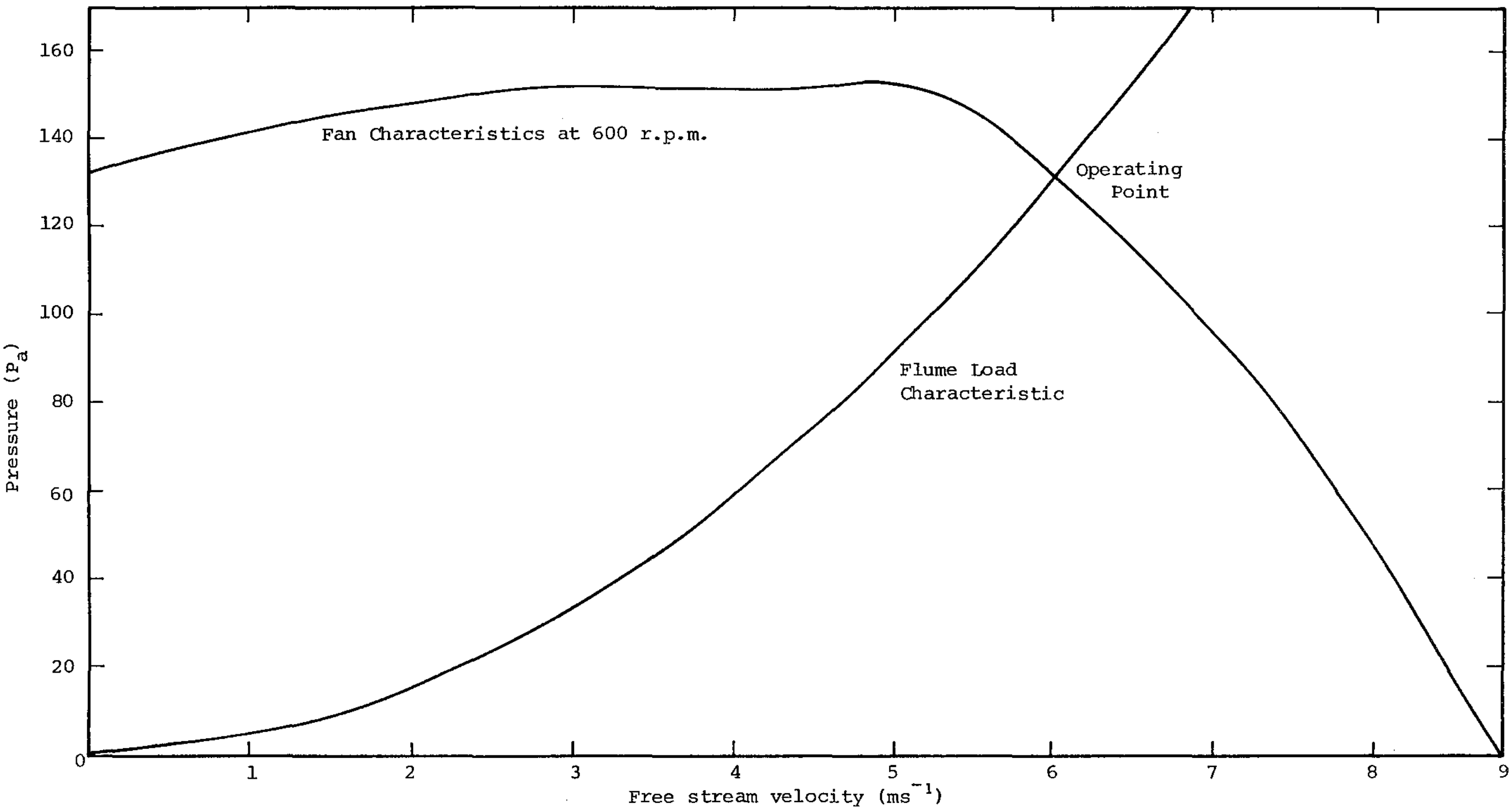

Figure 3.9 Fan and Flume Characteristics

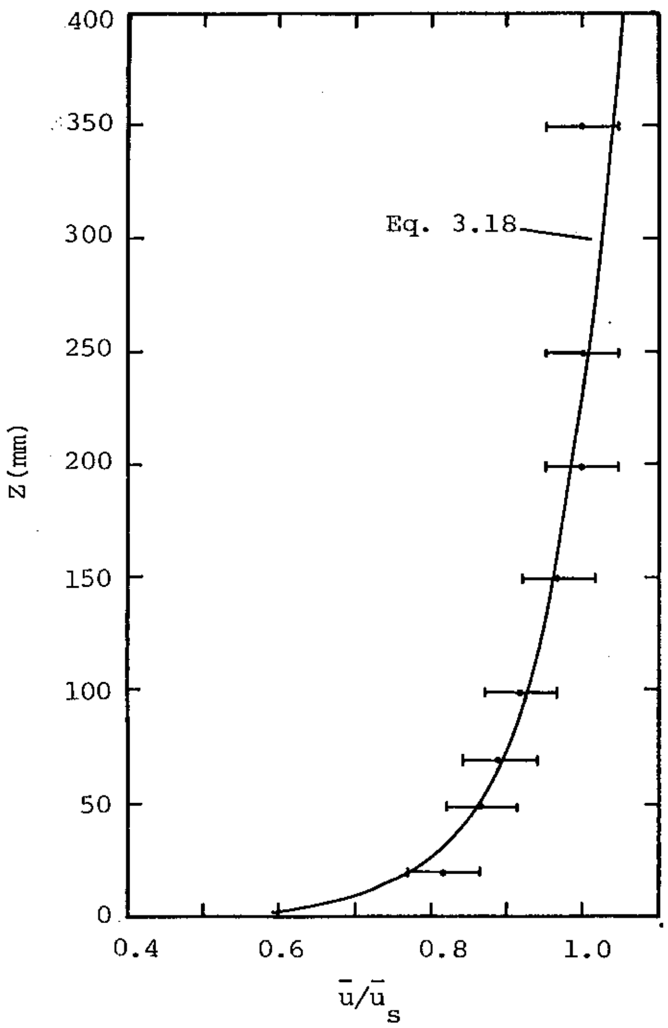

Figure 3.10 Mean velocity profile at flume inlet.

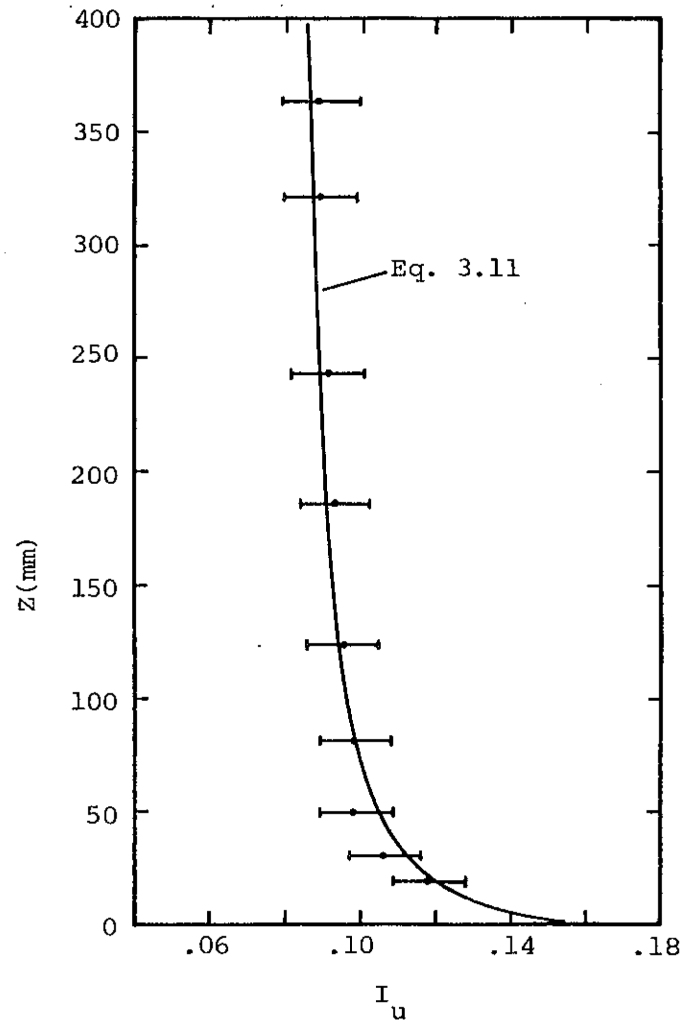

Figure 3.11 Profile of turbulence intensities at flume inlet.

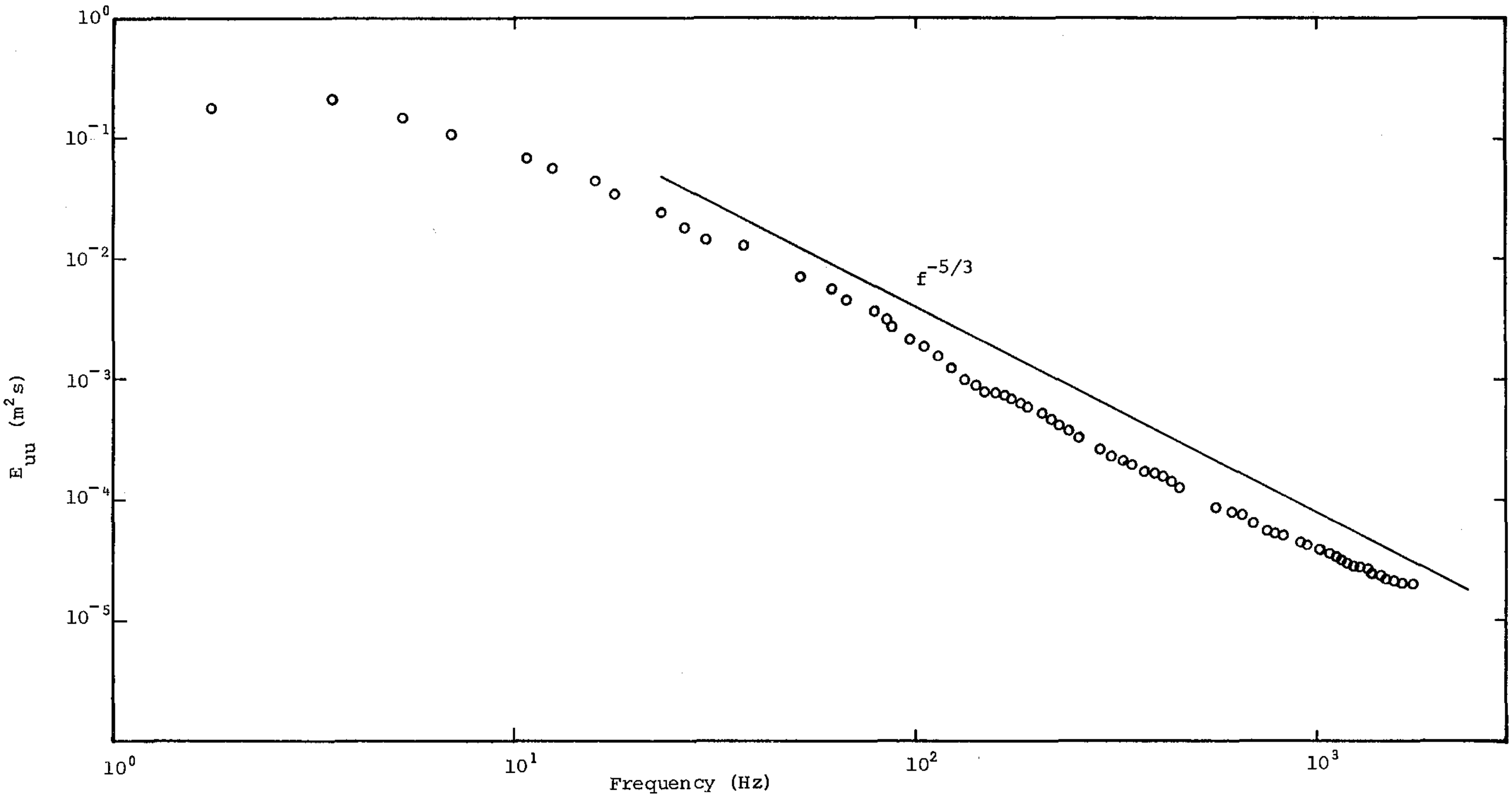

Figure 3.12 Spectrum of longitudinal wind turbulence at flume inlet.

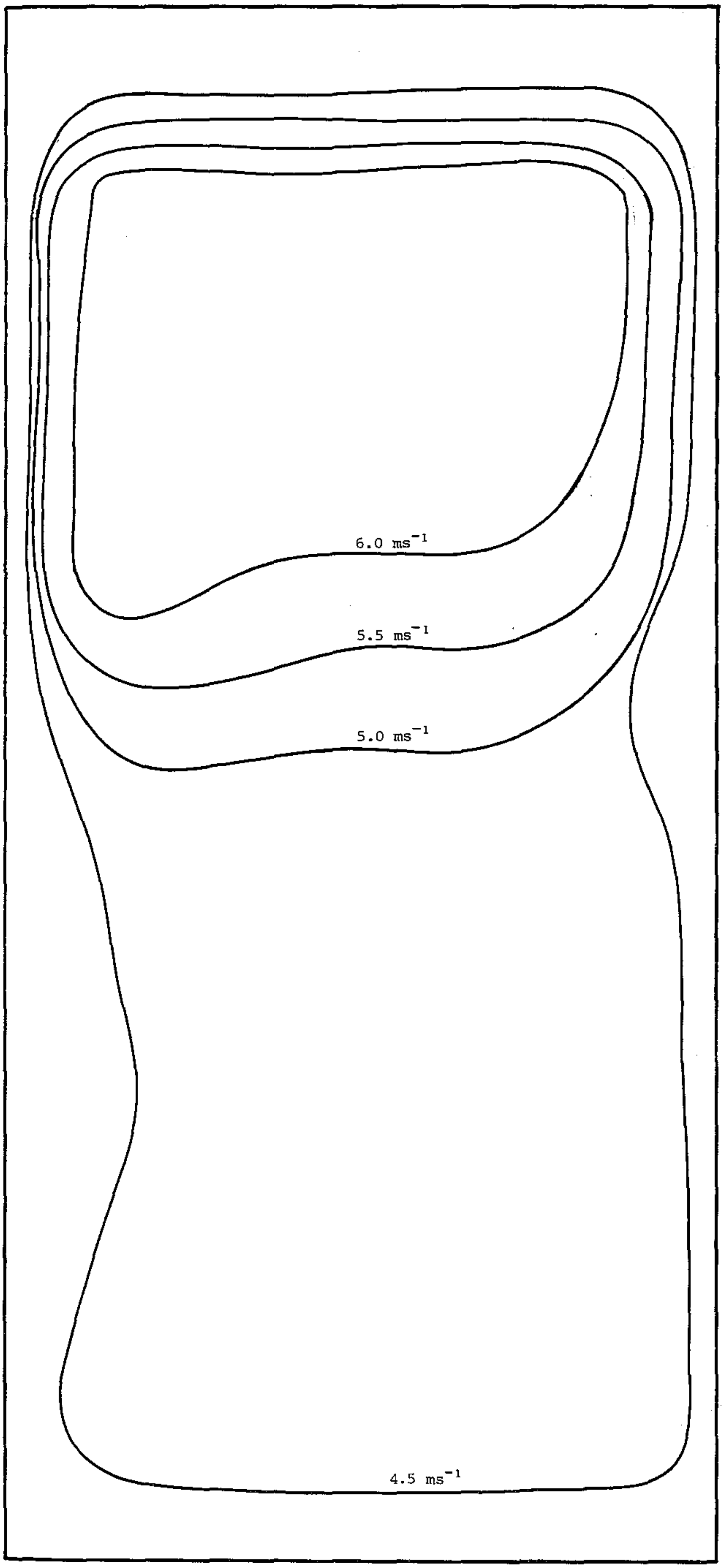

Figure 3.13a Cross-section velocity contours within the flume at the beach inlet.

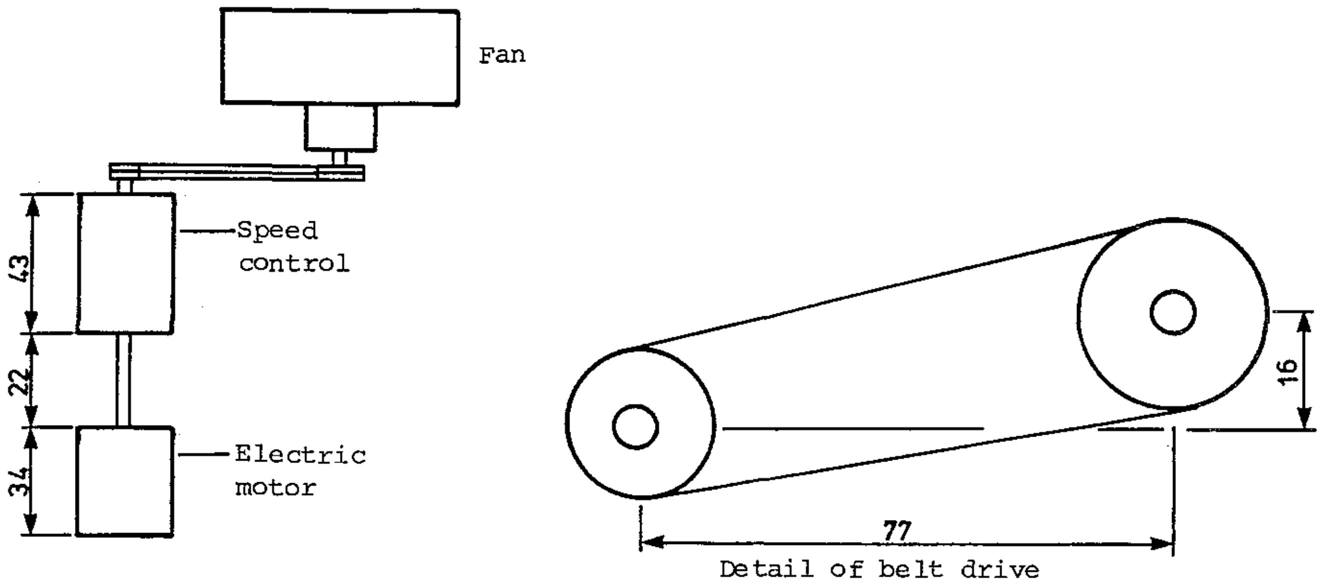

Figure 3.7 Plan of fan and drive assembly.

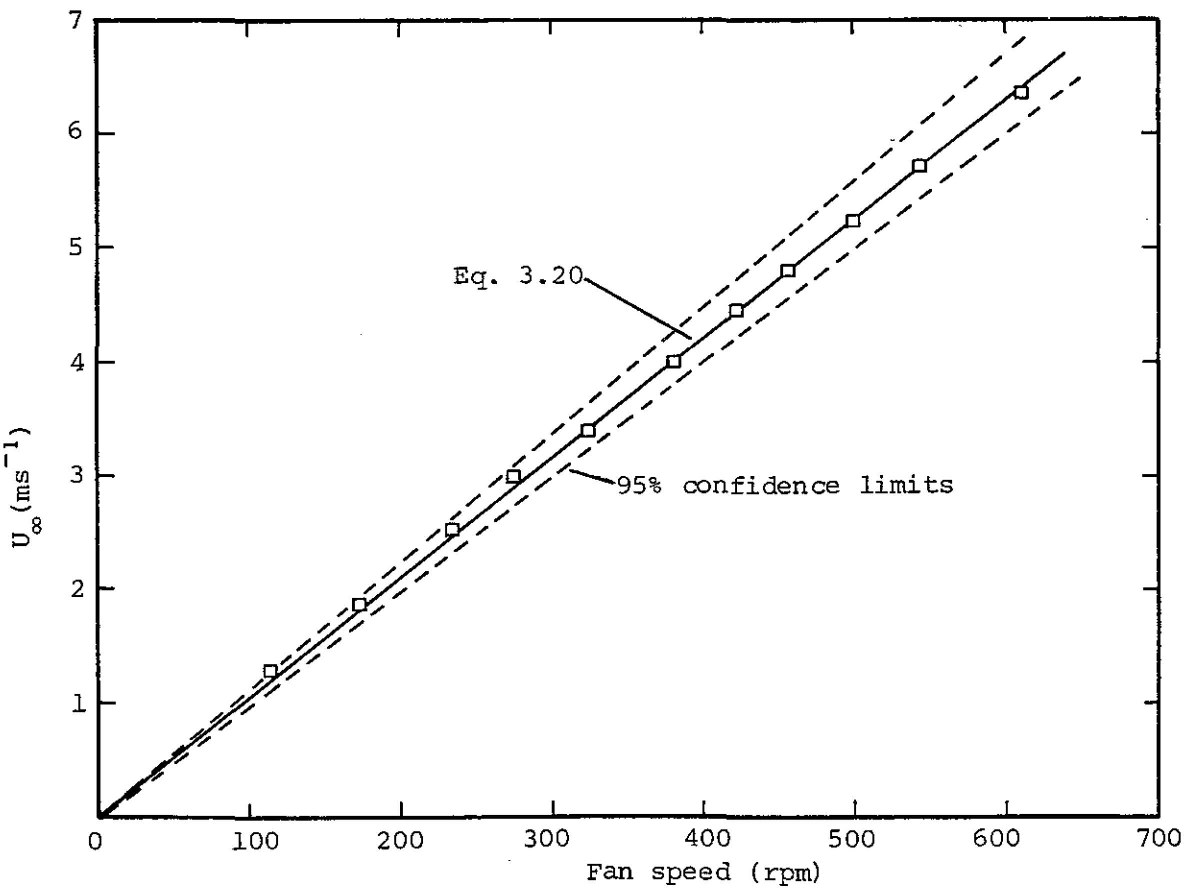

Figure 3.14 Relationship between fan speed and free stream wind velocity.

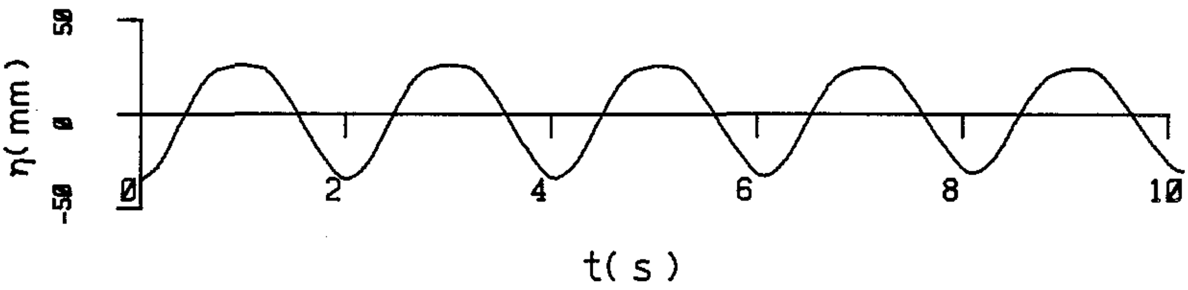

Frequency = 0.5 Hz

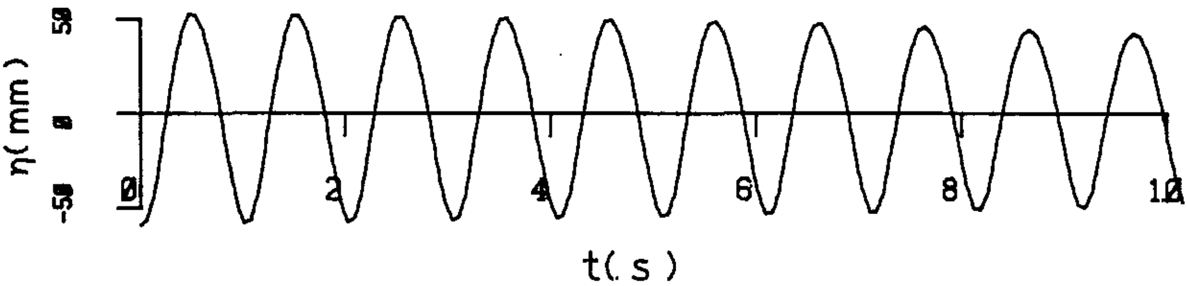

Frequency = 1.0 Hz

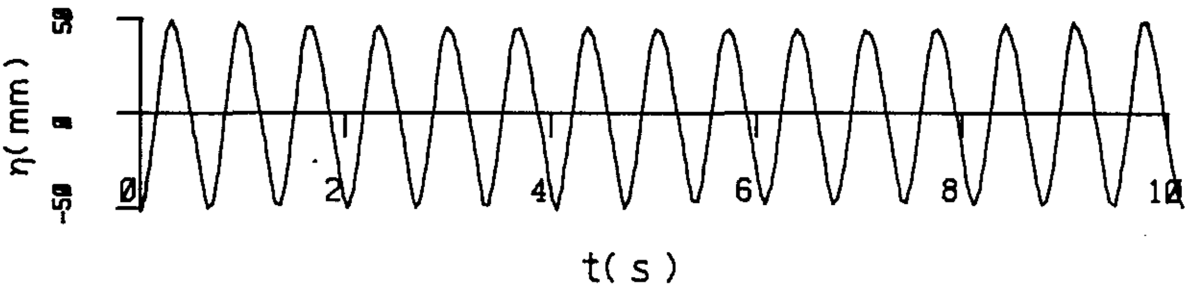

Frequency = 1.5 Hz

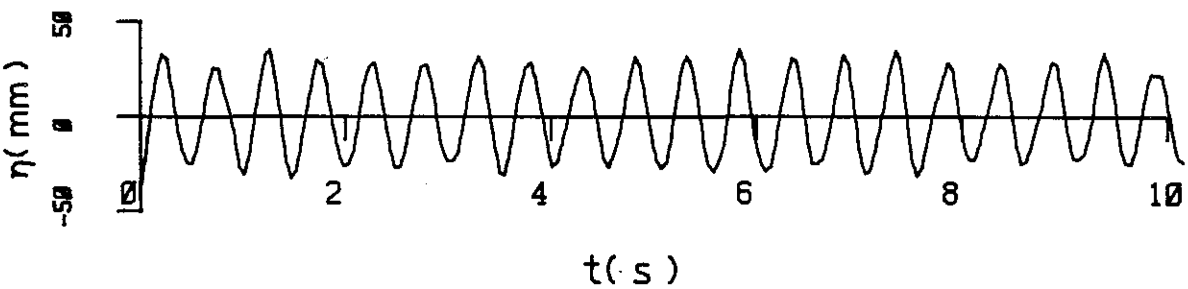

Frequency = 2.0 Hz

Figure 3.15 Time series of water surface elevation for sinusoidal wave maker motion at various frequencies.

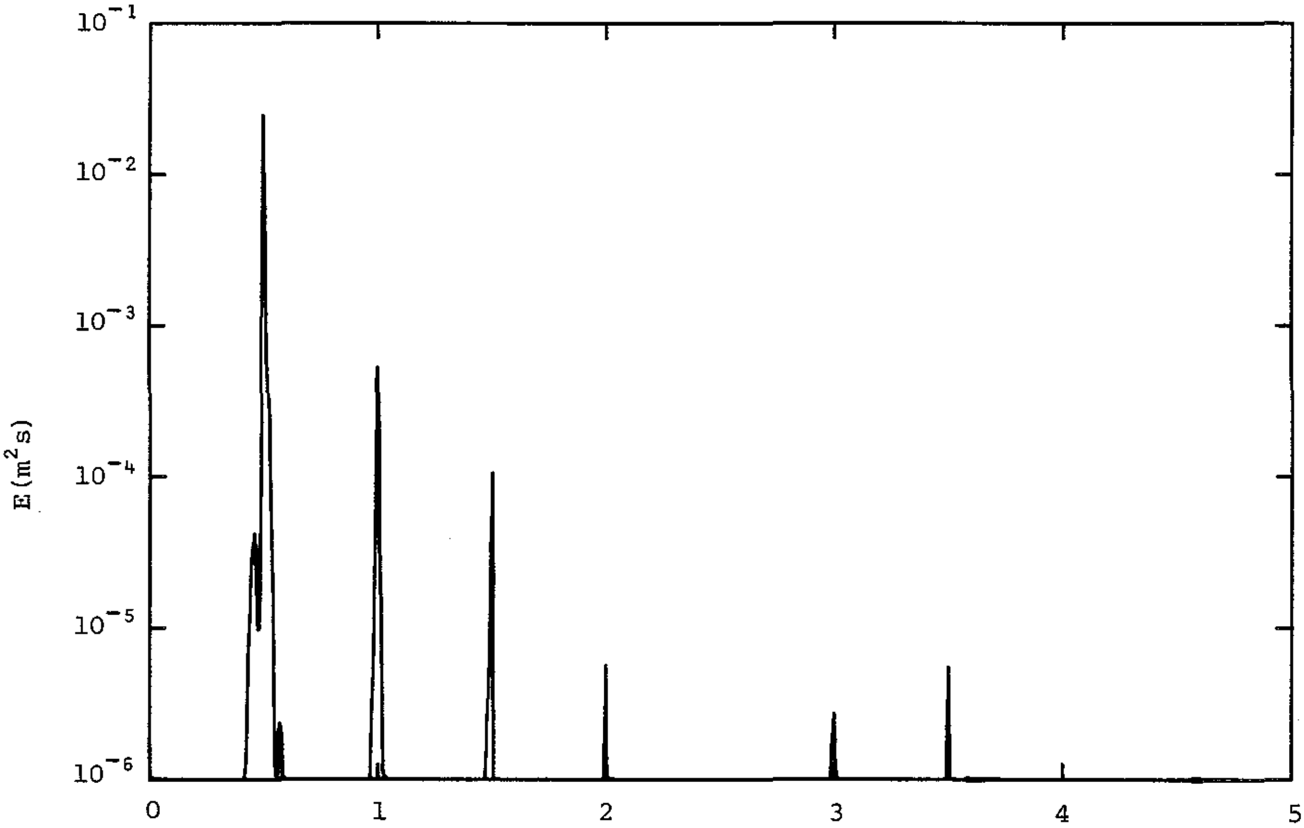

frequency = 0.5 Hz

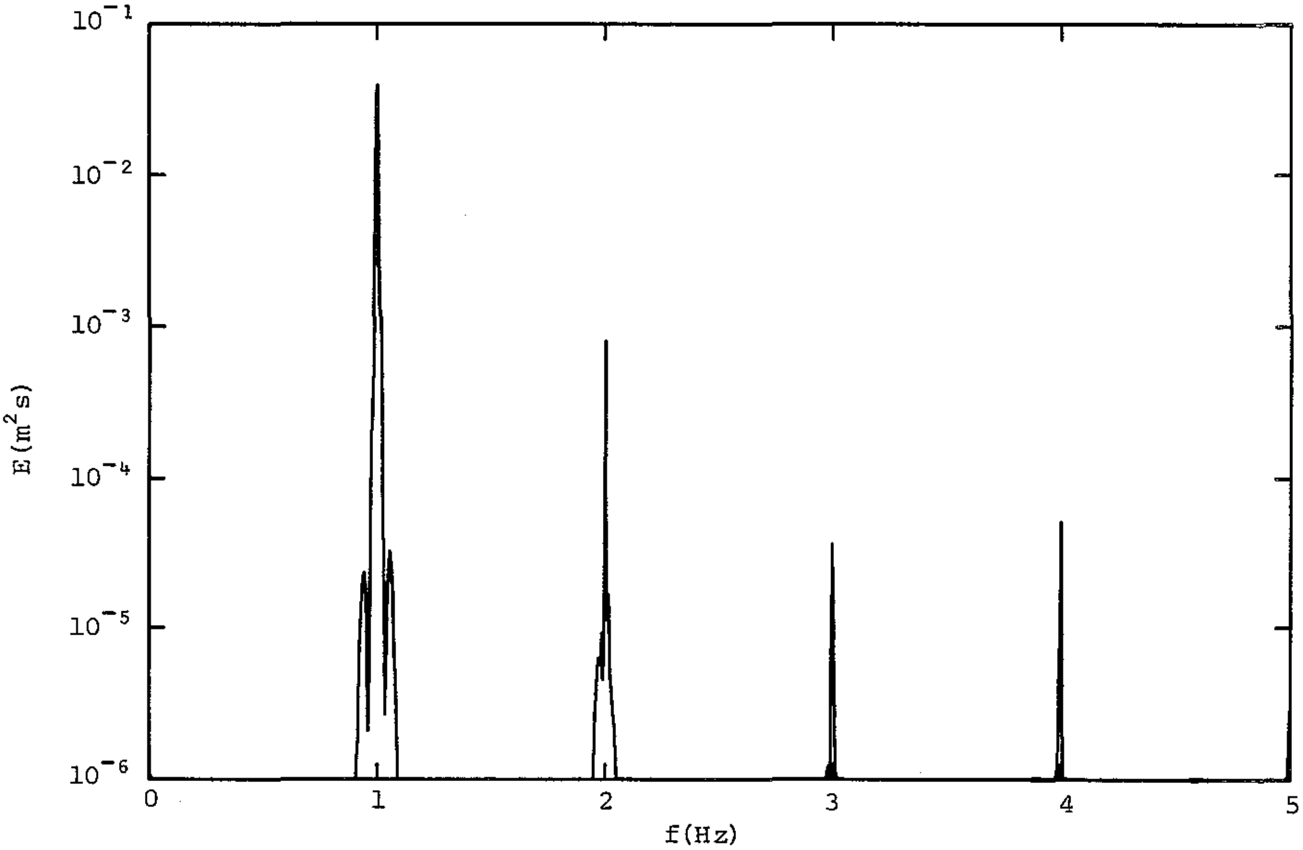

frequency = 1.0 Hz

Figure 3.16a Spectra of water surface elevation for sinusoidal wave maker motion at various frequencies.

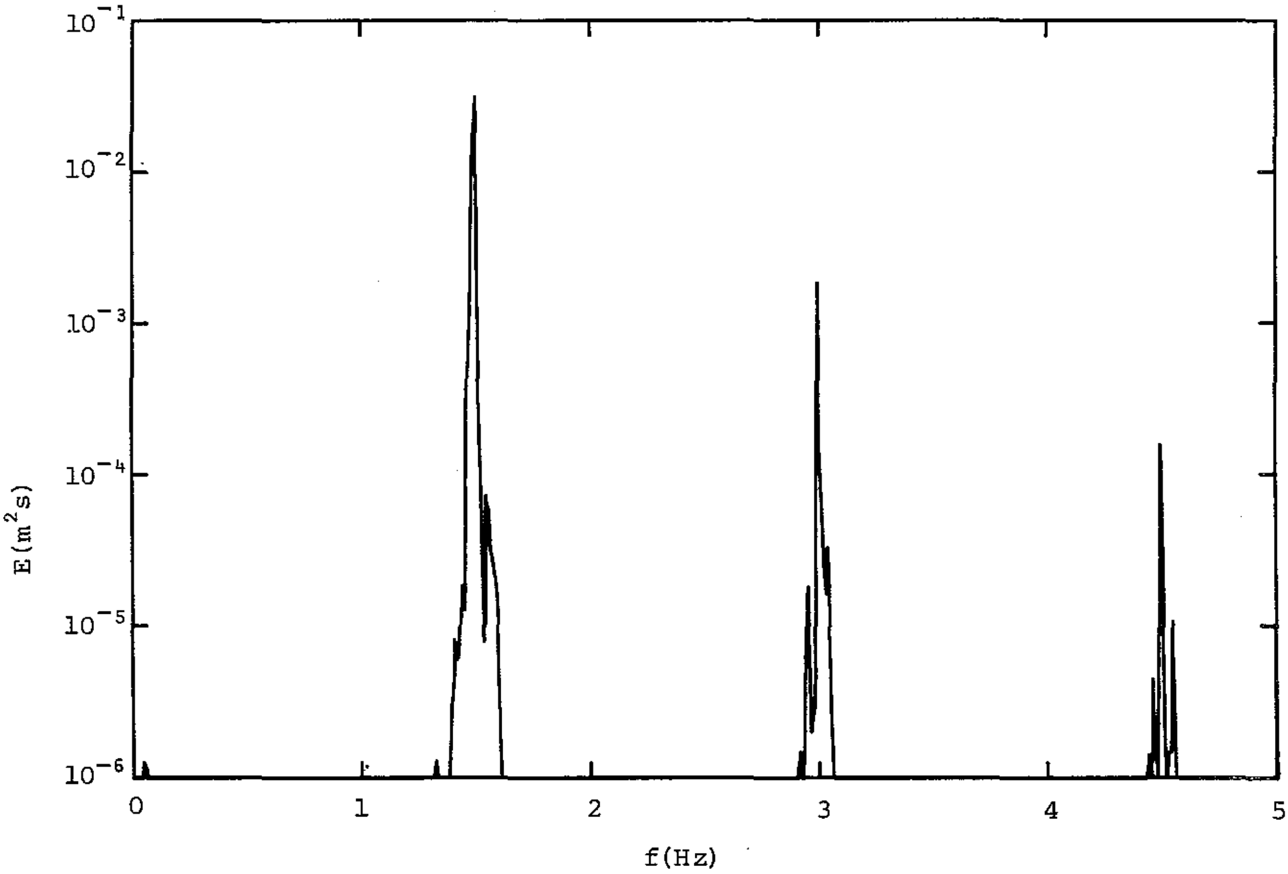

frequency = 1.5 Hz

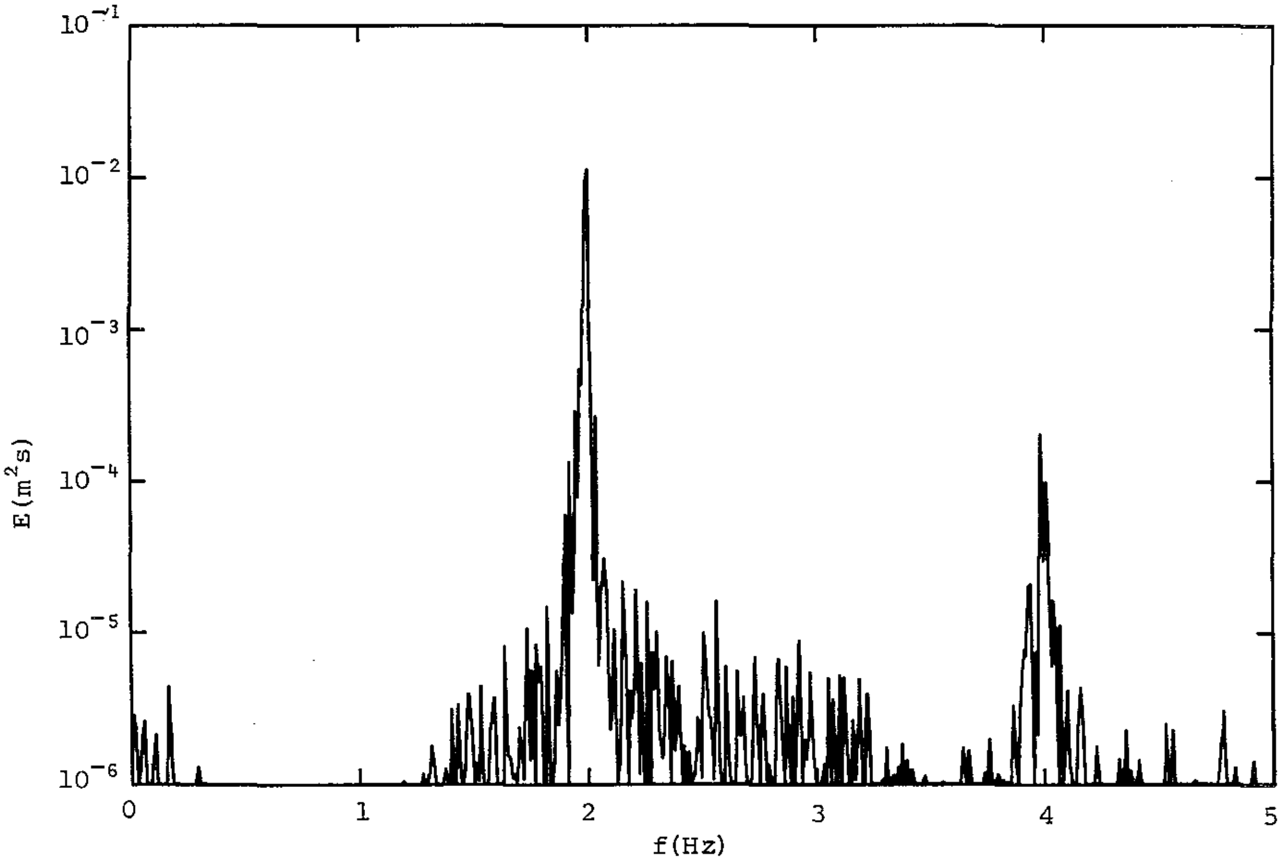

frequency = 2.0 Hz

Figure 3.16b Spectra of water surface elevation for sinusoidal wave maker motion of various frequencies.

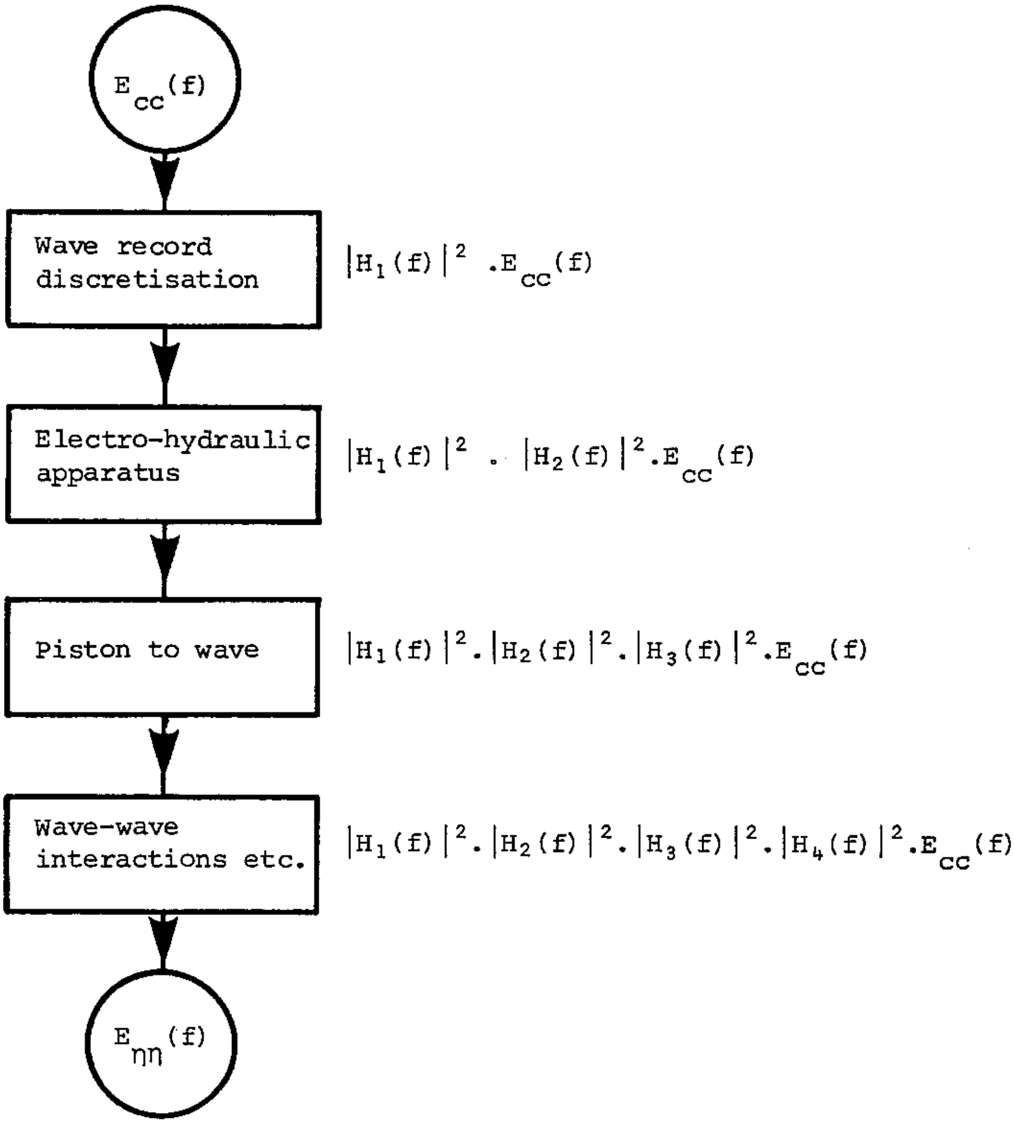

Figure 3.17 Transfer functions relating initial command wave record to realized water surface record.

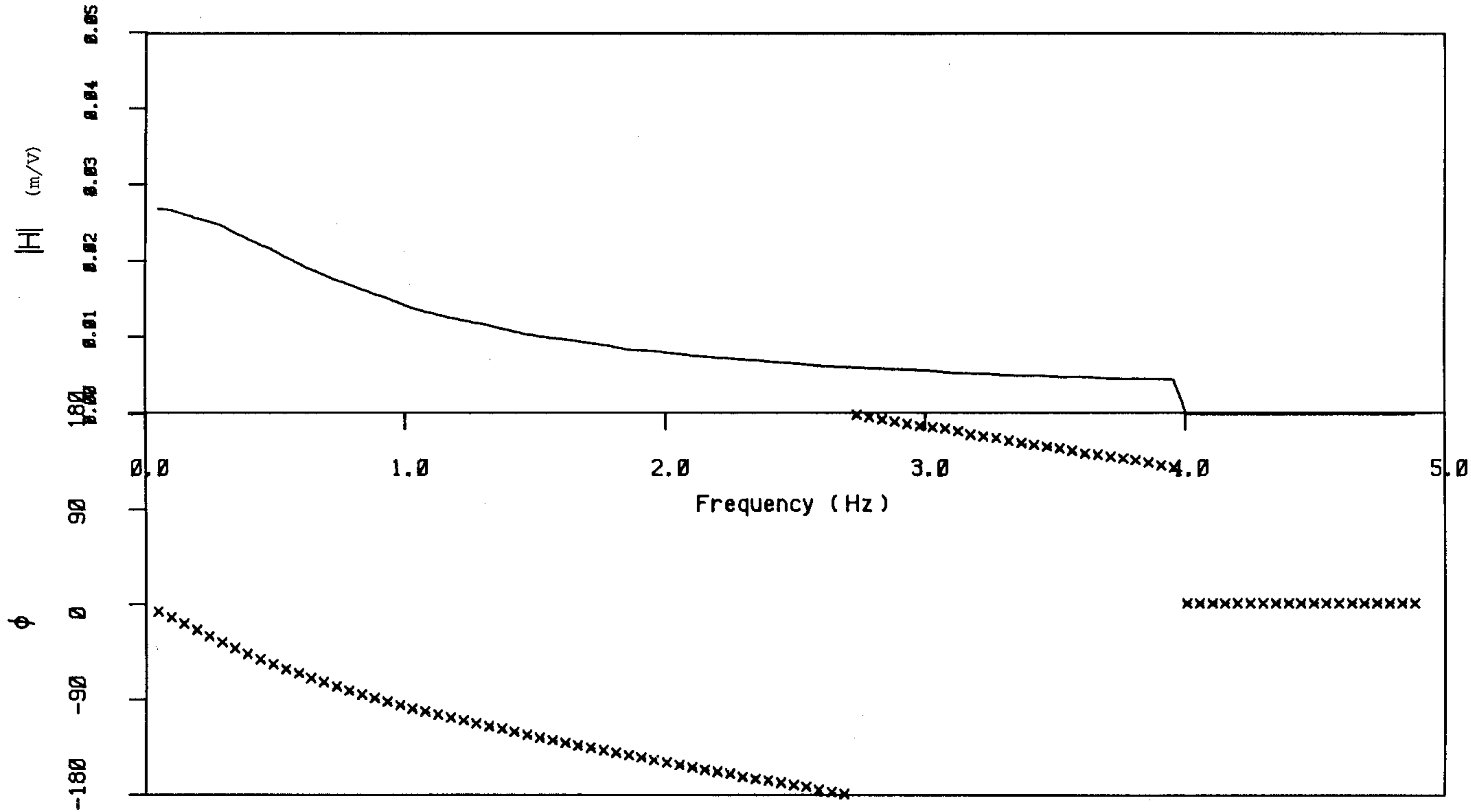

Figure 3.18 Transfer function relating command signal to wave maker motion.

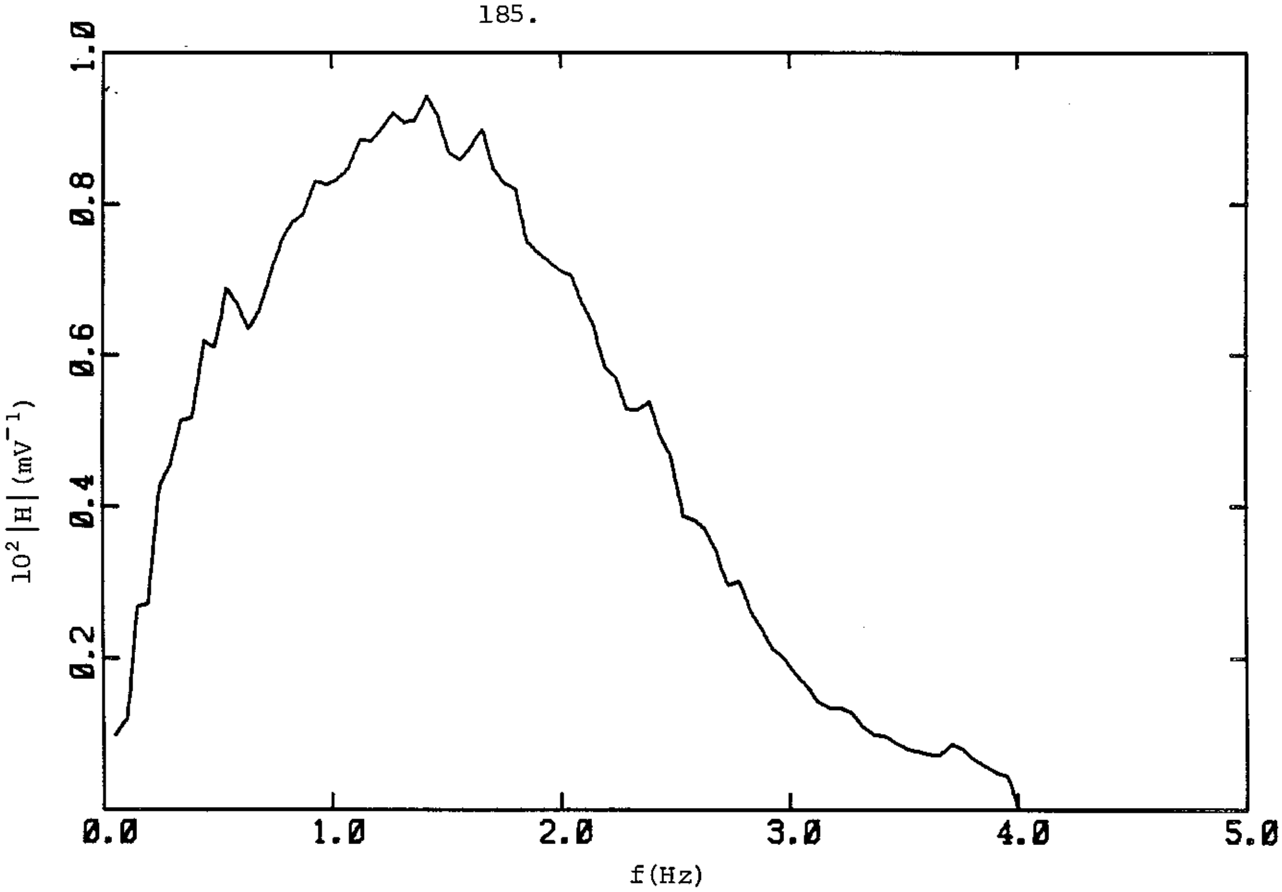

Figure 3.19a Wave maker transfer function at mid-flume working section. Input spectral variance = 0.7 V^2.

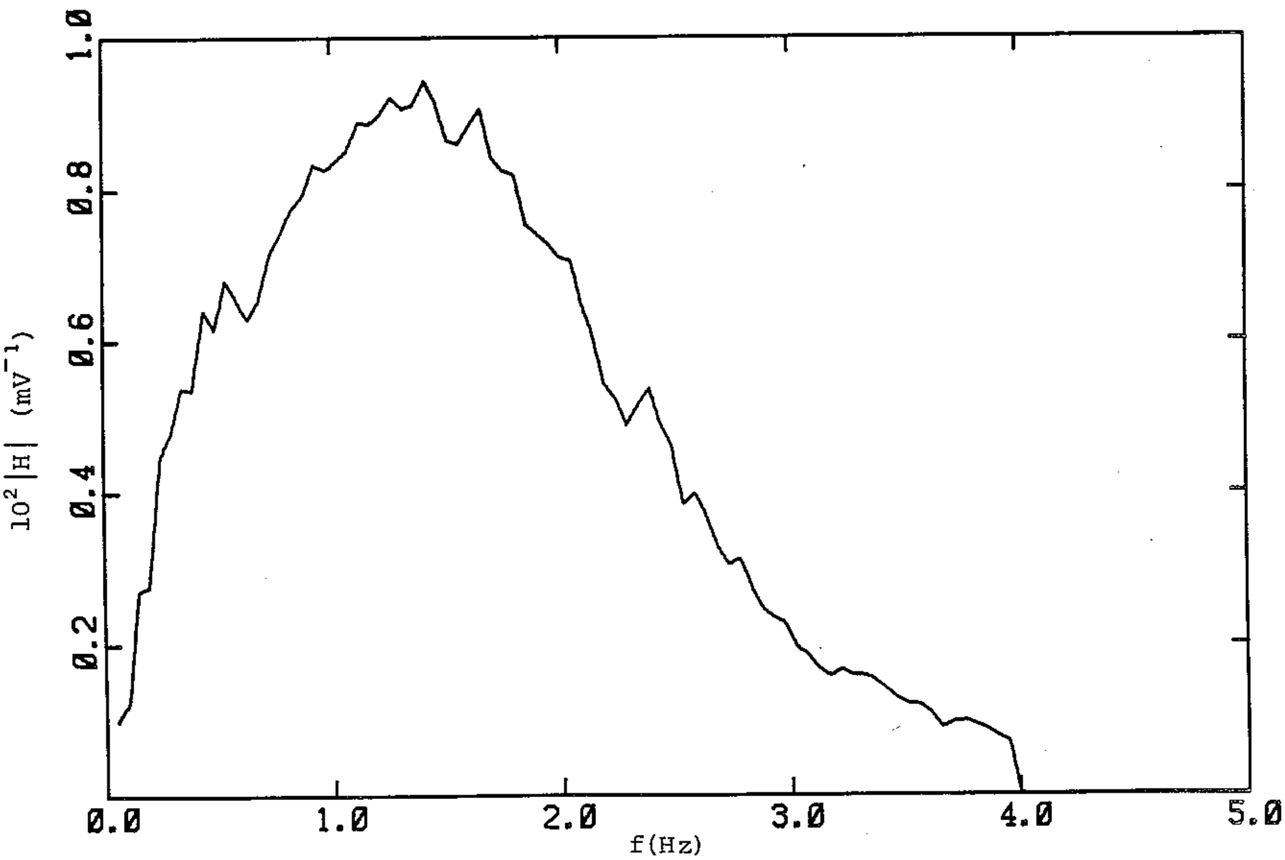

Figure 3.19b Wave maker transfer function at mid-flume working section. Input spectral variance = 1 V^2.

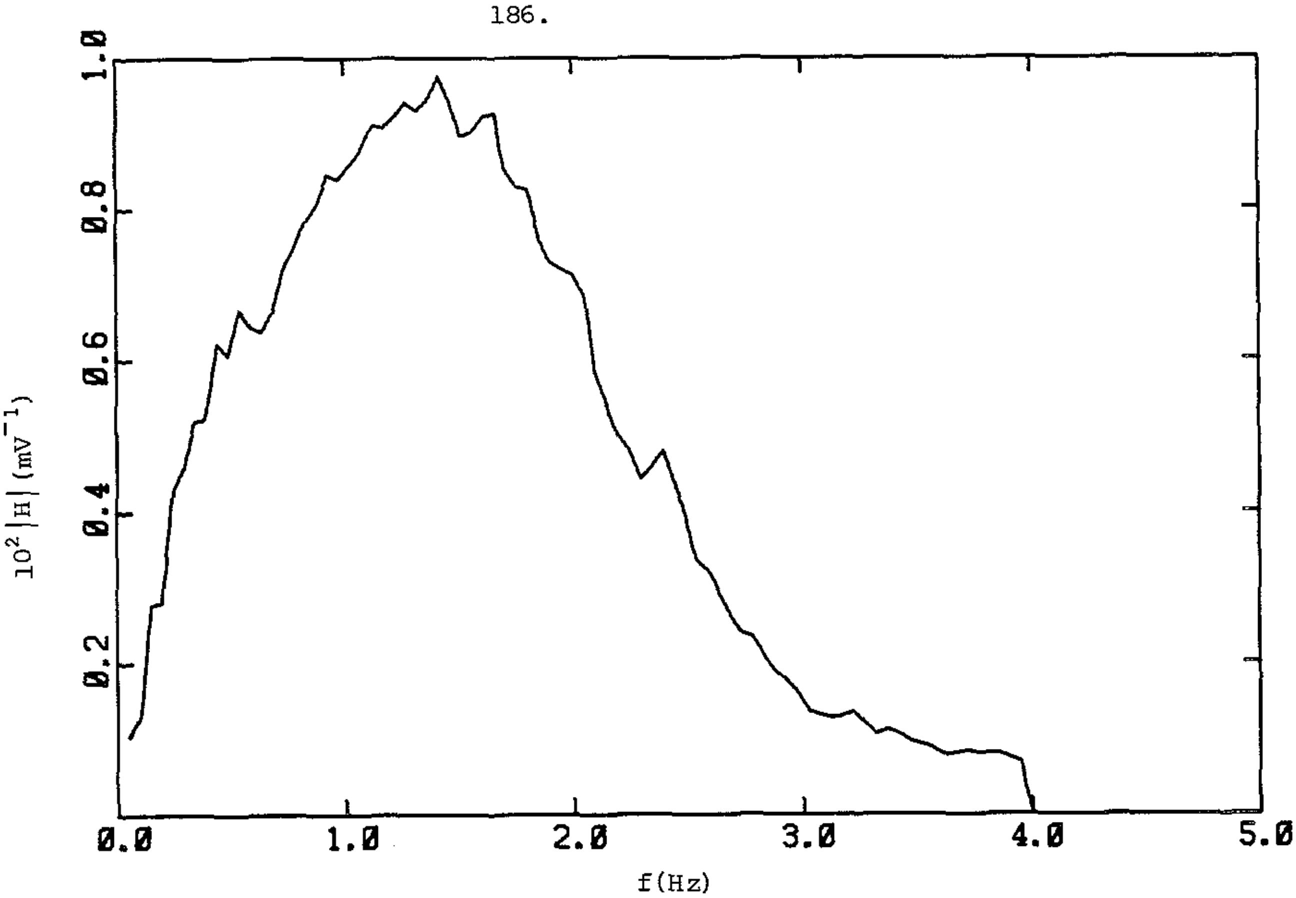

Figure 3.19c Wave maker transfer function at mid-flume working section. Input spectral variance = 1.5 V^2.

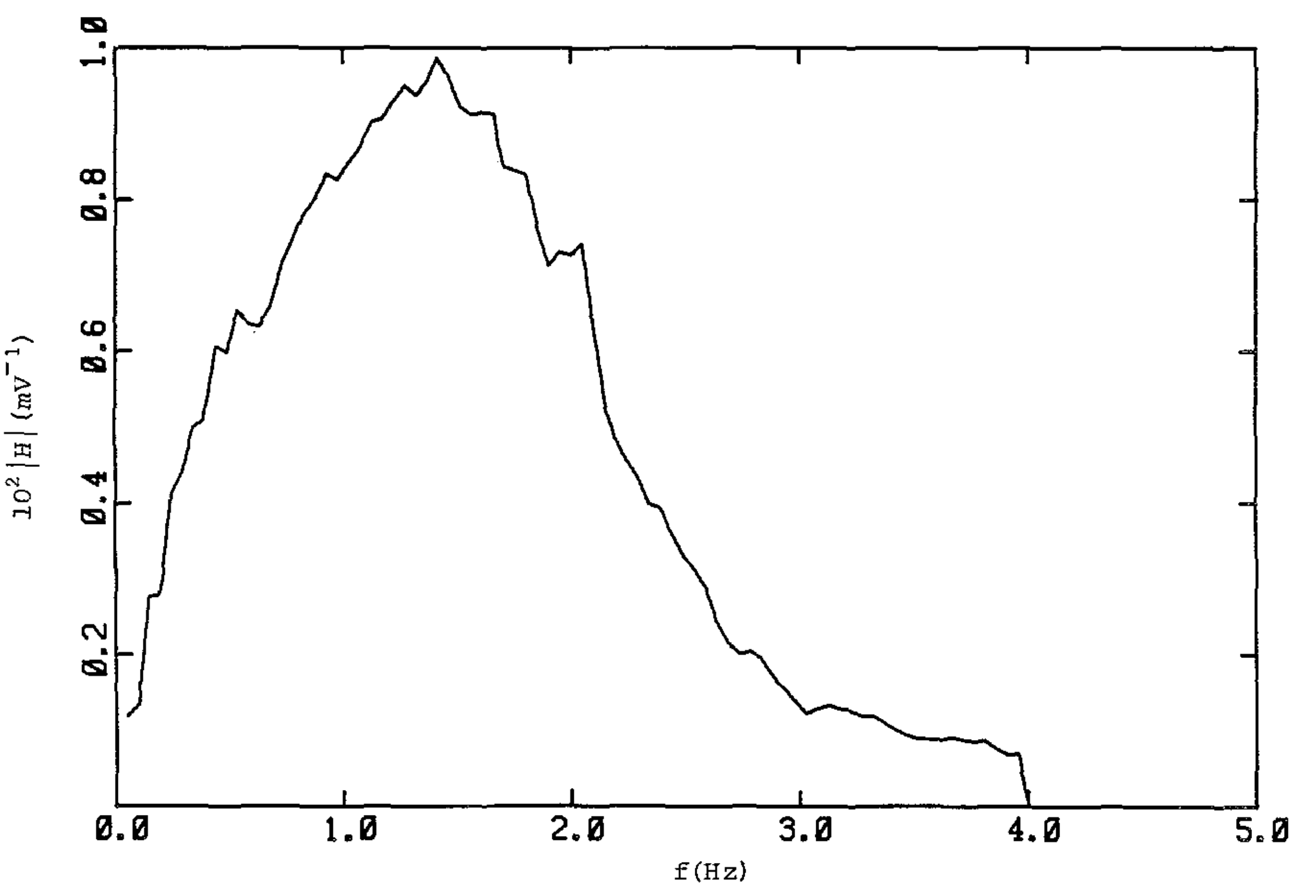

Figure 3.19d Wave maker transfer function at mid-flume working section. Input spectral variance = 2 V^2.

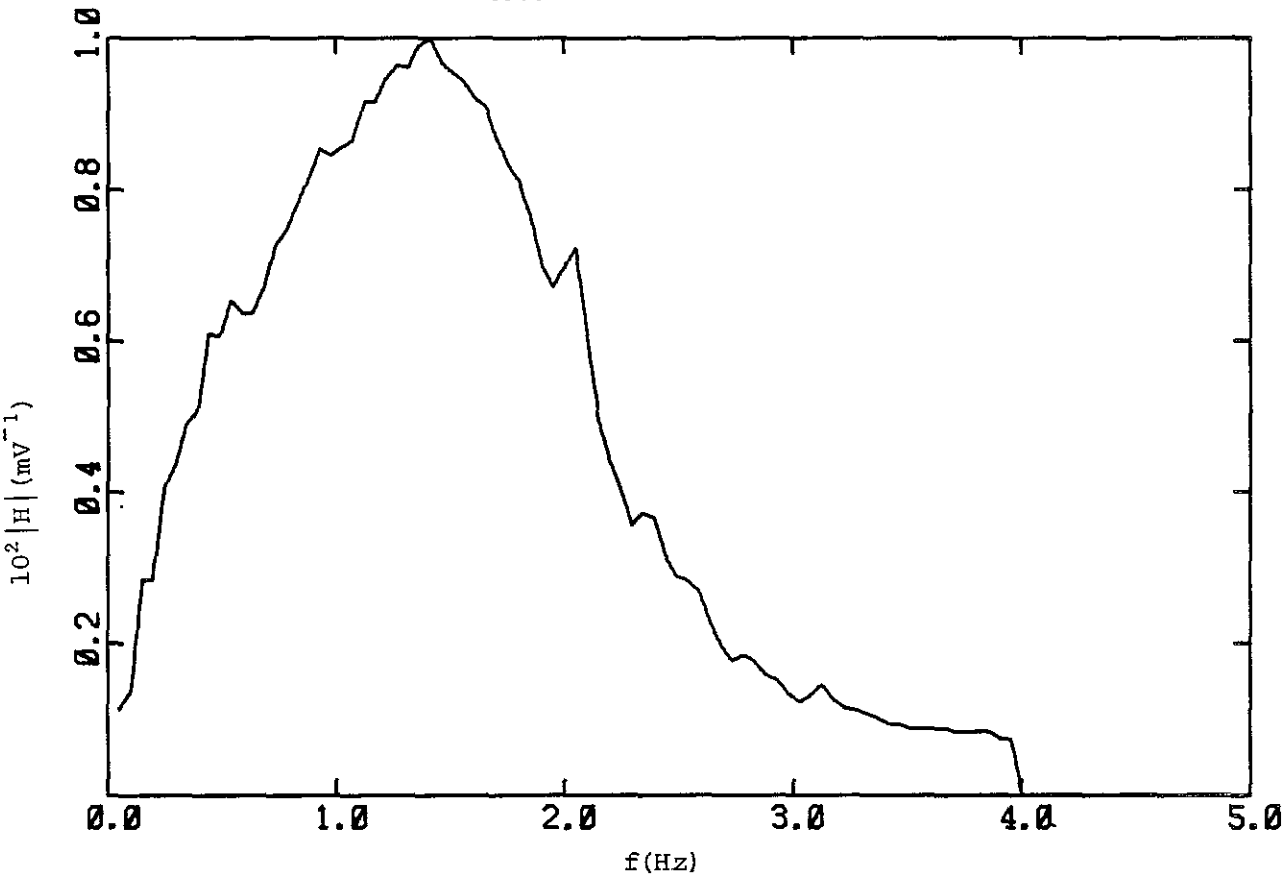

Figure 3.19e Wave maker transfer function at mid-flume working section. Input spectral variance = 2.5 V^2.

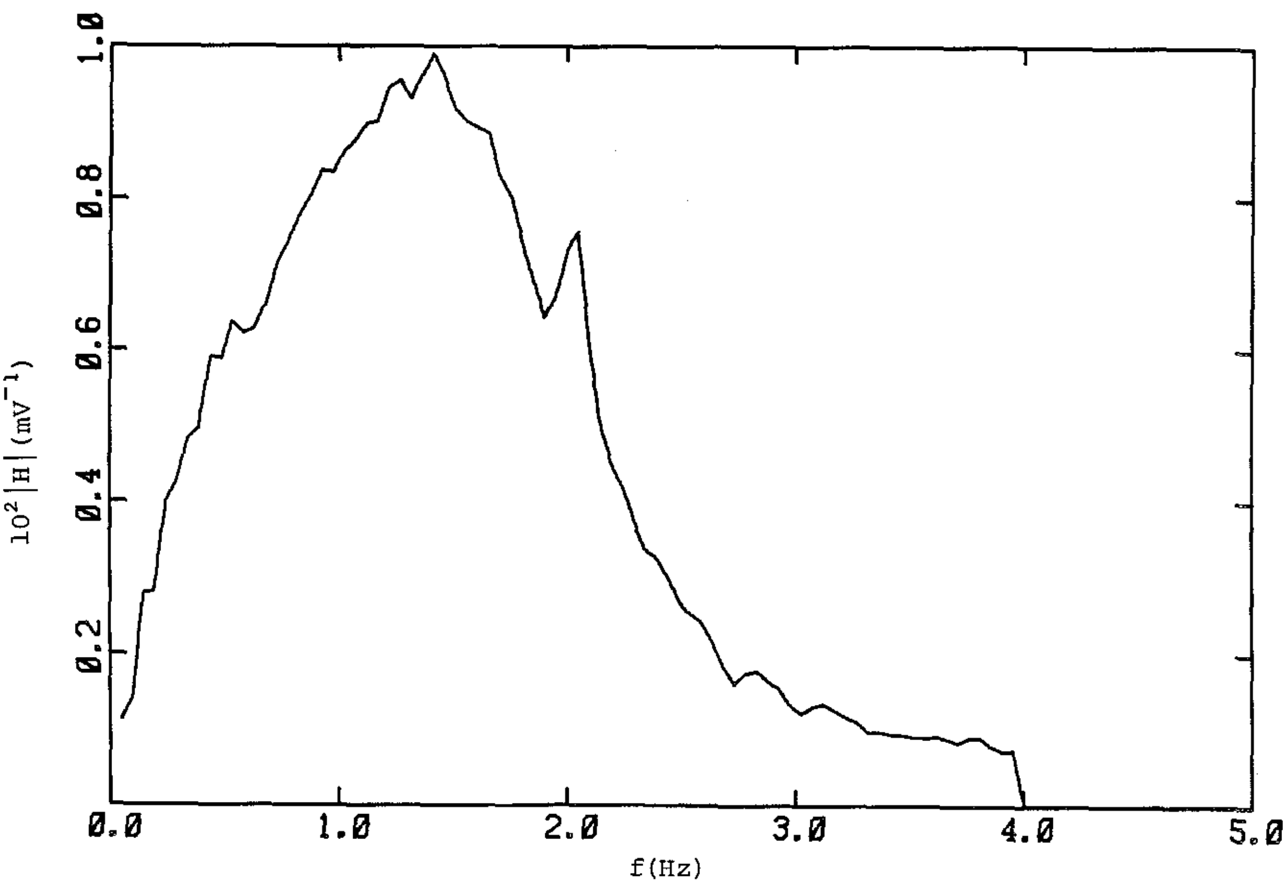

Figure 3.19f Wave maker transfer function at mid-flume working section. Input spectral variance = 3 V^2.

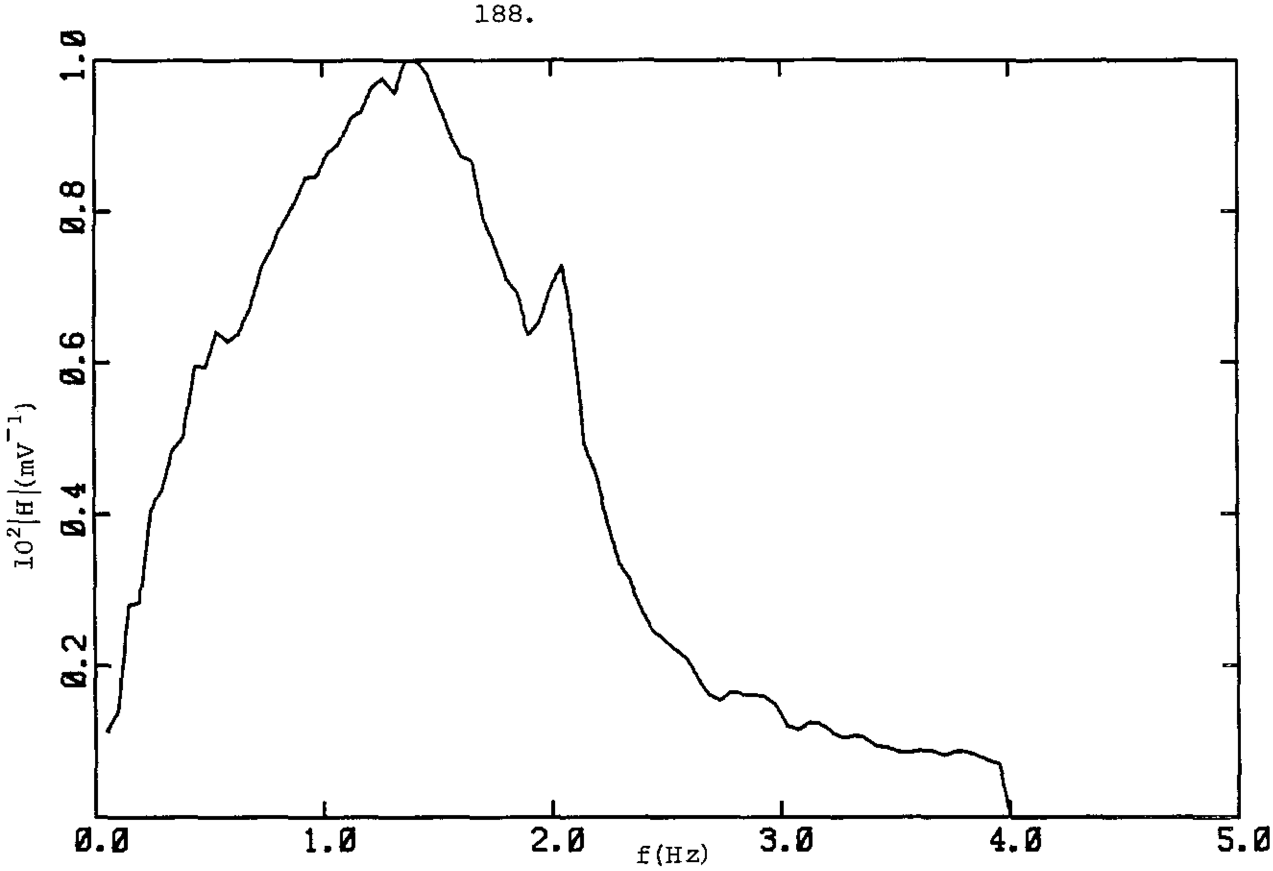

Figure 3.19g Wave maker transfer function at mid-flume working section. Input spectral variance = 3.5 V^2.

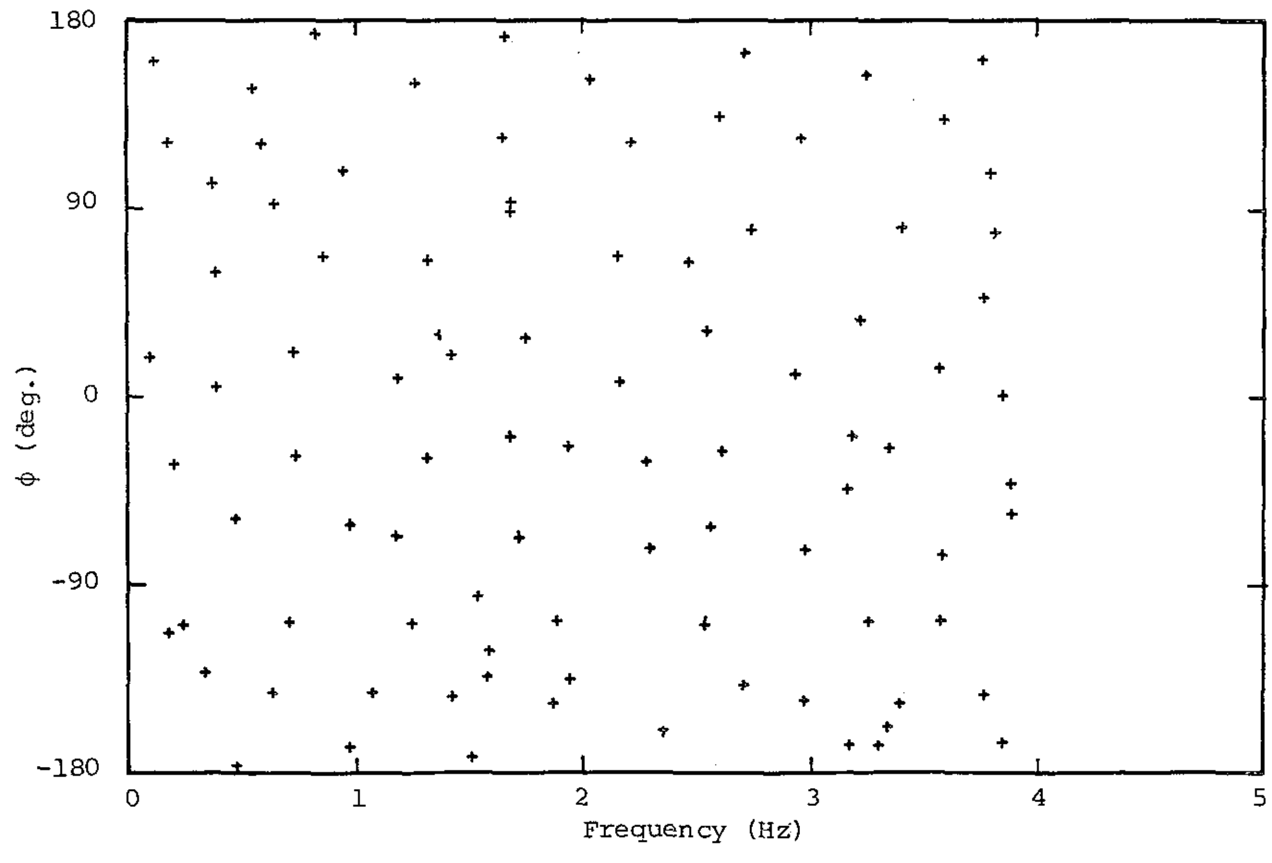

Figure 3.20 Phase of transfer function between command signal and water surface.

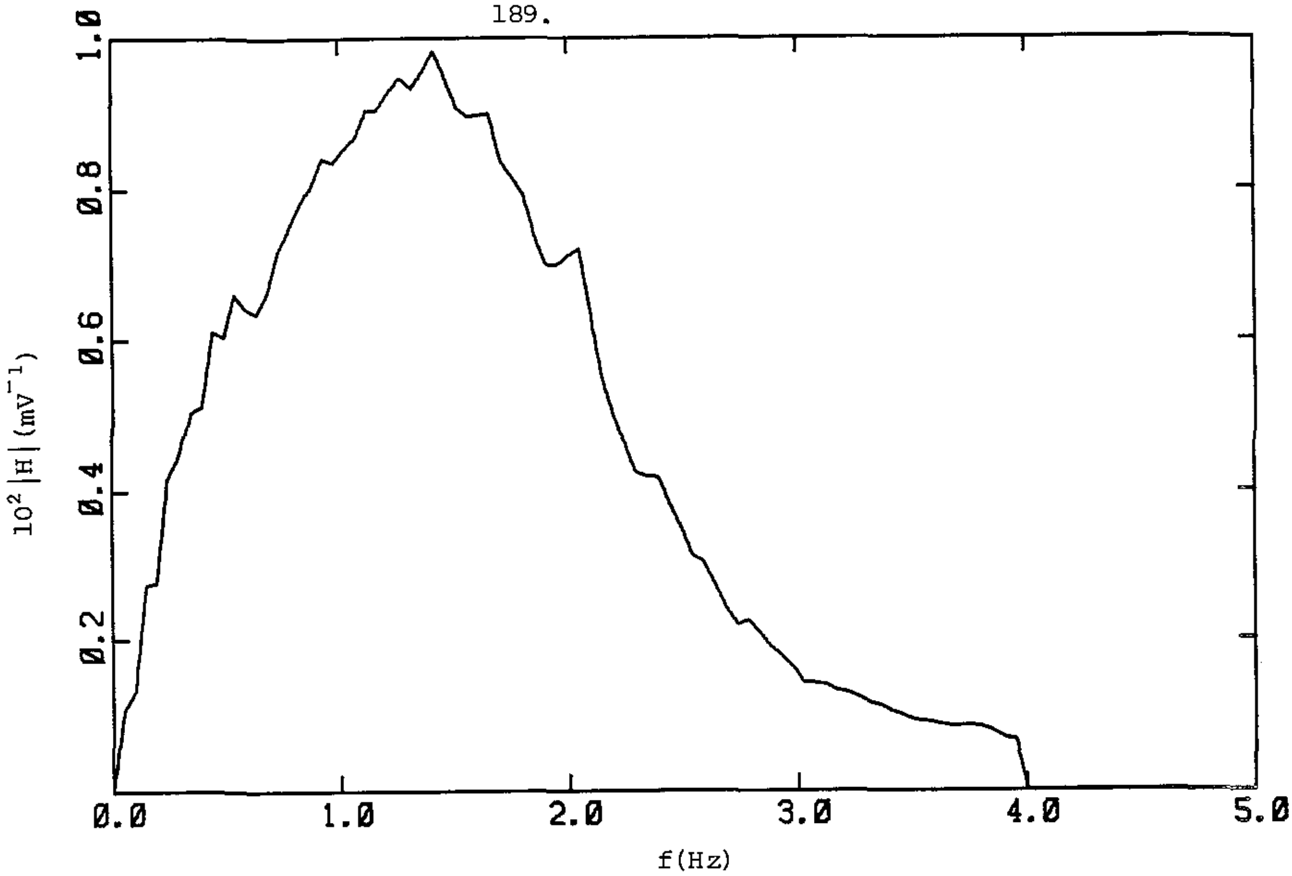

Figure 3.21 Average wave maker transfer function at mid-flume working section.

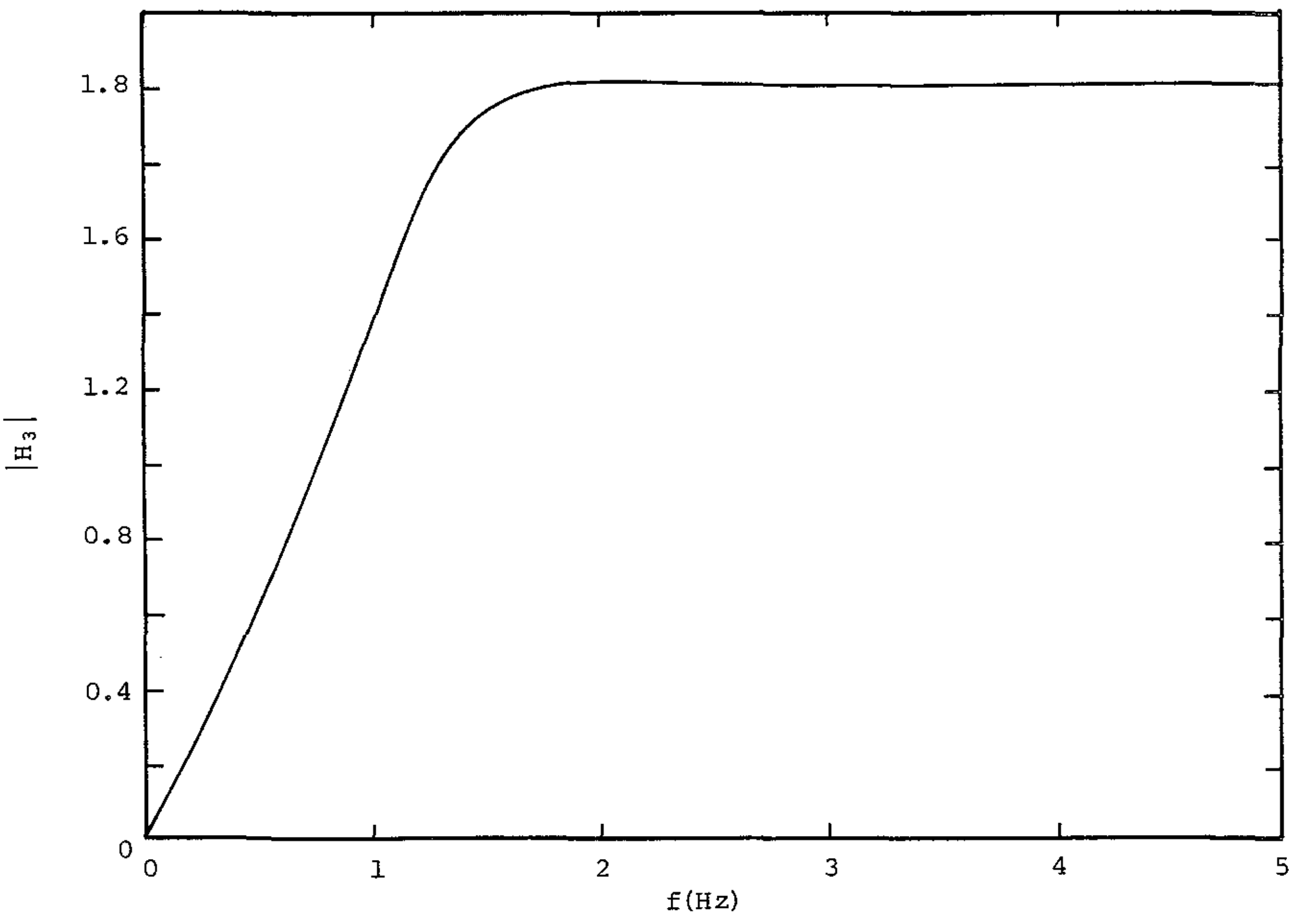

Figure 3.22 The theoretical transfer function H_3 between the piston stroke and wave as given by Eq. 3.22.

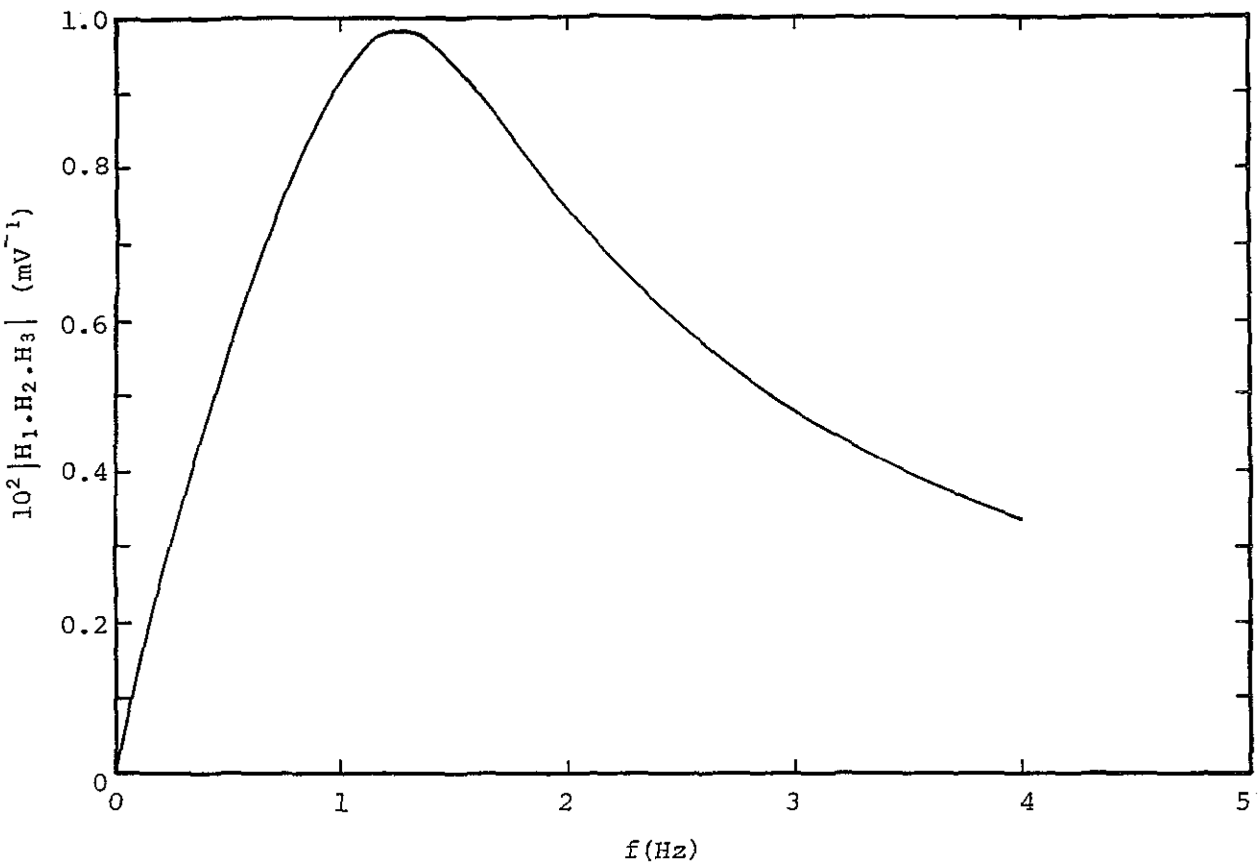

Figure 3.23 Theoretical transfer function between input signal and wave.

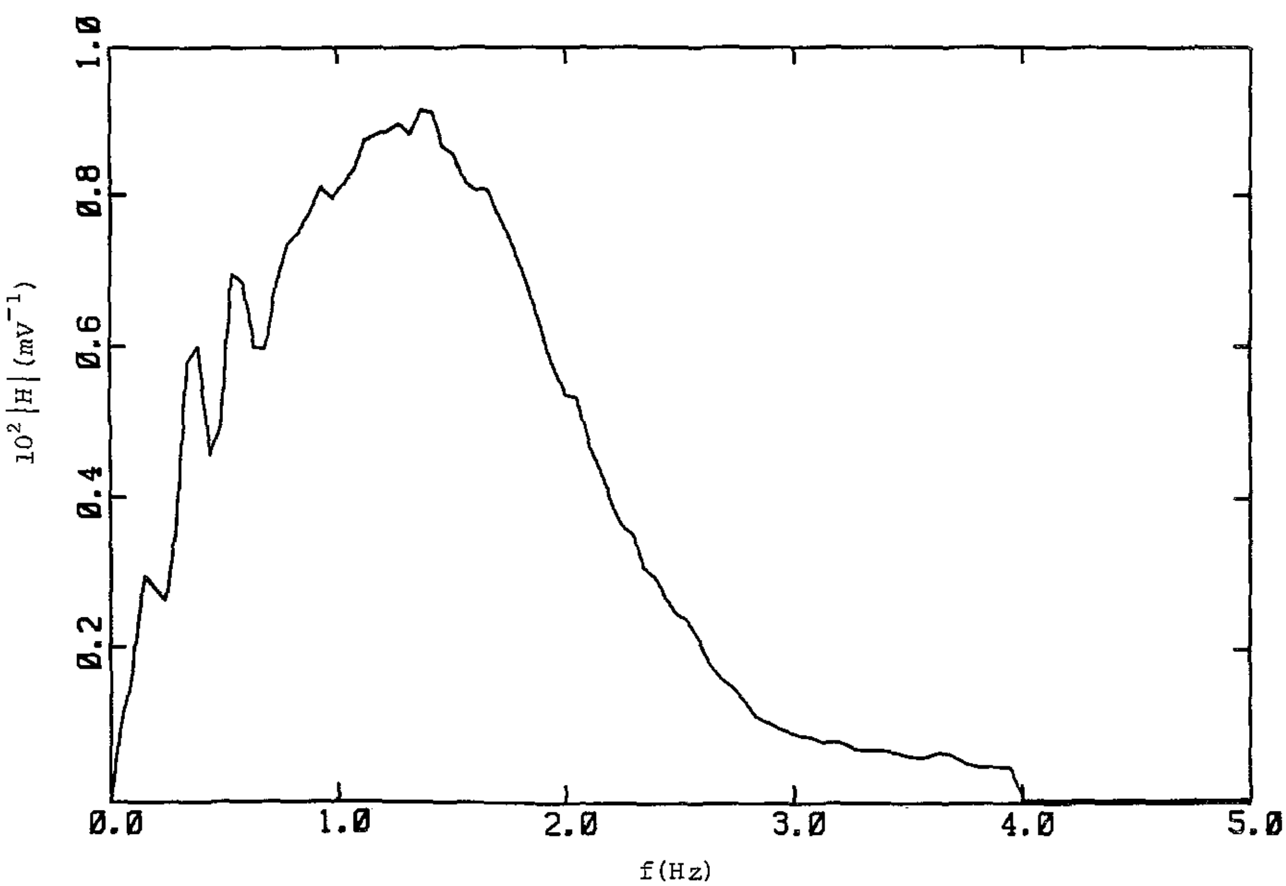

Figure 3.24 Average wave maker transfer function at beach station.

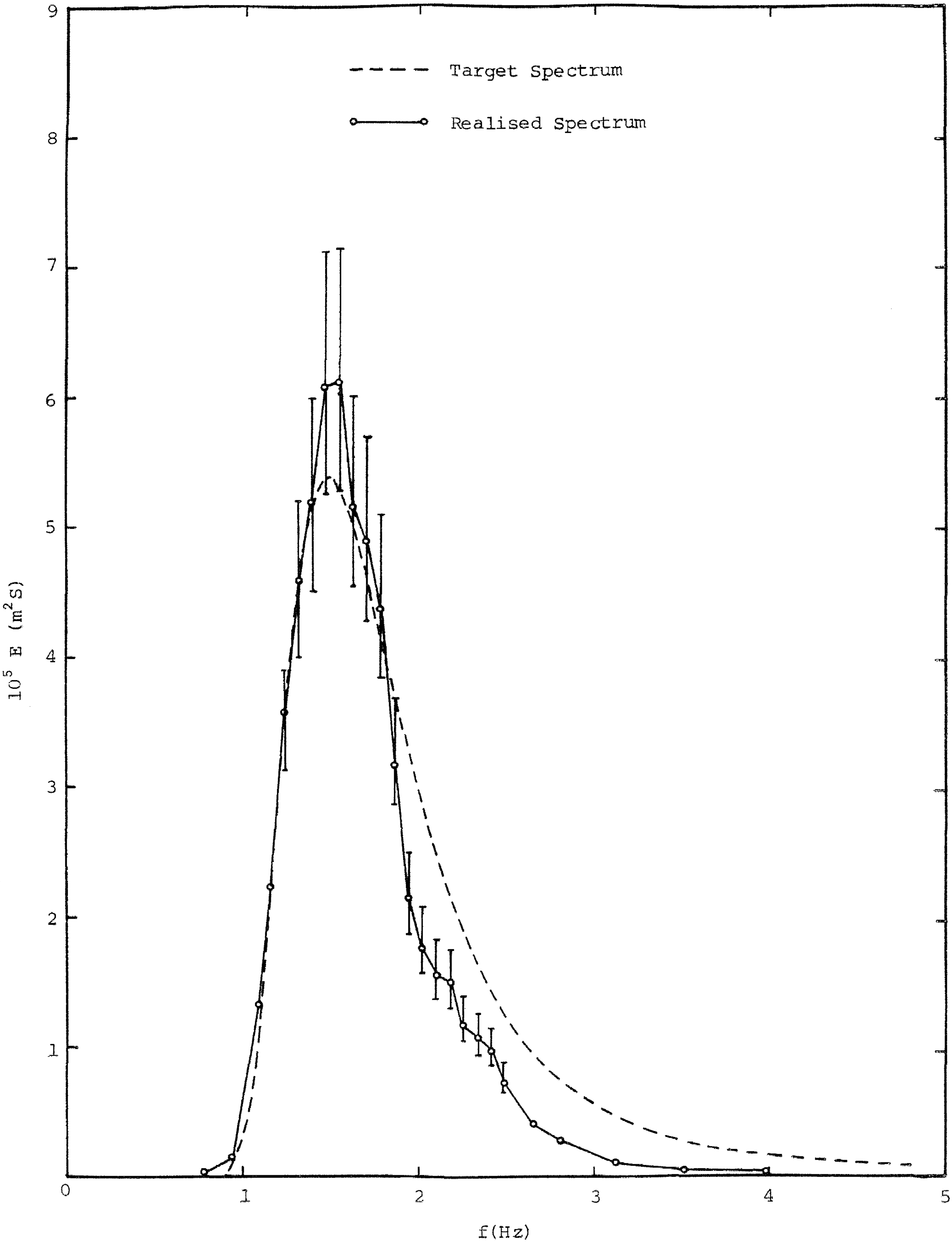

Figure 3.25 Comparison between target wave height spectrum and realised spectrum.

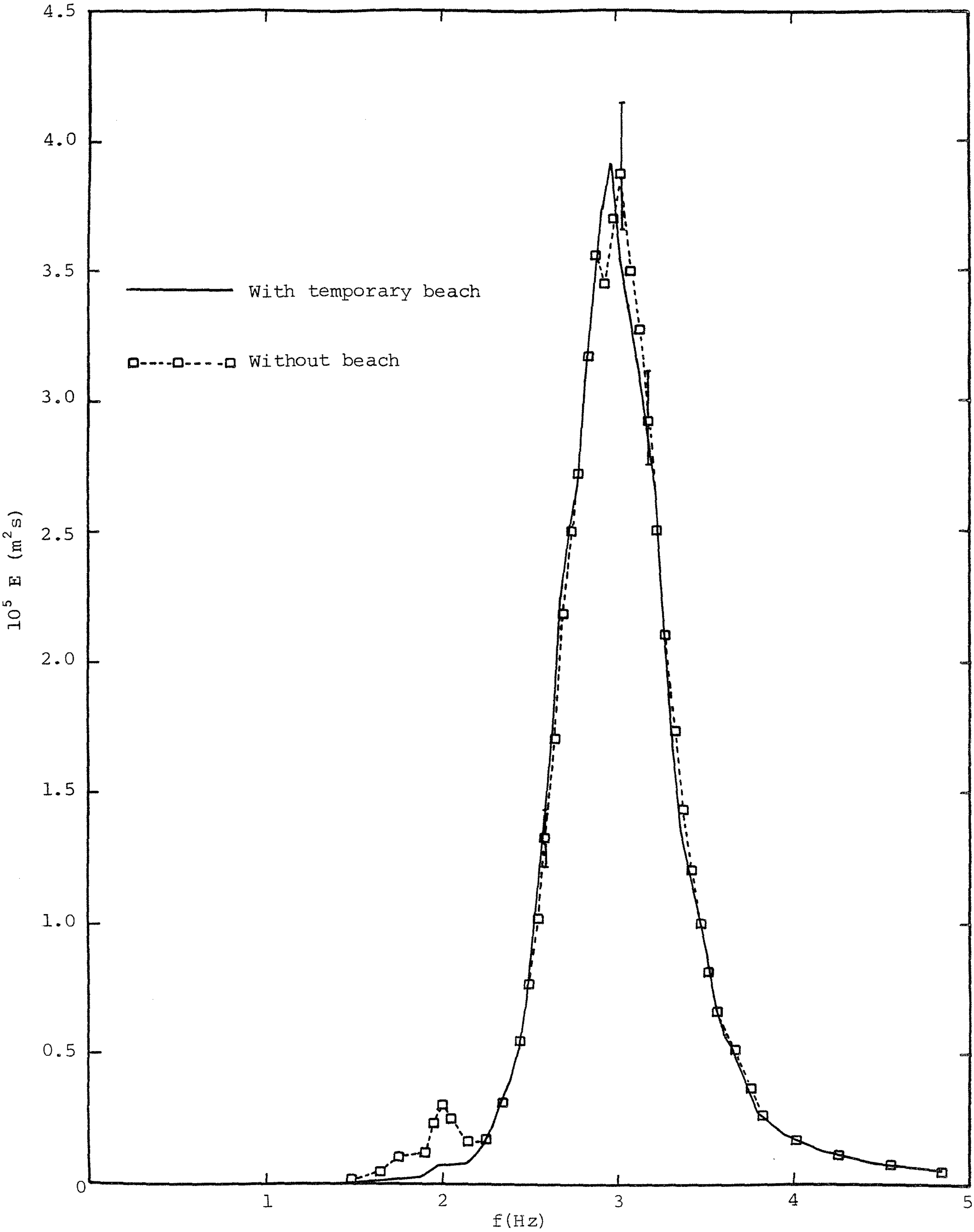

Figure 3.26 Comparison of wave height spectra at mid-flume with and without temporary absorbing beach at the wave maker.

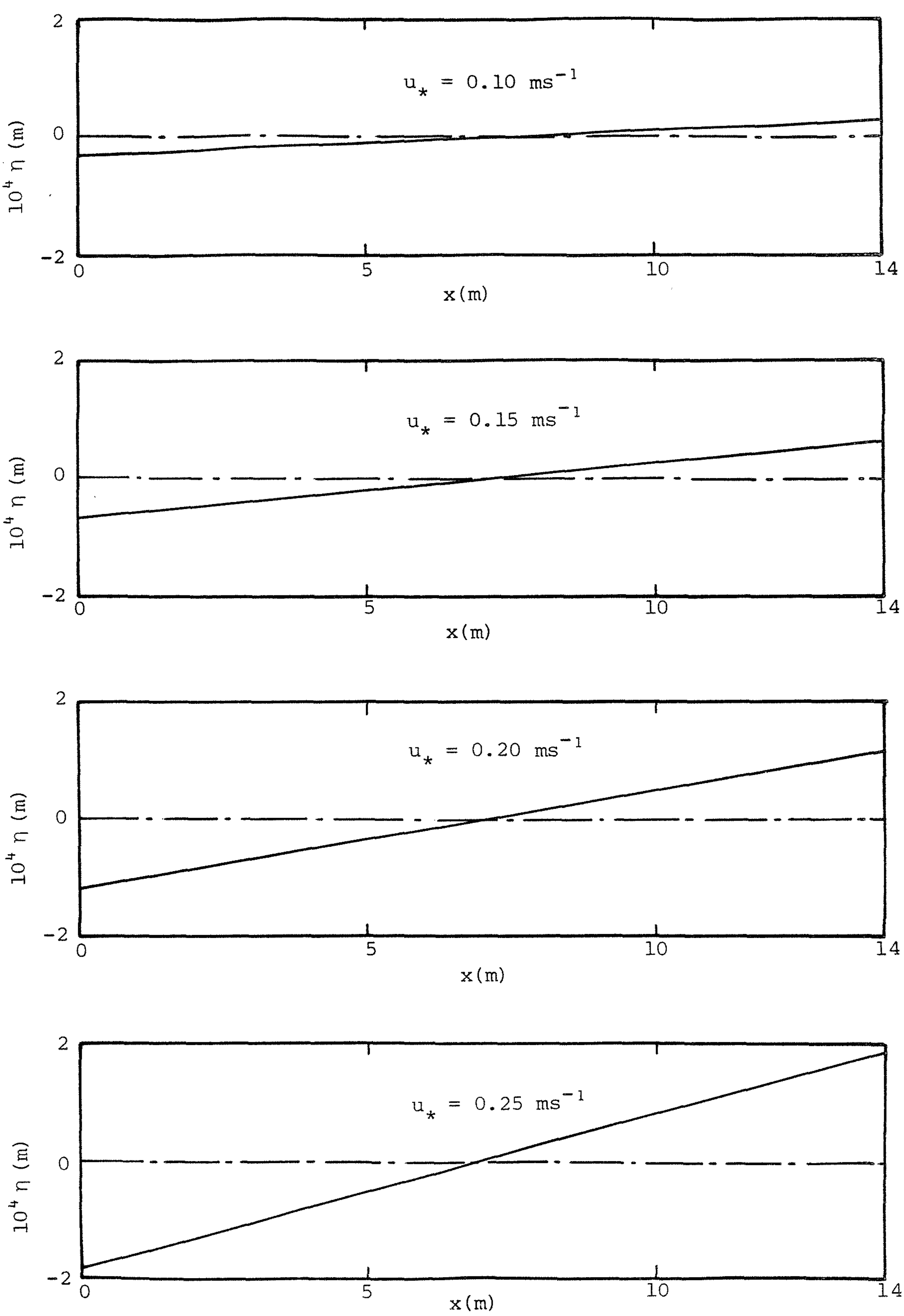

Figure 3.27 Water level setup for various values of u_*

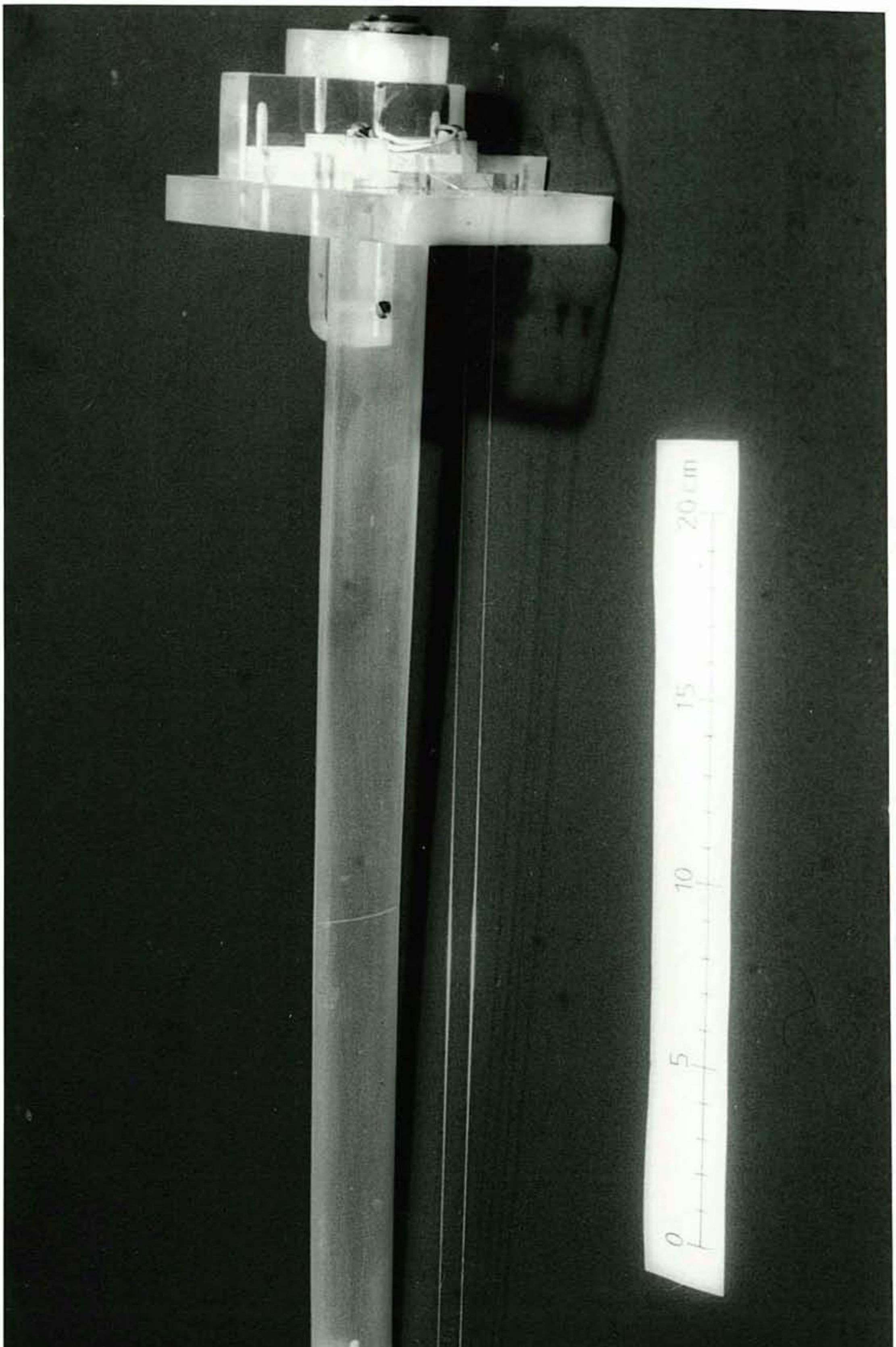

Figure 4.1 Photograph of wave height probe.

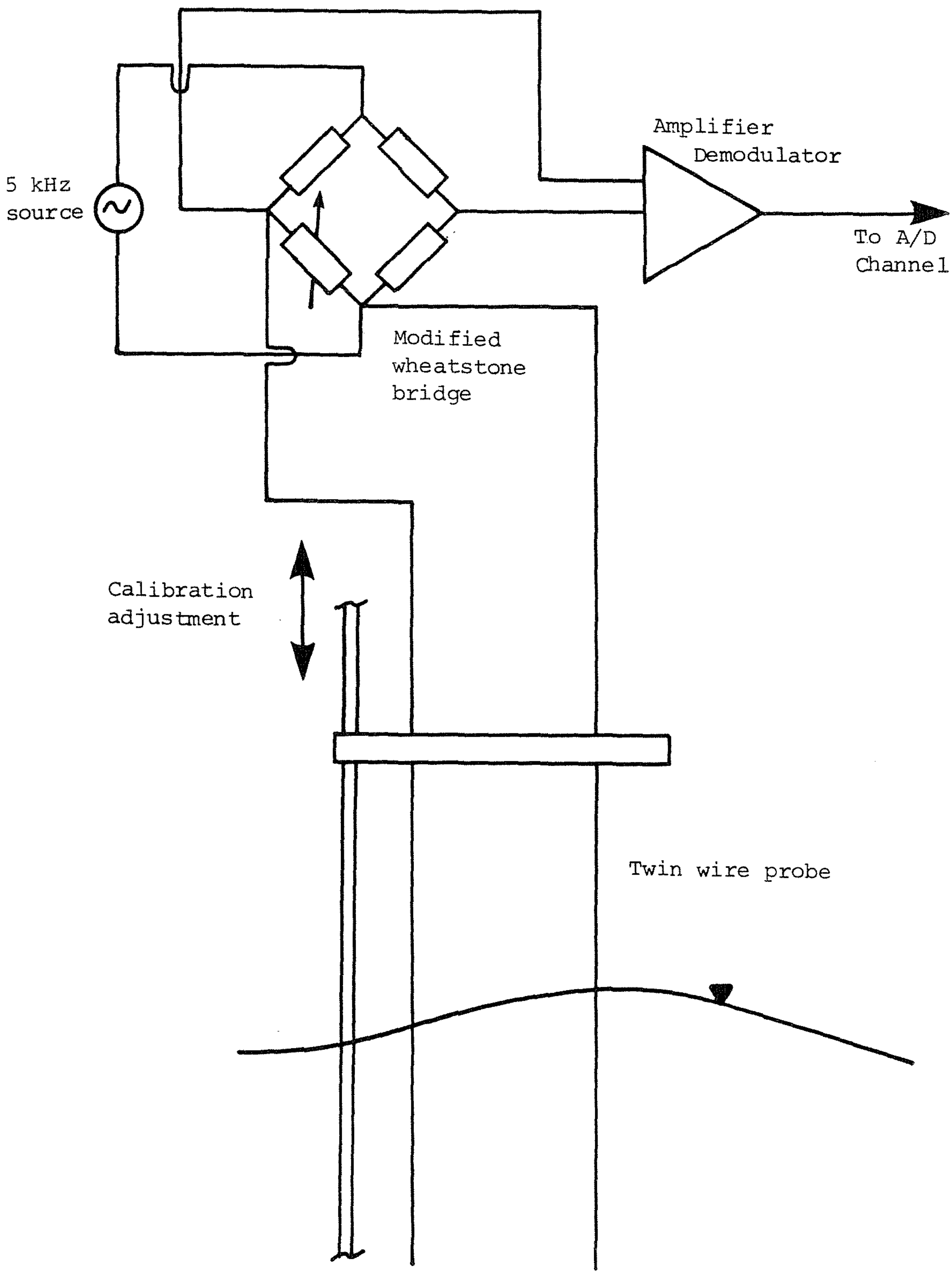

Figure 4.2 Schematic illustration of water surface elevation measurements system.

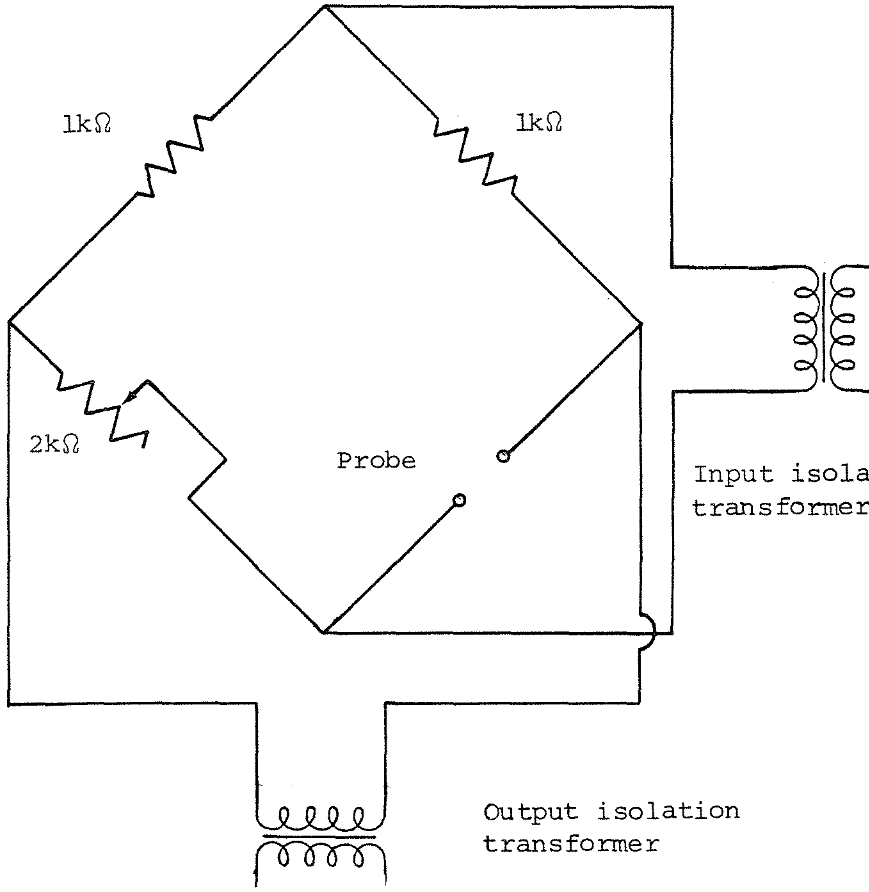

Figure 4.3 Circuit diagram of bridge for the electrical resistance wave gauges.

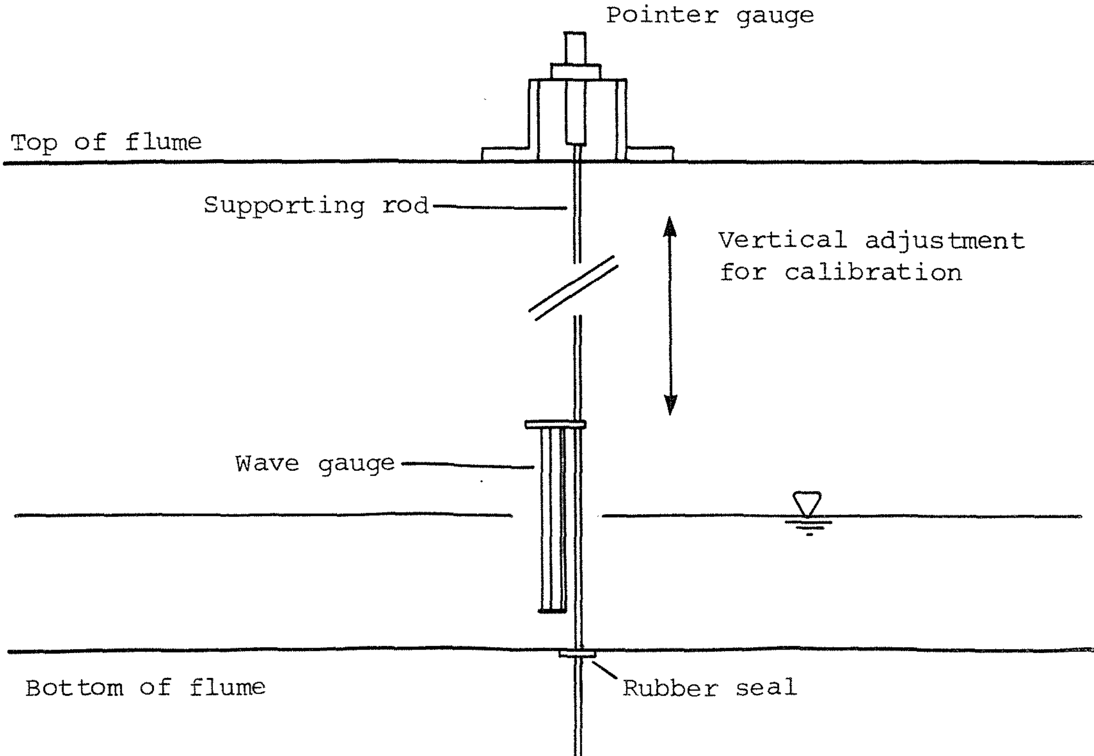

Figure 4.4 Wave gauge calibration and mounting system.

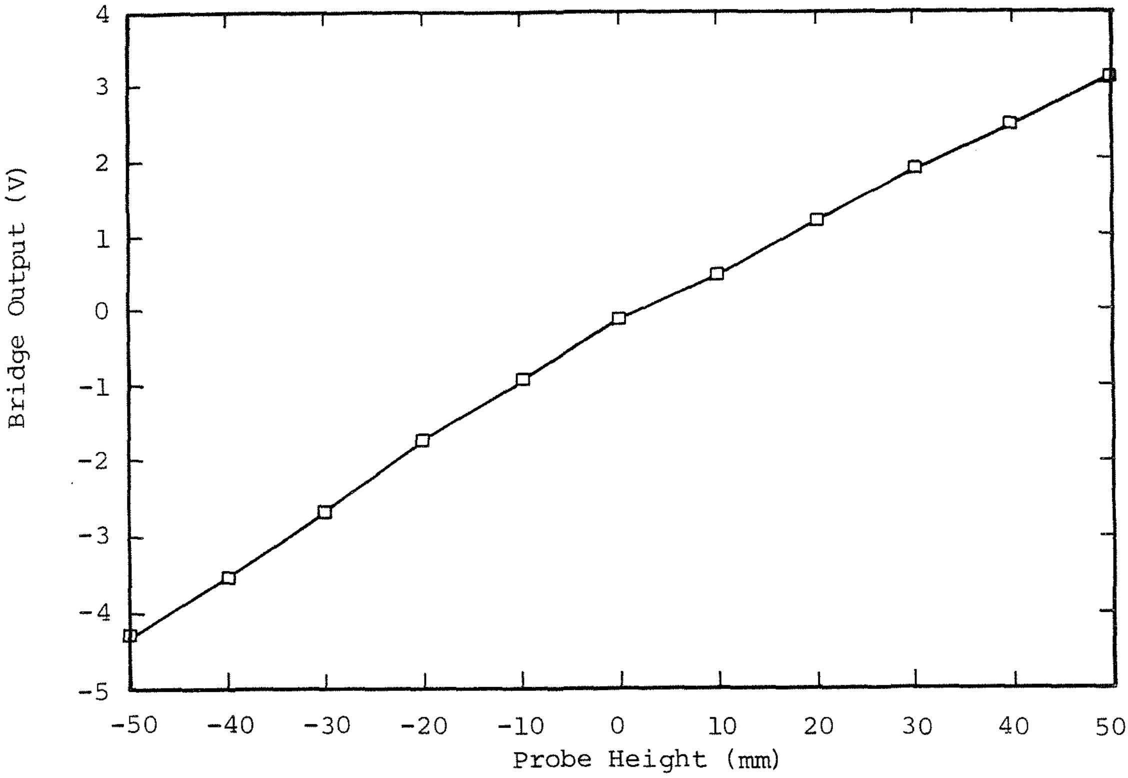

Figure 4.5 Typical wave gauge calibration curve.

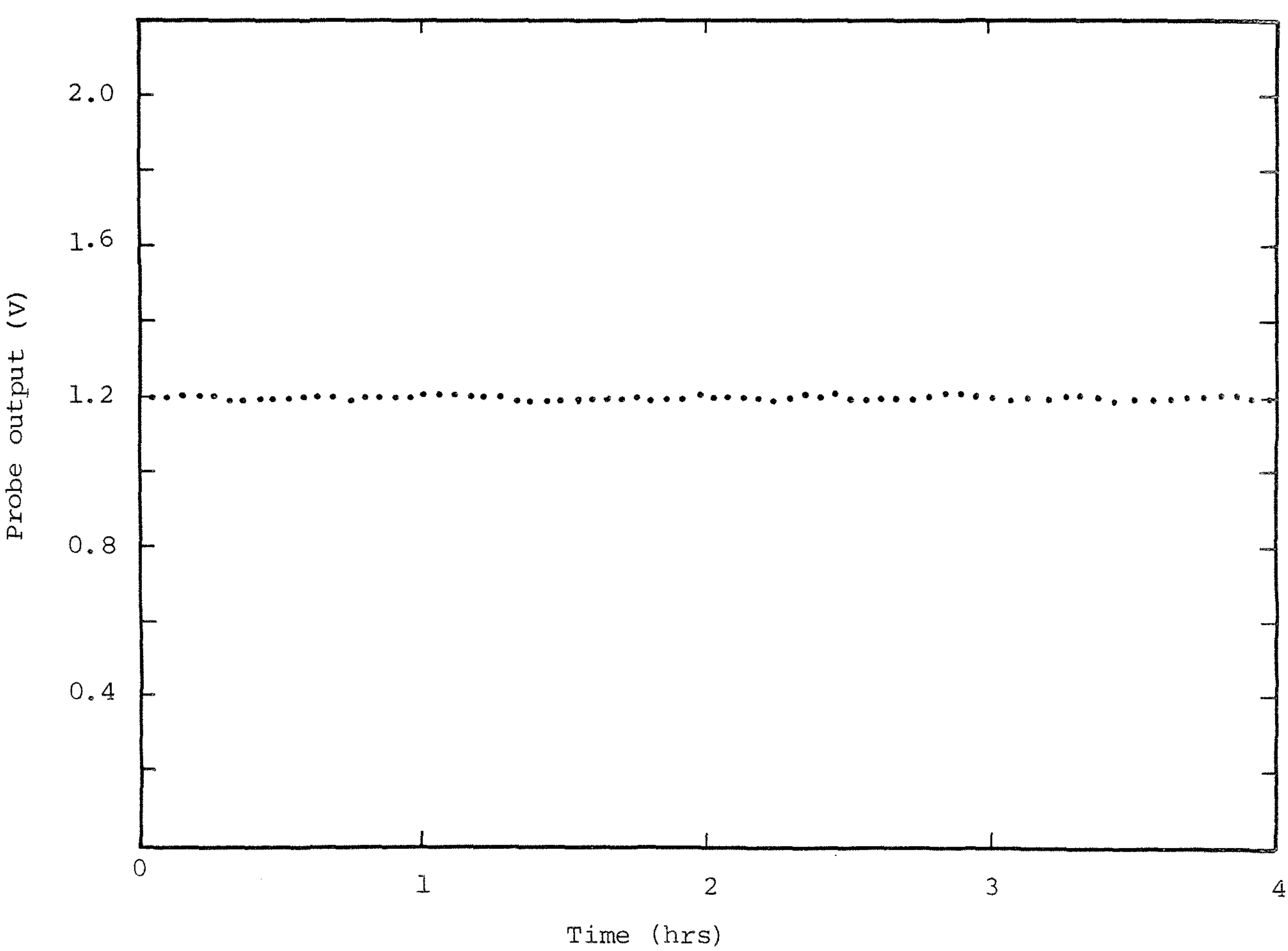

Figure 4.6 Stability of wave gauge output in still water.

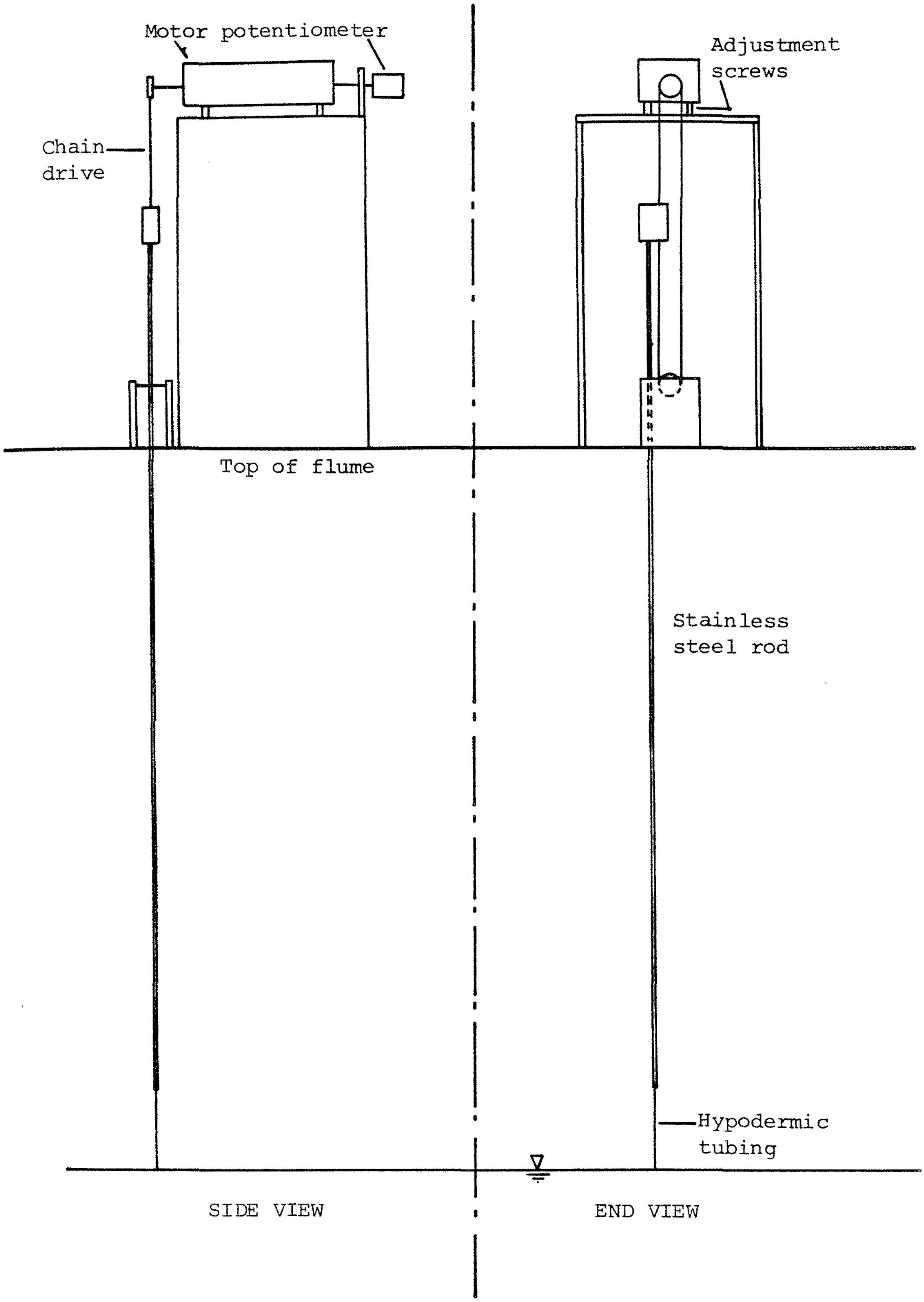

Figure 4.7 Wave follower system.

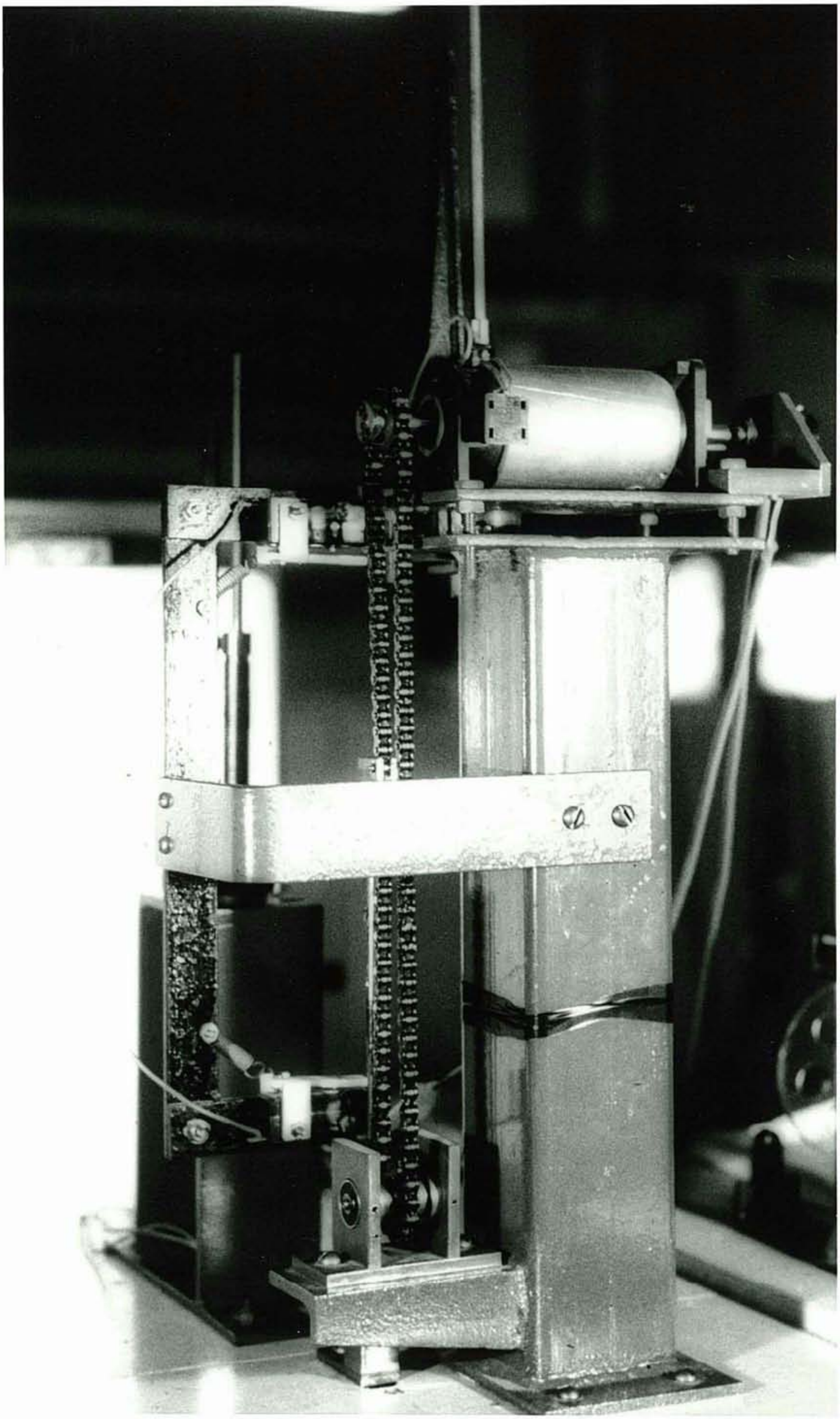

Figure 4.8 Photograph of wave follower drive system.

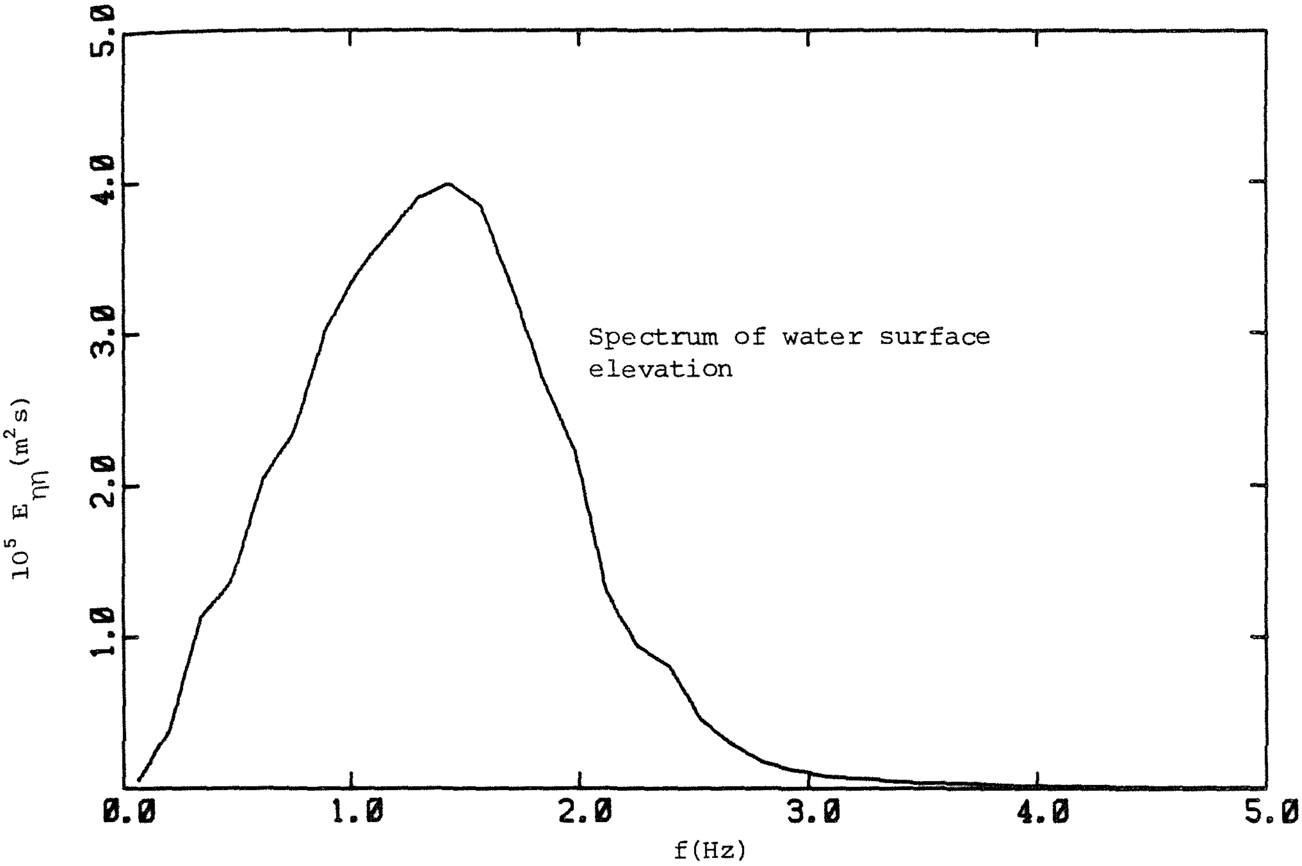

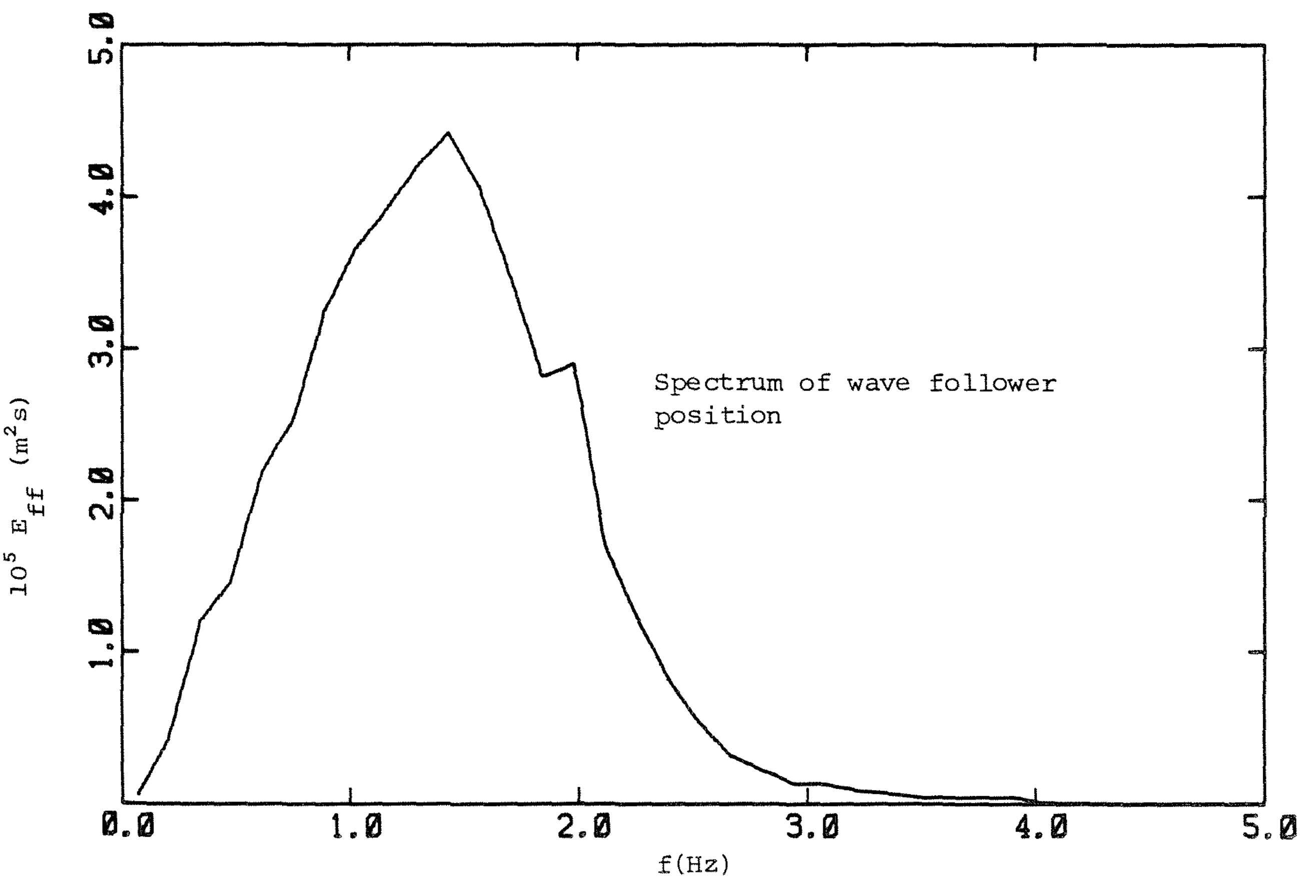

Figure 4.9 A comparison of the spectra of water surface elevation and motion of the wave follower.

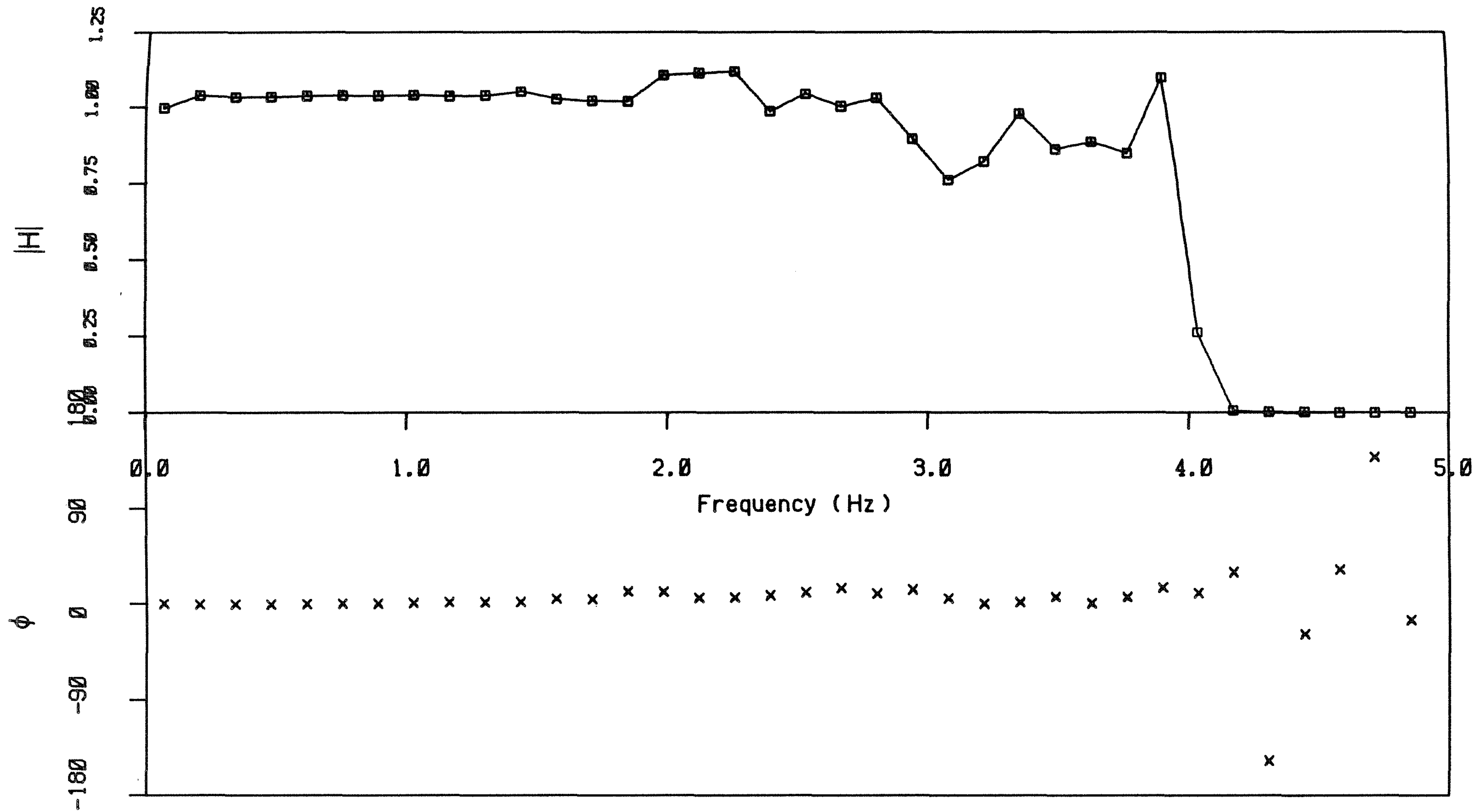

Figure 4.10 Transfer function between the water surface elevation and wave follower position.

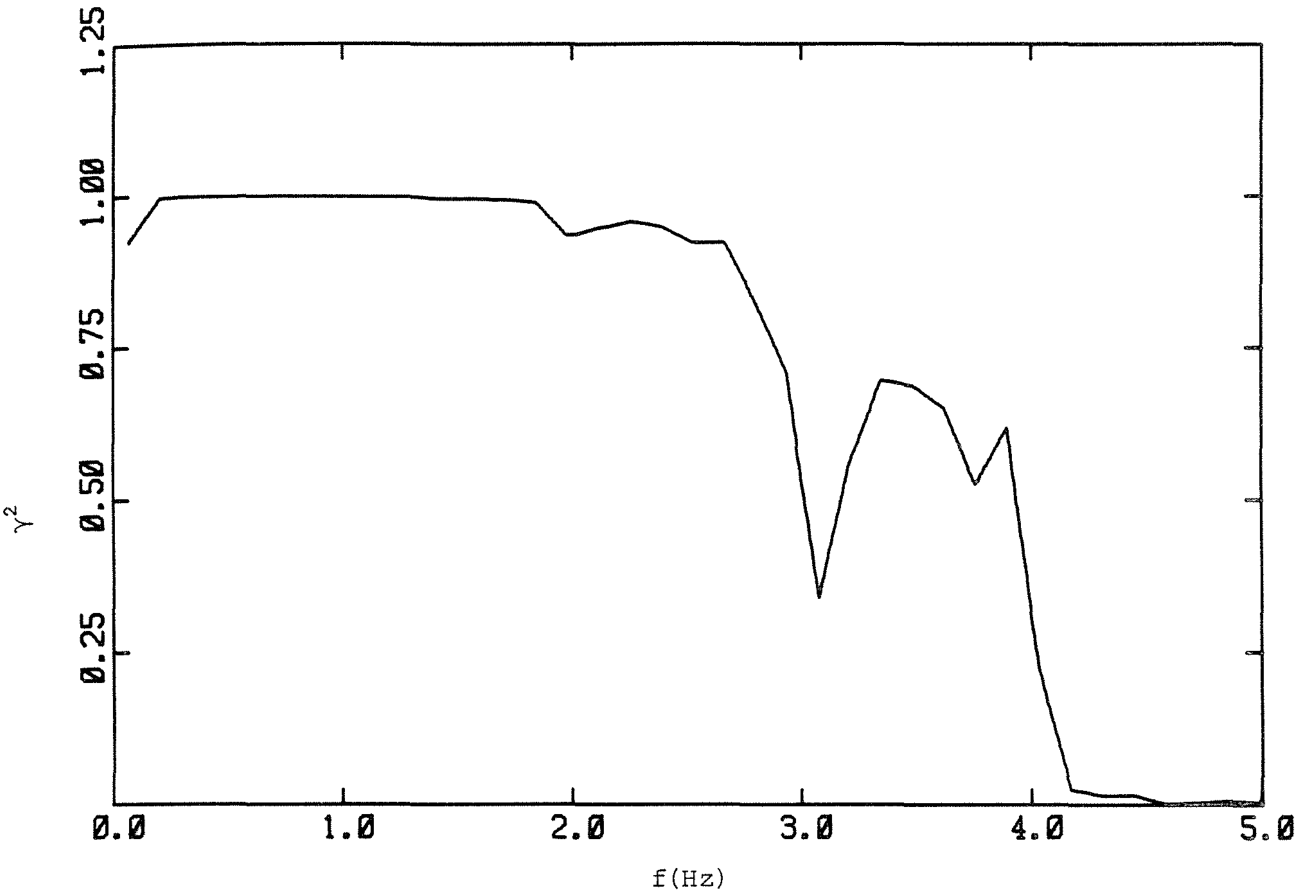

Figure 4.11 Coherence function between water surface elevation and wave follower position.

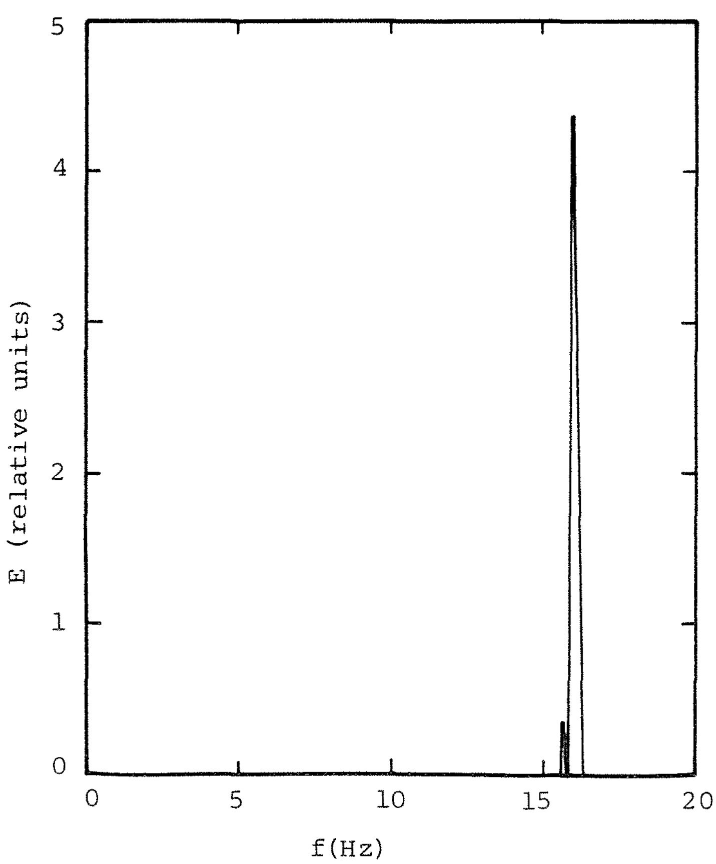

Figure 4.12 Spectrum of wave follower position in still water.

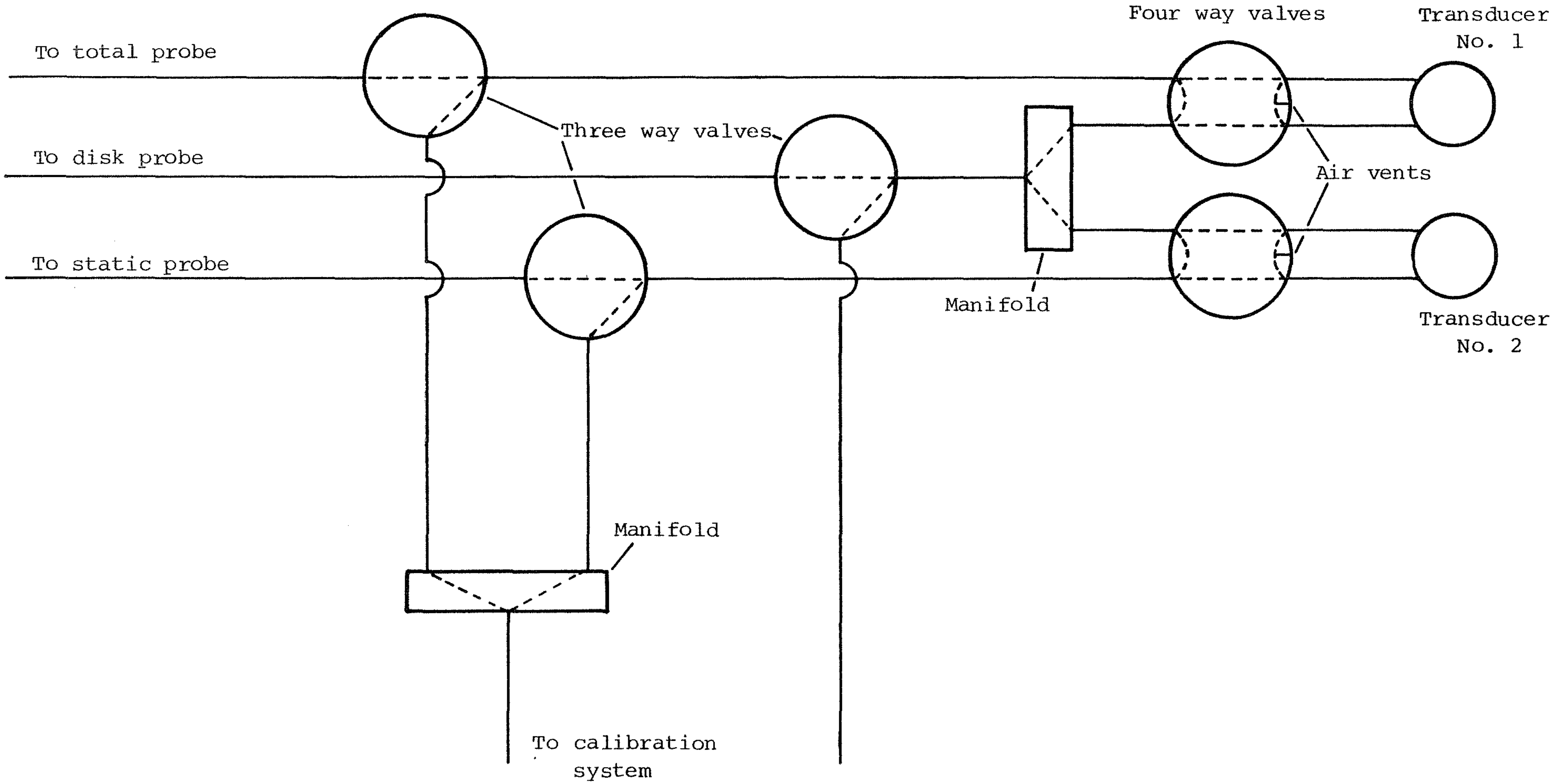

Figure 4.13 Schematic diagram of pressure transducer mounting system.

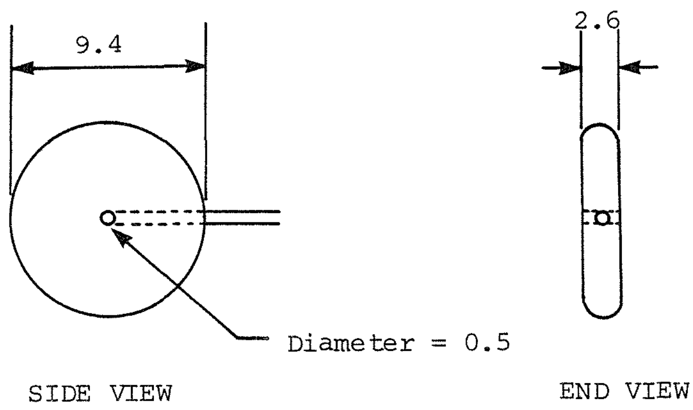

Figure 4.14   Dimensions of disk pressure probe.

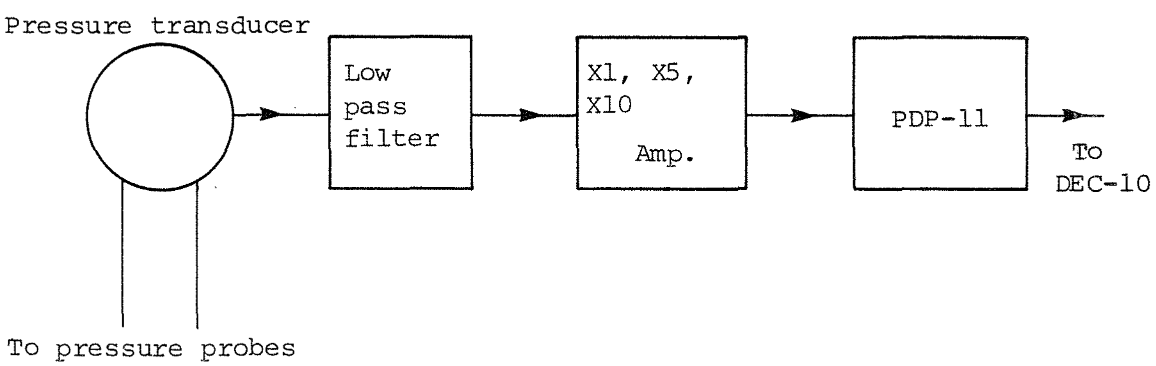

Figure 4.16   Schematic diagram of pressure recording system.

Figure 4.15   Photograph of pressure probes.

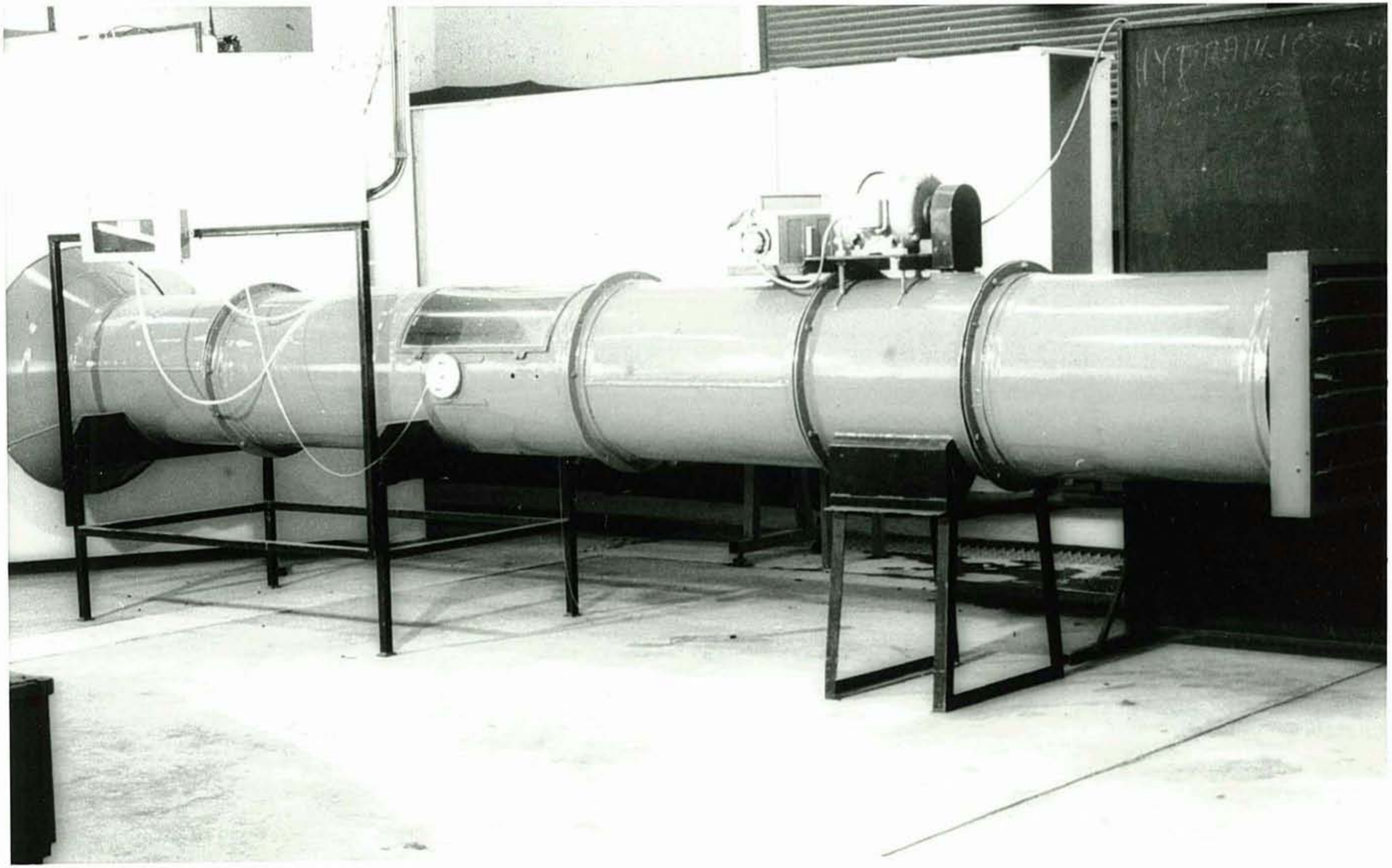

Figure 4.17 Photograph of calibration wind tunnel.

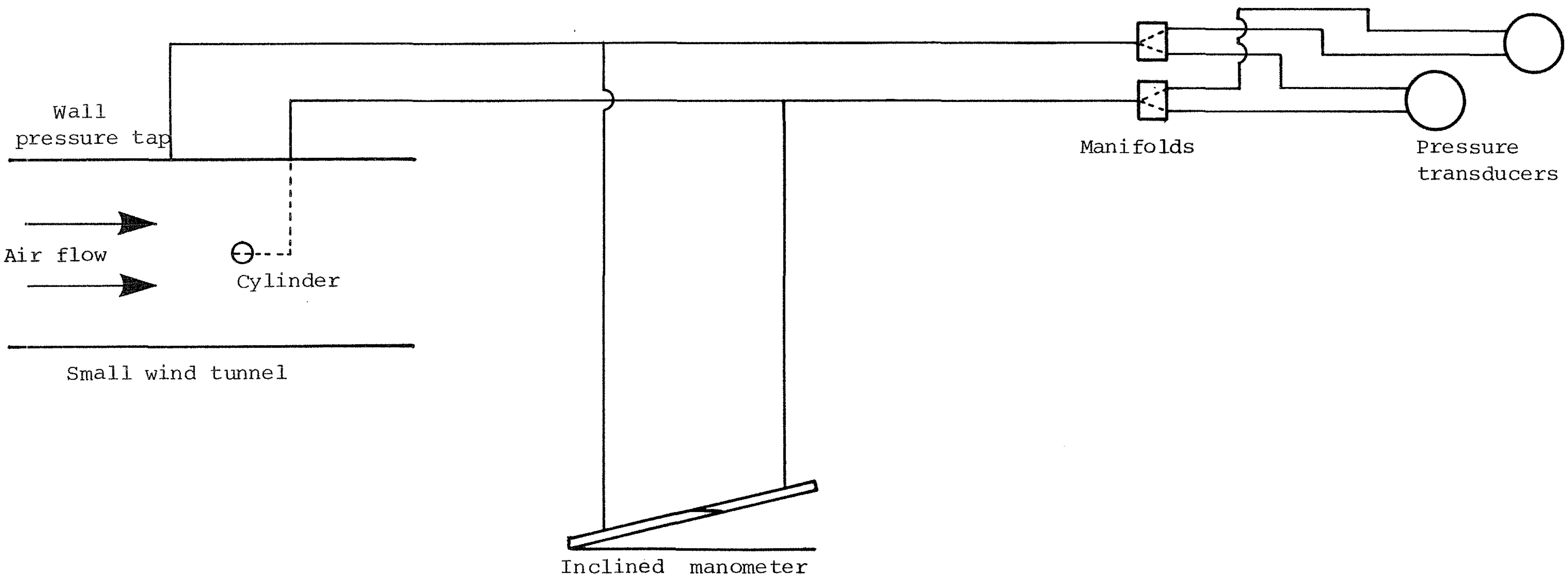

Figure 4.18 Schematic diagram of pressure transducer calibration system.

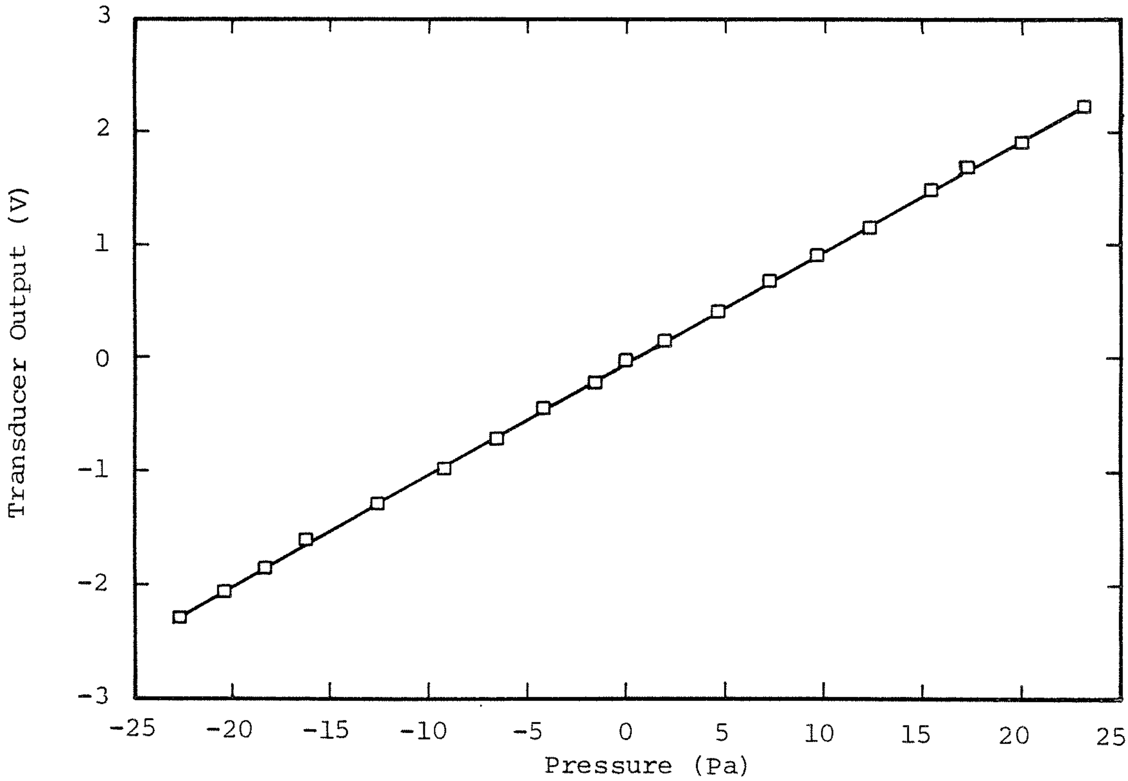

Figure 4.19 Typical pressure transducer calibration curve.

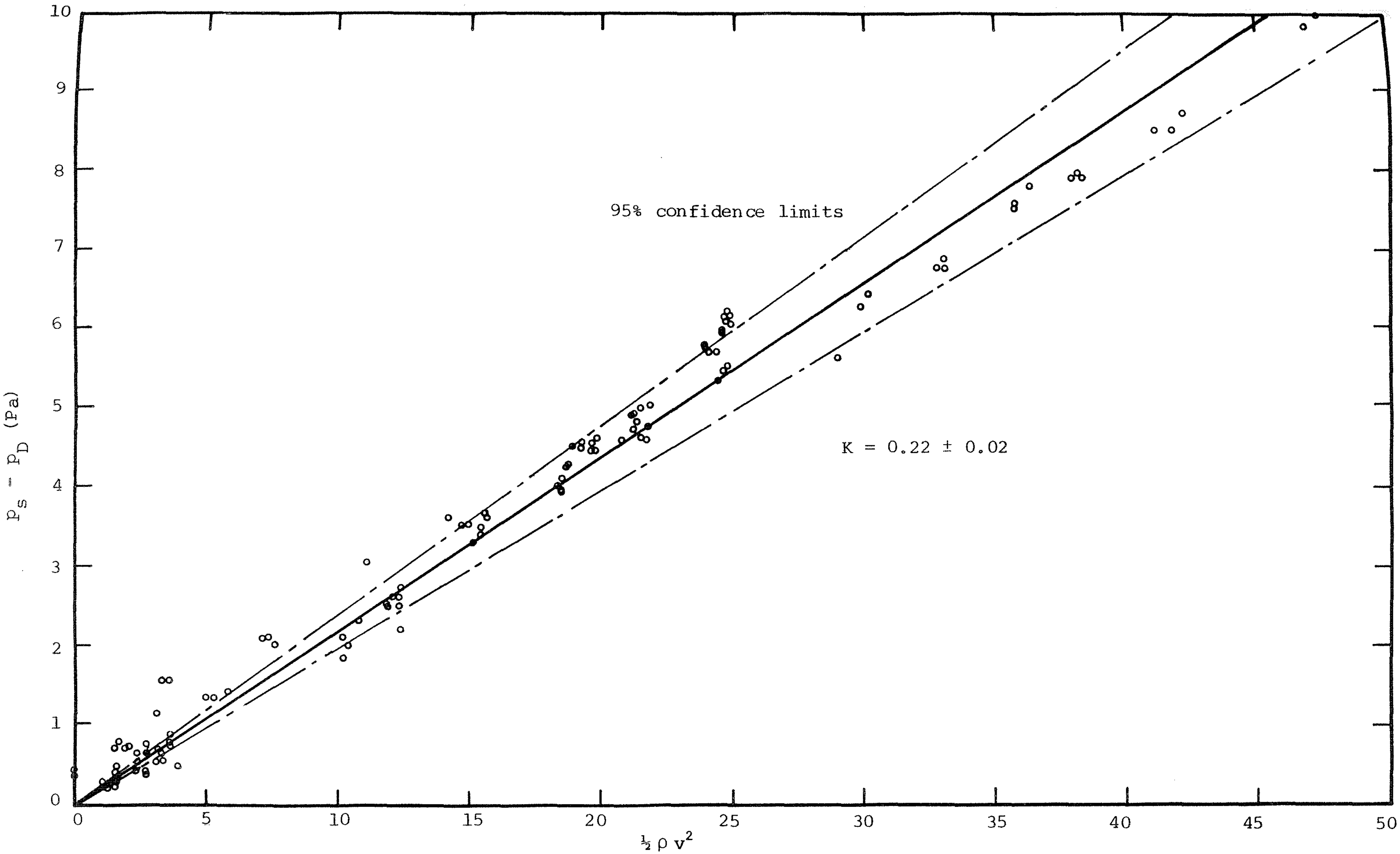

Figure 4.20 Calibration curve for disk pressure probe. $p_s - p_D = K \frac{1}{2}\rho v^2$ (P_a)

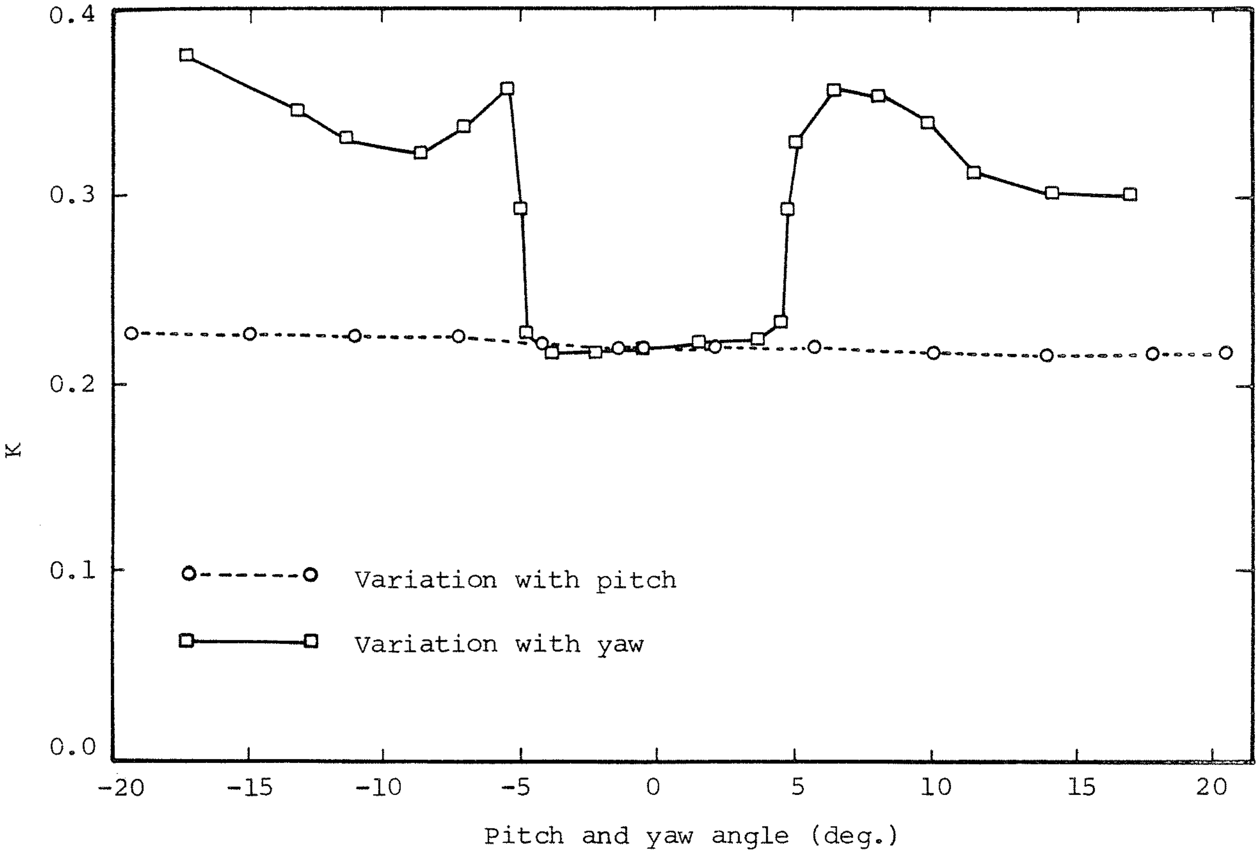

Figure 4.21 Variation in calibration constant K for disk probe with pitch and yaw.

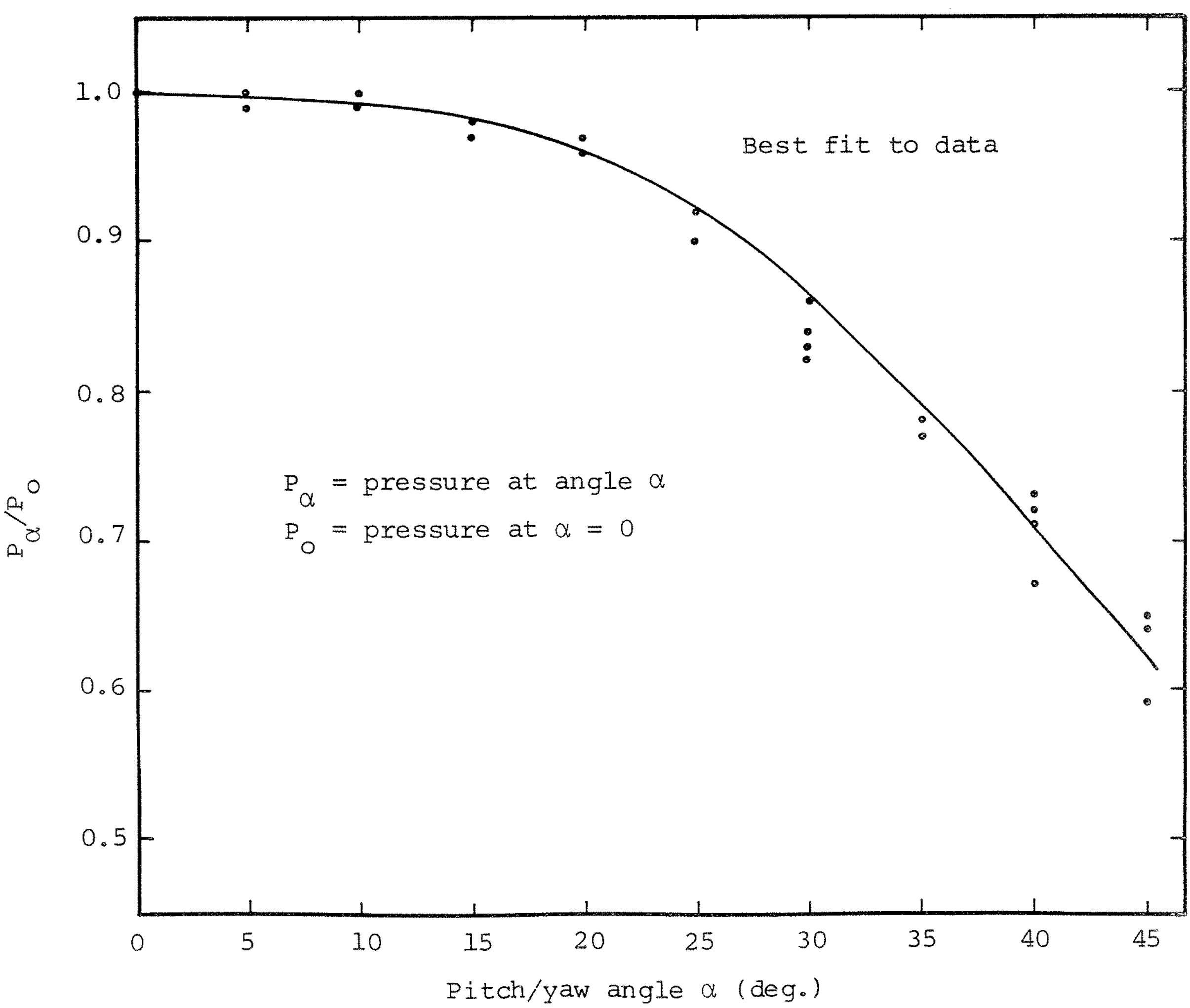

Figure 4.22 Response of total head probe to pitch or yaw

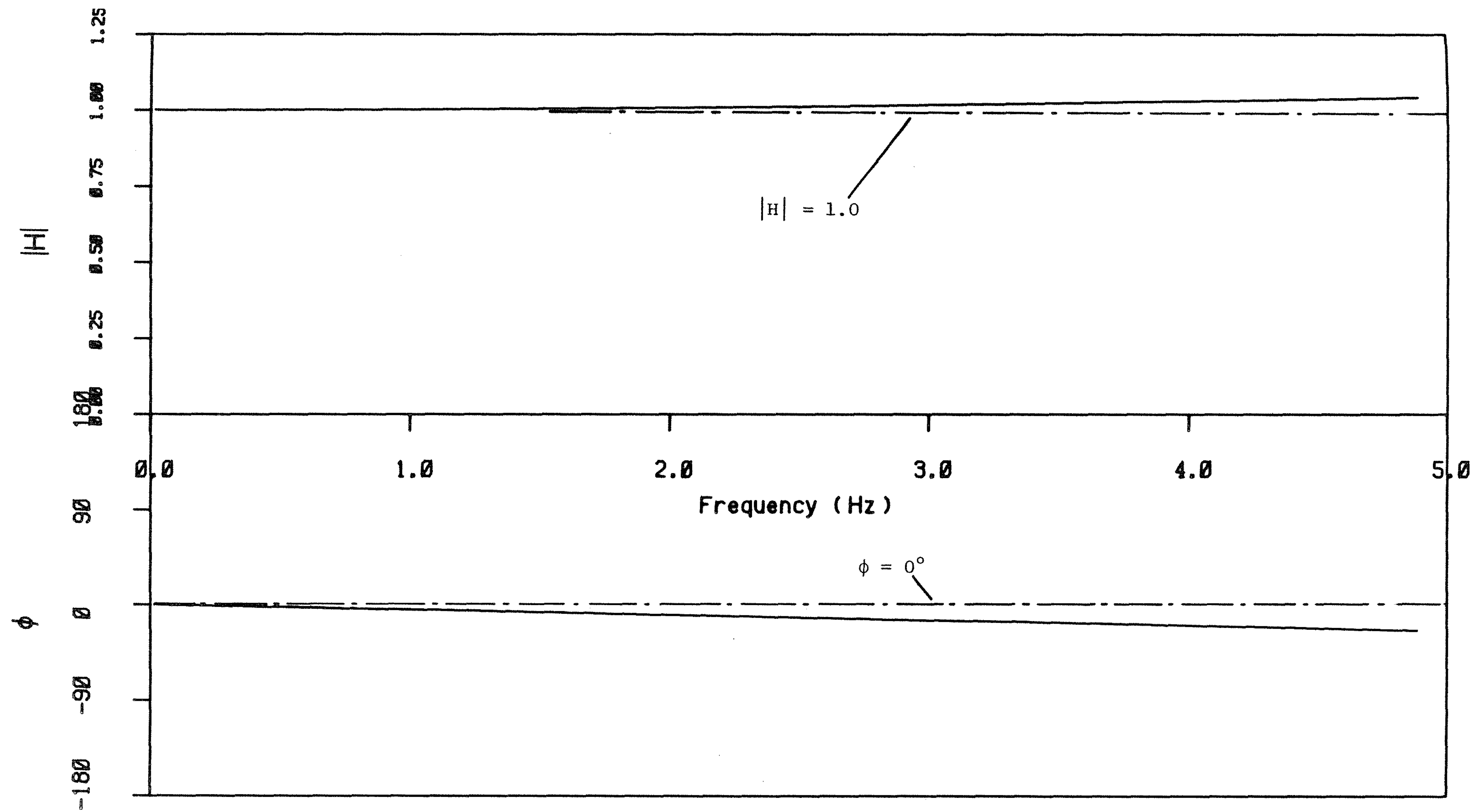

Figure 4.23a Theoretical pressure tube transfer function at low frequencies.

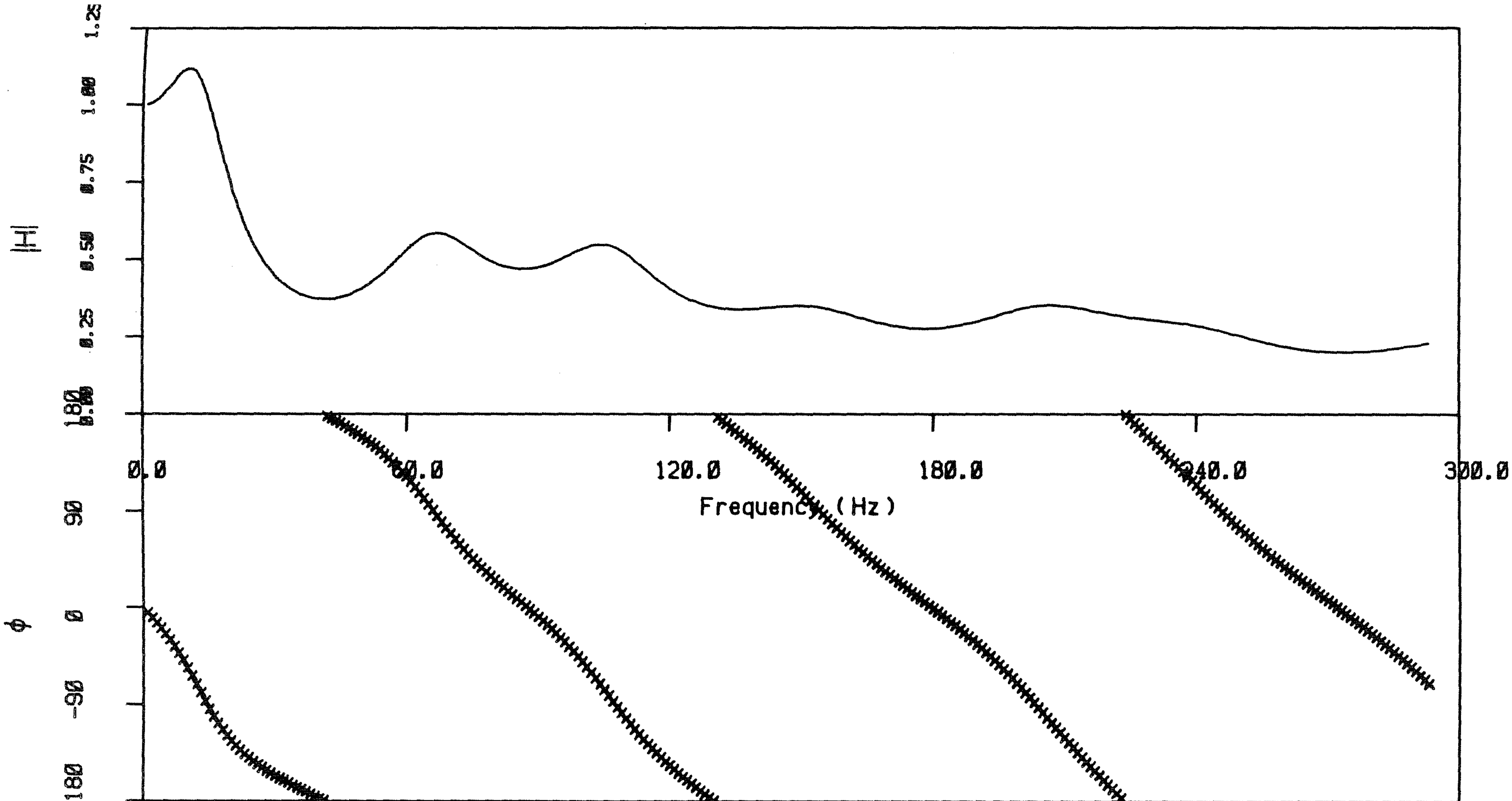

Figure 4.23b Theoretical pressure tube transfer function at high frequencies.

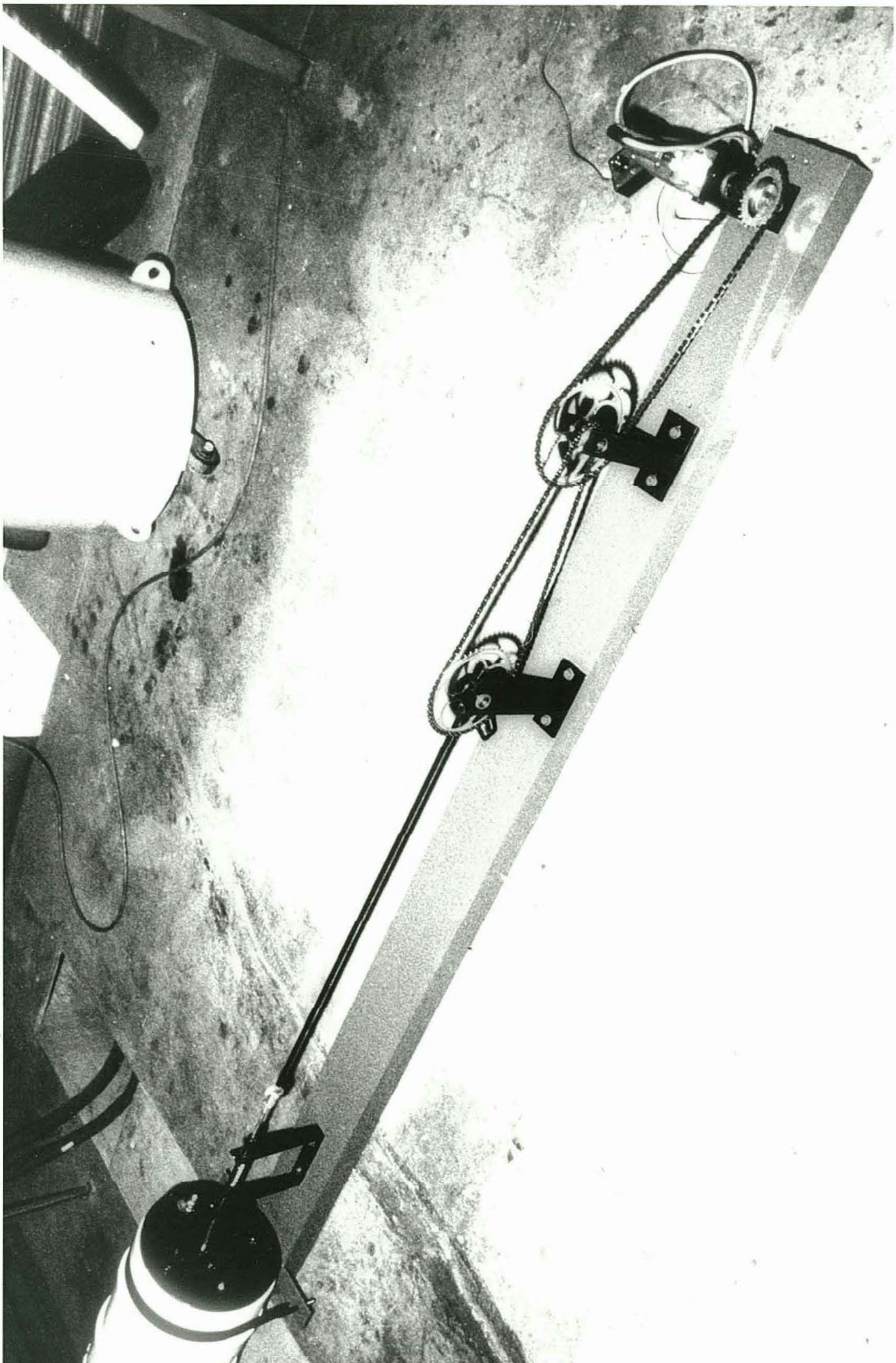

Figure 4.24 Photograph of dynamic pressure generating system.

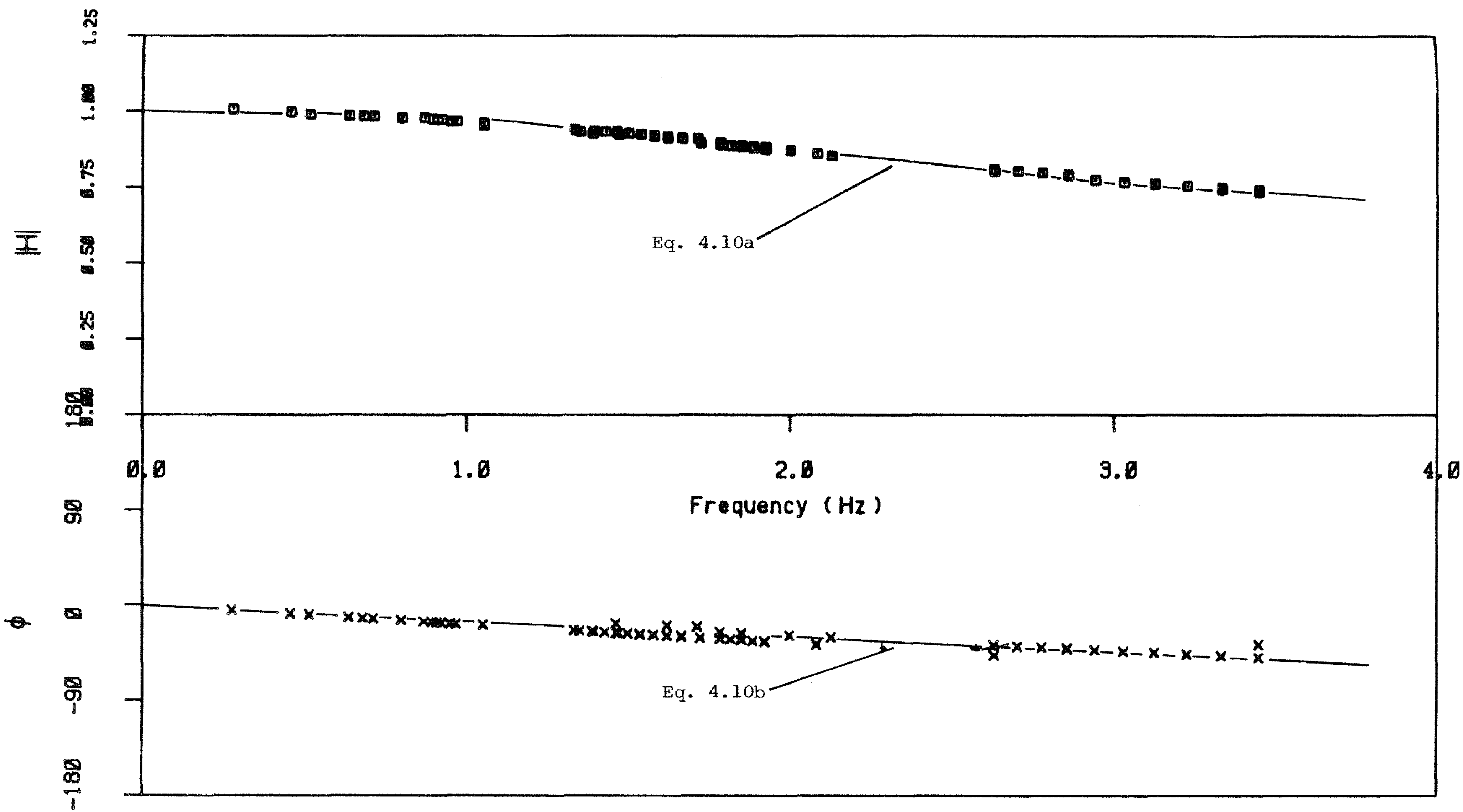

Figure 4.25a Transfer function for pressure tube connecting the disk probe to pressure transducer No. 1.

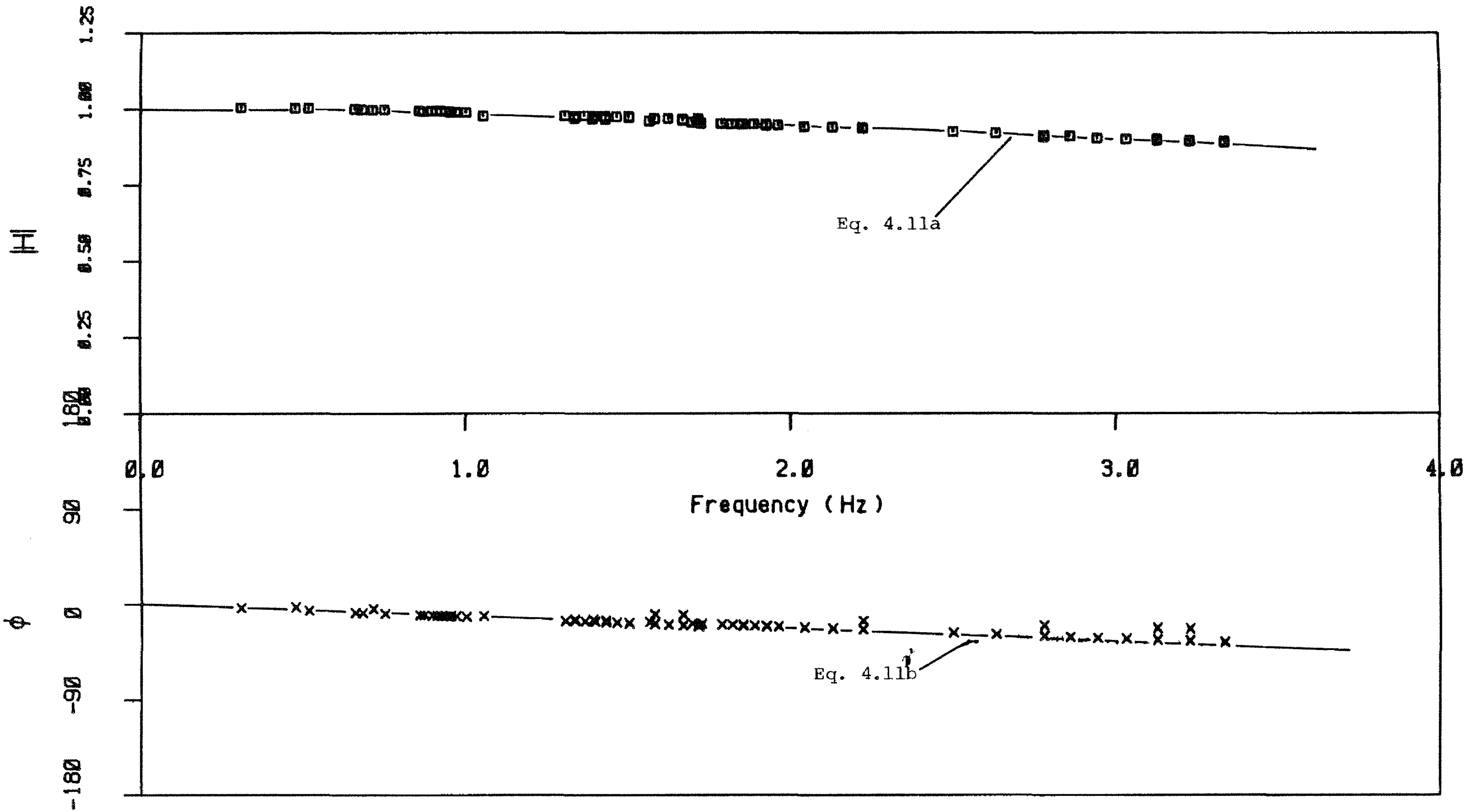

Figure 4.25b Transfer function for pressure tube connecting the total head probe to pressure transducer No. 1.

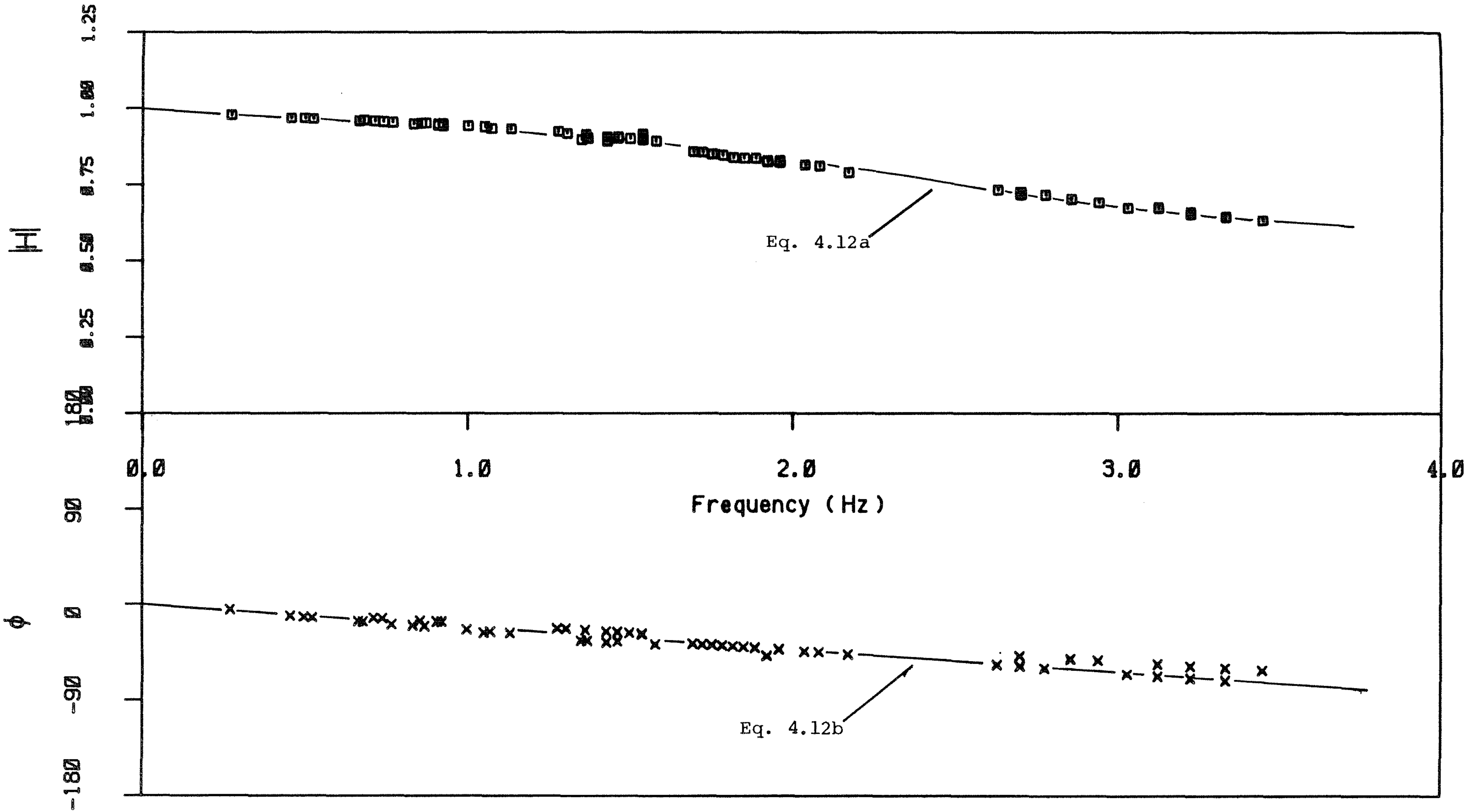

Figure 4.25c Transfer function for pressure tube connecting the disk probe to pressure transducer No. 2.

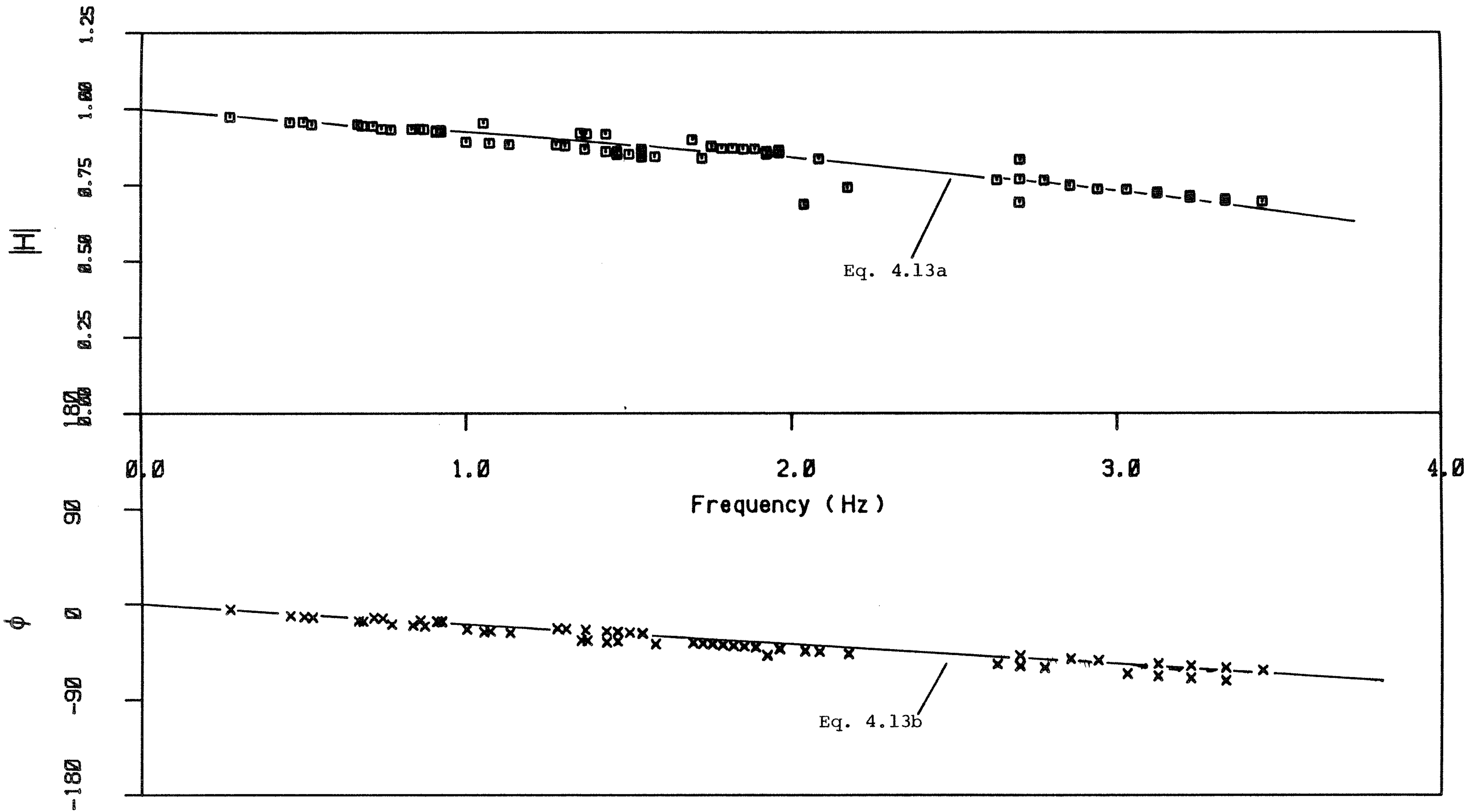

Figure 4.25d Transfer function for pressure tube connecting the static probe to pressure transducer No. 2.

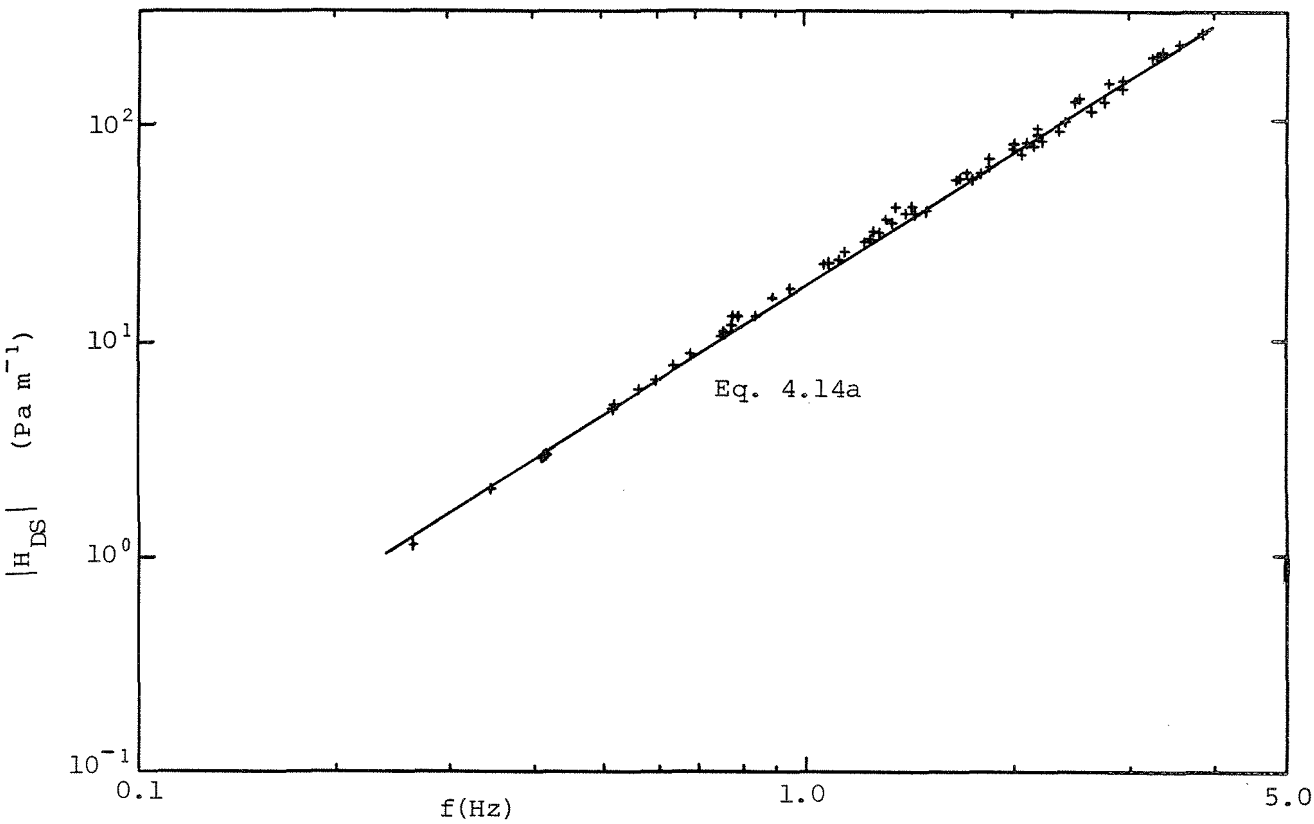

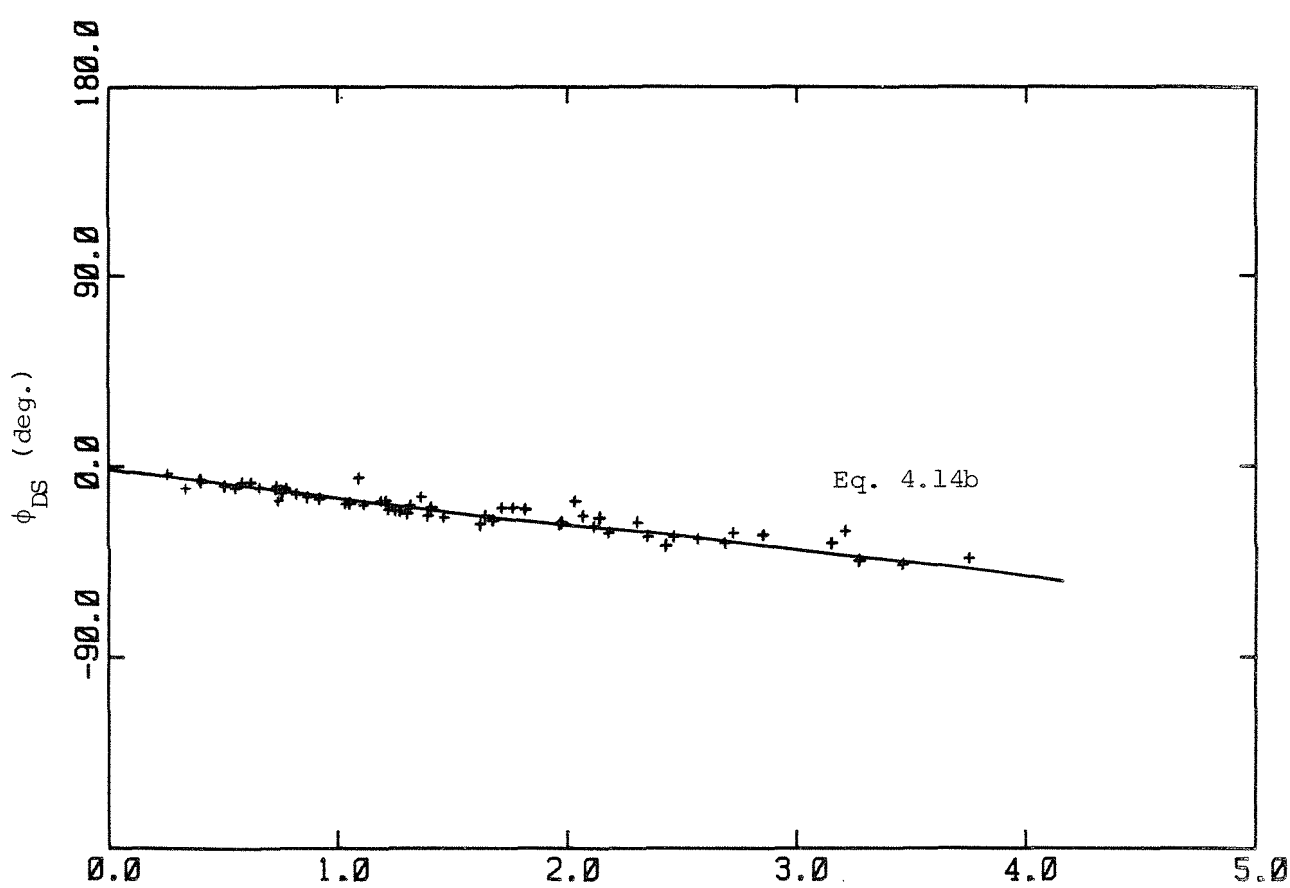

Figure 4.26a Transfer function between wave follower motion and induced pressure for the disk-static system.

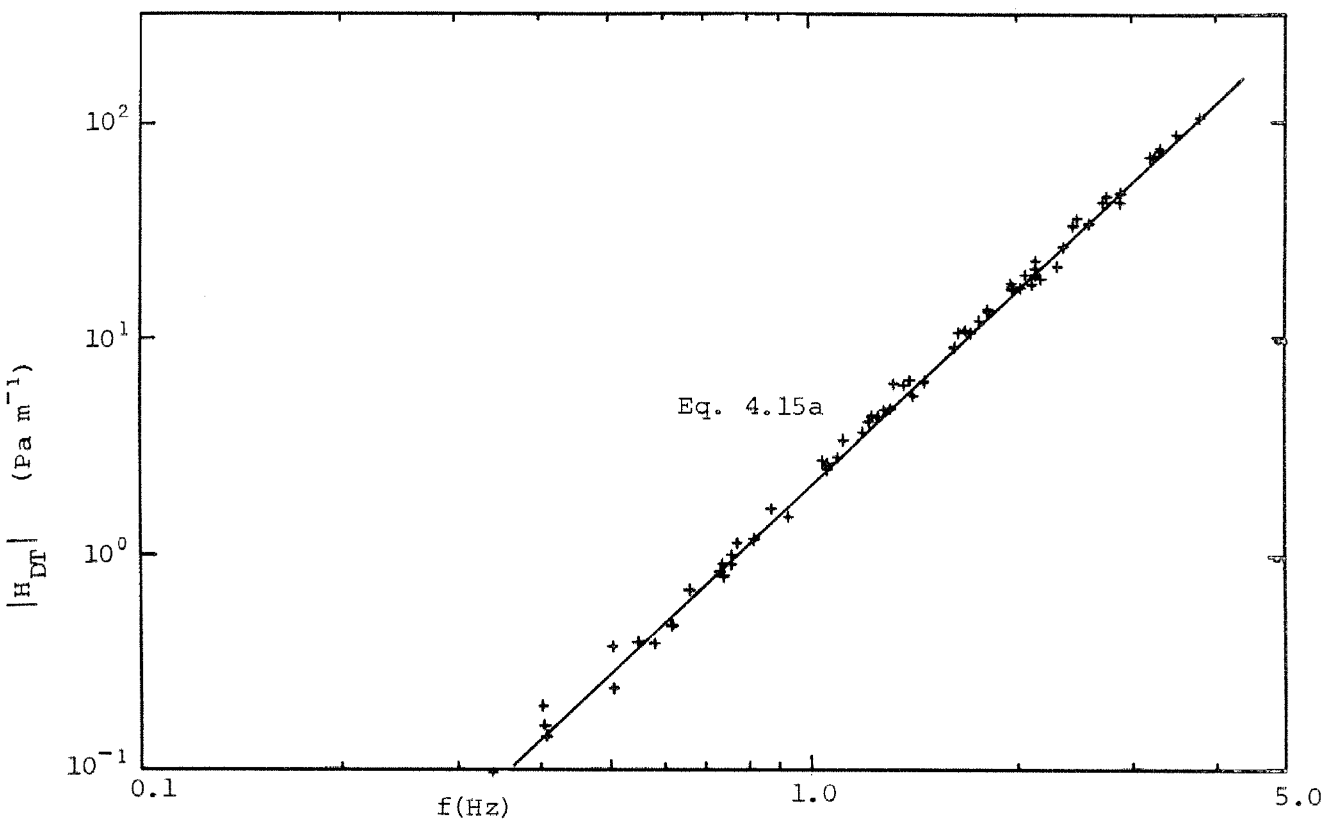

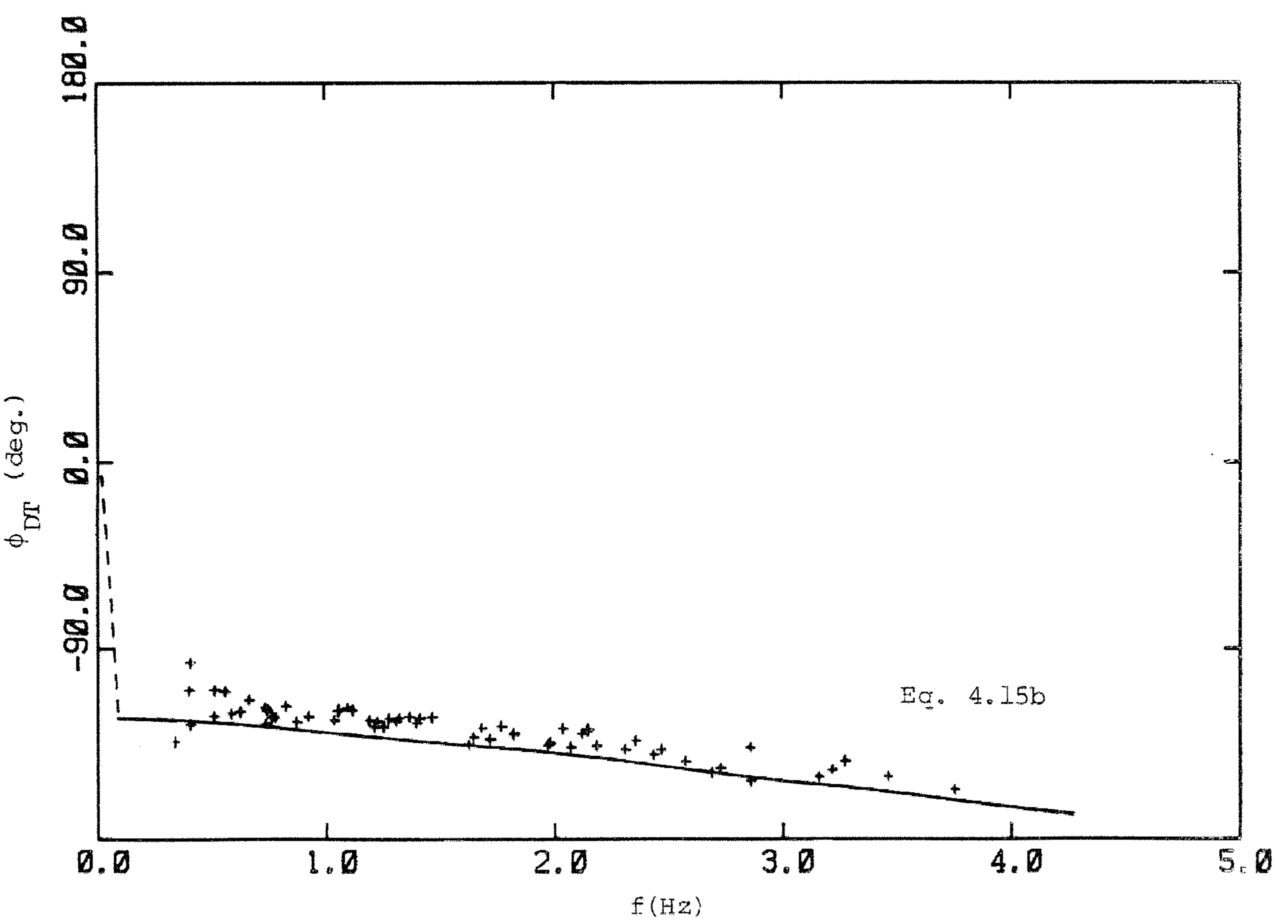

Figure 4.26b Transfer function between wave follower motion and induced pressure for the disk-total system.

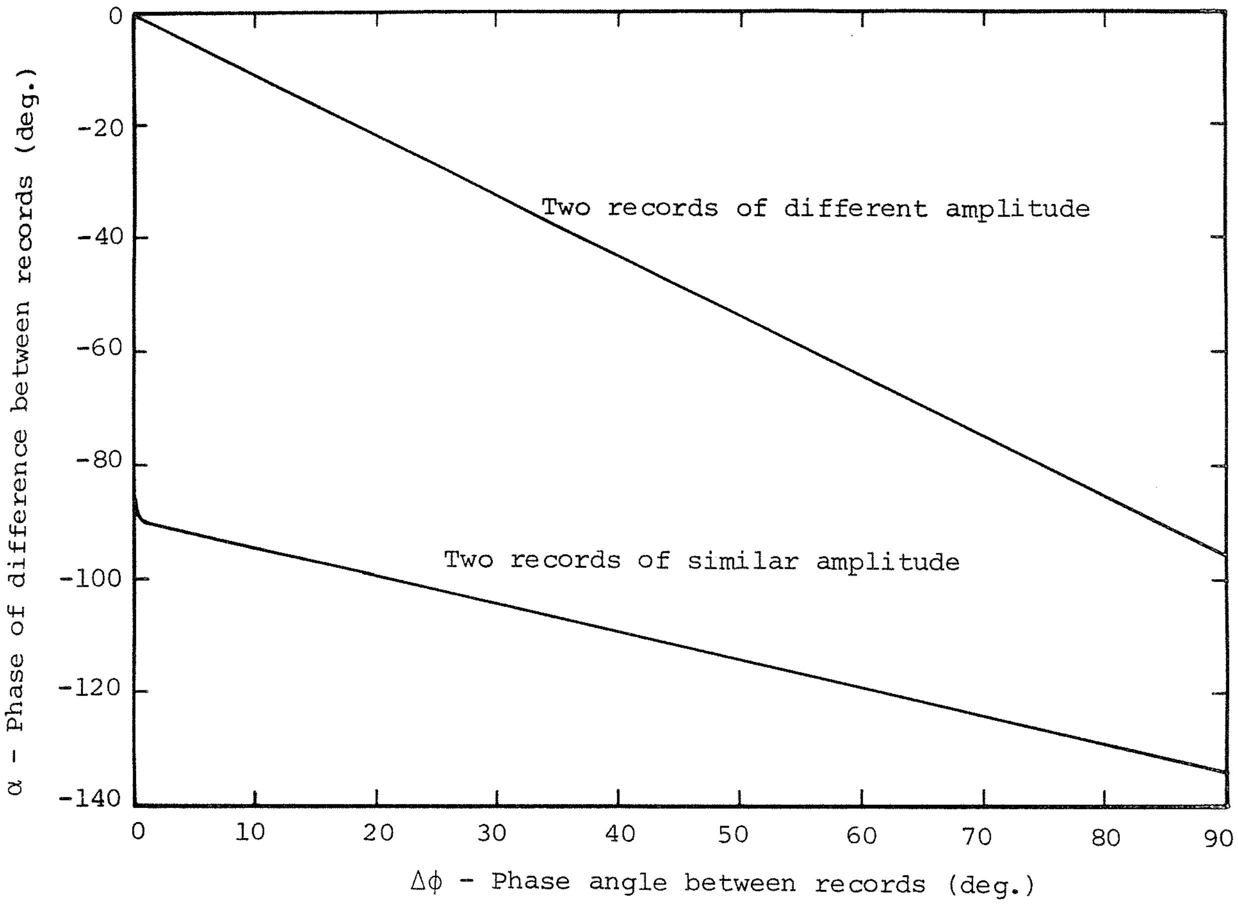

Figure 4.27 The resultant phase when two sinusoidal signals are subtracted.

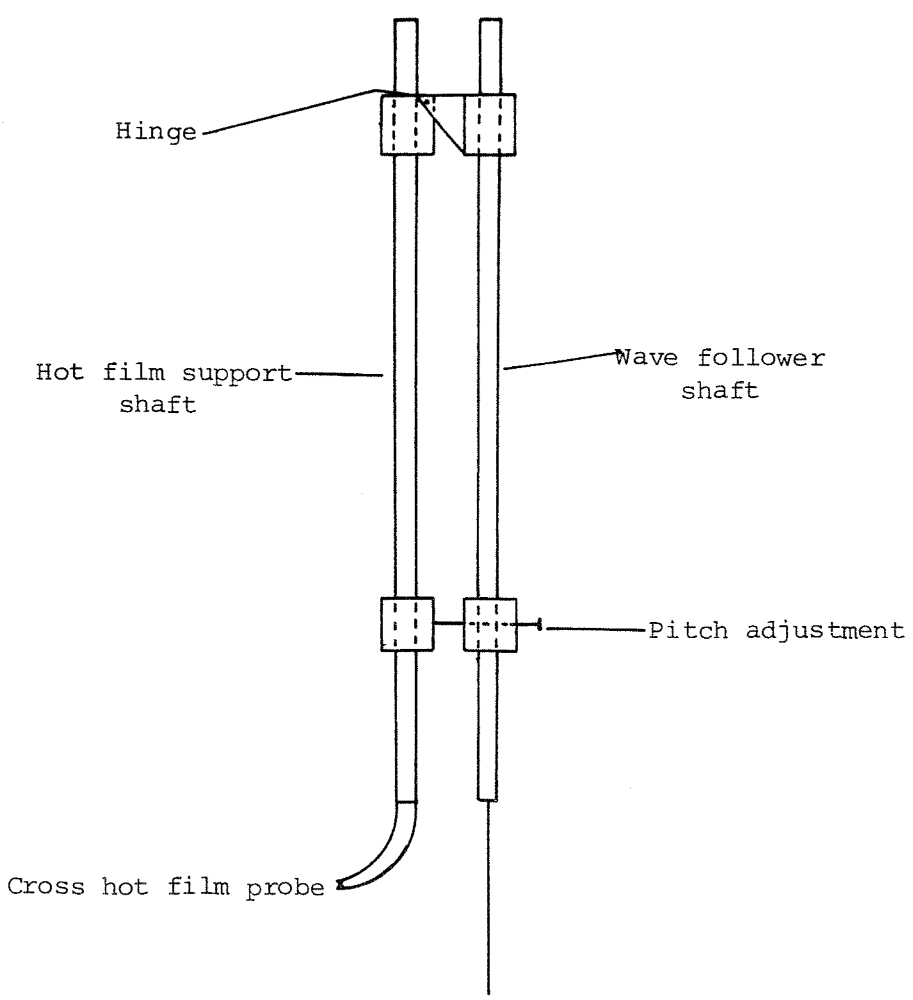

Figure 4.29 Mounting and adjustment system for hot film probe.

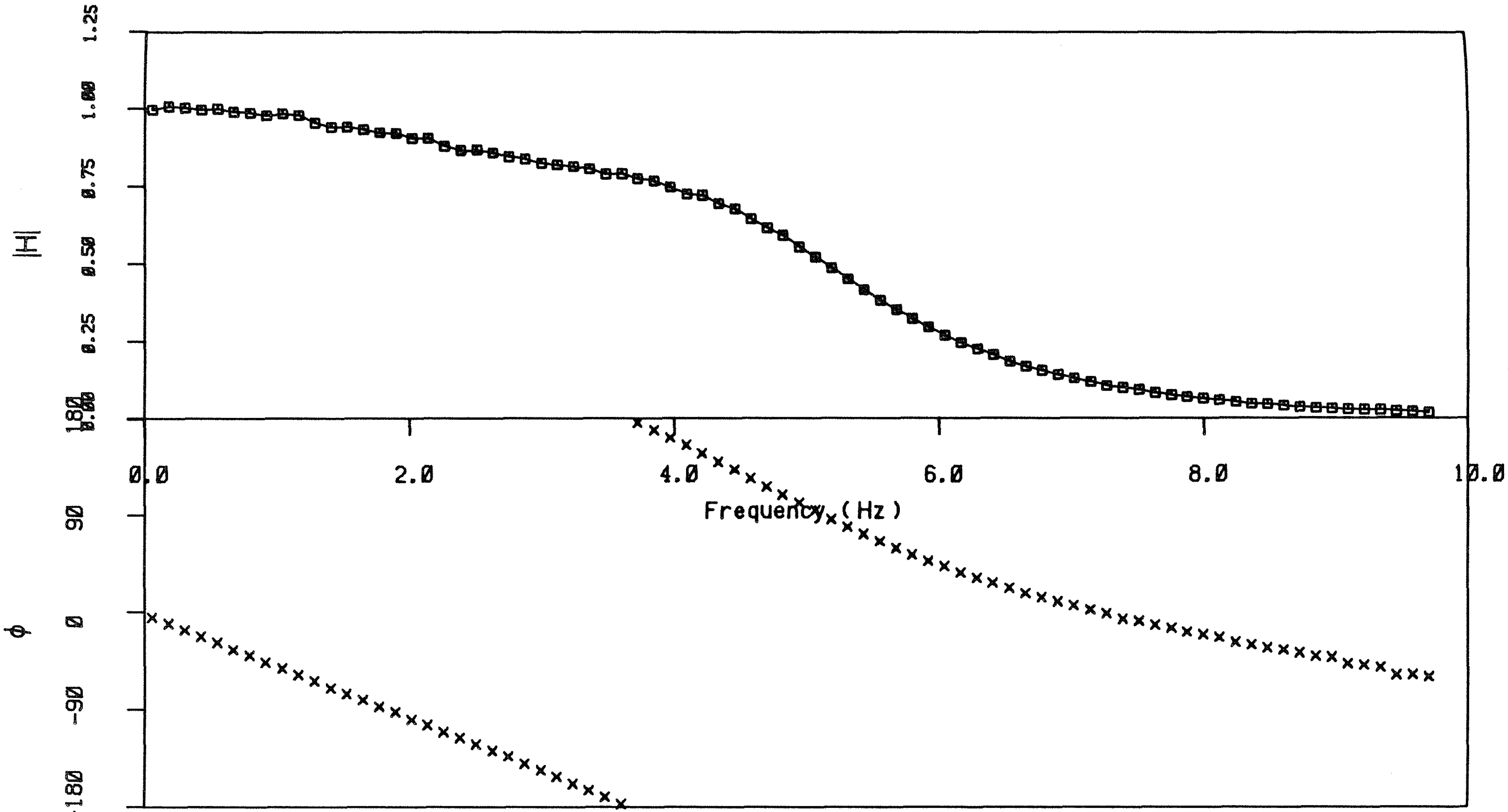

Figure 4.28a Transfer function for 5 Hz low pass analog filter No. 1.

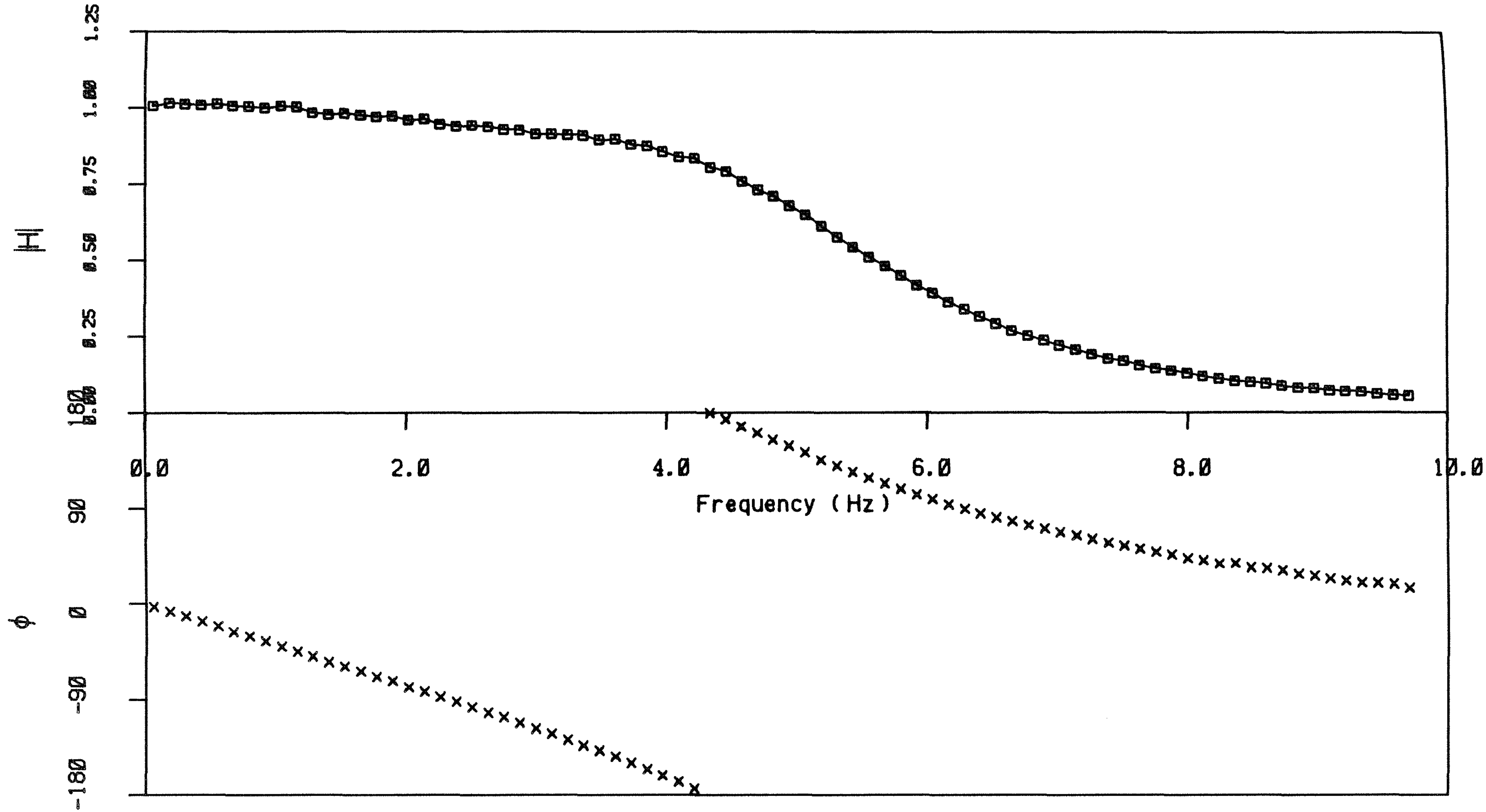

Figure 4.28b Transfer function for 5 Hz low pass analog filter No. 2.

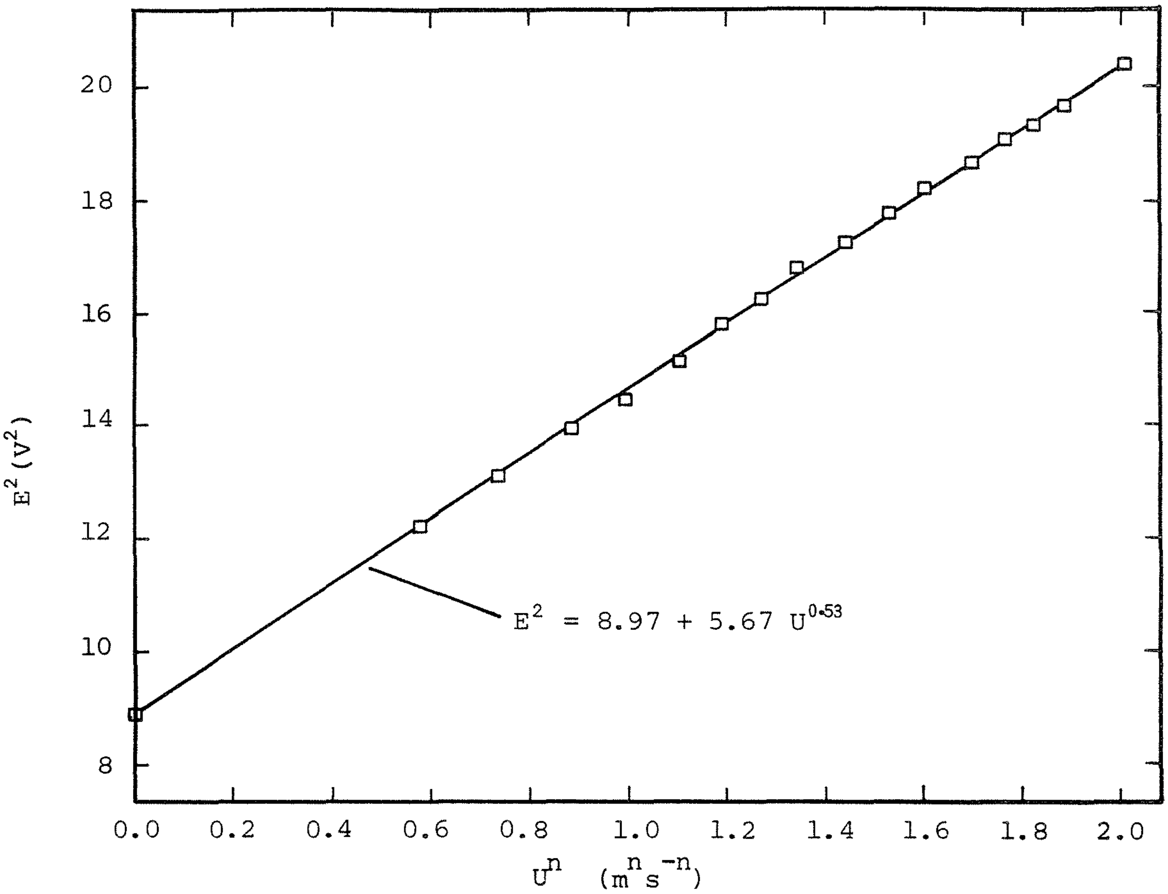

Figure 4.30 Typical hot film calibration curve.

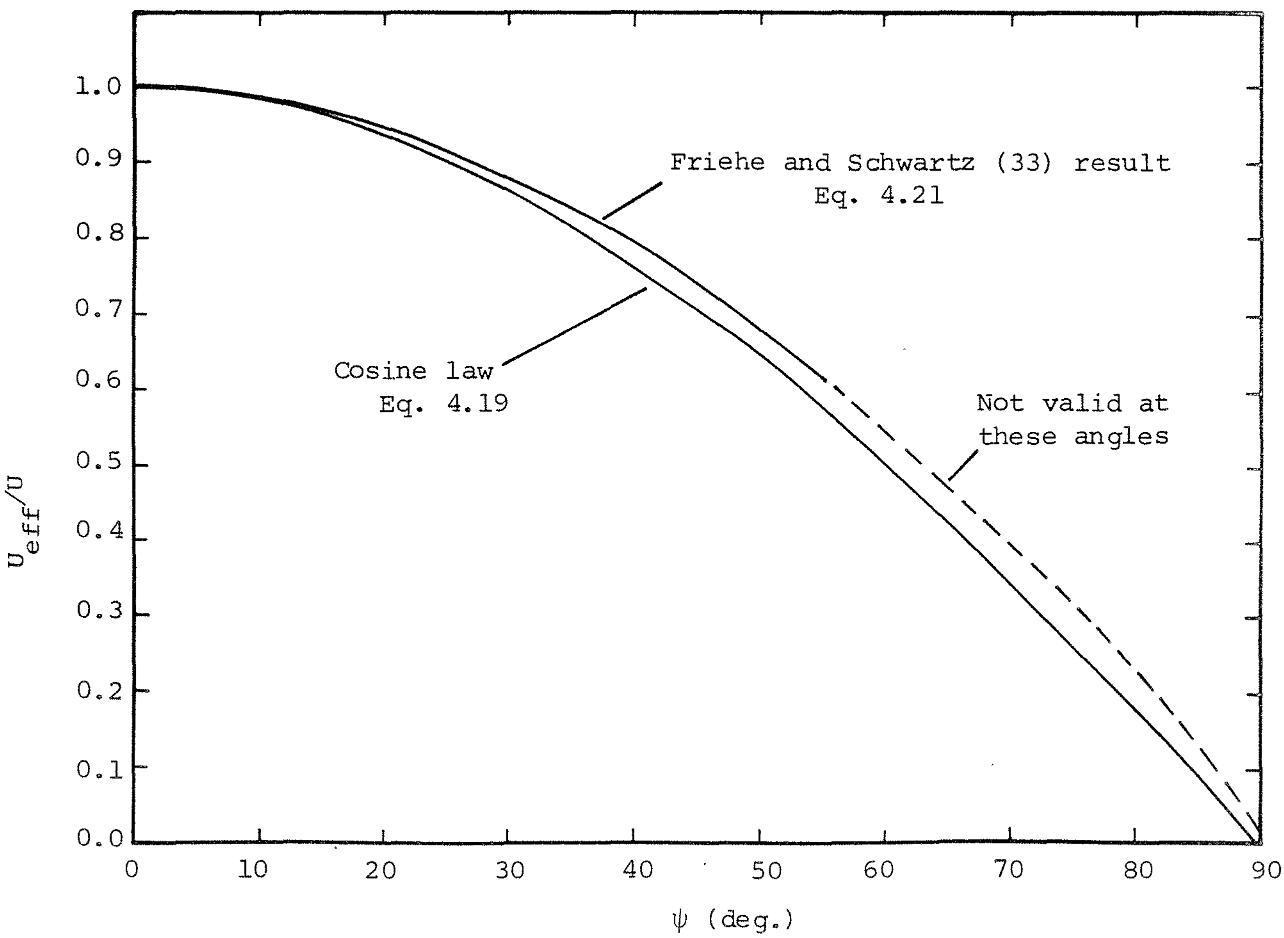

Figure 4.31 Anemometer cooling laws for the probe at an angle ψ to the fluid flow.

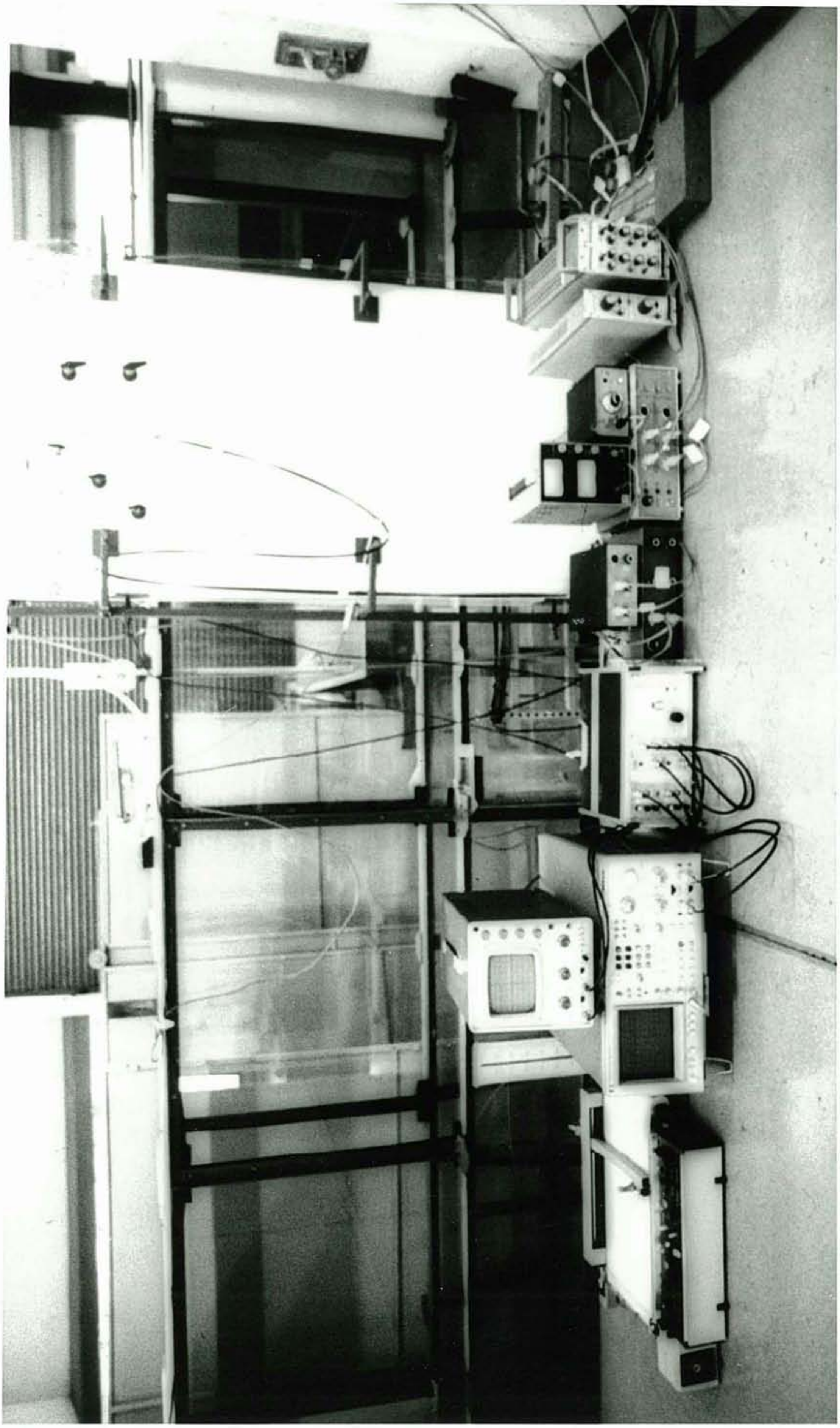

Figure 4.32 Photograph of wave flume instrumentation.

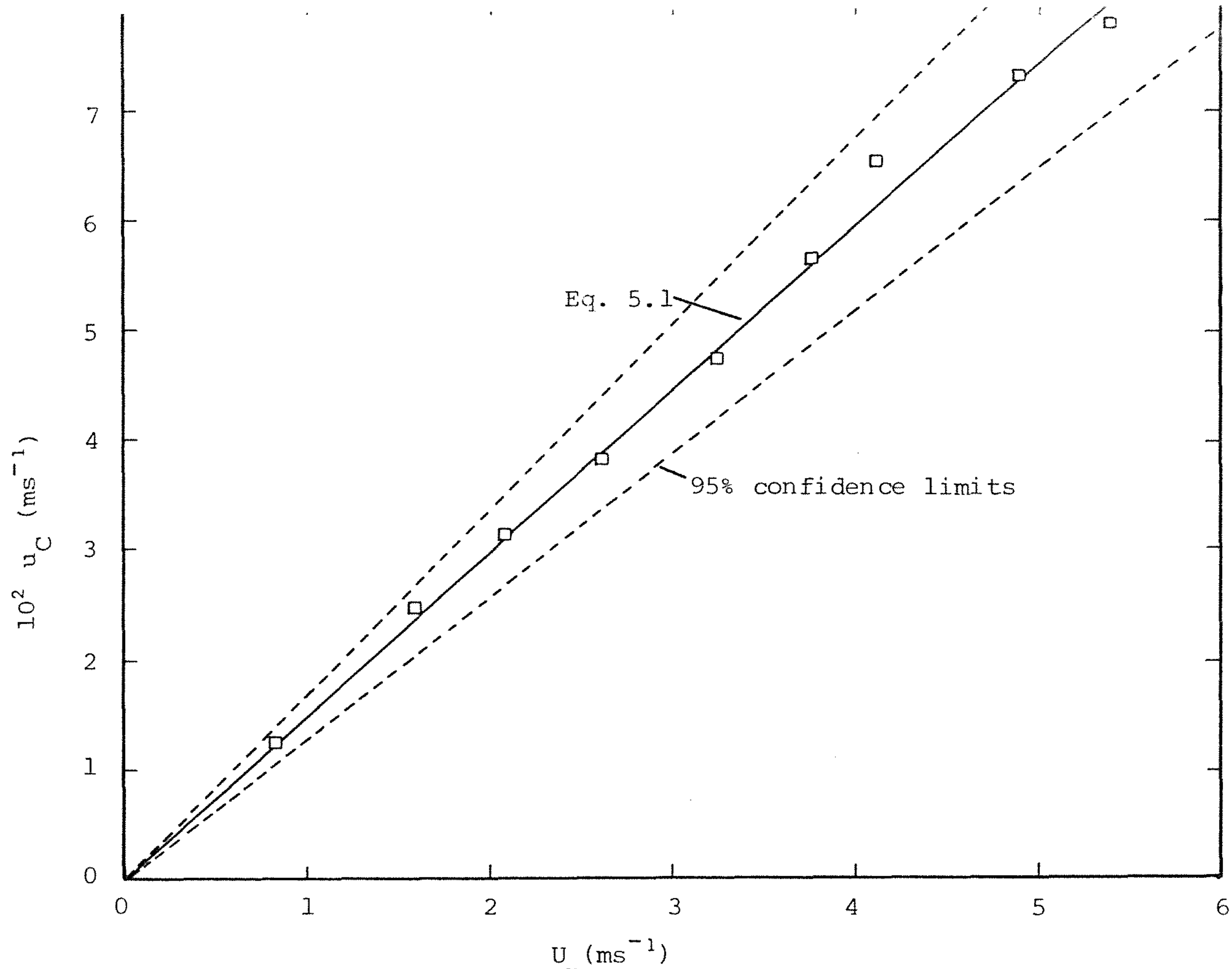

Figure 5.1 Surface drift current as a function of free stream wind velocity.

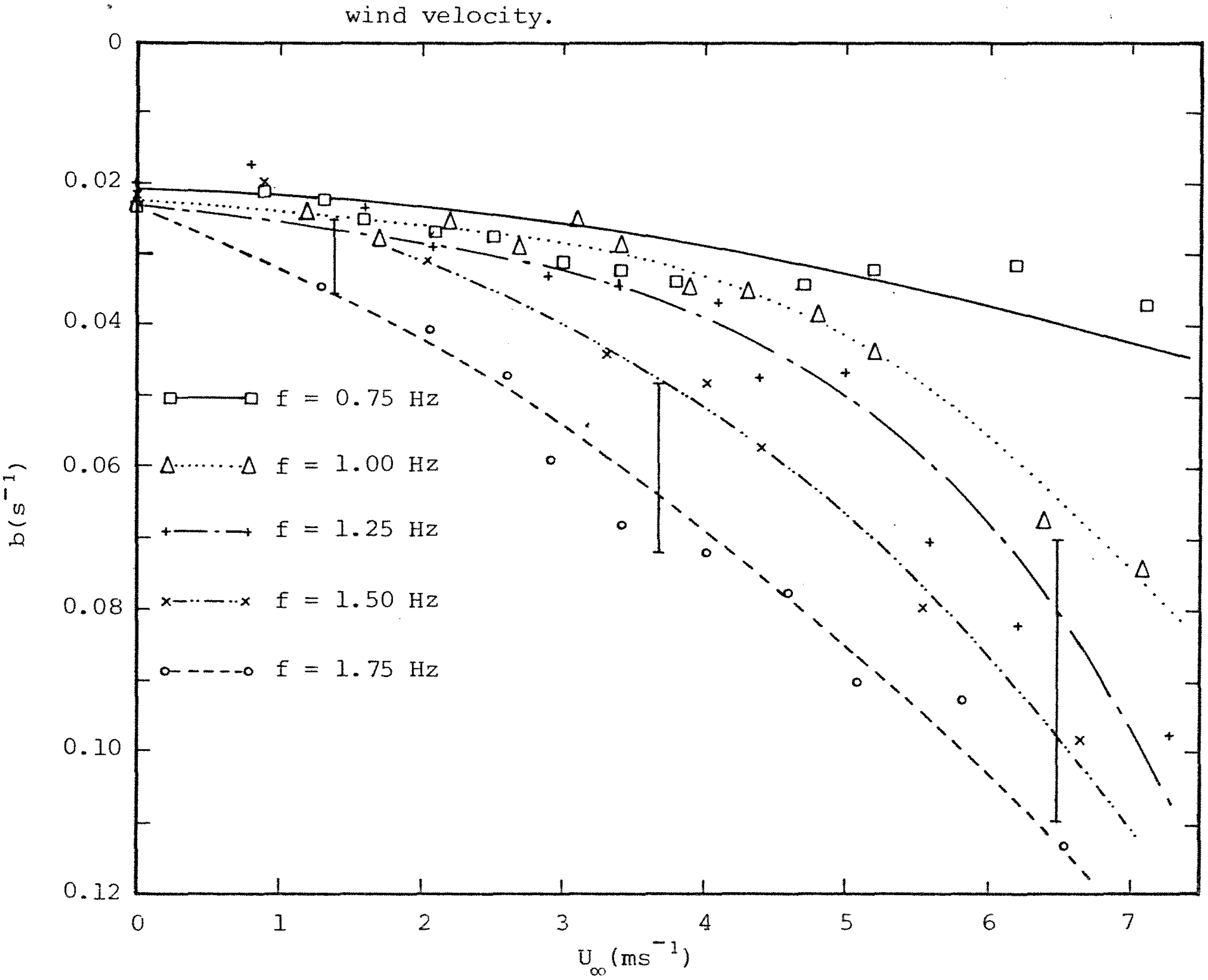

Figure 6.1 Spatial wave decay along the flume for various frequency waves as a function of free stream wind velocity. Error bars represent 95% confidence limits on b.

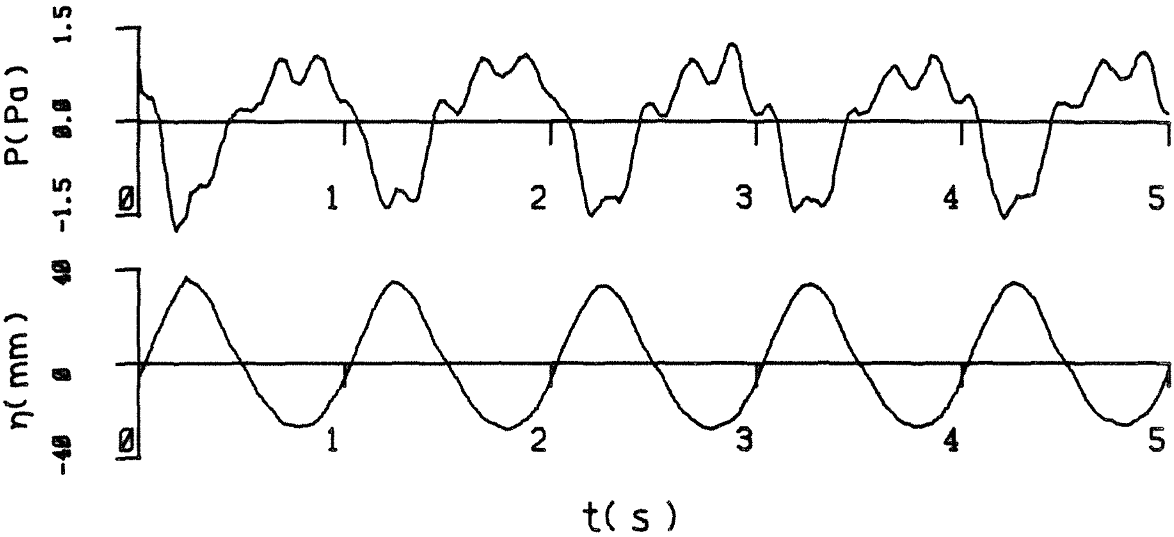

Fan speed = 170 rpm

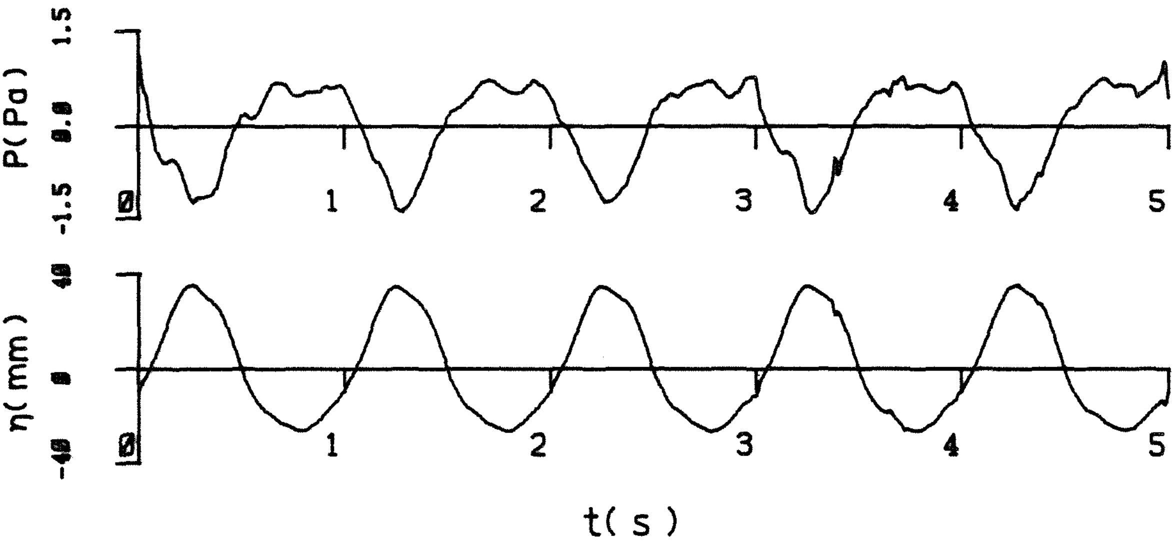

Fan speed = 140 rpm

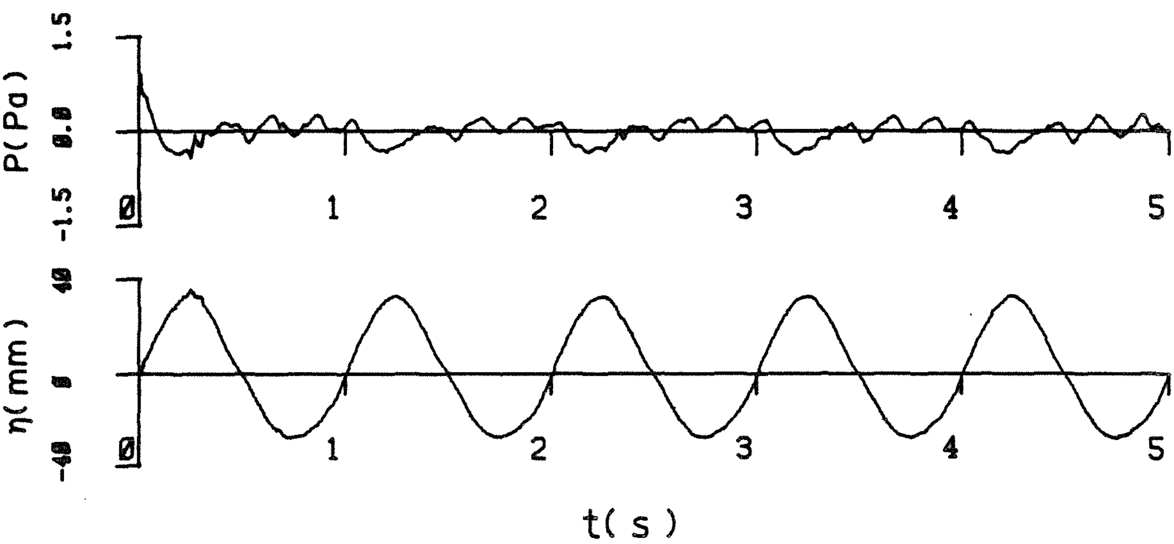

Fan speed = 0 rpm

Figure 7.1a Water surface elevation and wave induced pressure records for various wind speeds.

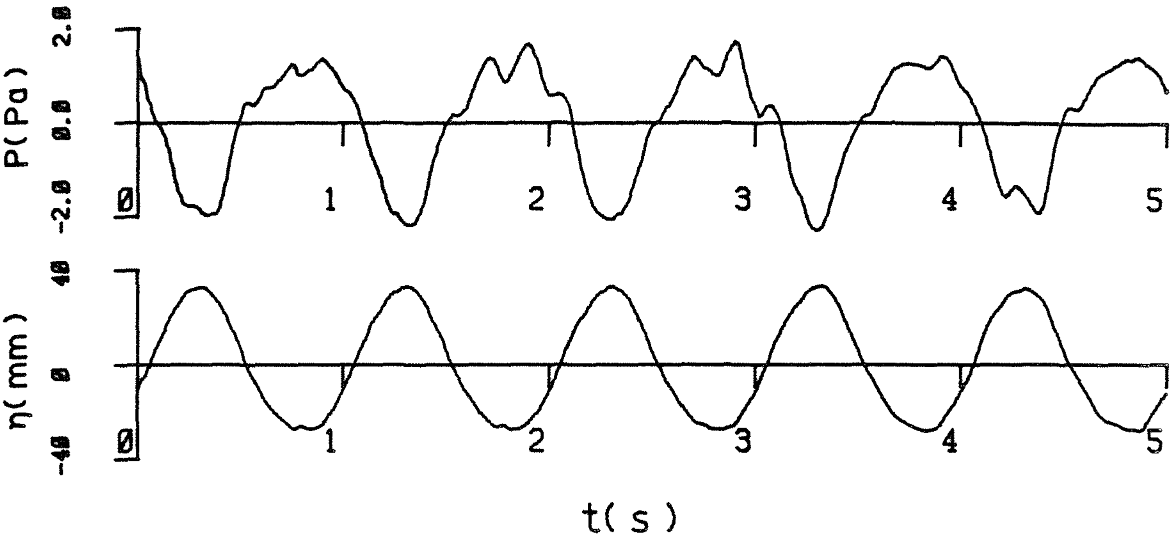

Fan speed = 230 rpm

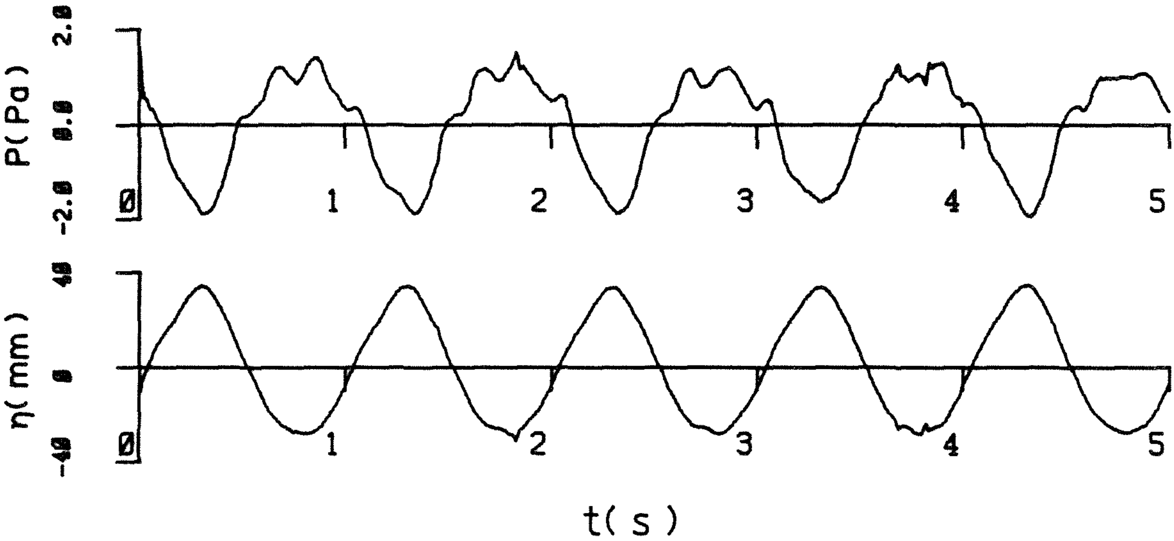

Fan speed = 205 rpm

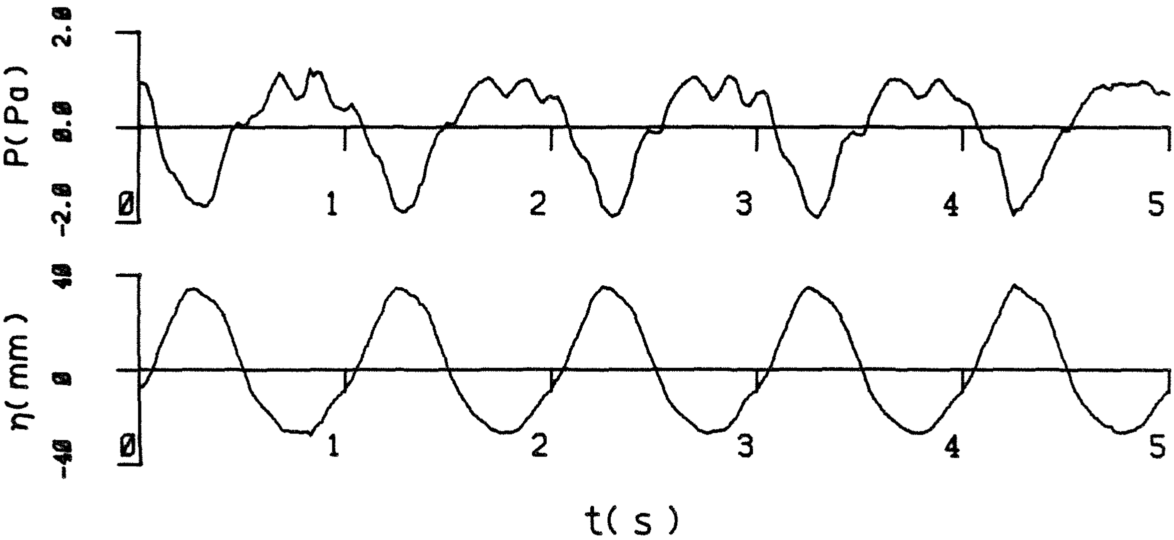

Fan speed = 185 rpm

Figure 7.1b Water surface elevation and wave induced pressure records for various wind speeds.

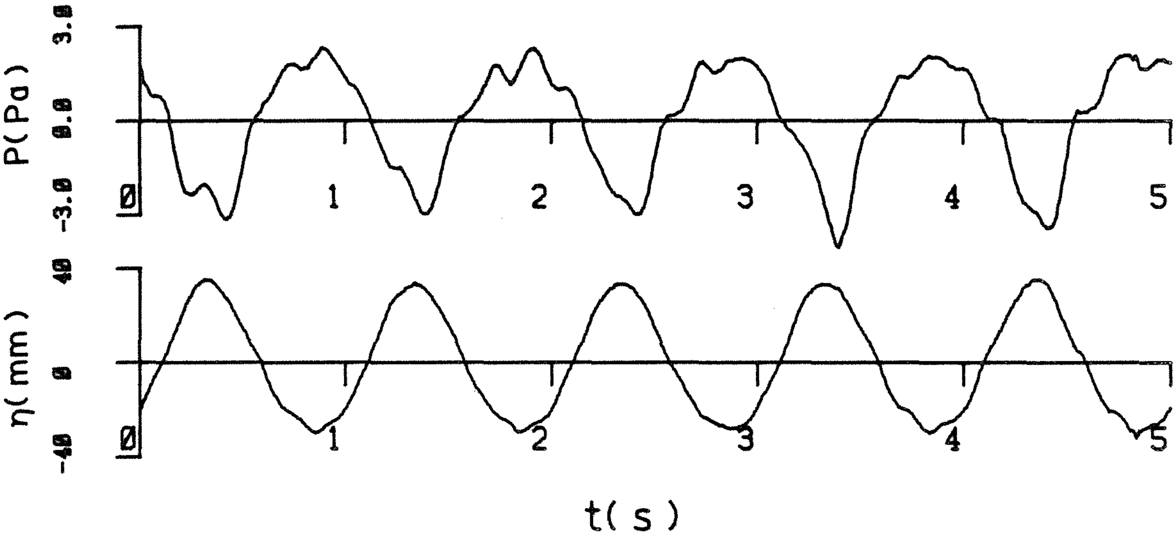

Fan speed = 310 rpm

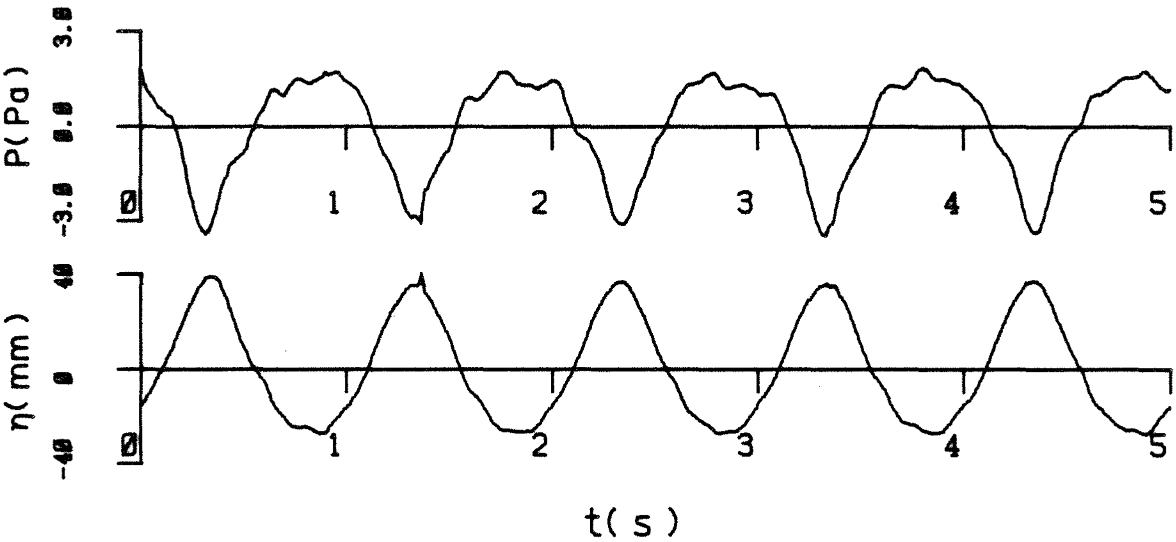

Fan speed = 280 rpm

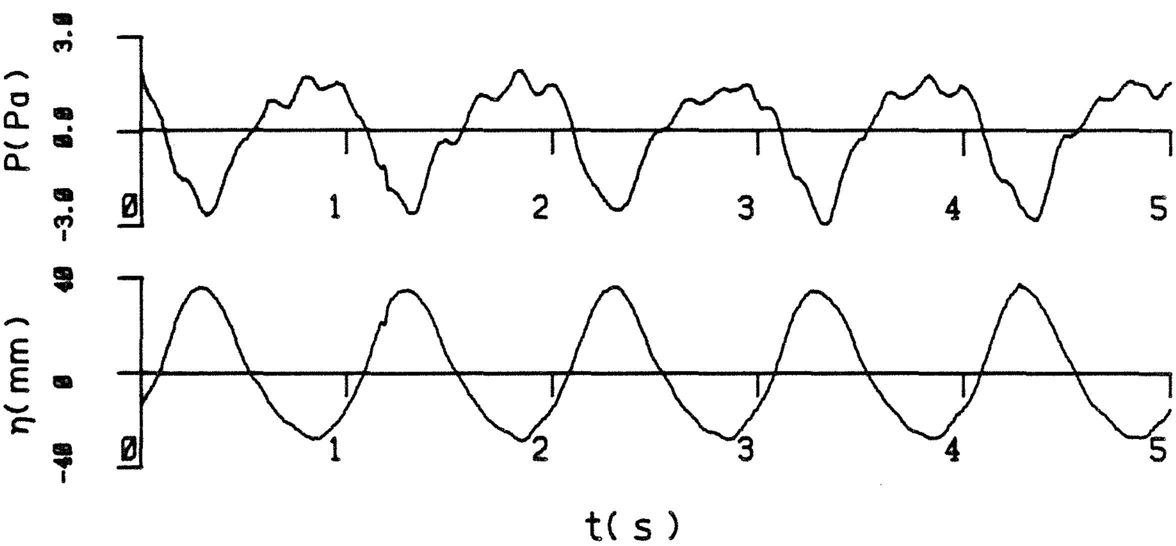

Fan speed = 260 rpm

Figure 7.1c Water surface elevation and wave induced pressure records for various wind speeds.

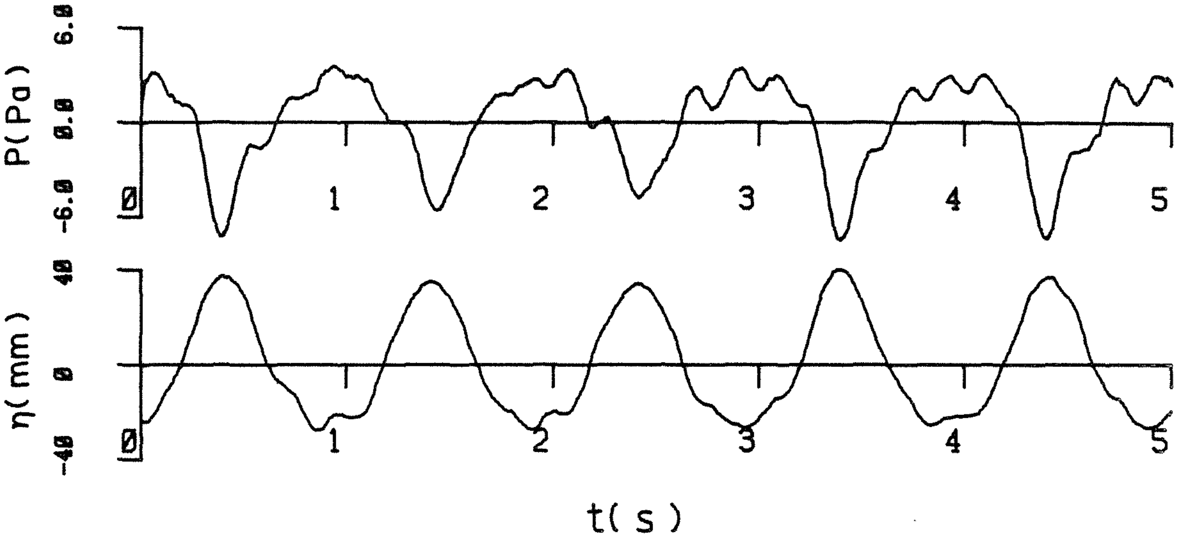

Fan speed = 415 rpm

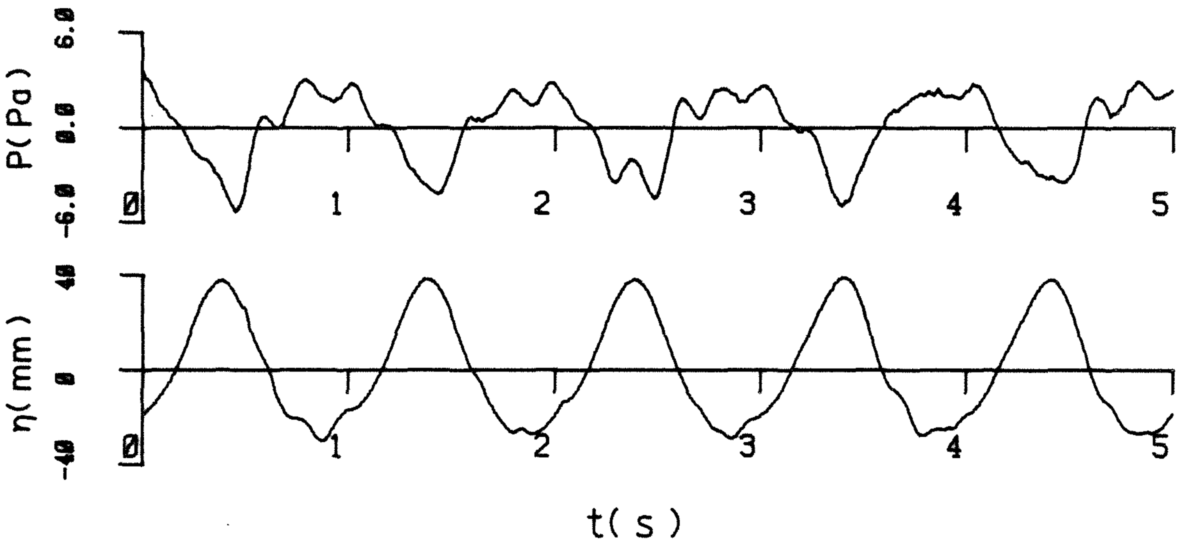

Fan speed = 380 rpm

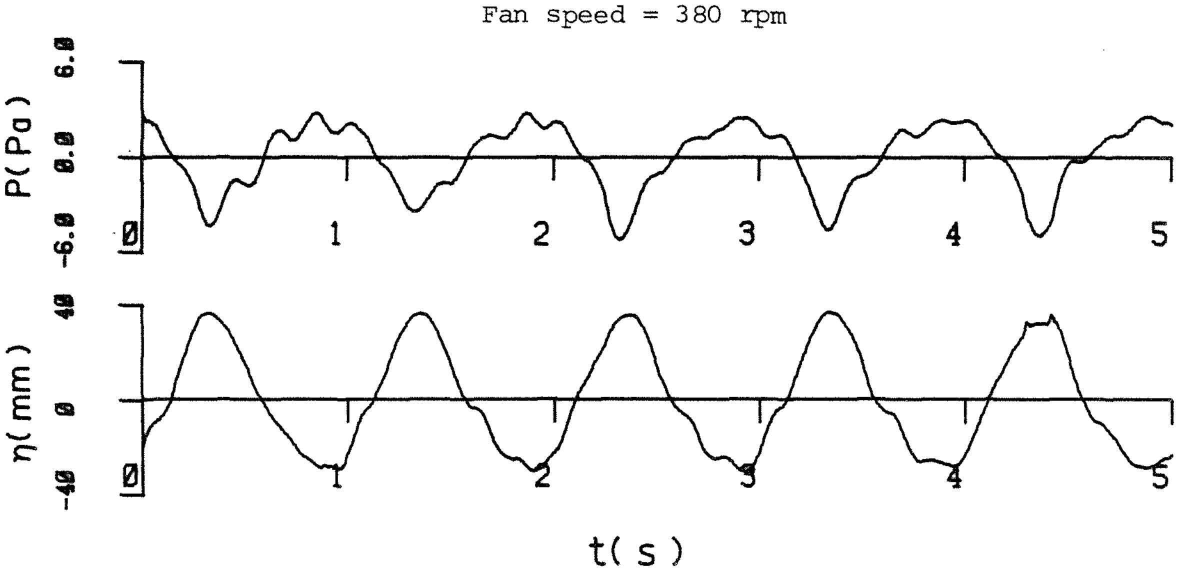

Fan speed = 345 rpm

Figure 7.1d Water surface elevation and wave induced pressure records for various wind speeds.

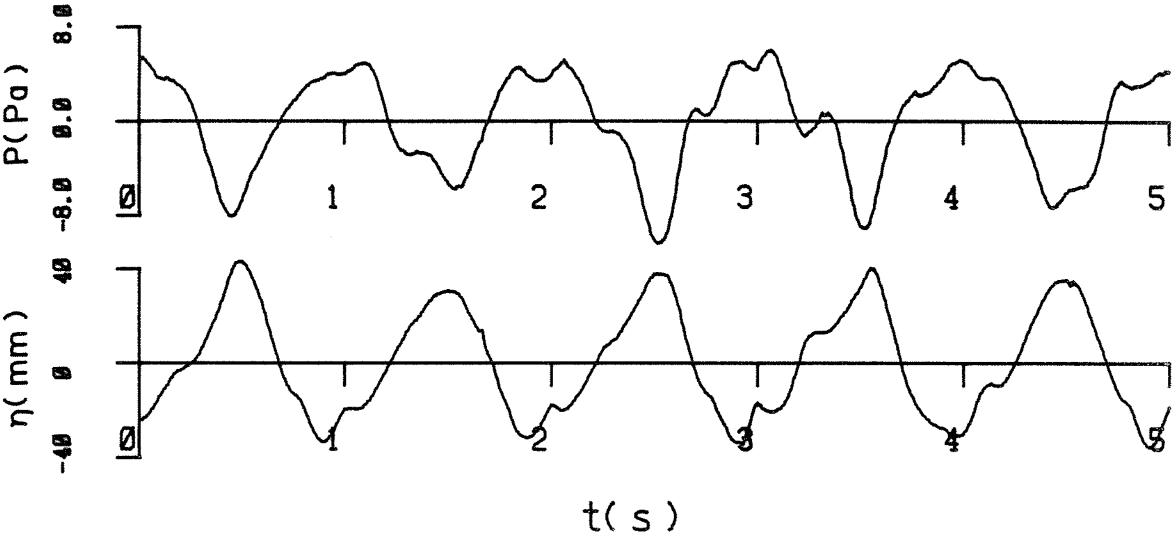

Fan speed = 550 rpm

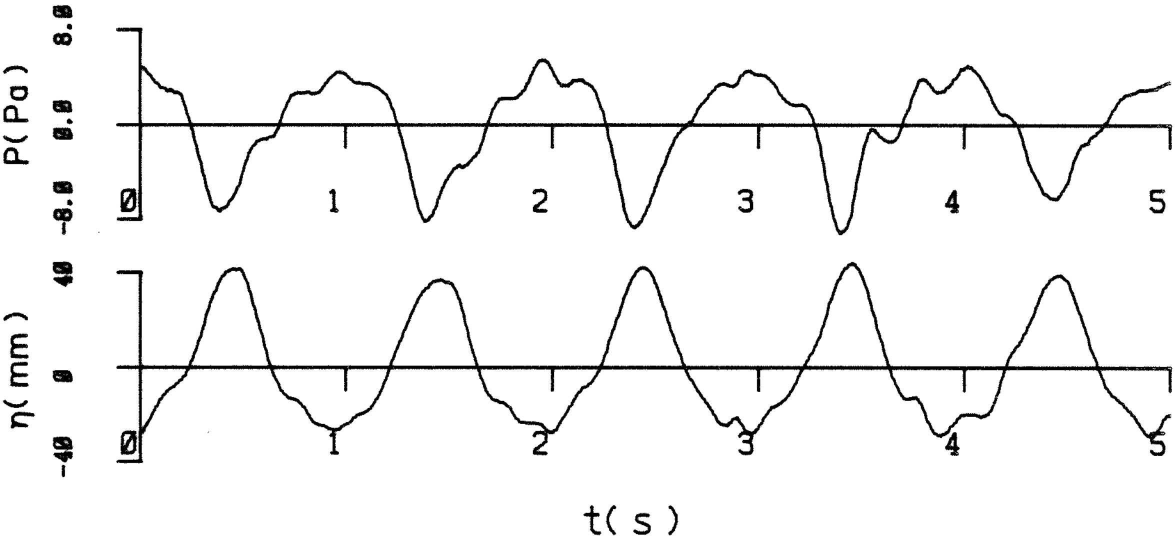

Fan speed = 500 rpm

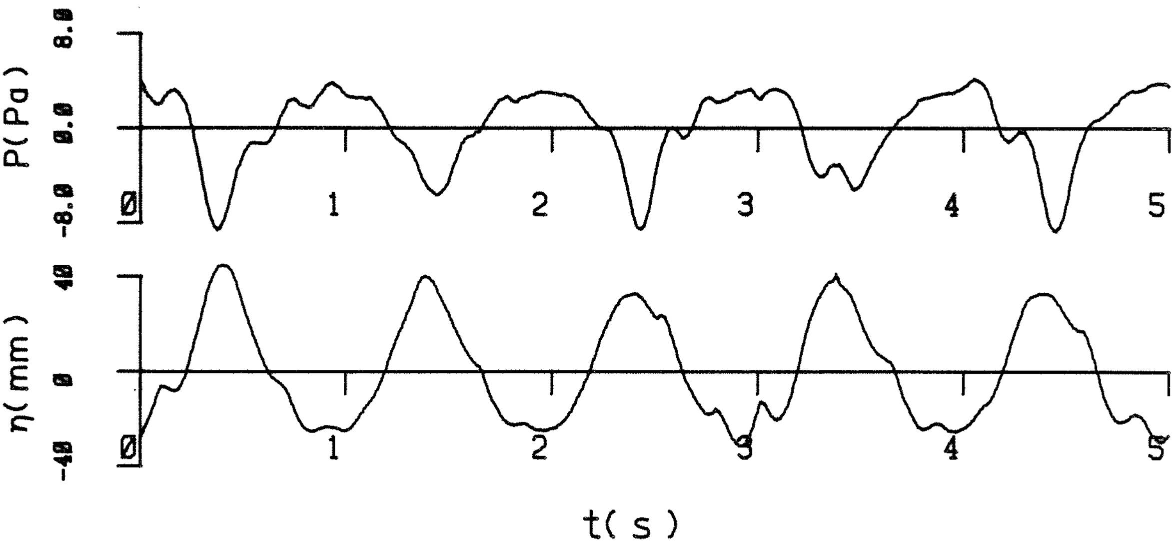

Fan speed = 455 rpm

Figure 7.1e Water surface elevation and wave induced pressure records for various wind speeds.

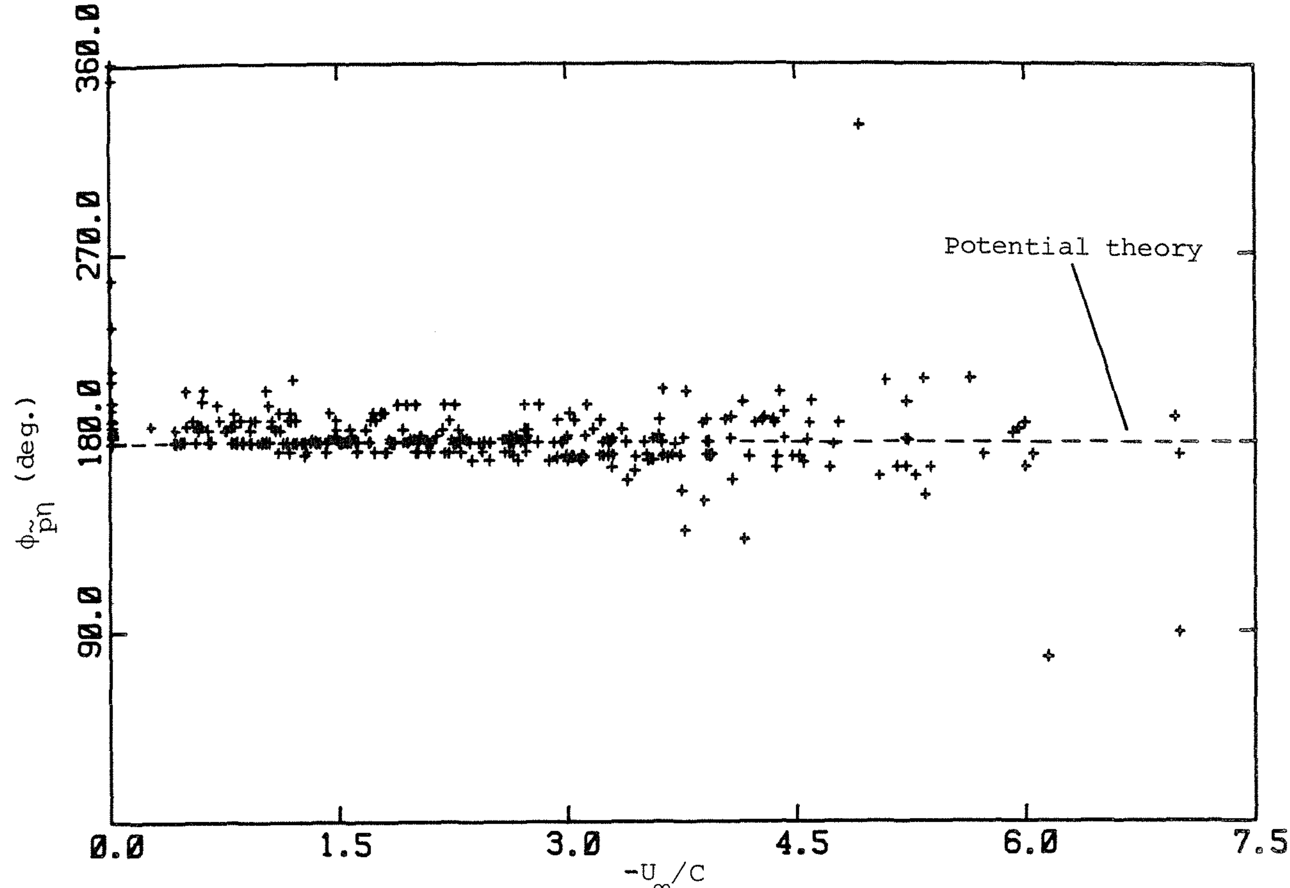

Figure 7.2 Phase angle between wave induced pressure and water surface elevation as a function of U_∞/C.

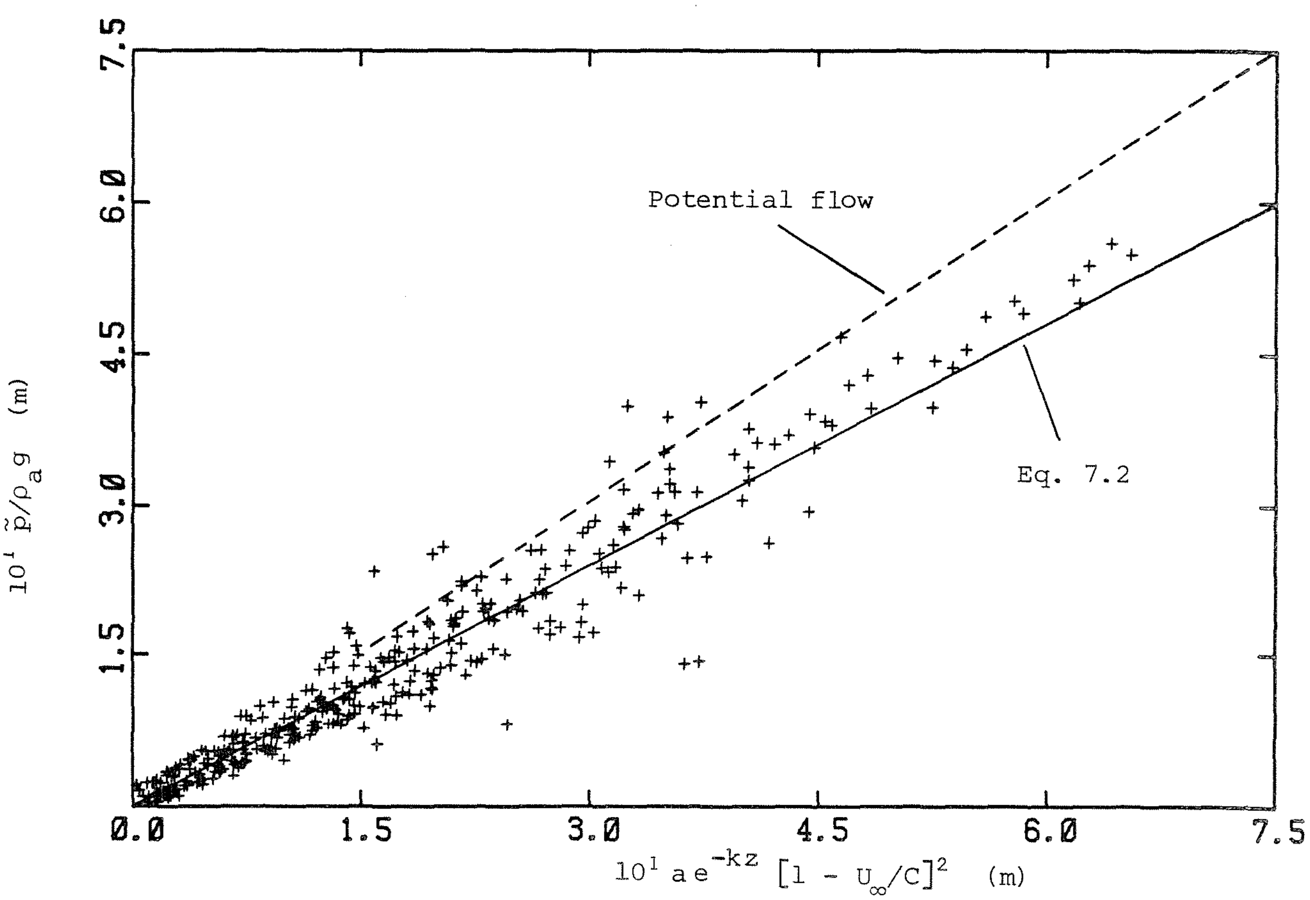

Figure 7.3 Wave induced pressure as a function of the potential flow solution.

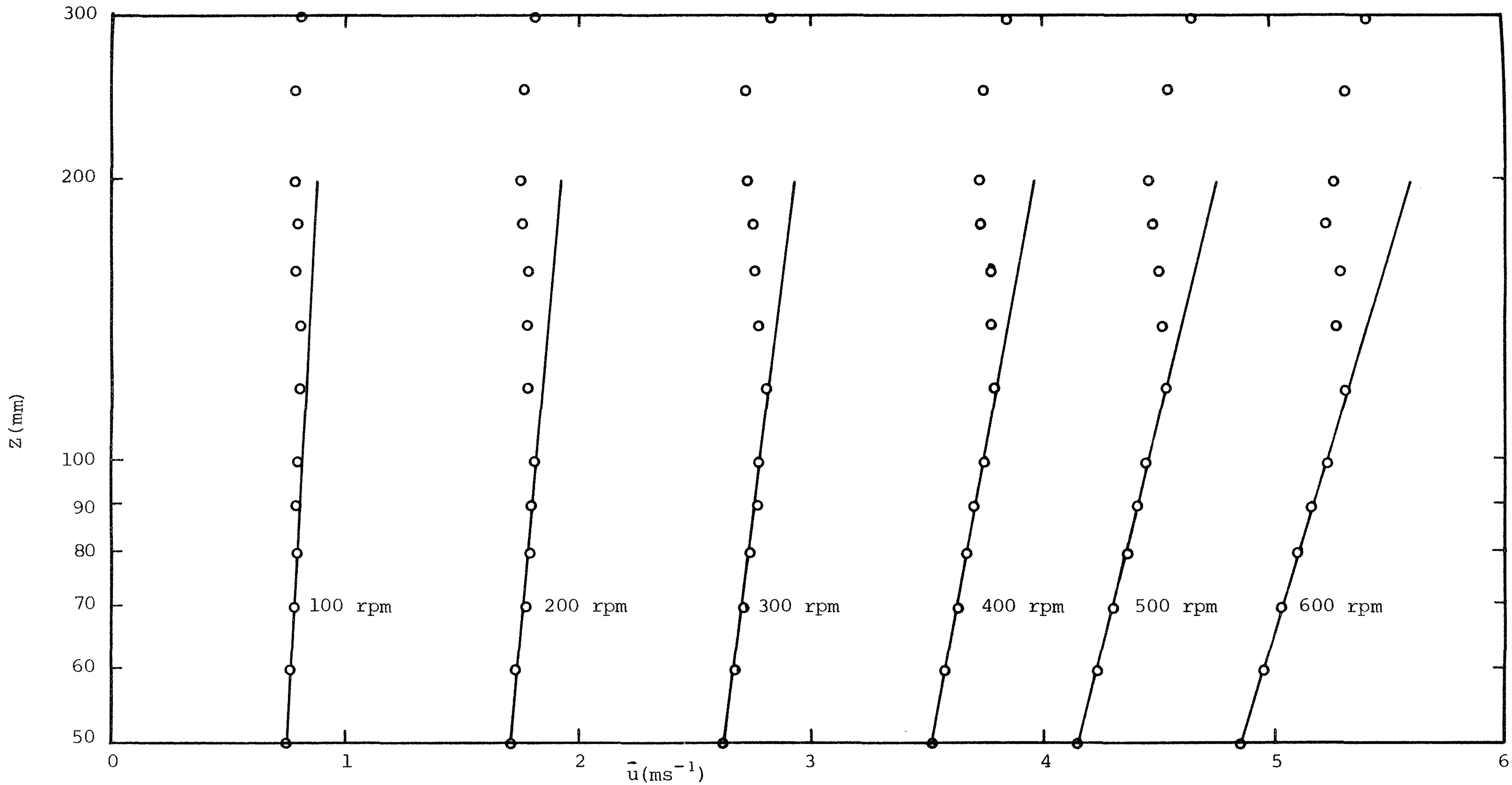

Figure 8.1a Velocity profiles above mechancially generated waves with f = 0.75 Hz.

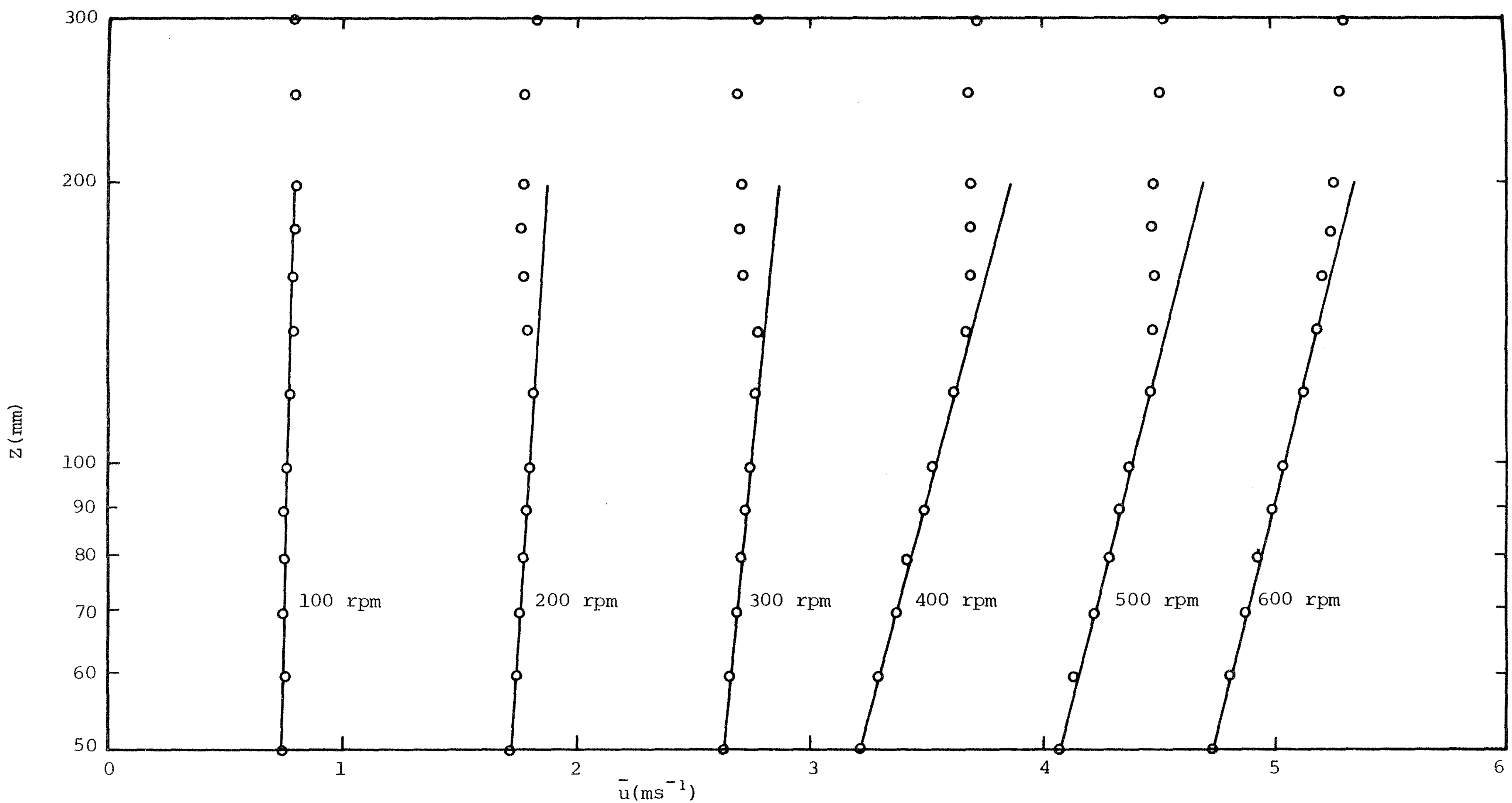

Figure 8.1b Velocity profiles above mechancially generated waves with f = 1.00 Hz.

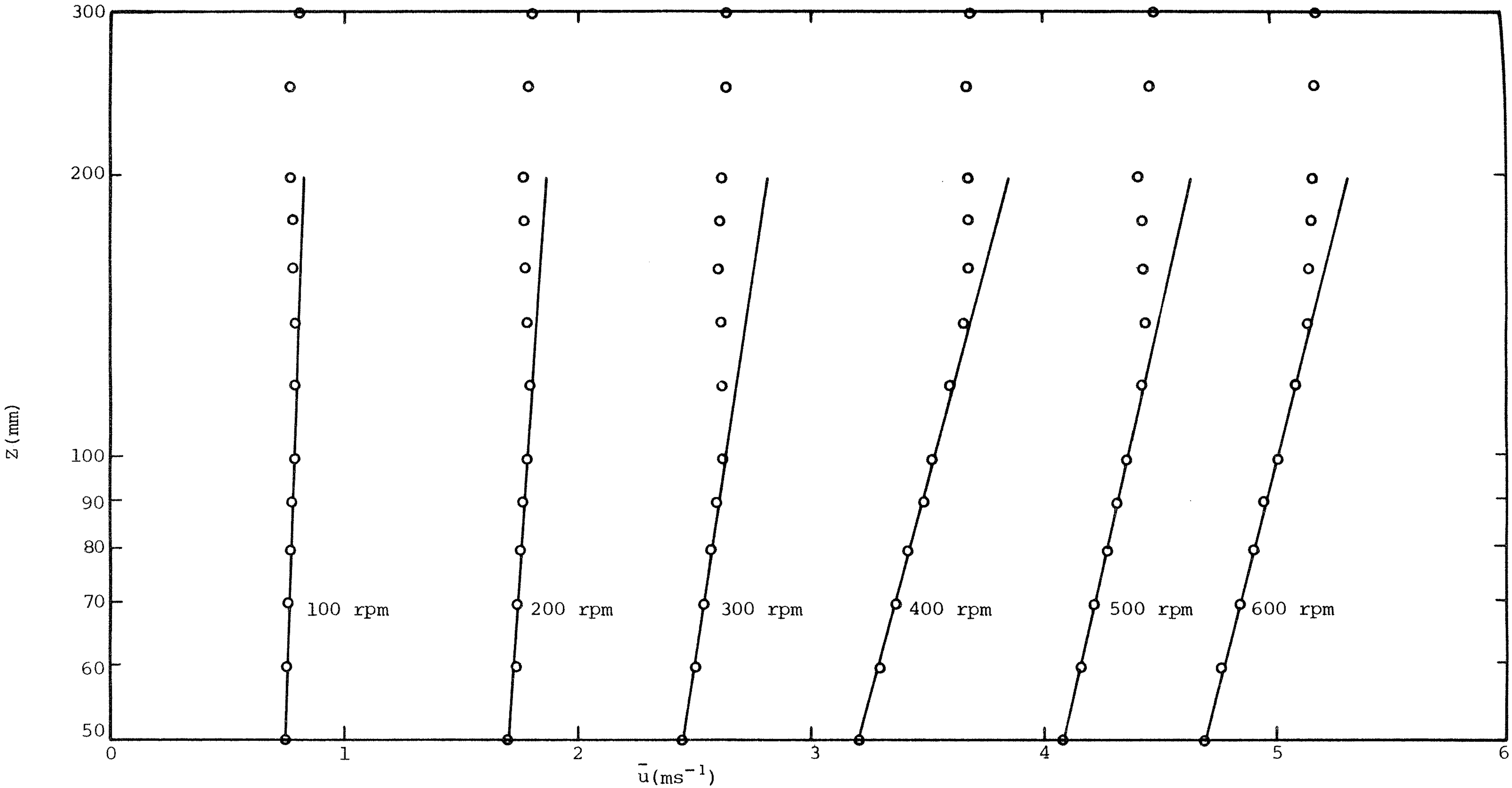

Figure 8.1c Velocity profiles above mechanically generated waves with f = 1.25 Hz.

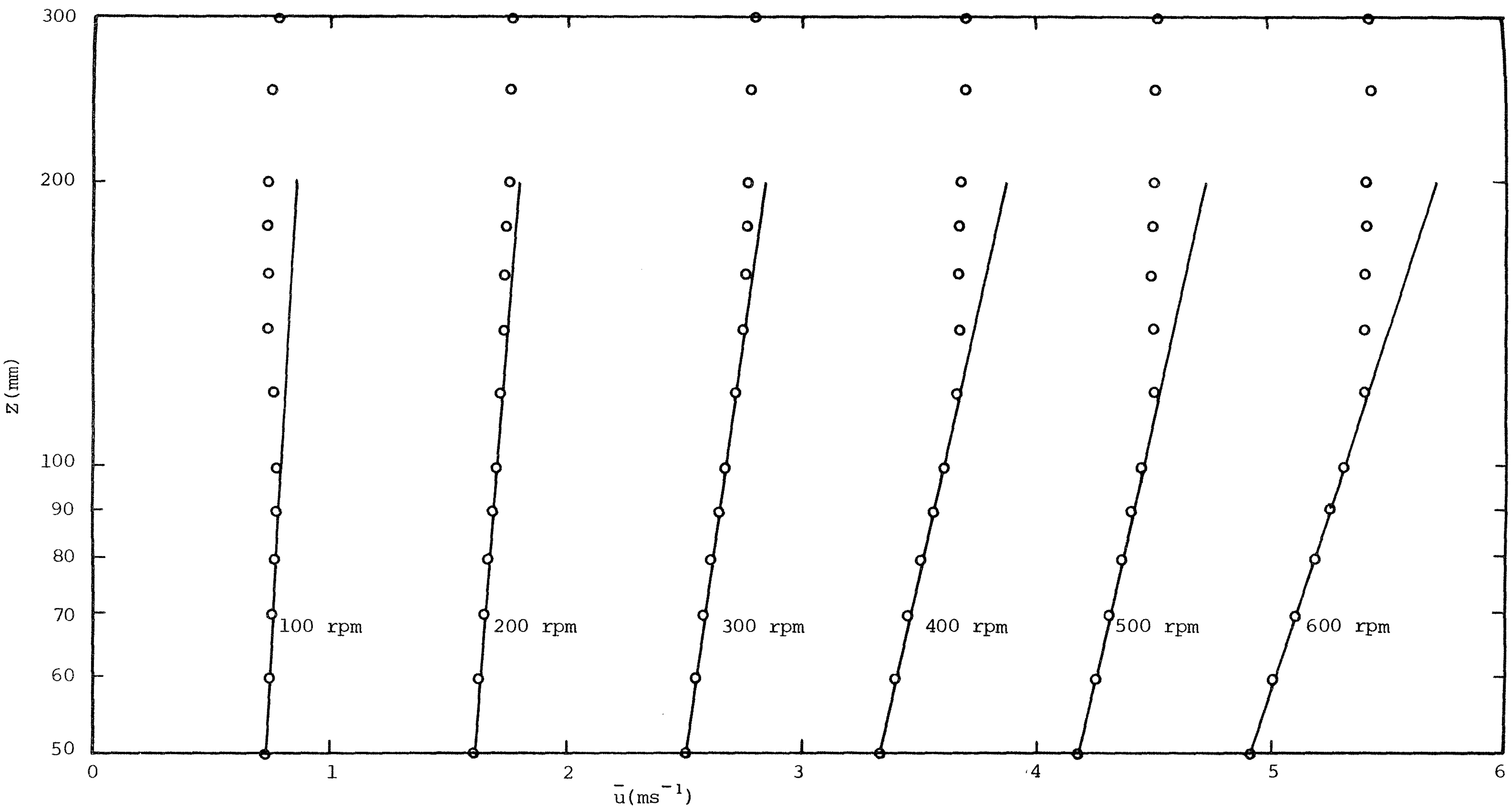

Figure 8.1d Velocity profiles above mechanically generated waves with f = 1.50 Hz.

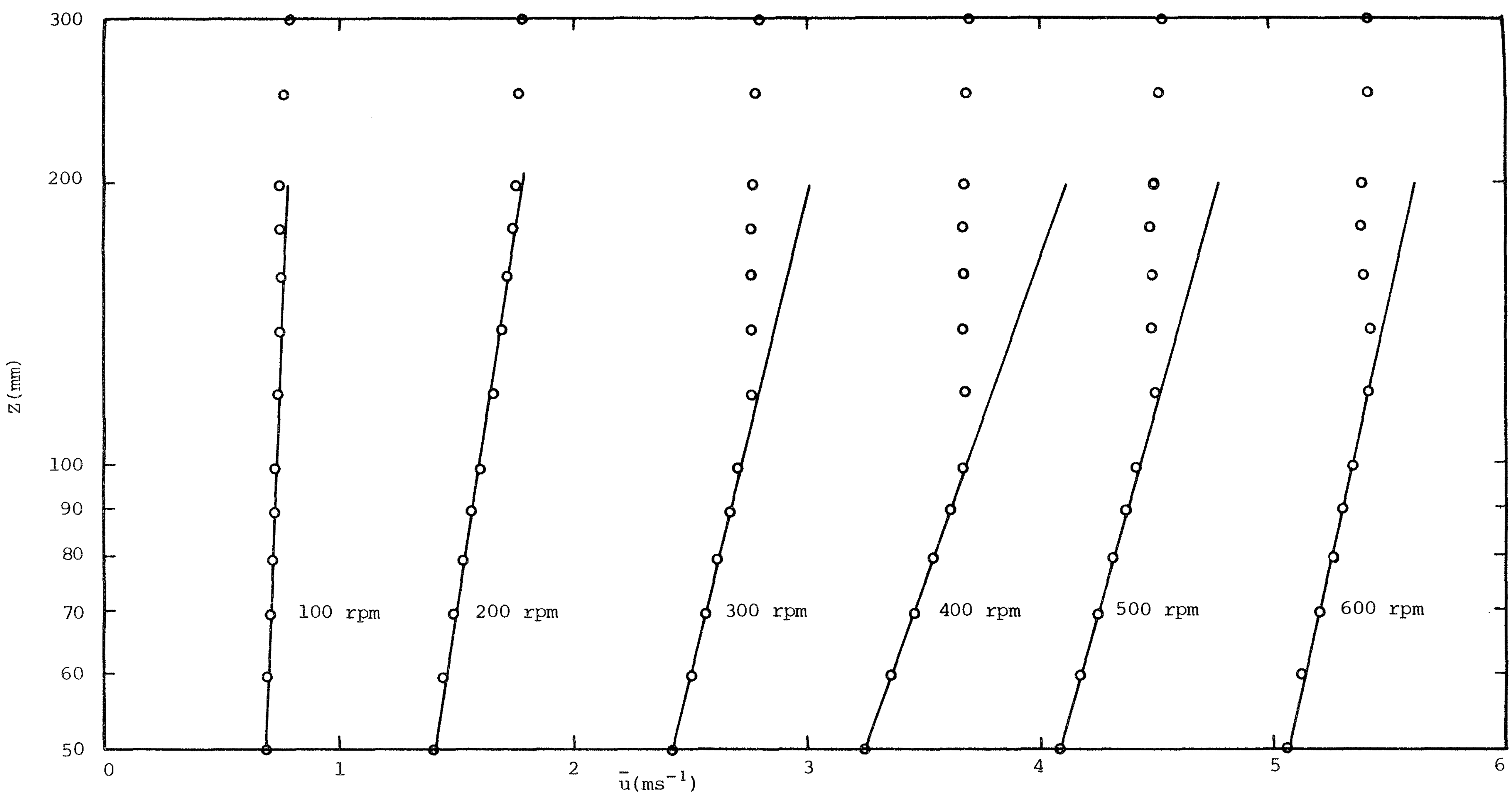

Figure 8.1e Velocity profiles above mechanically generated waves with f = 1.75 Hz.

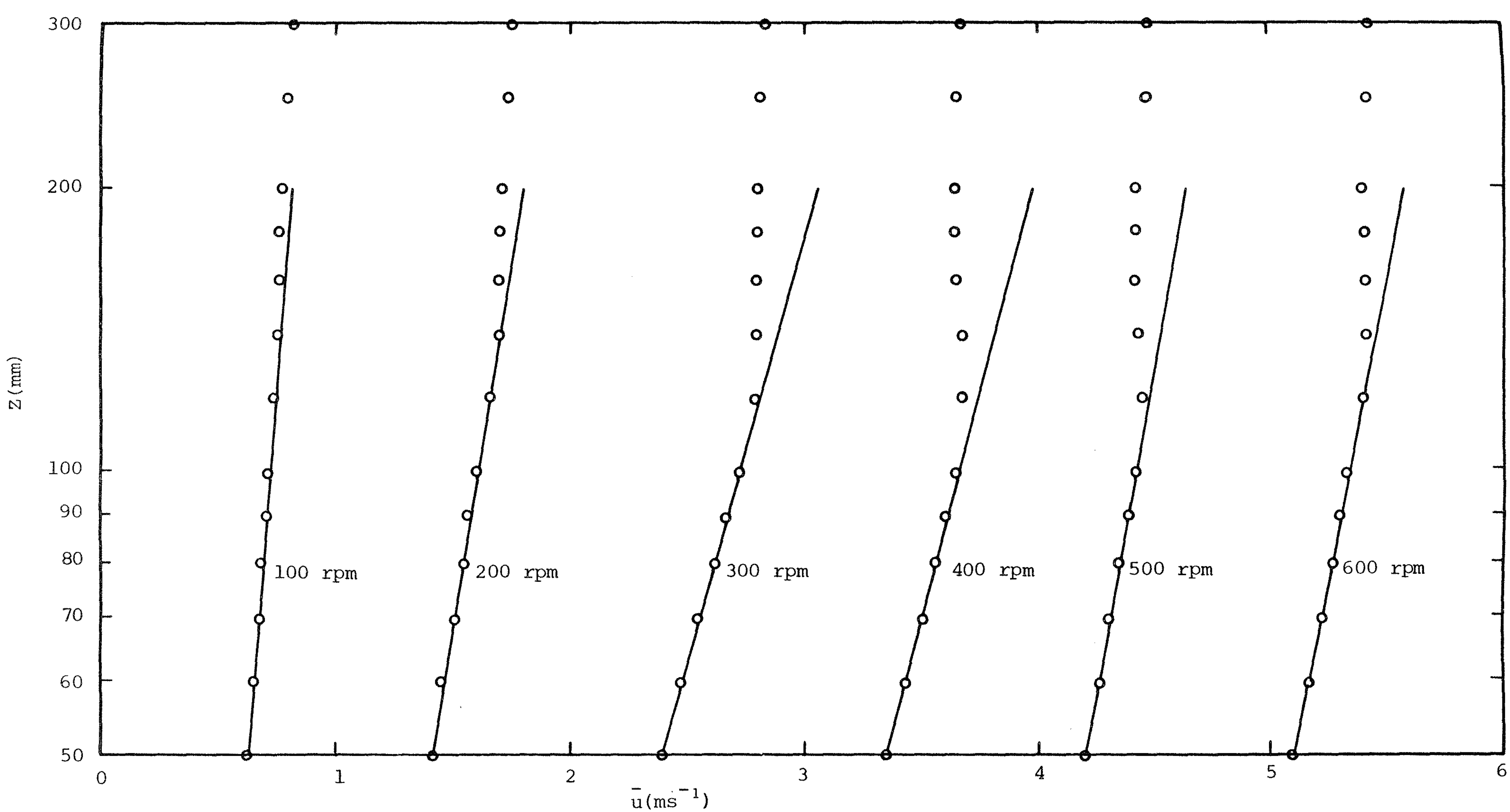

Figure 8.1f Velocity profiles above mechanically generated waves with f = 2.00 Hz.

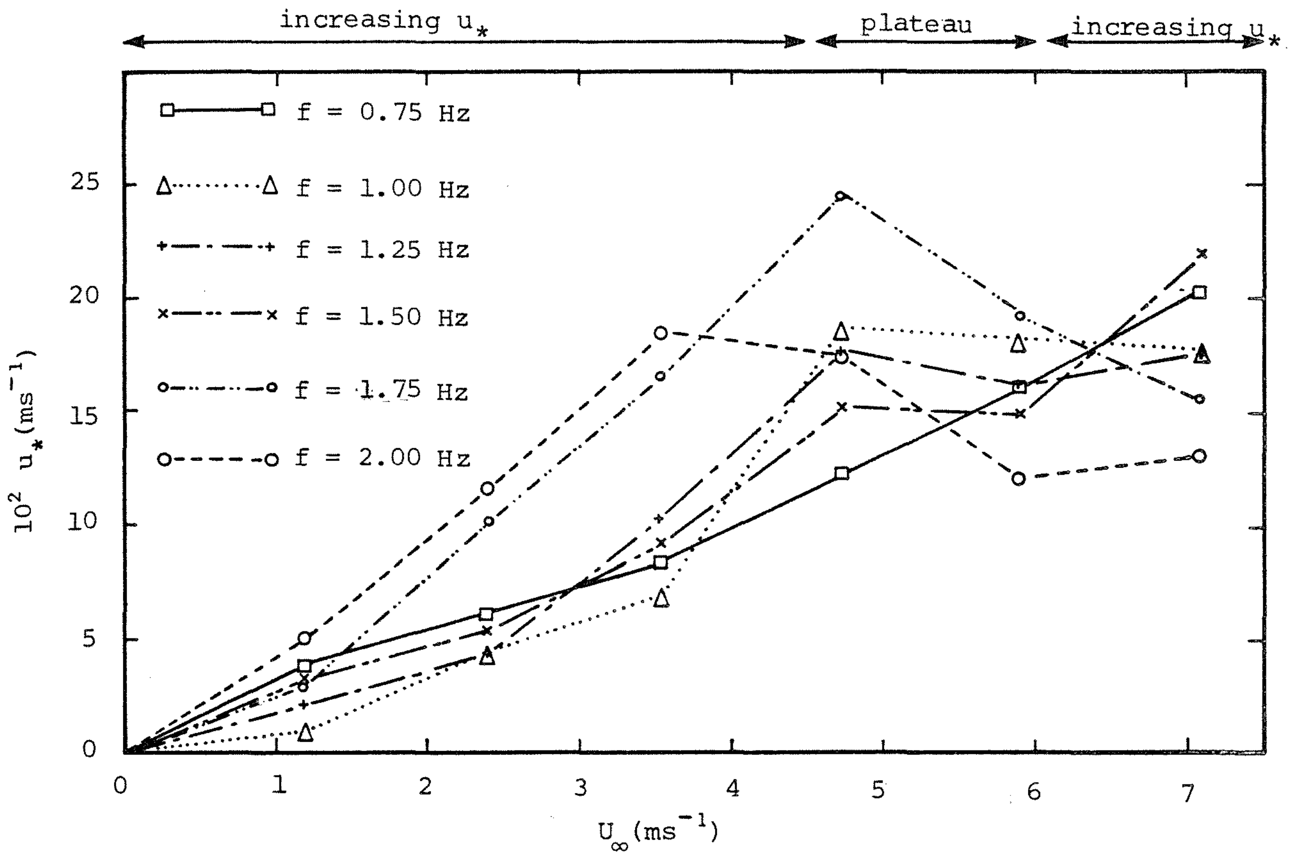

Figure 8.2 Shear velocity u_* as a function of U_∞ for various frequencies of mechanically generated waves.

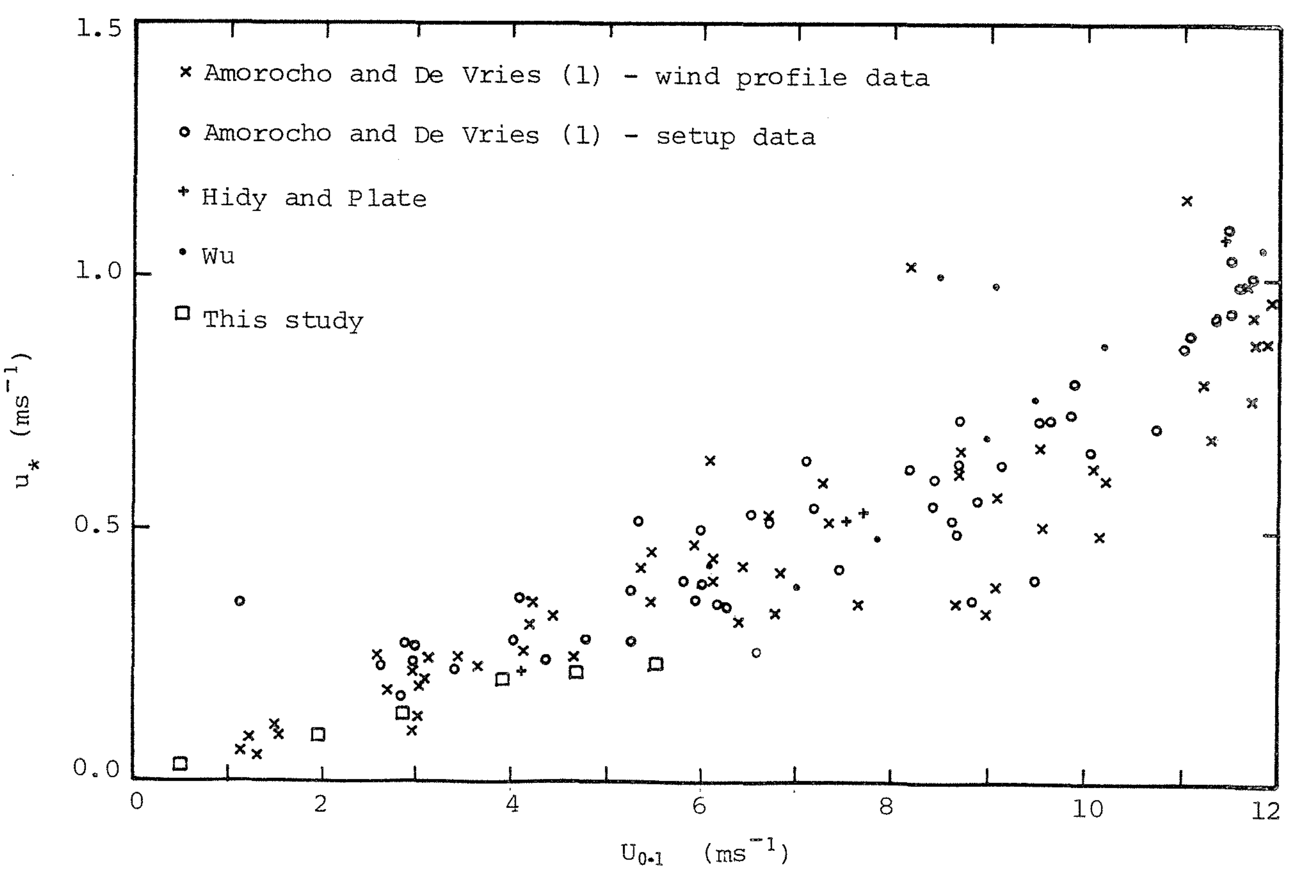

Figure 8.3 Comparison of u_* values from this study with data from following wind studies.

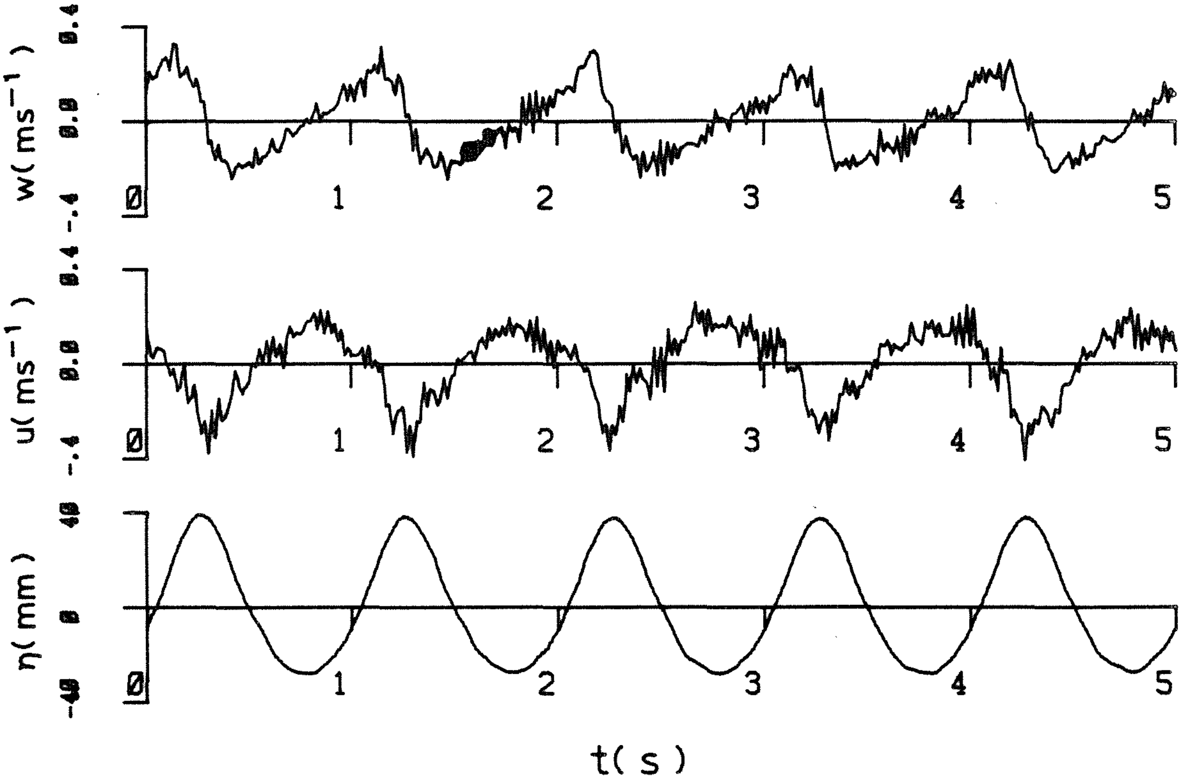

Fan speed = 150 rpm

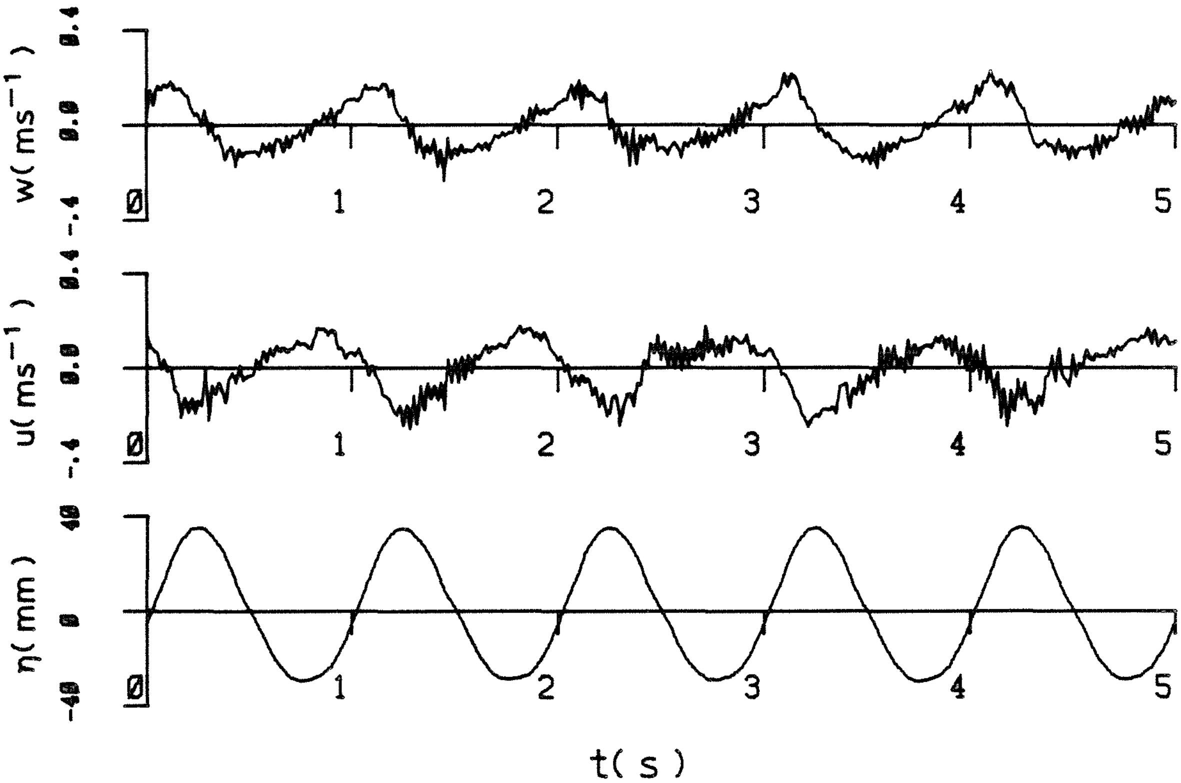

Fan speed = 100 rpm

Figure 8.4a Water surface elevation and velocity records for various wind speeds.

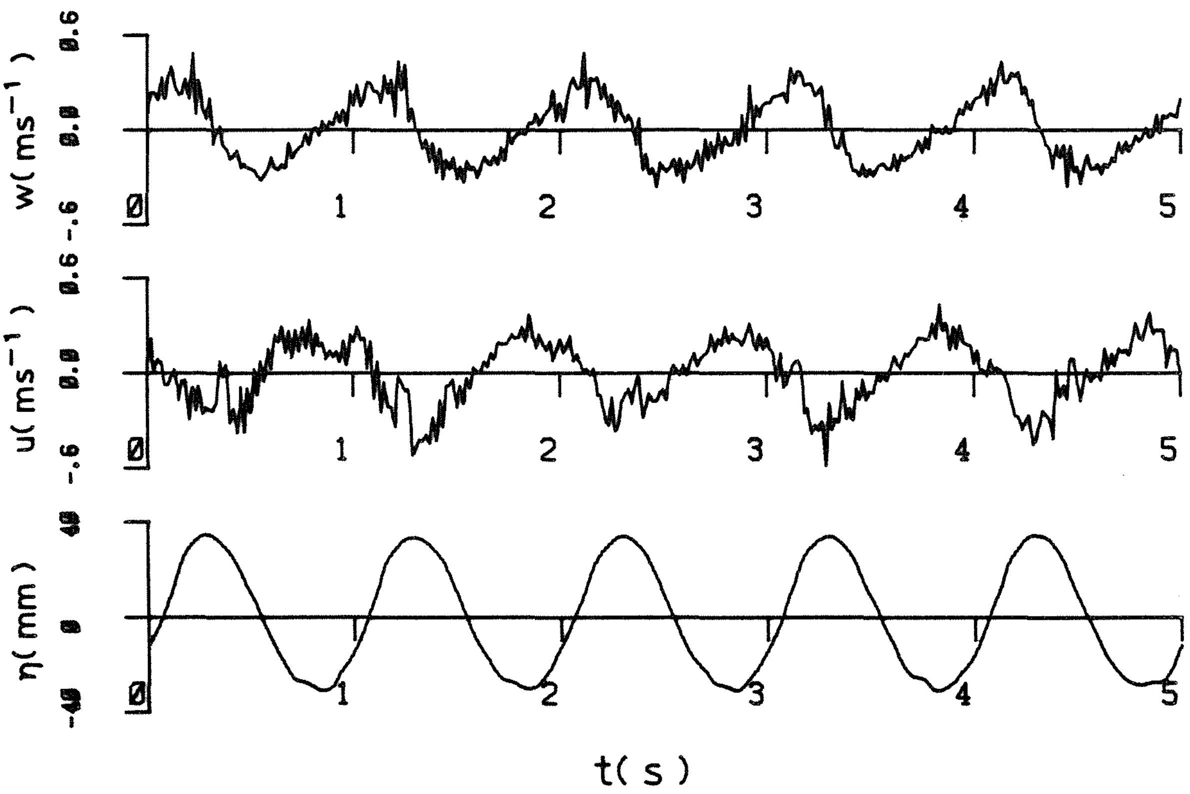

Fan speed = 250 rpm

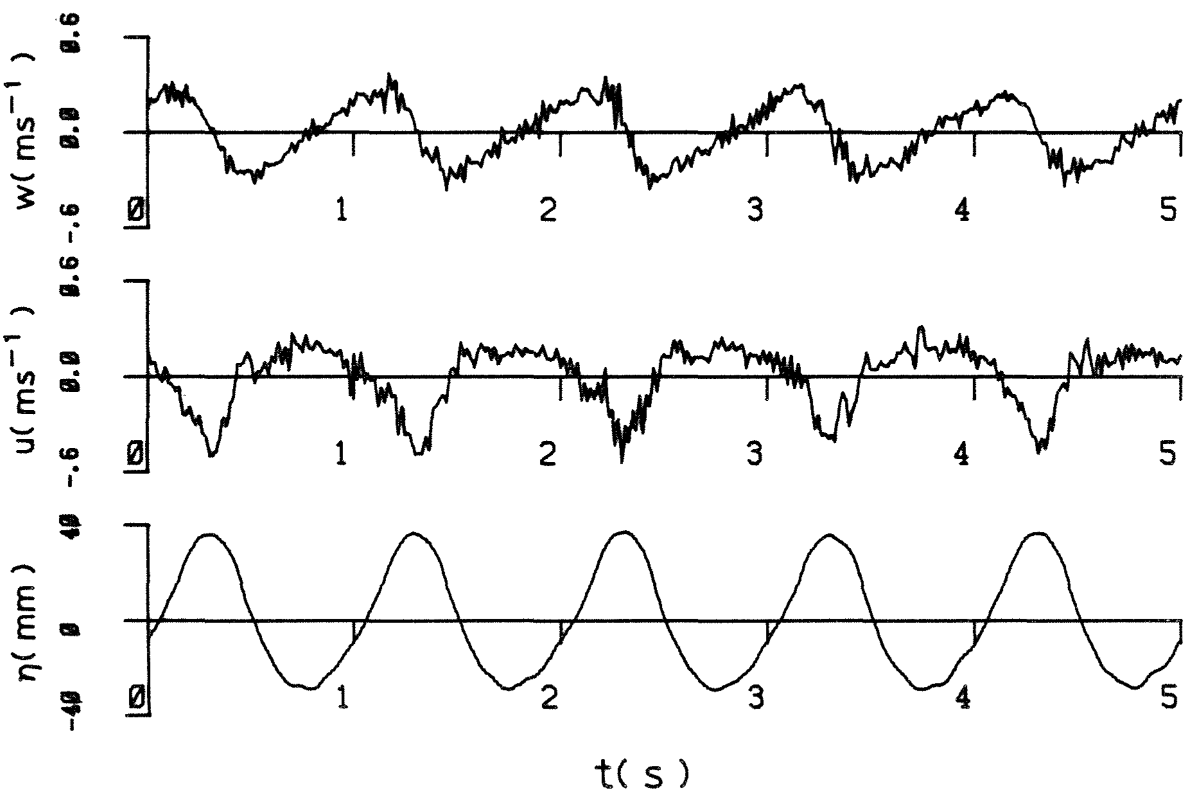

Fan speed = 200 rpm

Figure 8.4b Water surface elevation and velocity records for various wind speeds.

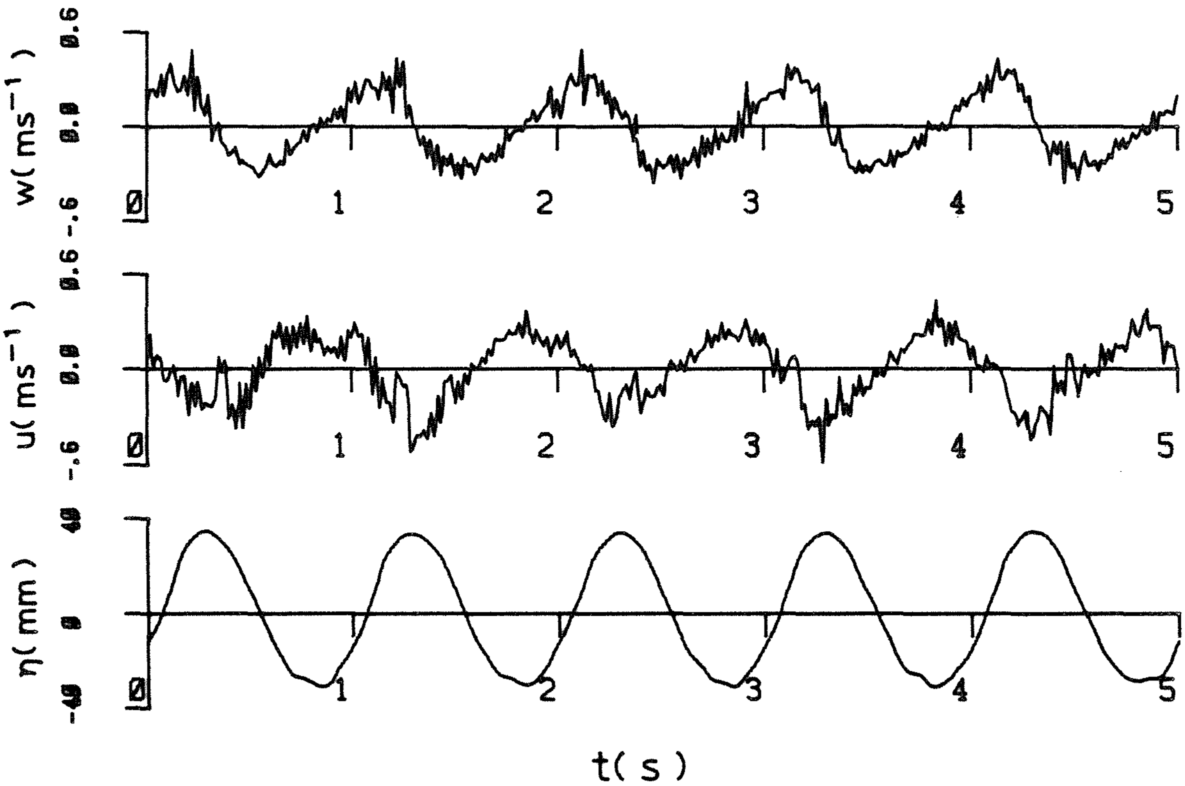

Fan speed = 250 rpm

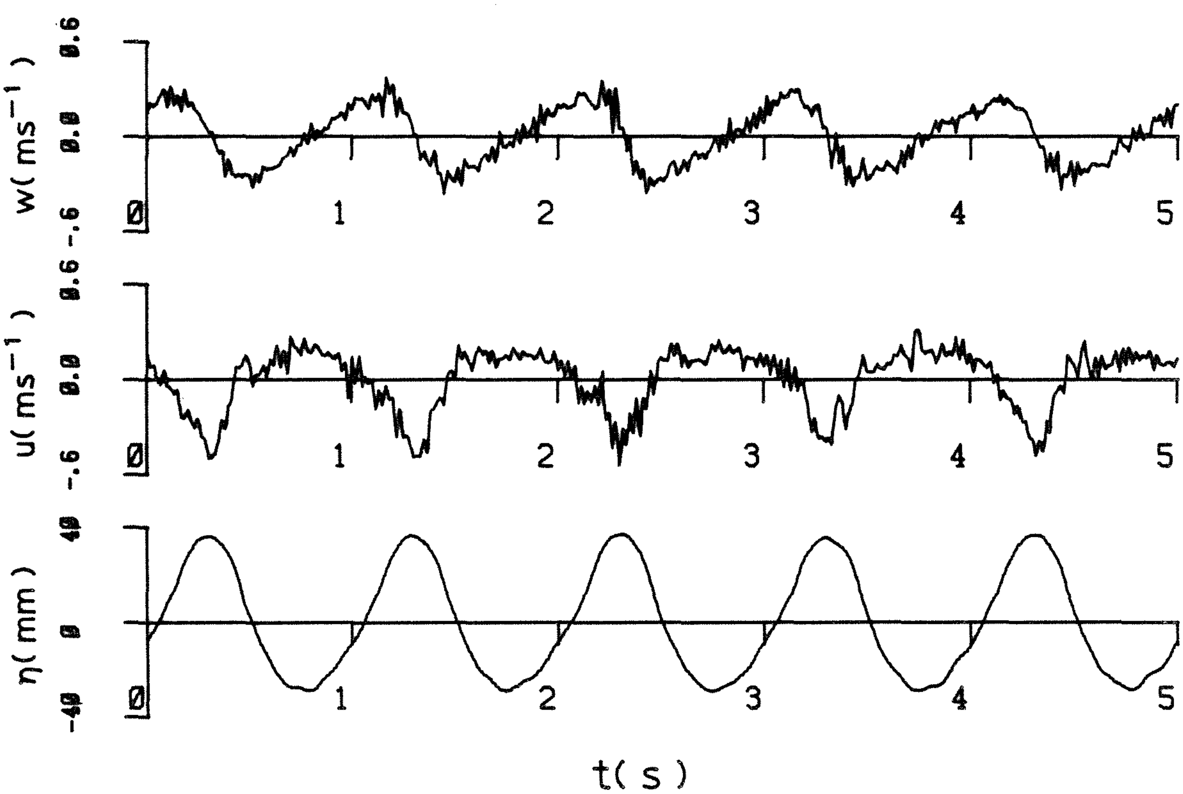

Fan speed = 200 rpm

Figure 8.4b Water surface elevation and velocity records for various wind speeds.

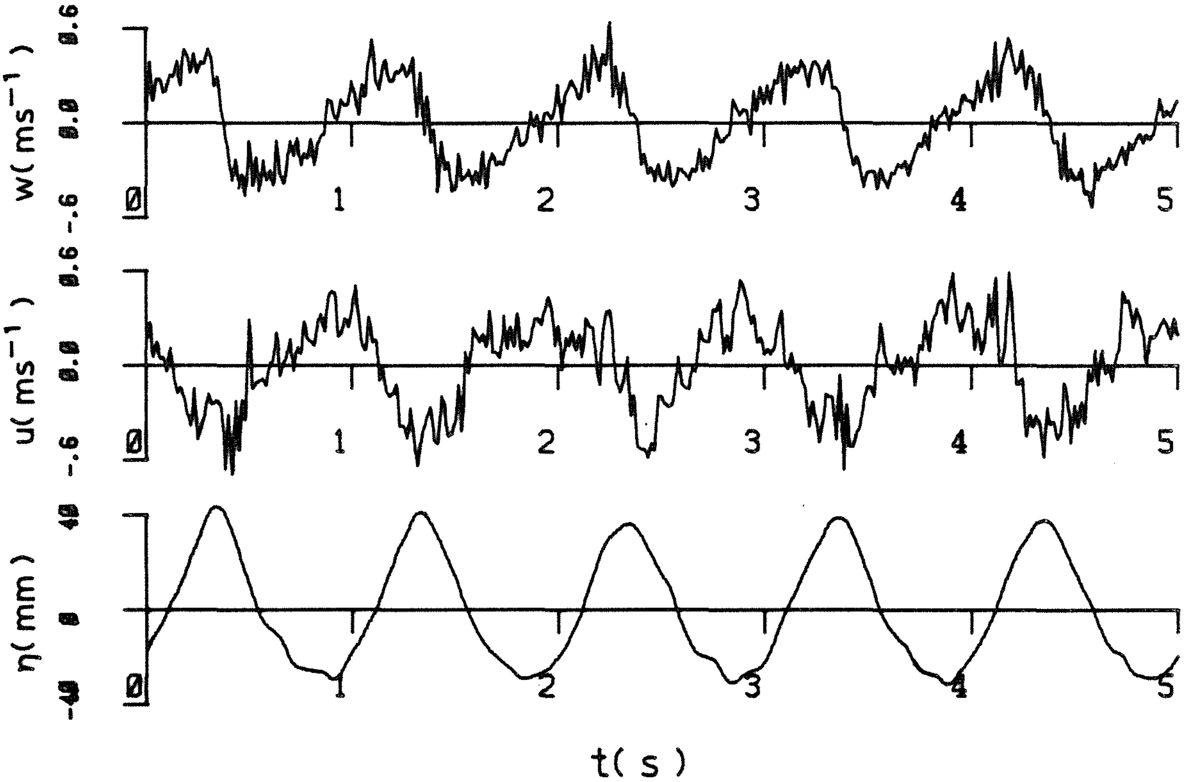

Fan speed = 350 rpm

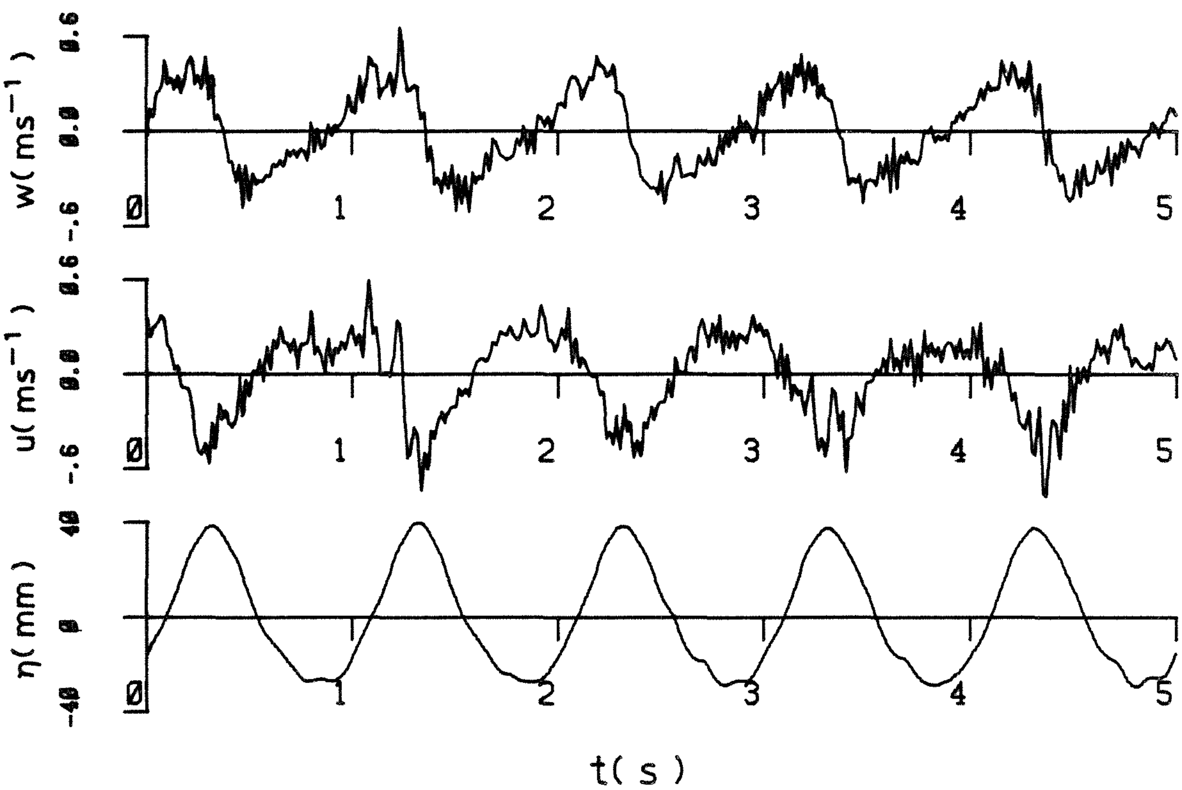

Fan speed = 300 rpm

Figure 8.4c Water surface elevation and velocity records for various wind speeds.

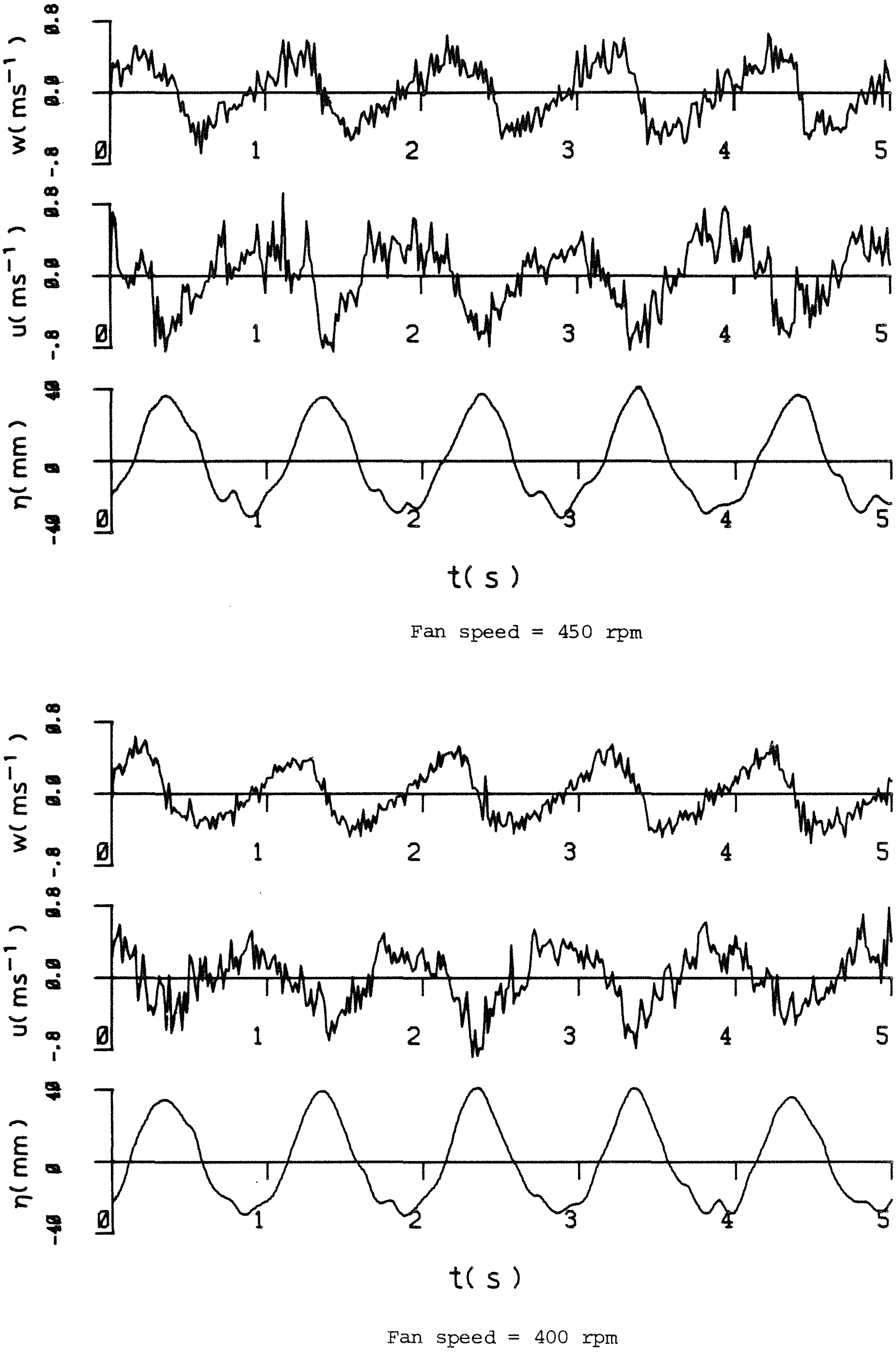

Figure 8.4d Water surface elevation and velocity records for various wind speeds.

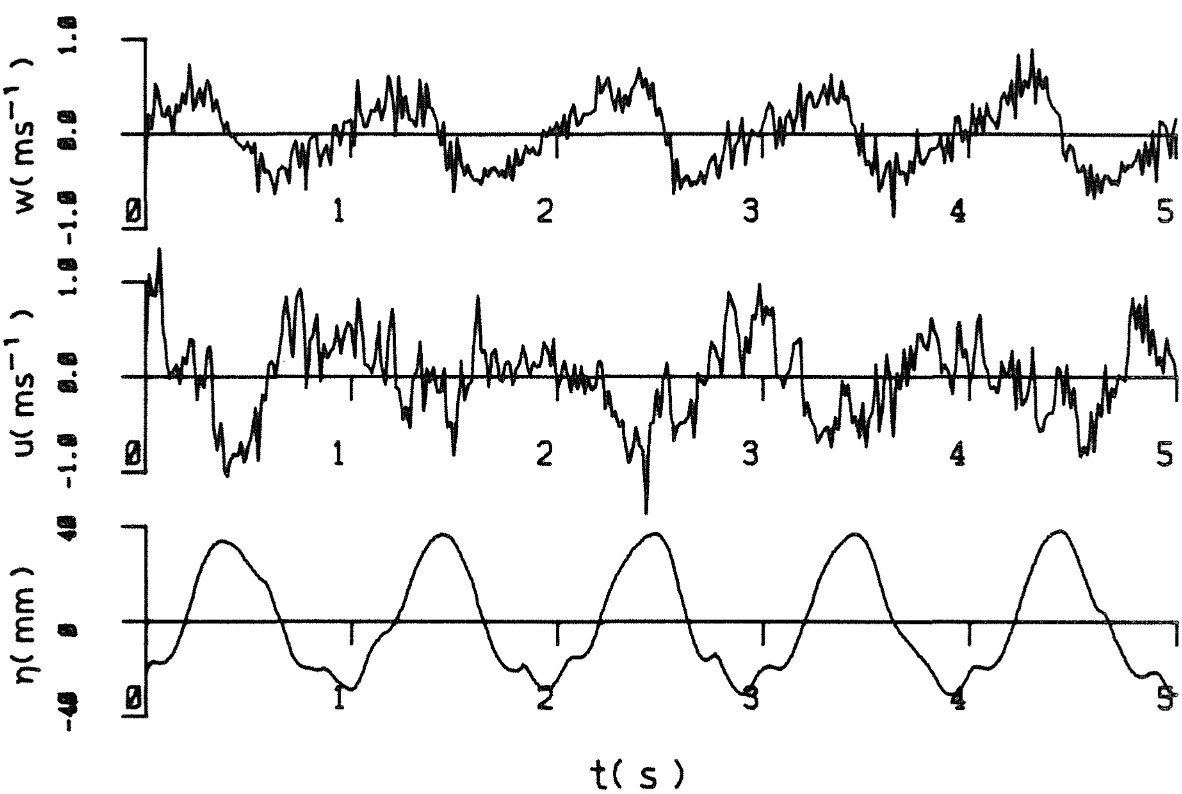

Fan speed = 550 rpm

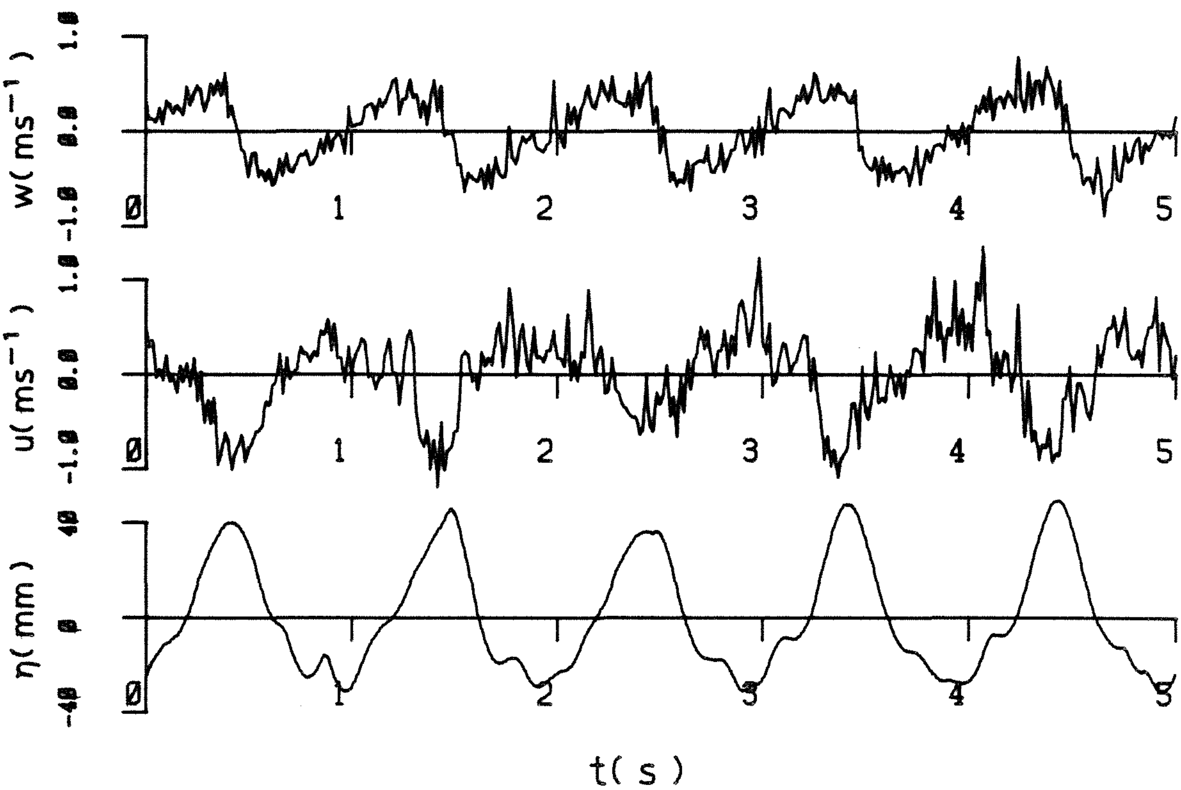

Fan speed = 500 rpm

Figure 8.4e Water surface elevation and velocity records for various wind speeds.

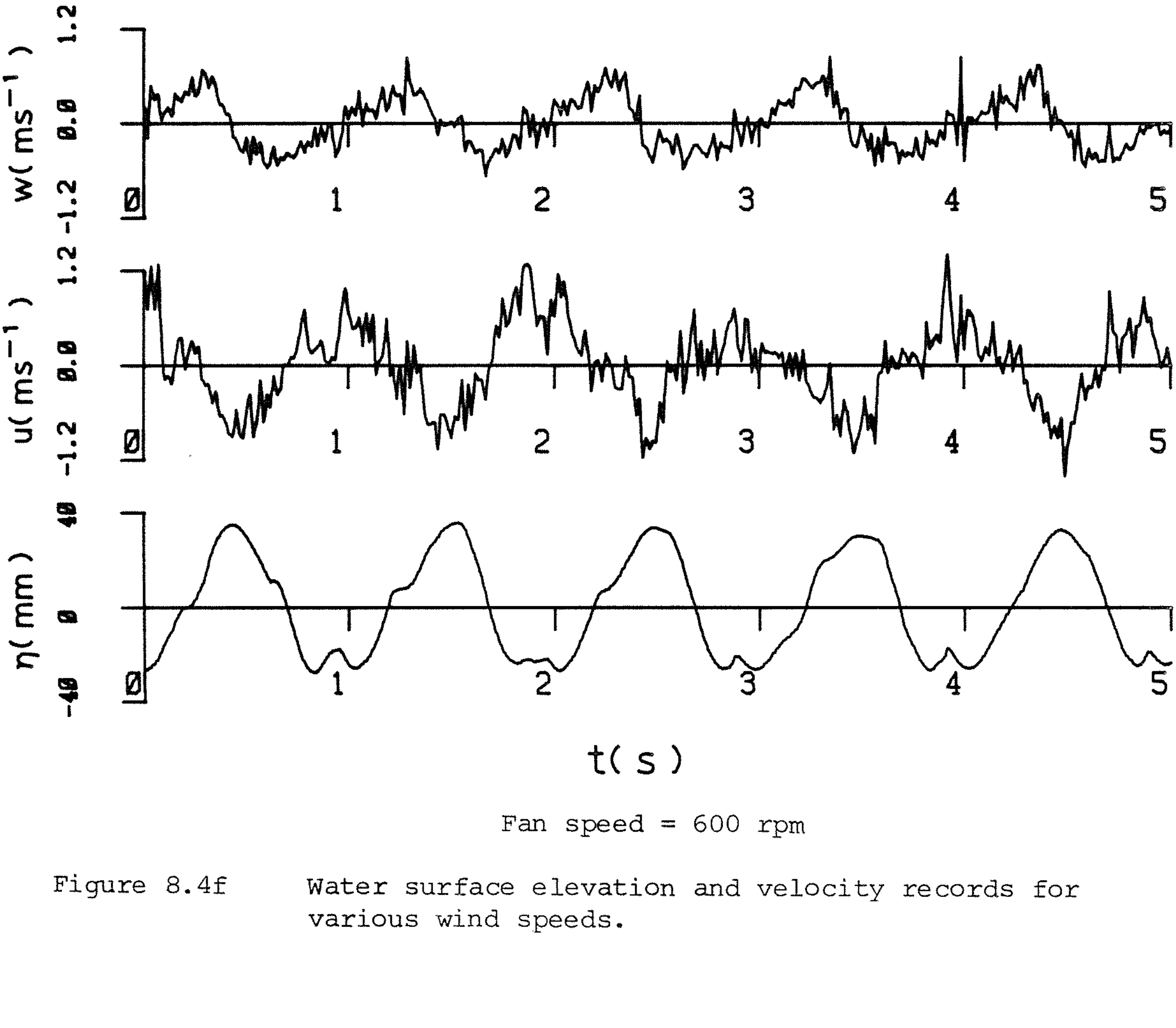

Fan speed = 600 rpm

Figure 8.4f Water surface elevation and velocity records for various wind speeds.

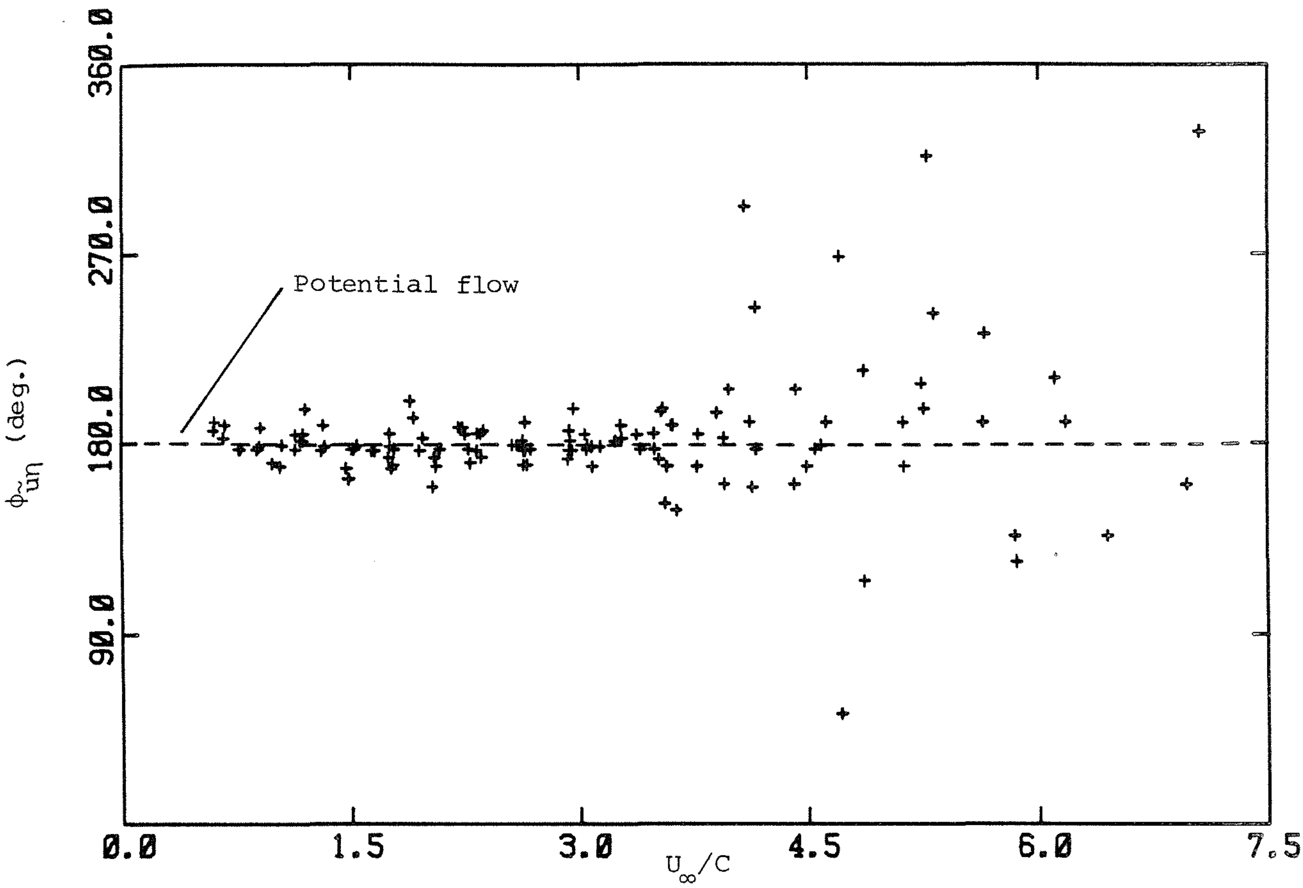

Figure 8.5 Phase angle between $\tilde{u}$ and η in a stationary coordinate system as a function of U_∞/C.

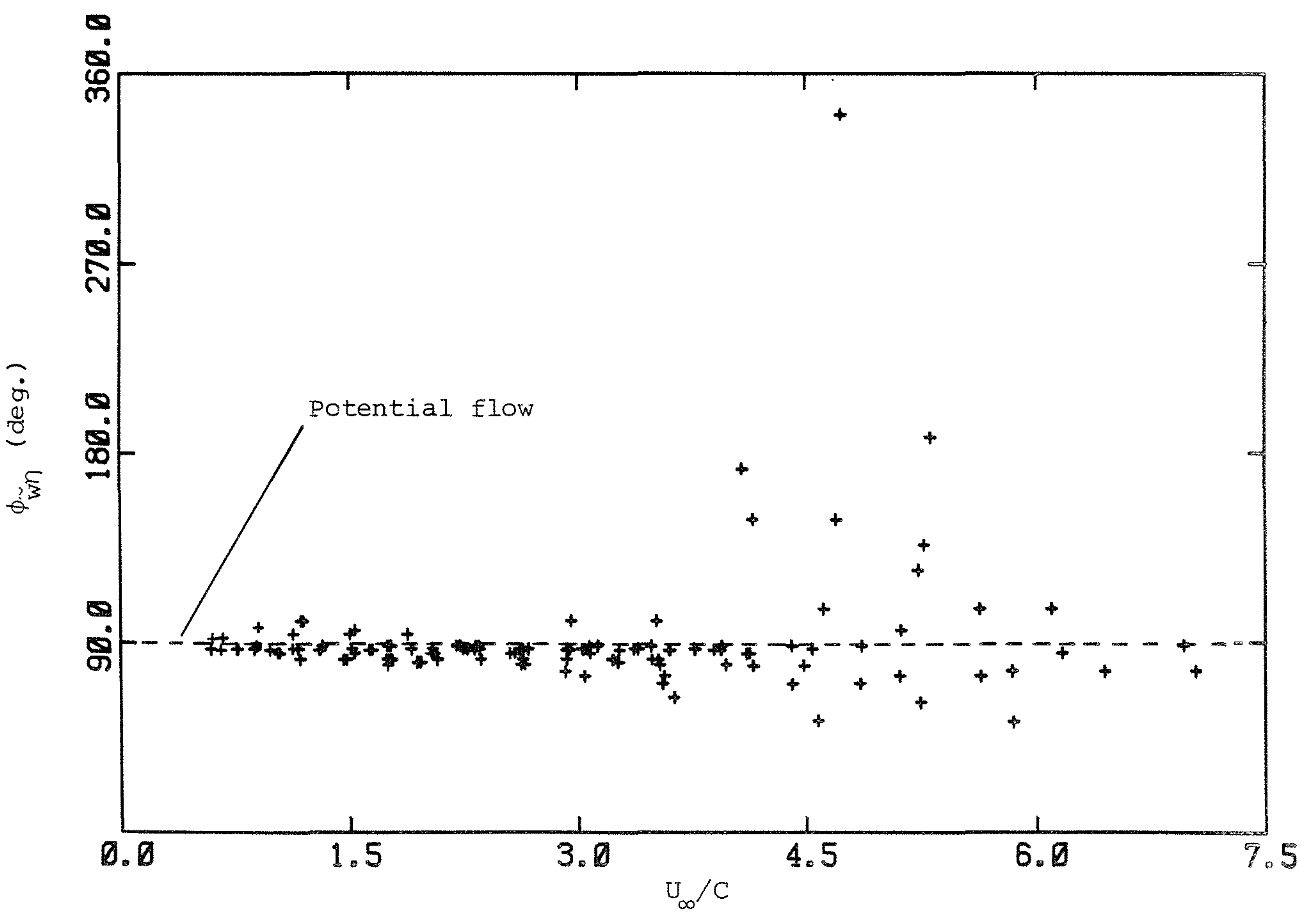

Figure 8.6 Phase angle between $\tilde{w}$ and η in a stationary coordinate system as a function of U_∞/C.

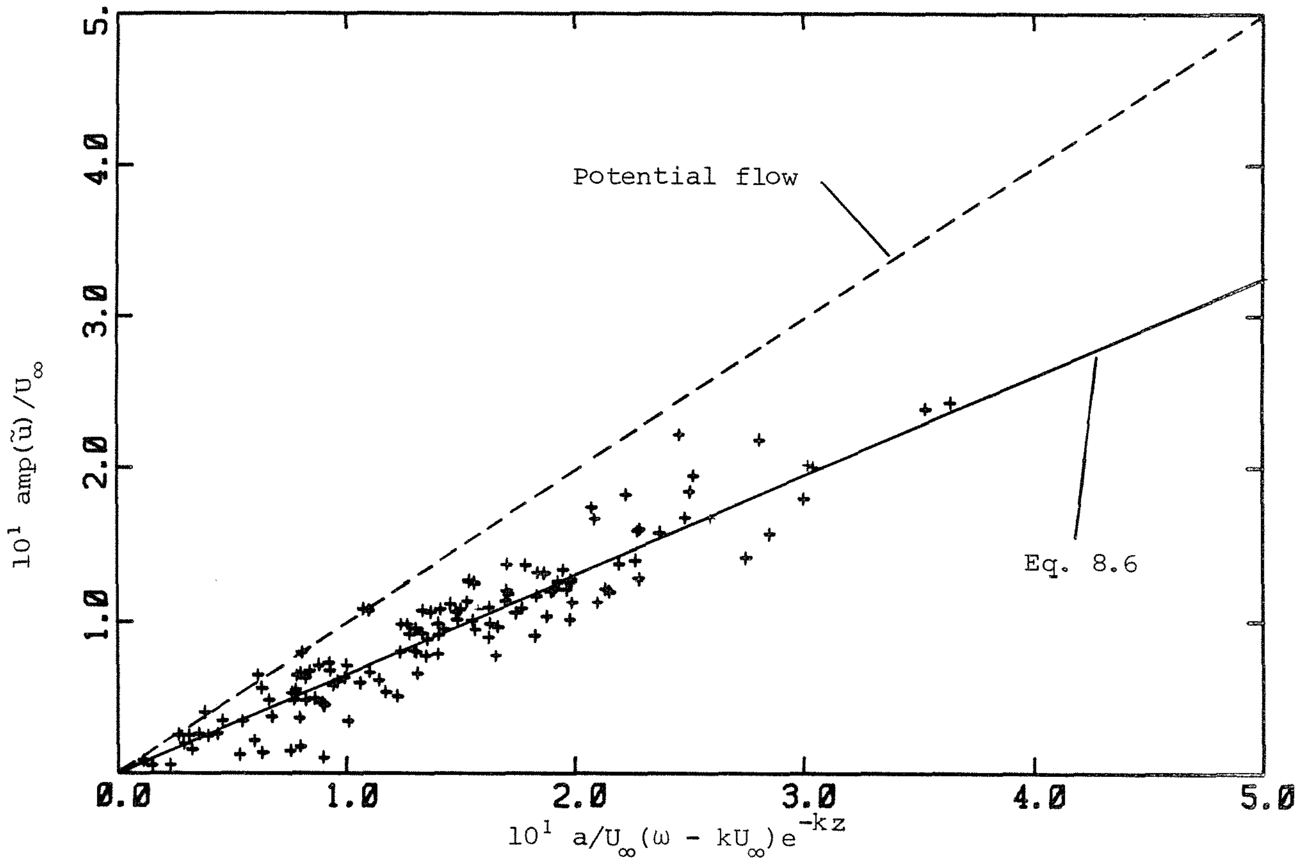

Figure 8.7 Wave induced velocity in the x direction in a stationary coordinate system as a function of the potential flow solution.

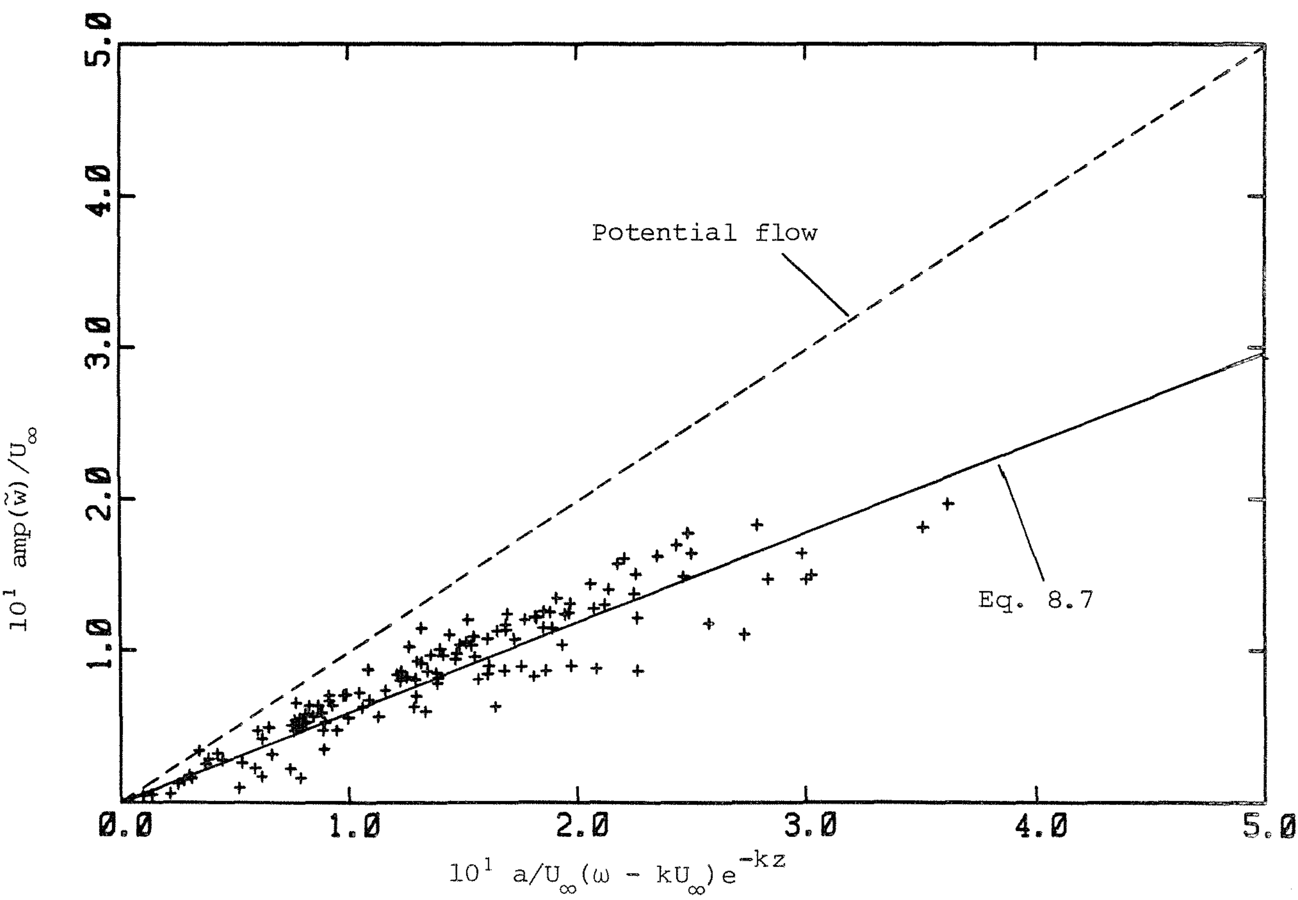

Figure 8.8 Wave induced velocity in the z direction in a stationary coordinate system as a function of the potential flow solution.

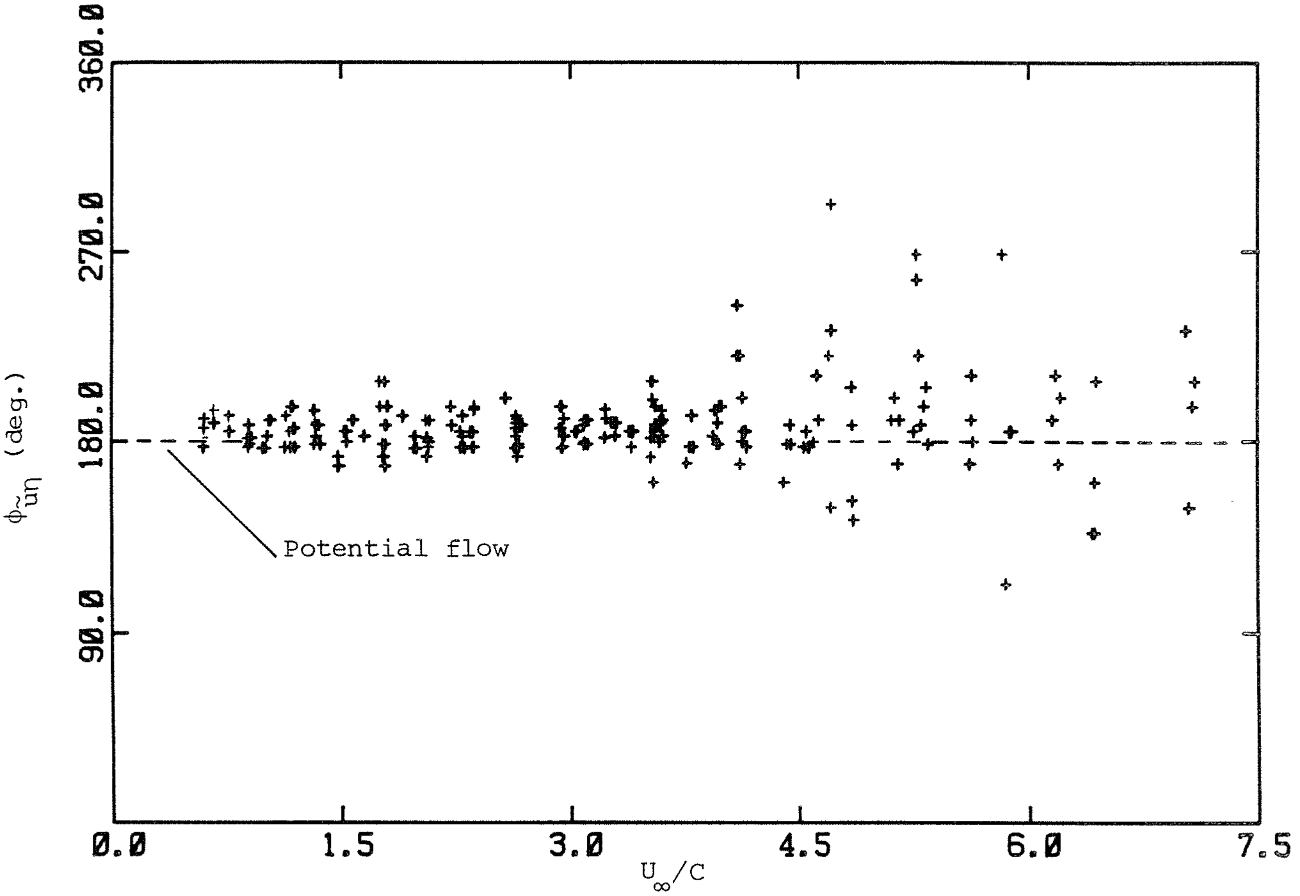

Figure 8.9 Phase angle between $\tilde{u}$ and η in a wave following coordinate system as a function of U_∞/C.

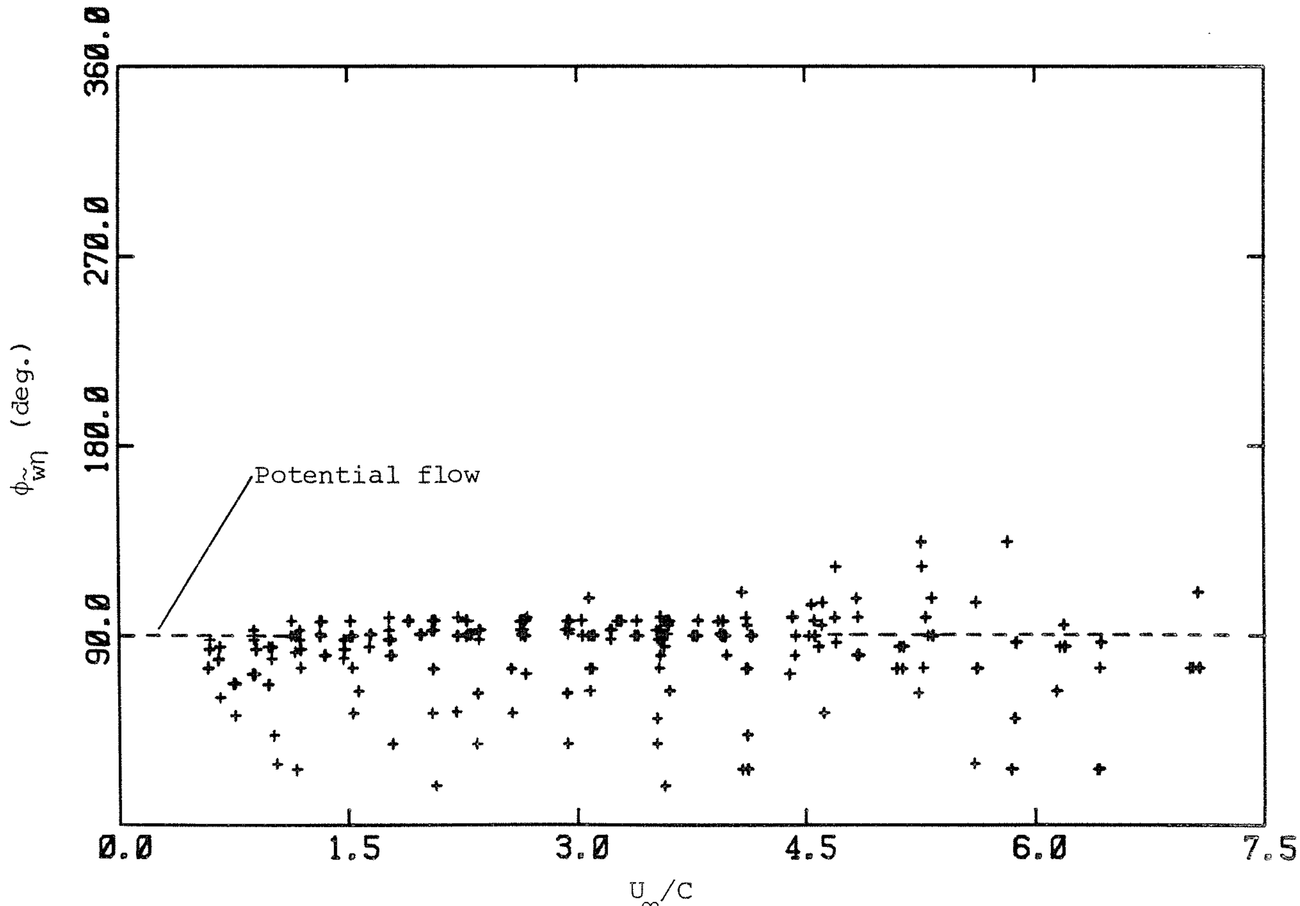

Figure 8.10 Phase angle between $\tilde{w}$ and η in a wave following coordinate system as a function of U_∞/C.

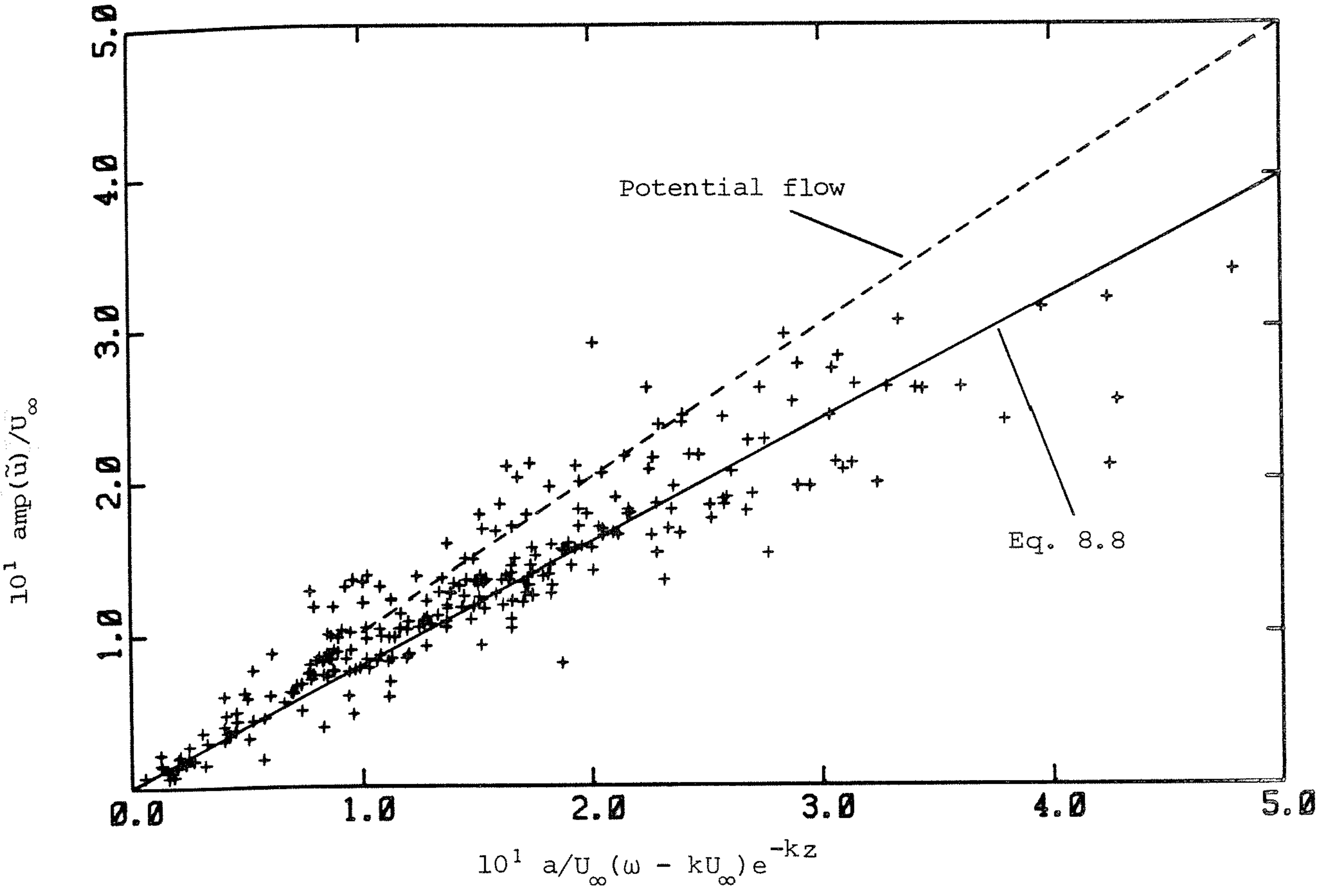

Figure 8.11 Wave induced velocity in the x direction in a wave following coordinate system as a function of the potential flow solution.

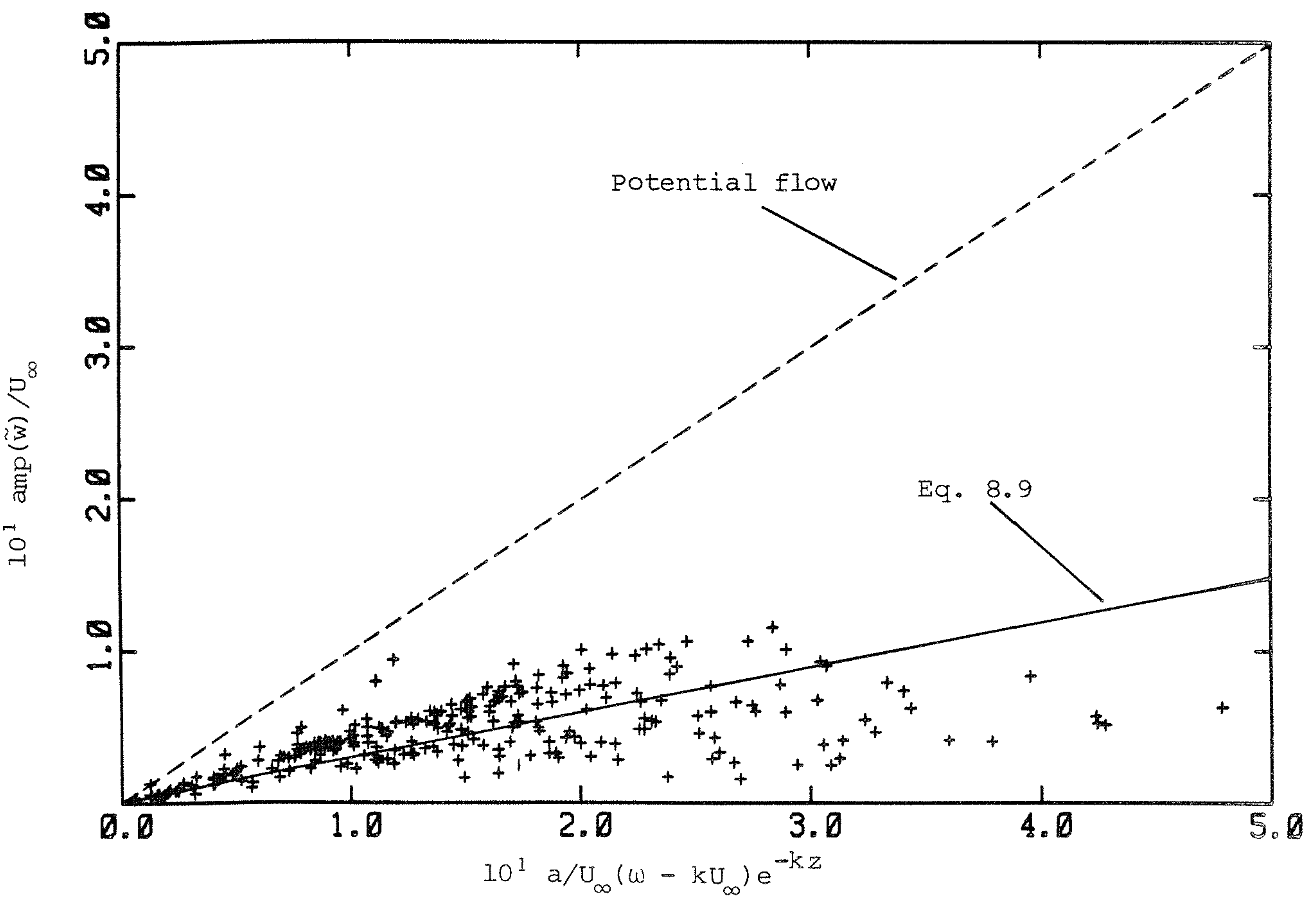

Figure 8.12 Wave induced velocity in the z direction in a wave following coordinate system as a function of the potential flow solution.

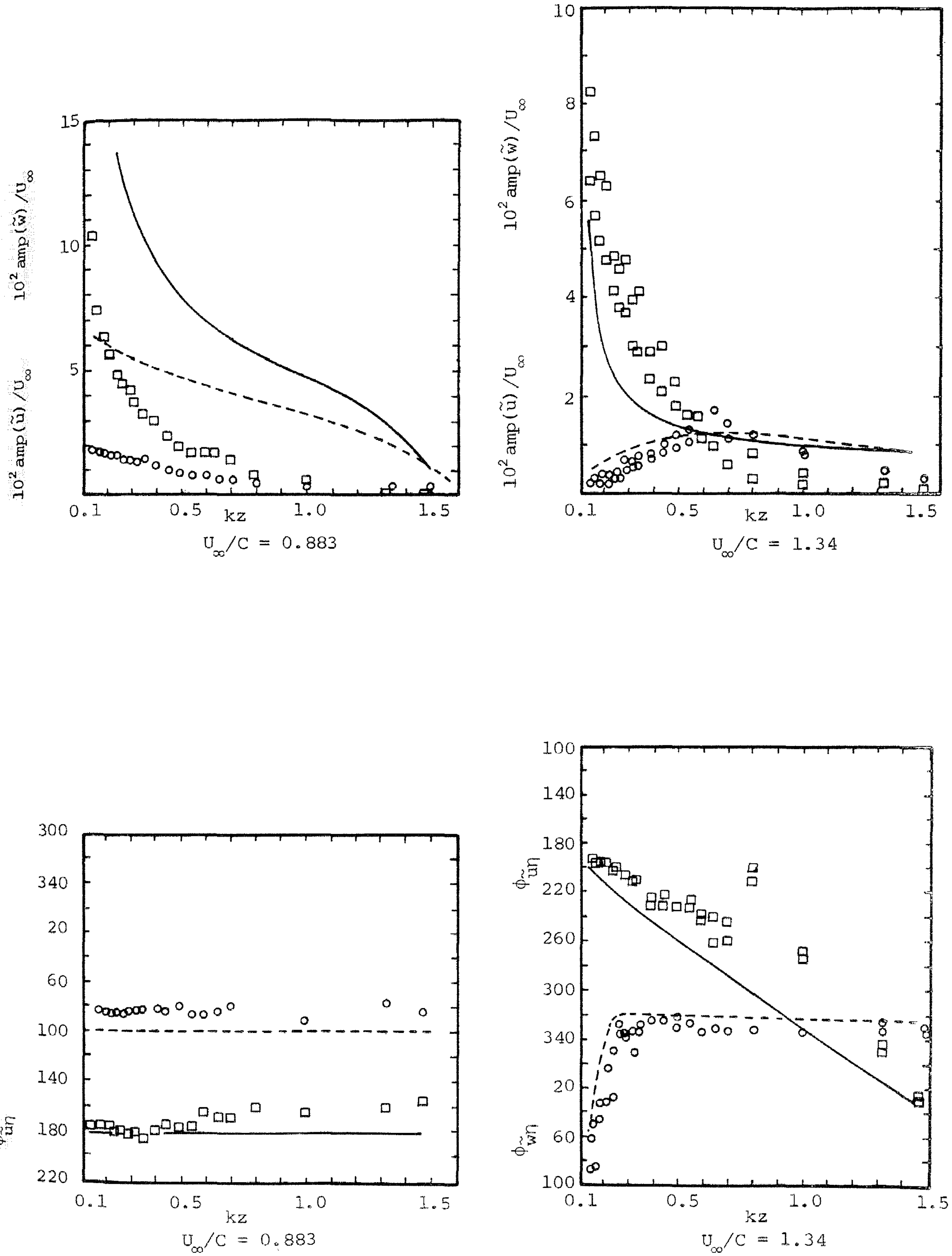

Figure 8.13 Wave induced velocities for $U_\infty/C > 1$ and $U_\infty/C < 1$. □ ○ Chao and Hsu (21), ——— - - - - Stewart (123).

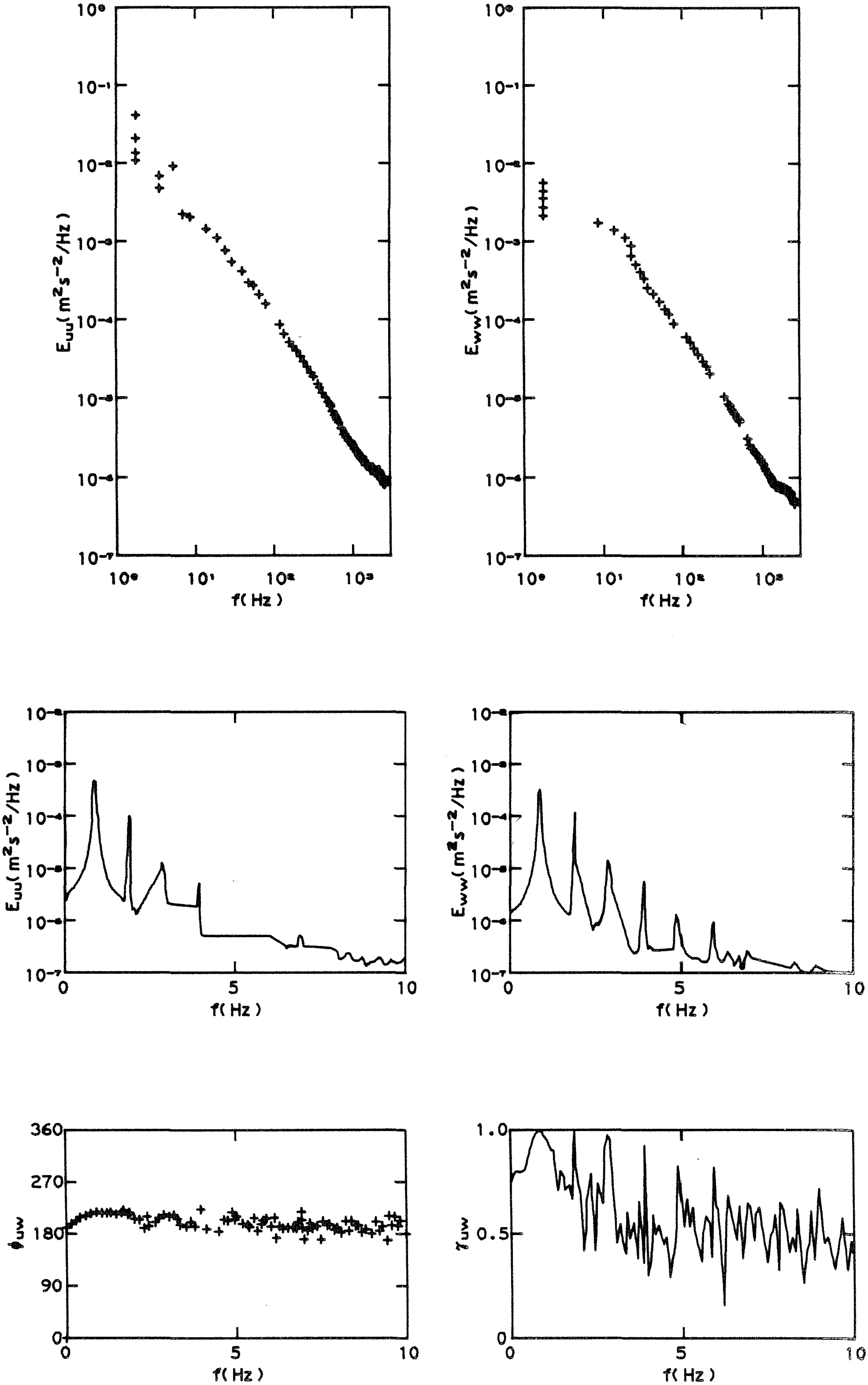

Figure 8.14a   Spectra, phase and coherence results for 1 Hz waves and a fan speed of 100 rpm.

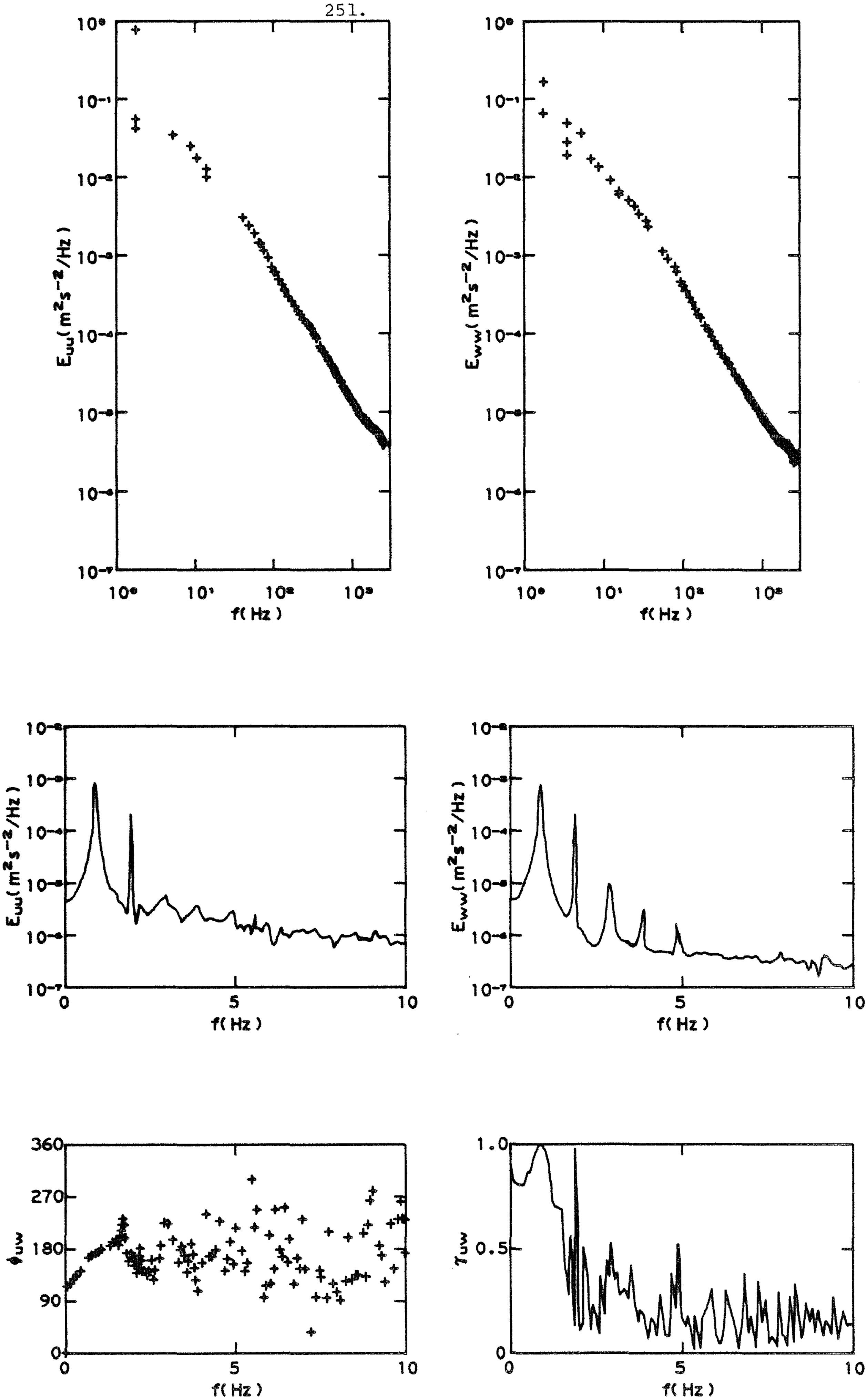

Figure 8.14b Spectra, phase and coherence results for 1 Hz waves and a fan speed of 200 rpm.

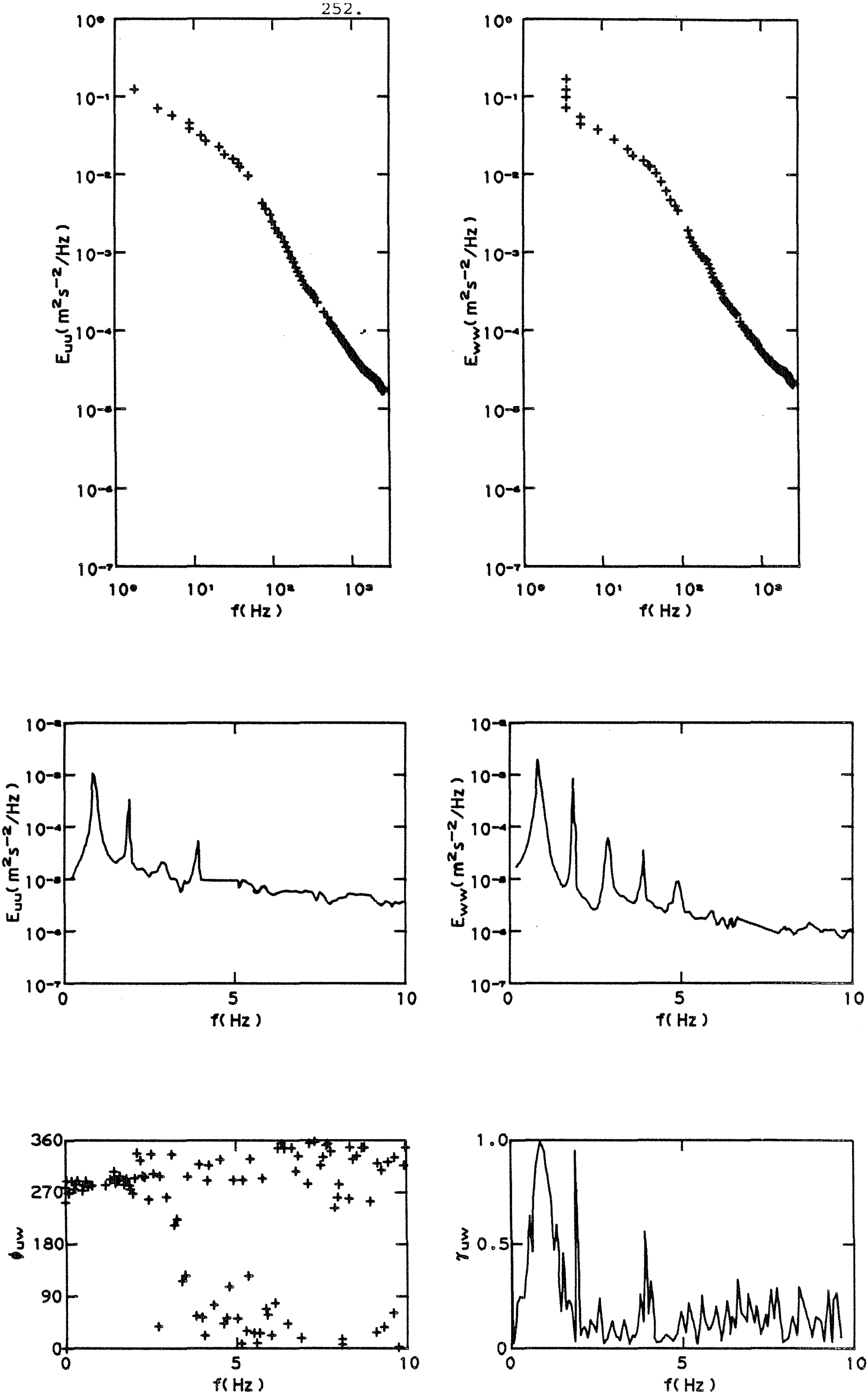

Figure 8.14c Spectra, phase and coherence results for 1 Hz waves and a fan speed of 300 rpm.

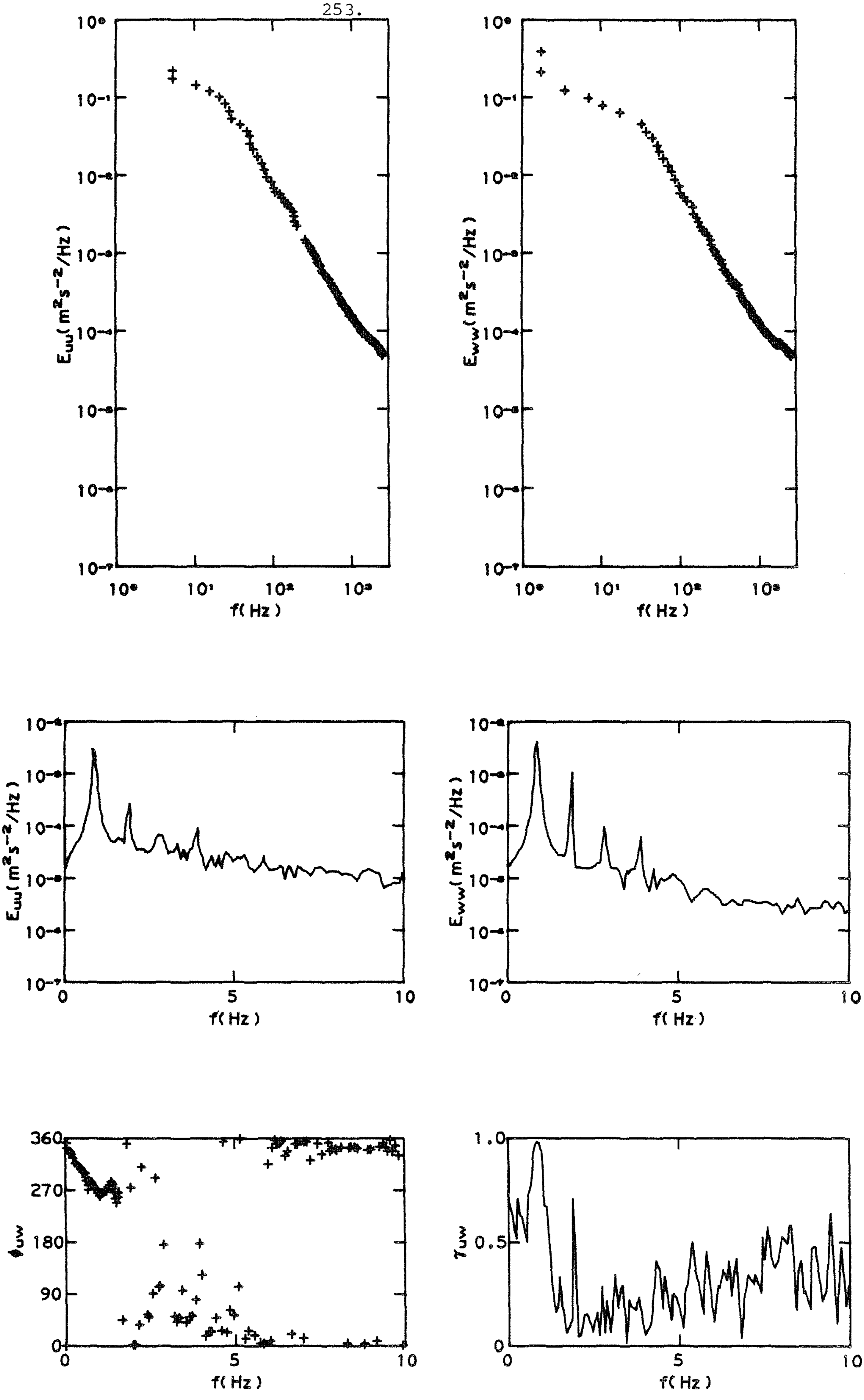

Figure 8.14d Spectra, phase and coherence results for 1 Hz waves and a fan speed of 400 rpm.

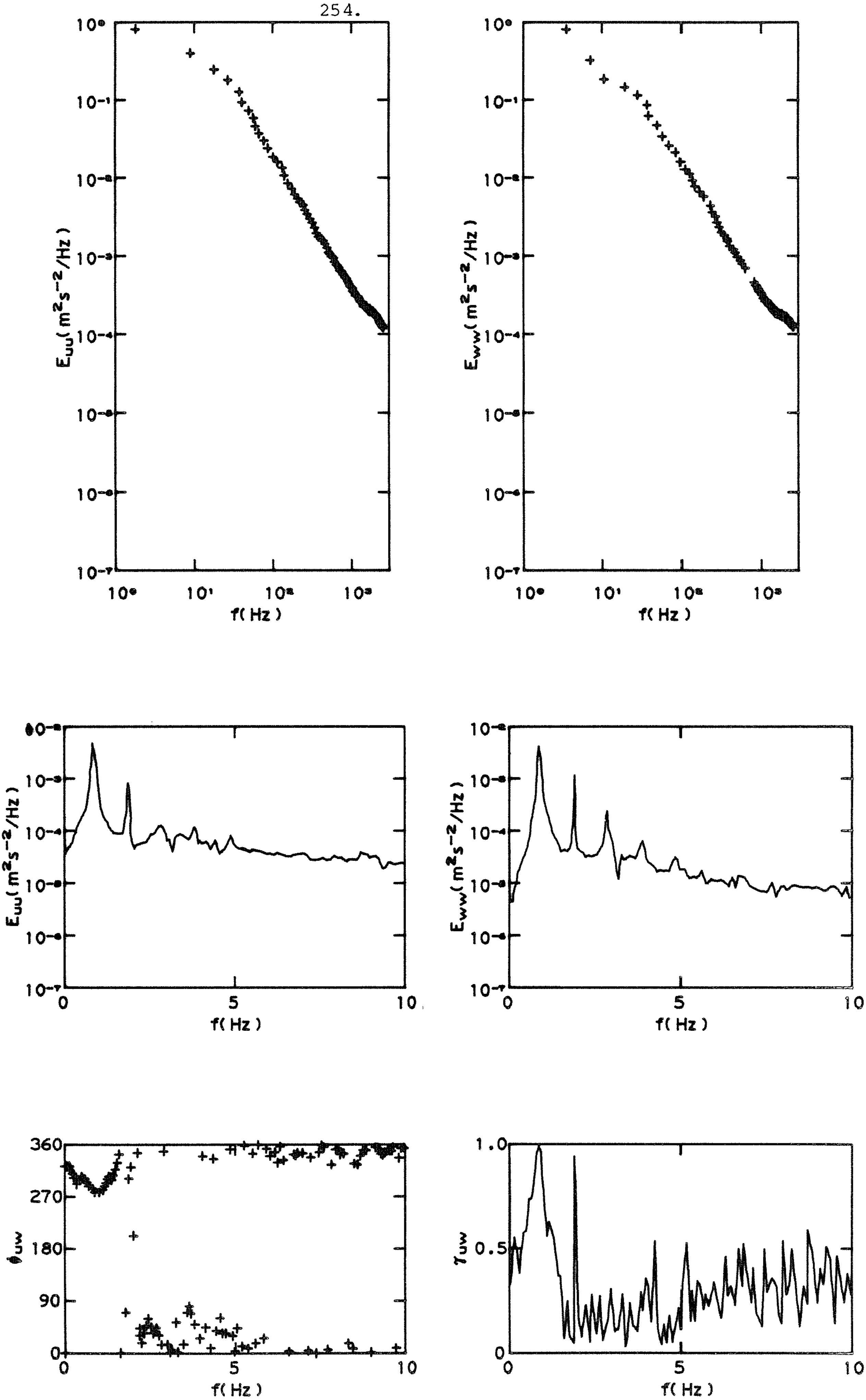

Figure 8.14e Spectra, phase and coherence results for 1 Hz waves and a fan speed of 500 rpm.

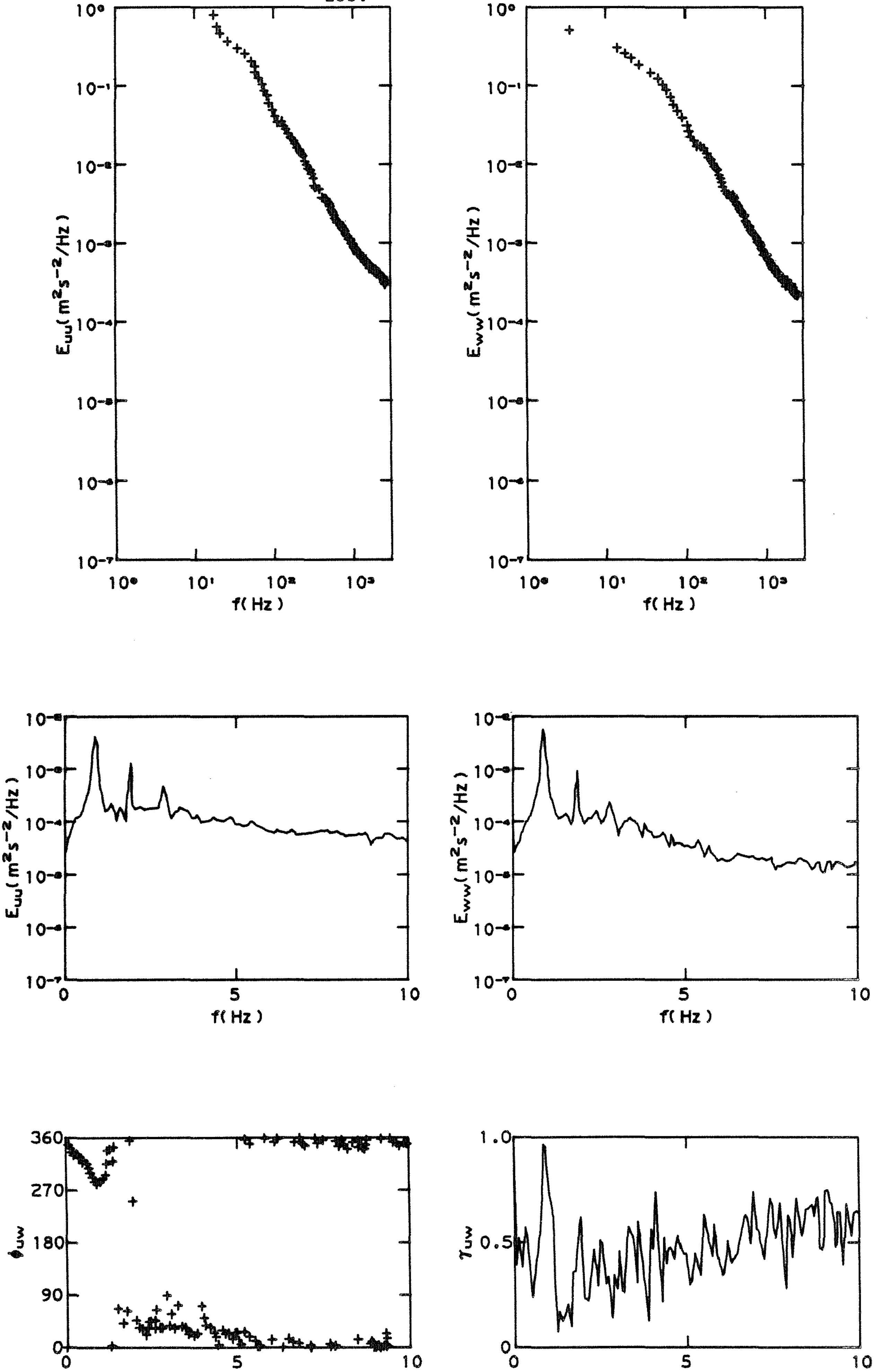

Figure 8.14f Spectra, phase and coherence results for 1 Hz waves and a fan speed of 600 rpm.

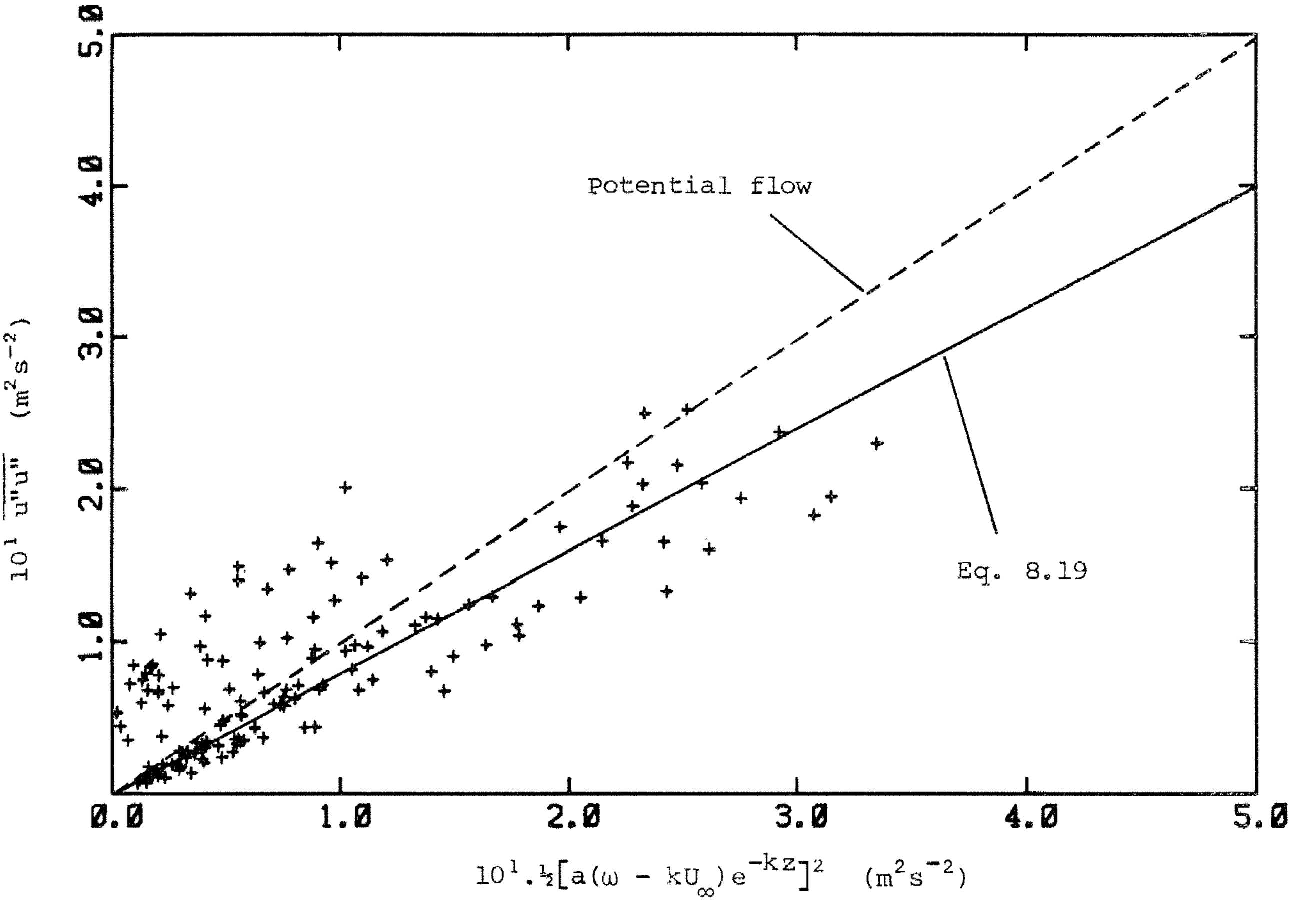

Figure 8.15 The total Reynolds stress $\overline{u''u''}$ as a function of the wave induced Reynolds stress predicted by potential theory. (stationary coordinate system).

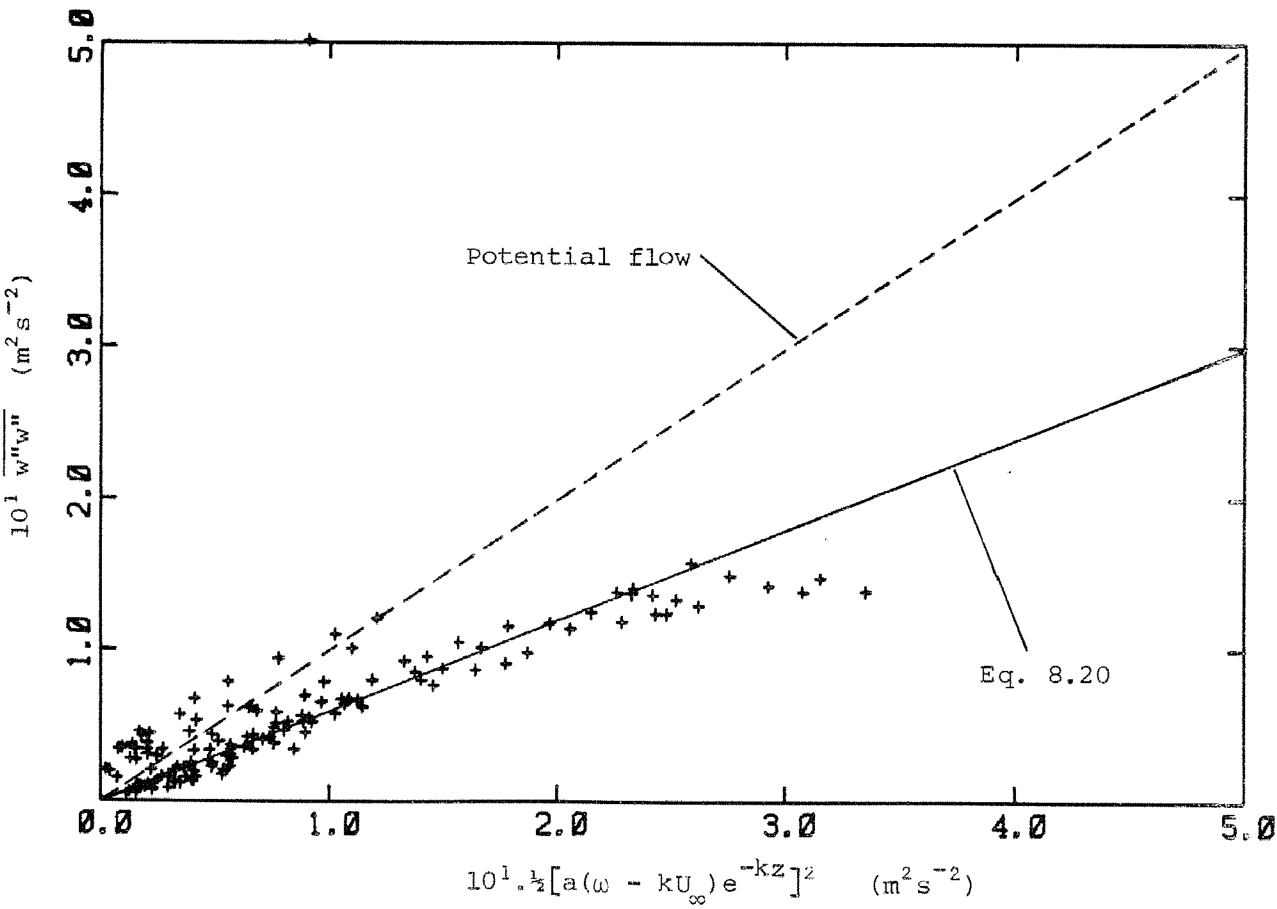

Figure 8.16 The total Reynolds stress $\overline{w''w''}$ as a function of the wave induced Reynolds stress predicted by potential coordinate system).

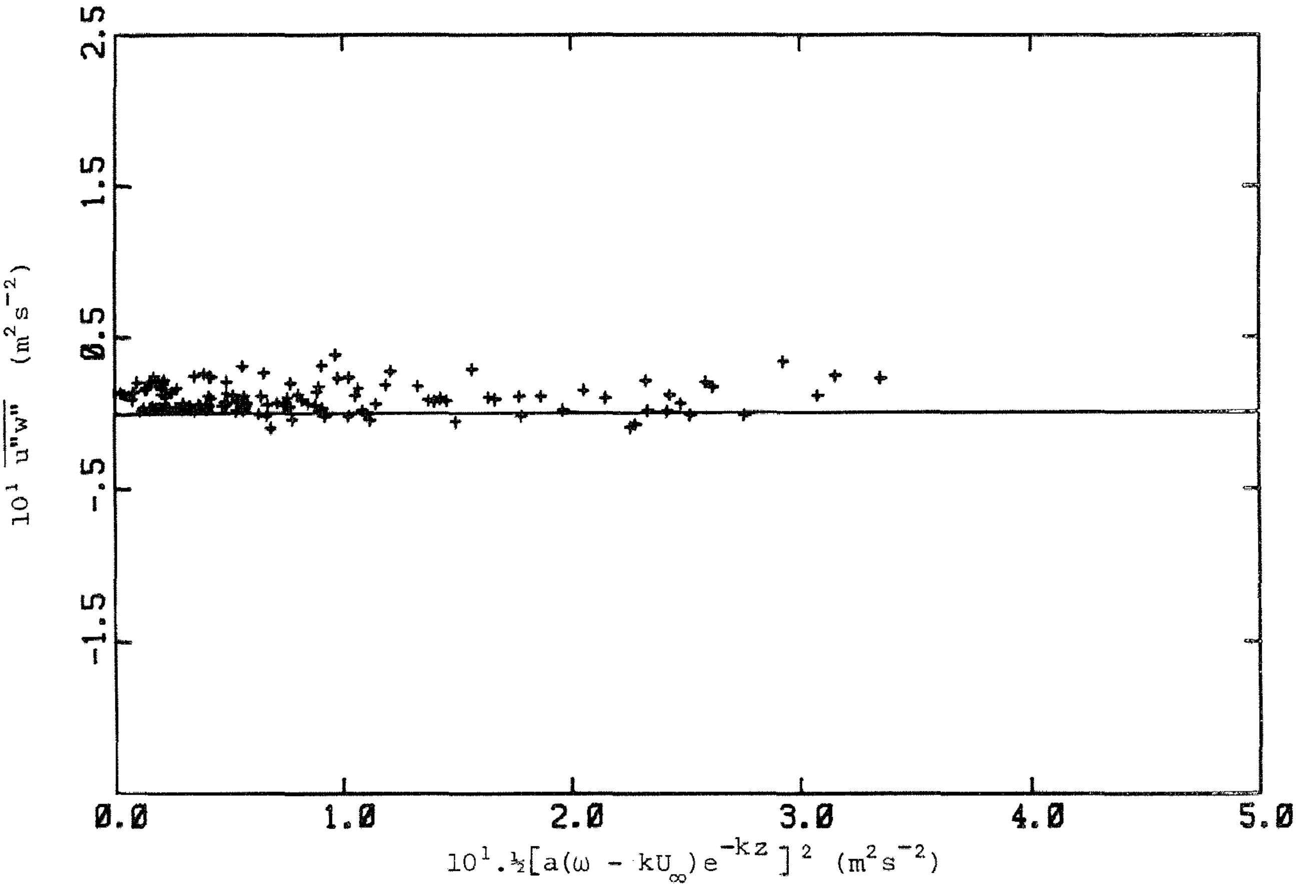

Figure 8.17 The total Reynolds stress $\overline{u''w''}$ as a function of the wave induced velocity function squared. (stationary coordinate system).

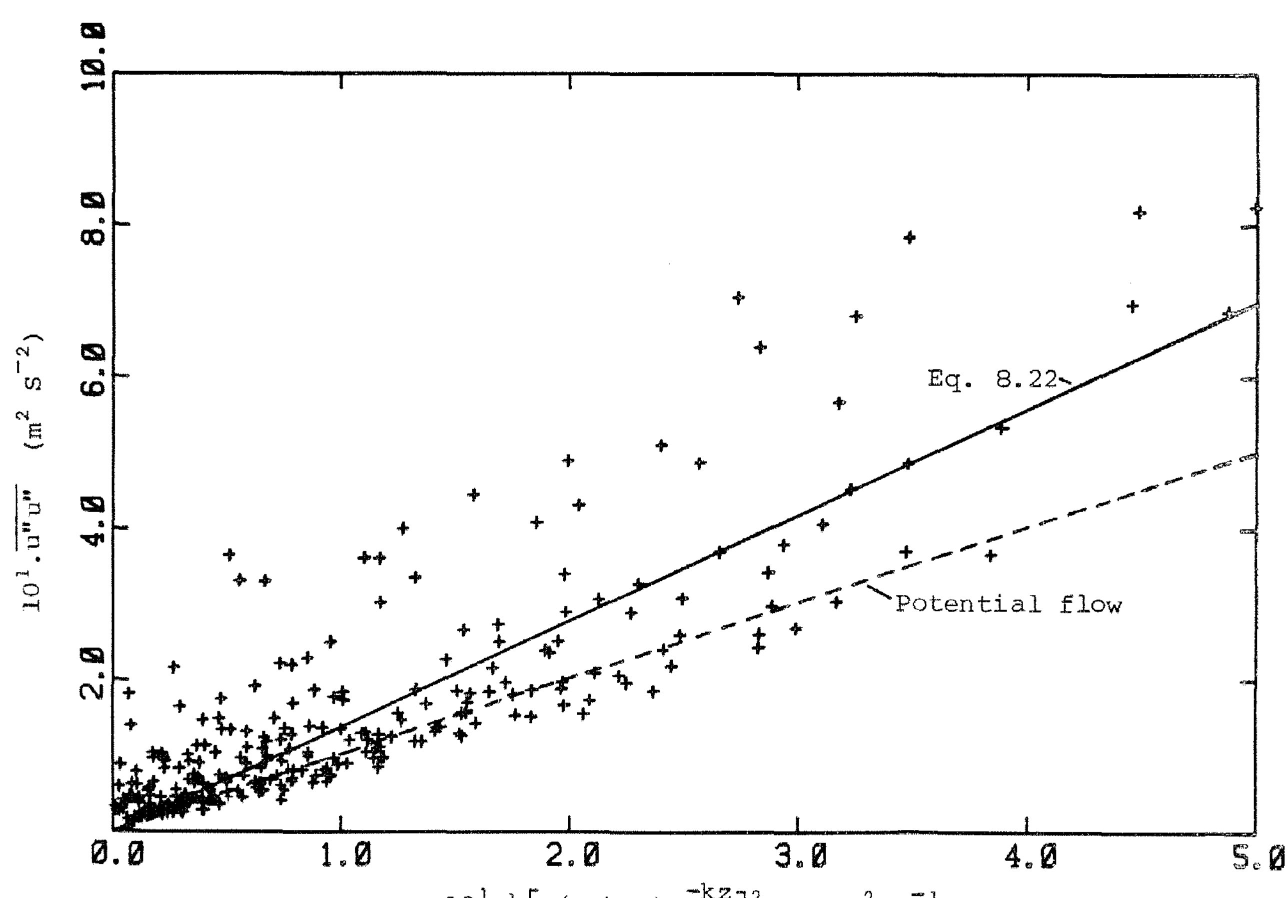

Figure 8.18 The total Reynolds stress $\overline{u''u''}$ as a function of the wave-induced Reynolds stress predicted by potential theory. (Wave following coordinate system).

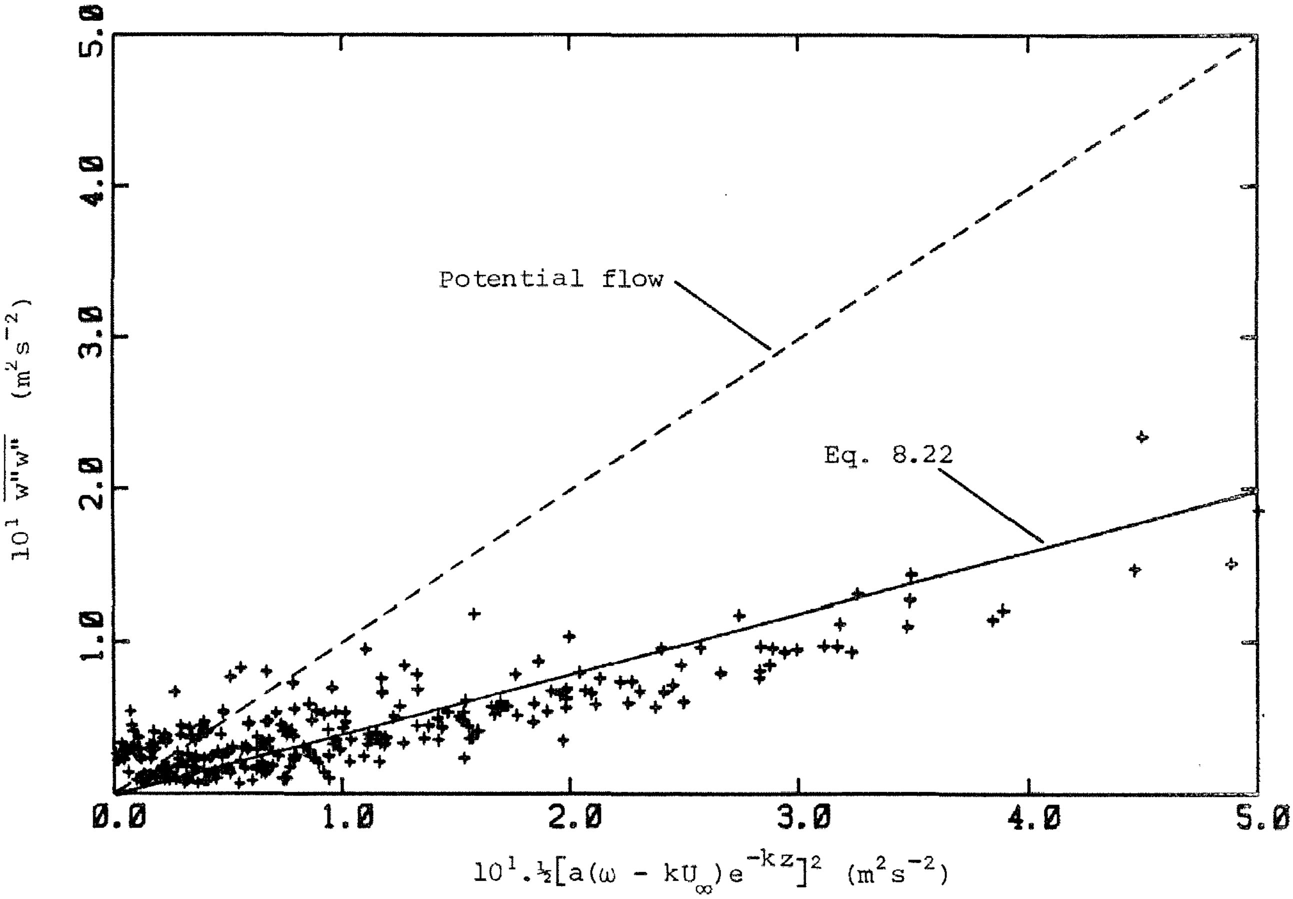

Figure 8.19 The total Reynolds stress $\overline{w''w''}$ as a function of the wave induced Reynolds stress predicted by potential theory. (wave following coordinate system).

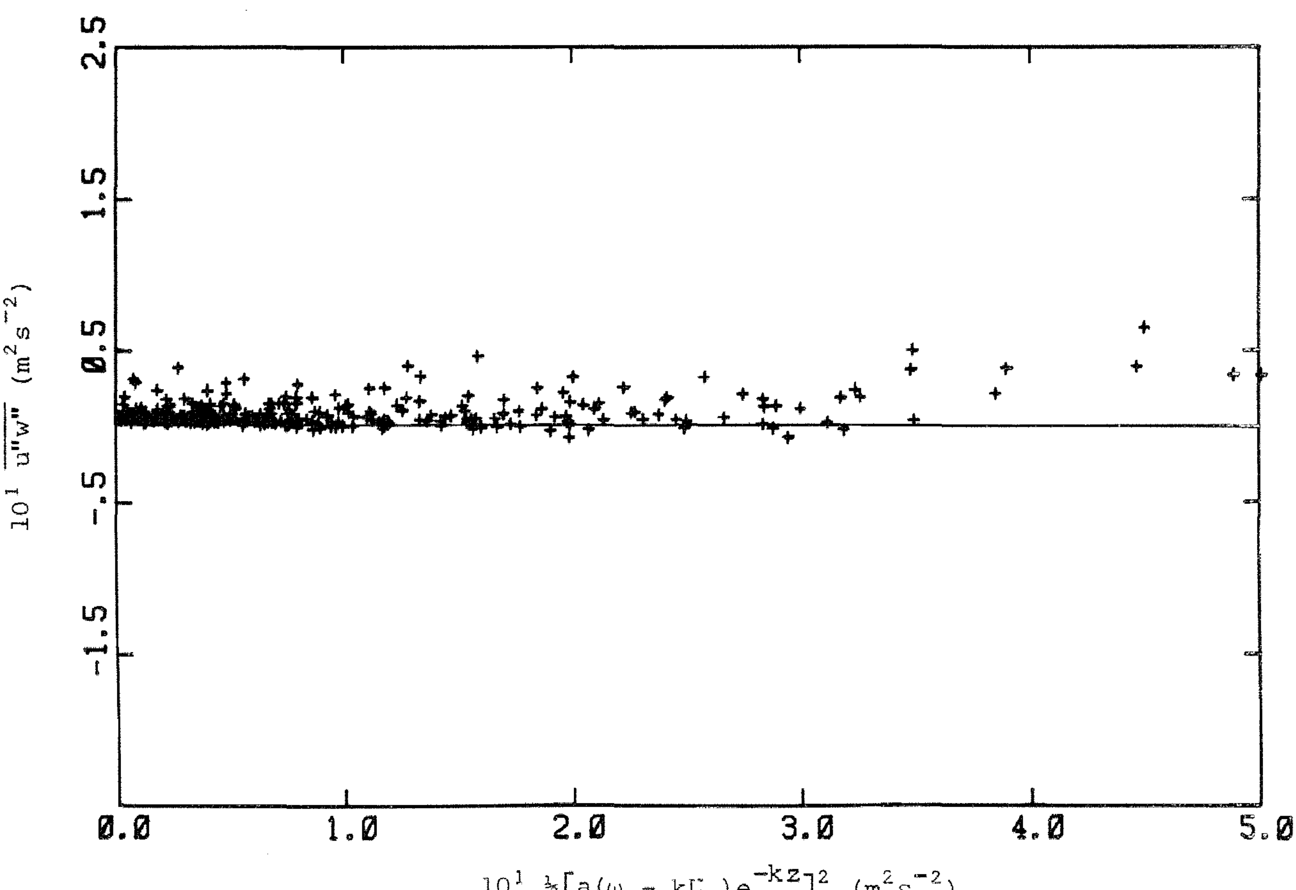

Figure 8.20 The total Reynolds stress $\overline{u''w''}$ as a function of the wave induced velocity function squared. (wave following coordinate system).

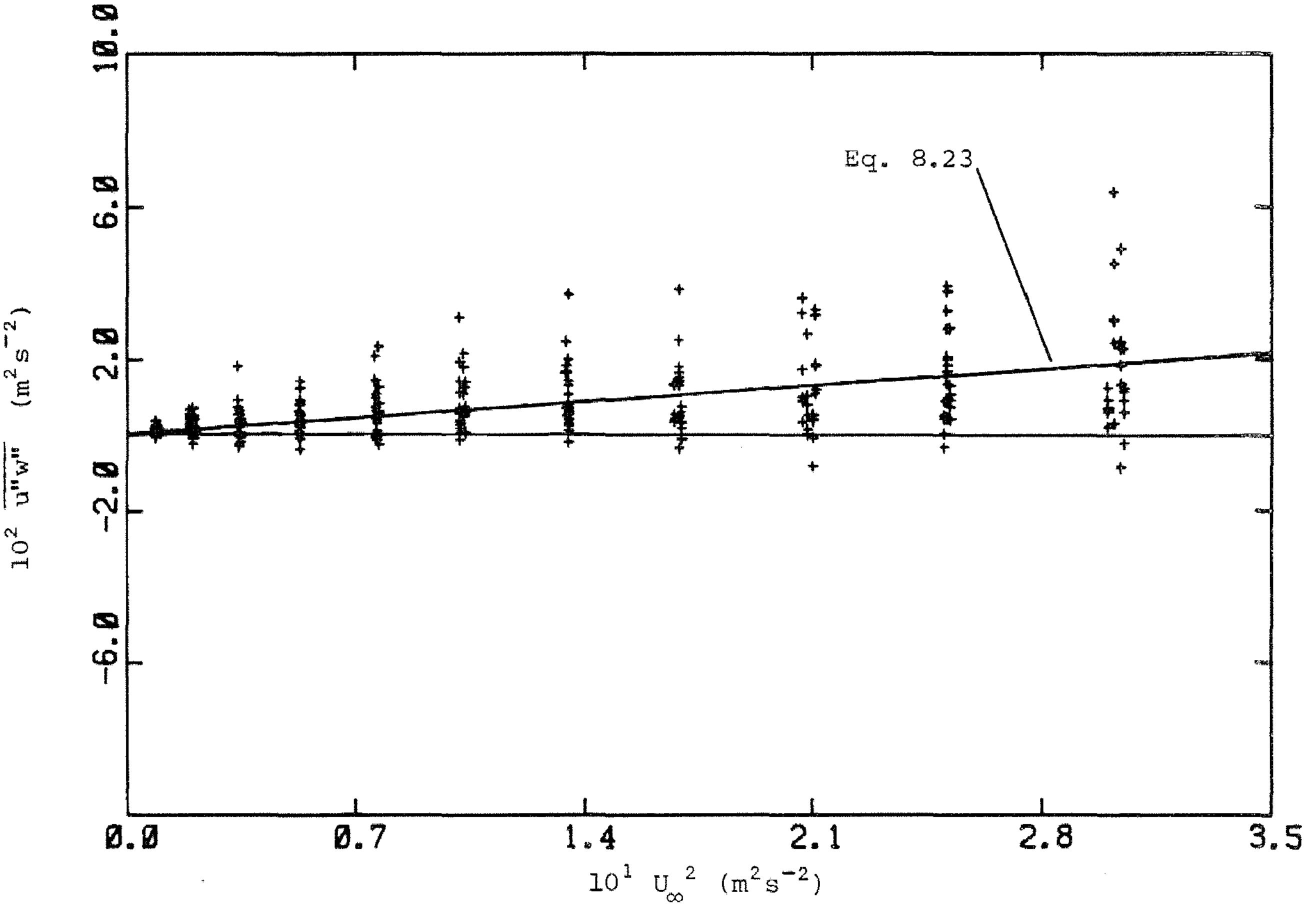

Figure 8.21 The total Reynolds stress $\overline{u''w''}$ as a function of U_∞^2 (wave following coordinate system).

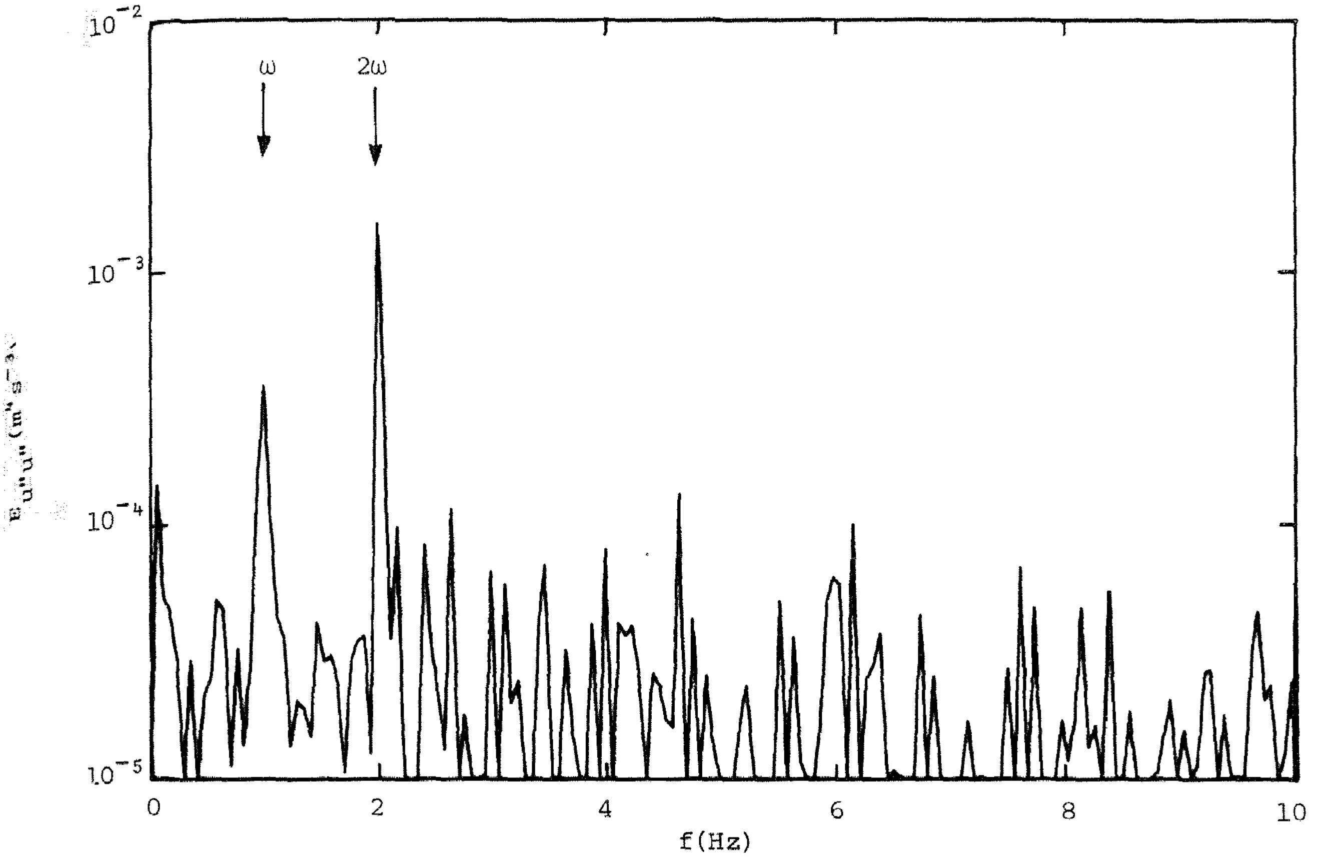

Figure 8.22a Spectrum of the product u"u".

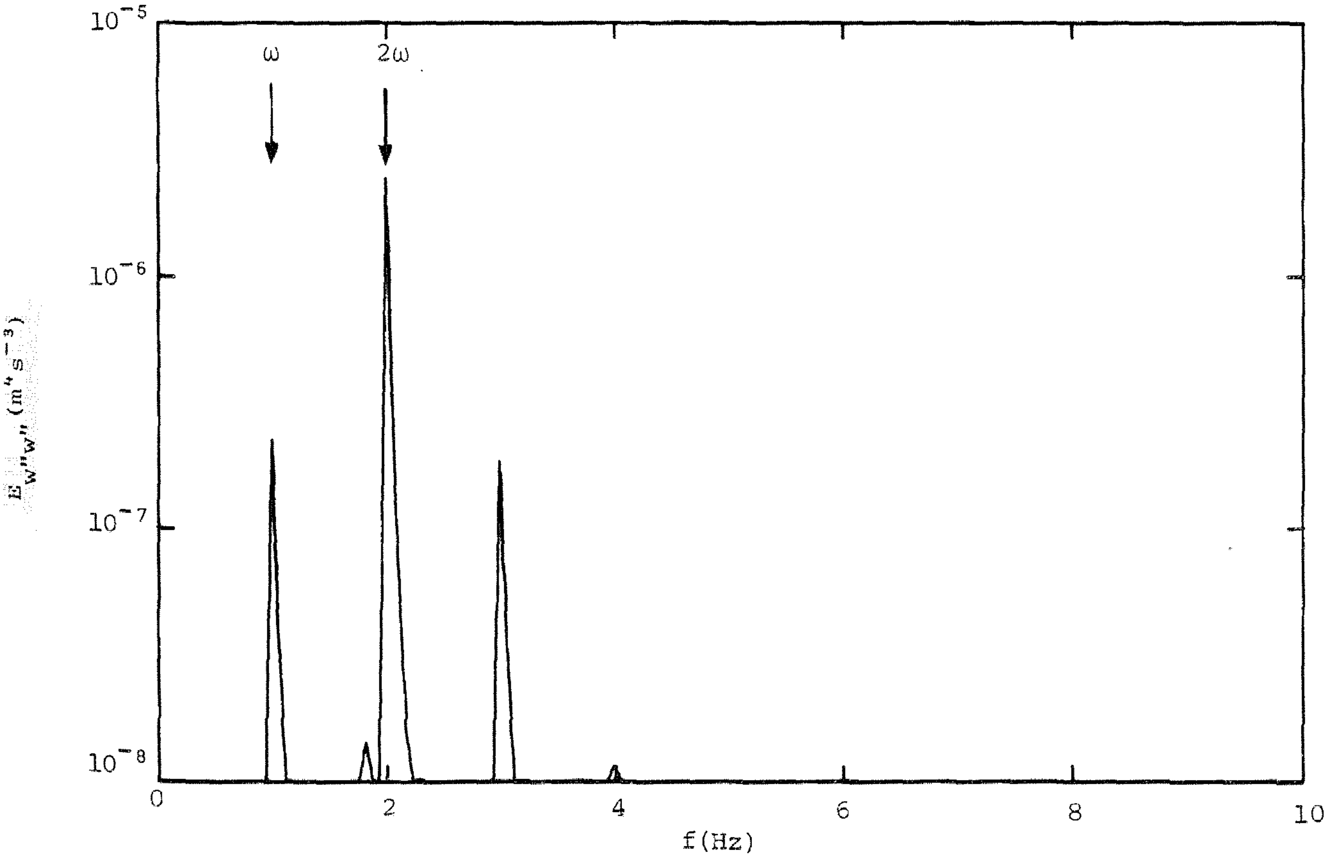

Figure 8.22b Spectrum of the product w"w".

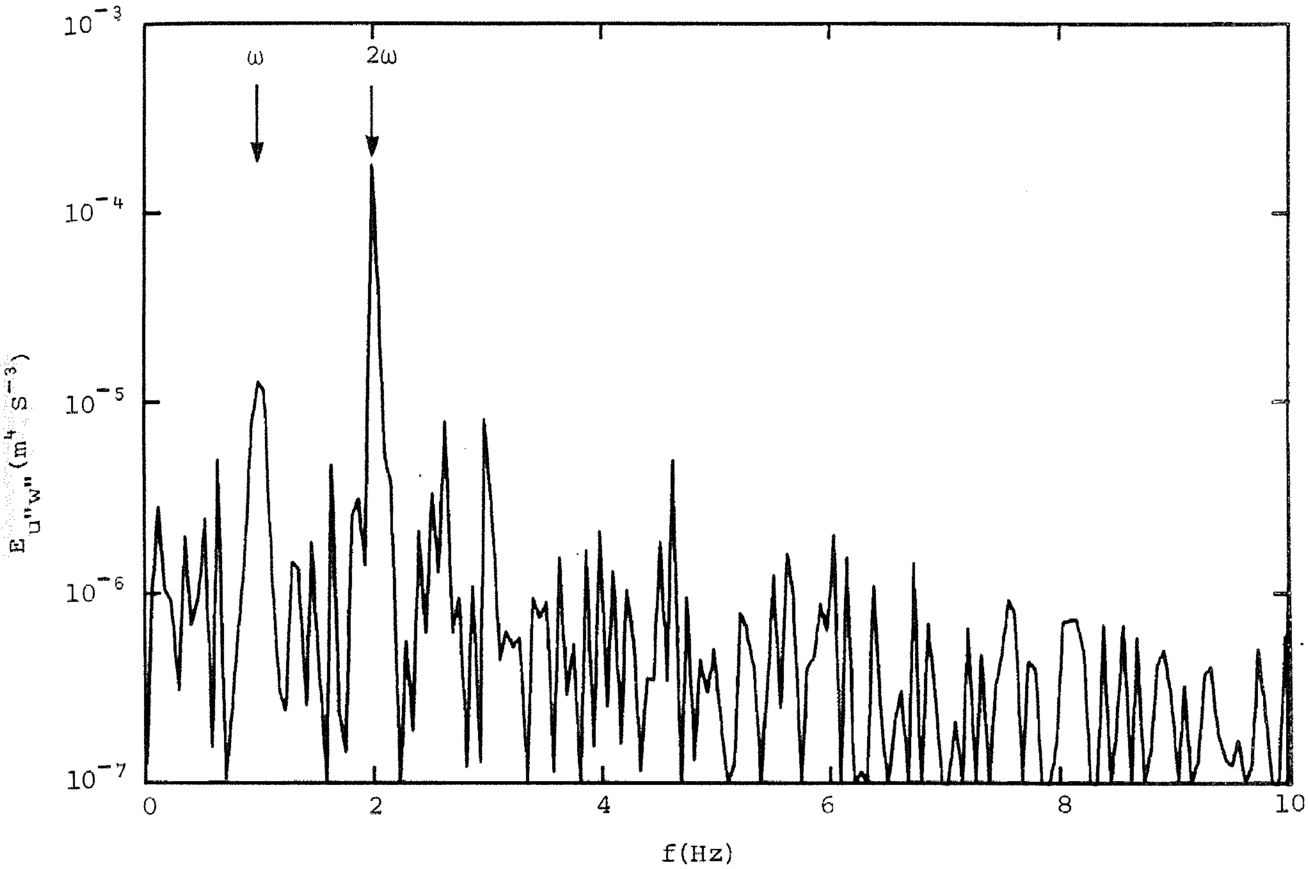

Figure 8.22c Spectrum of the product u"w".

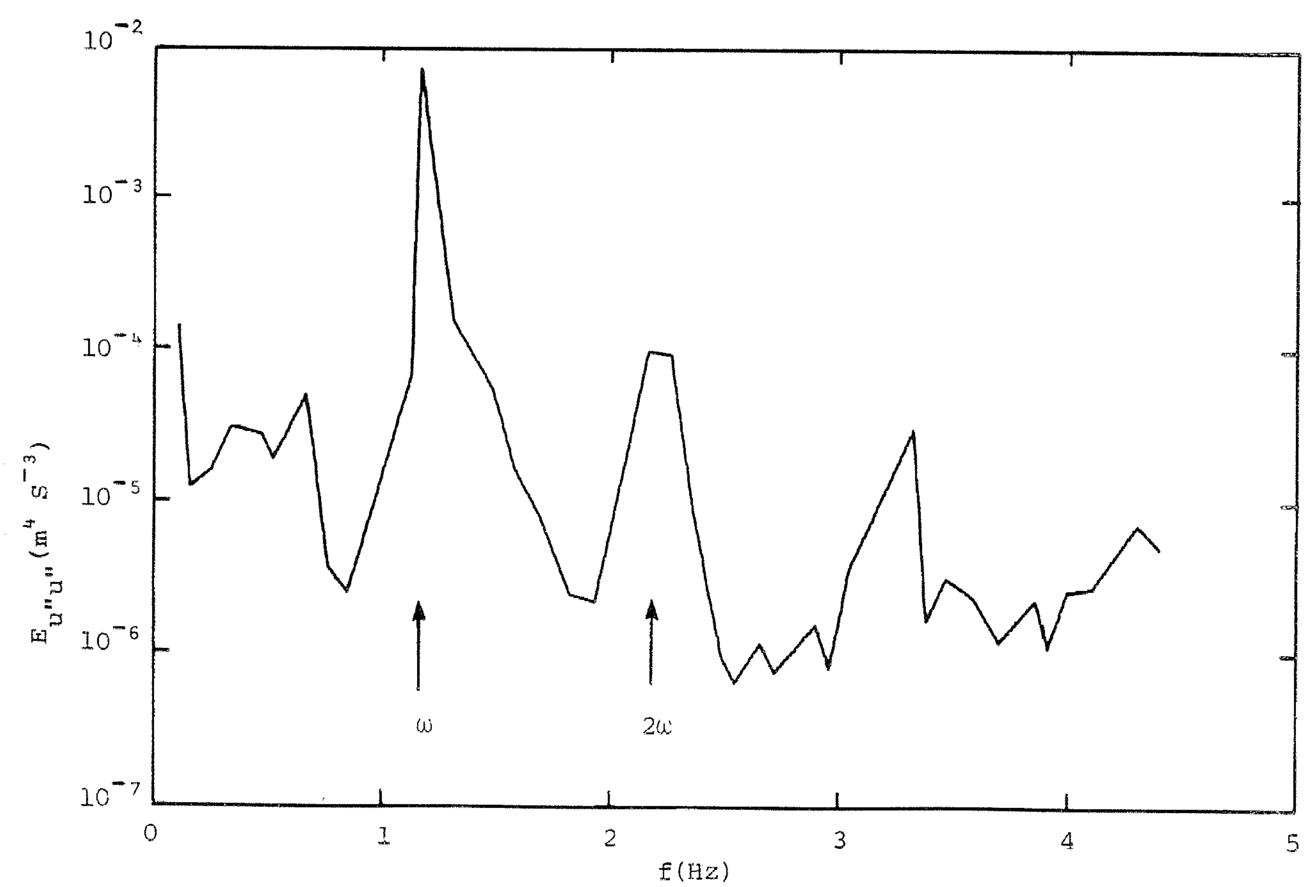

Figure 8.22d Spectrum of the momentum flux term u"w" in a following wind. [after Chao and Hsu (21)].

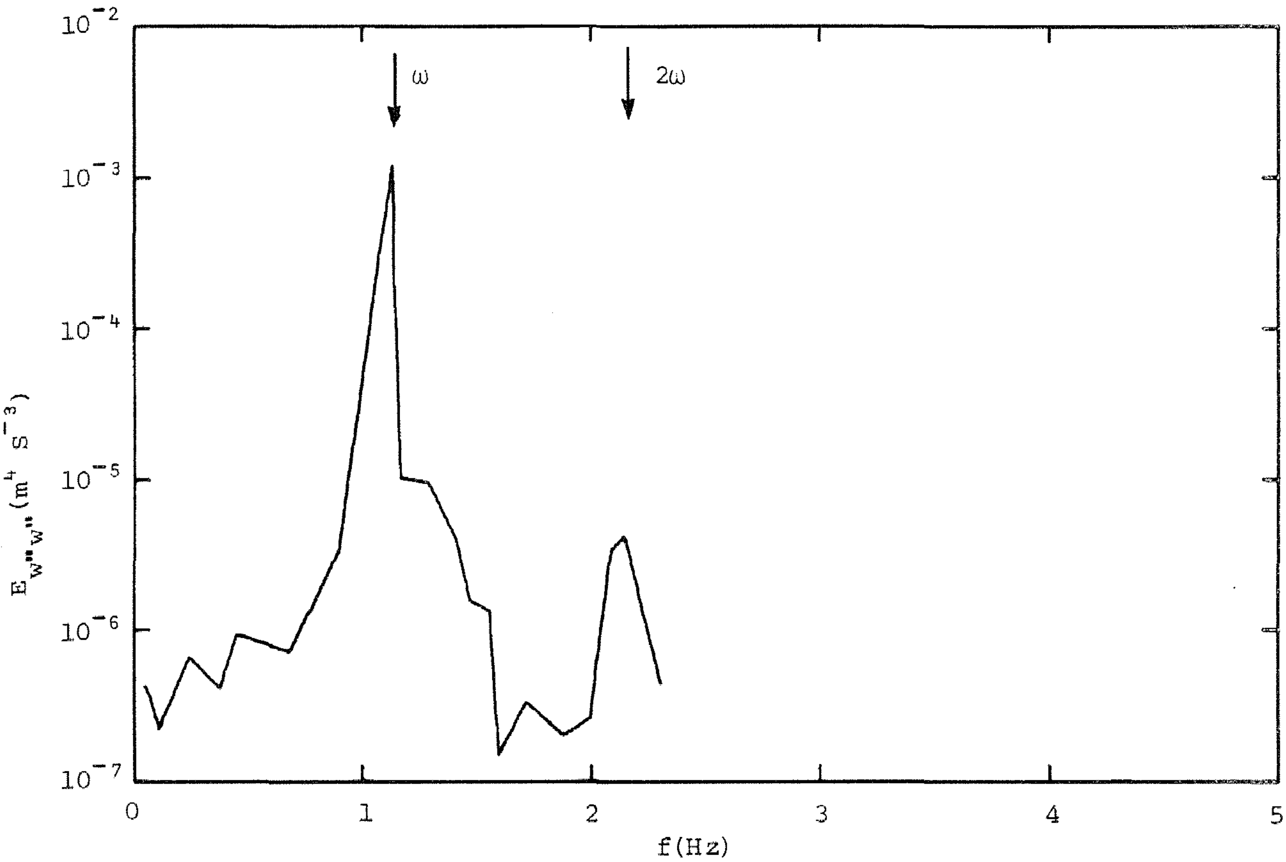

Figure 8.22e Spectrum of the momentum flux term w"w" in a following wind. [after Chao and Hsu (21)].

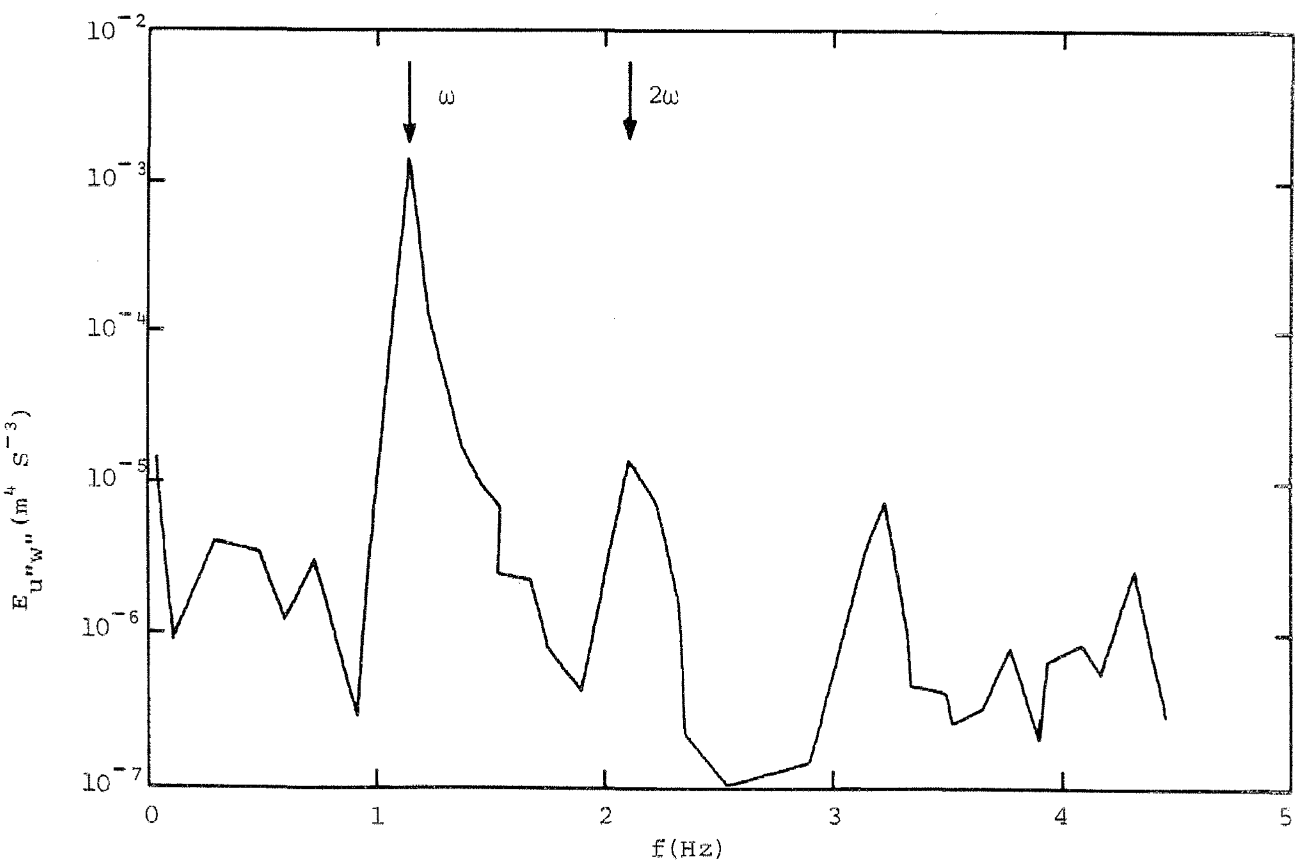

Figure 8.22f Spectrum of the momentum flux term u"w" in a following wind. [after Chao and Hsu (21)].

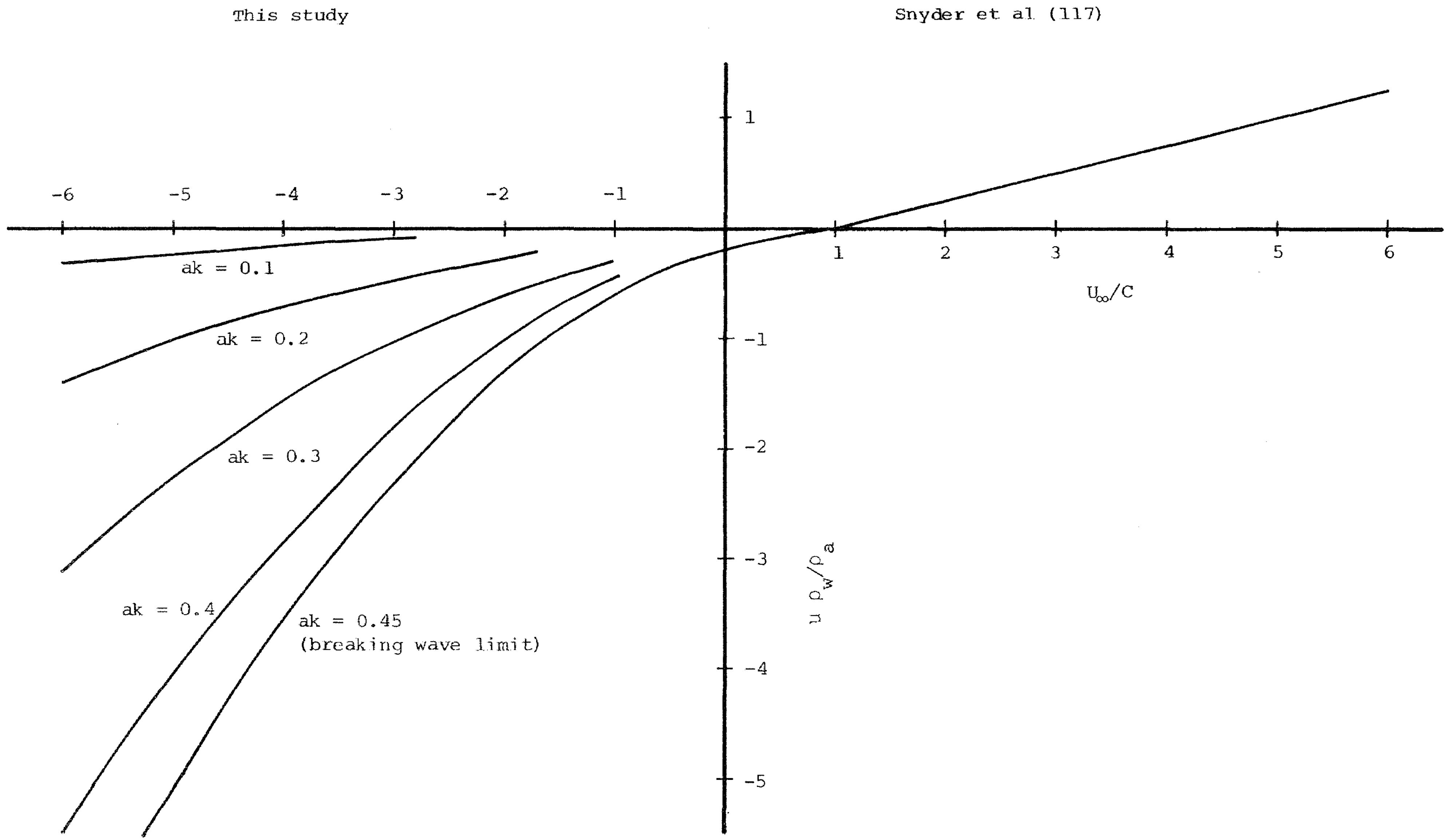

Figure 9.1 The exponential coupling coefficient, μ for following and opposing winds.

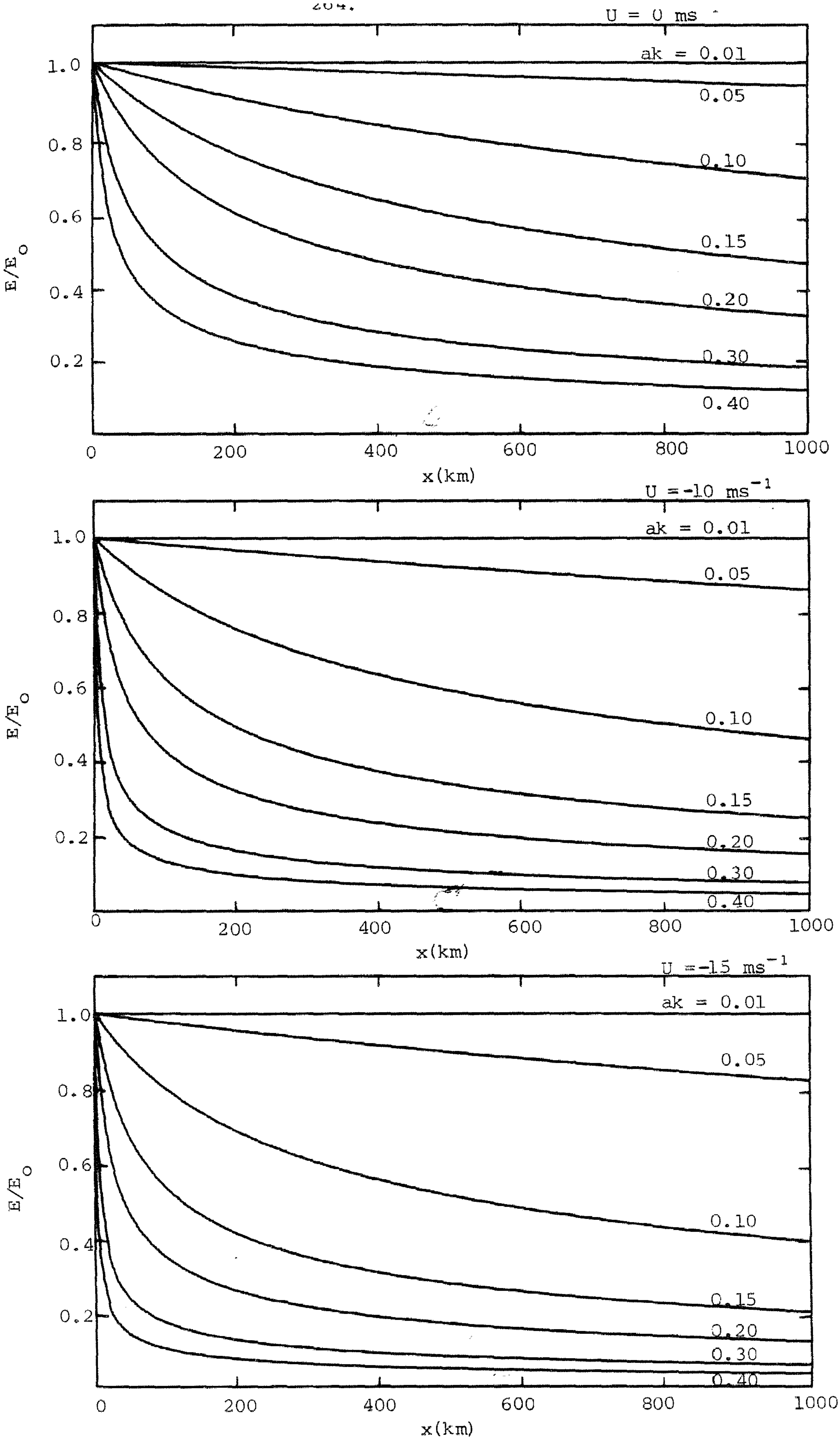

Figure 9.2a Wave decay in an opposing wind as a function of fetch.

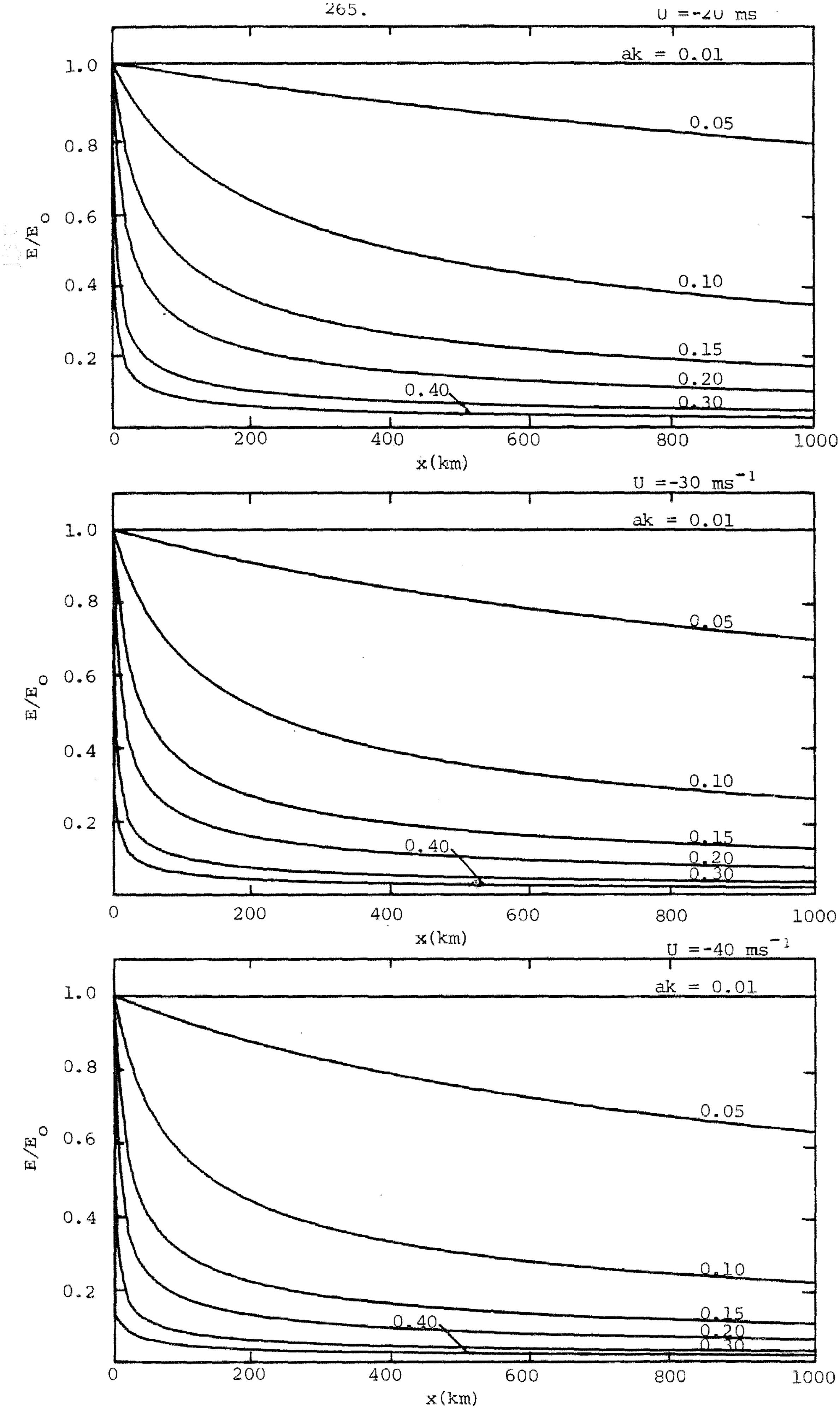

Figure 9.2b Wave decay in an opposing wind as a function of fetch.

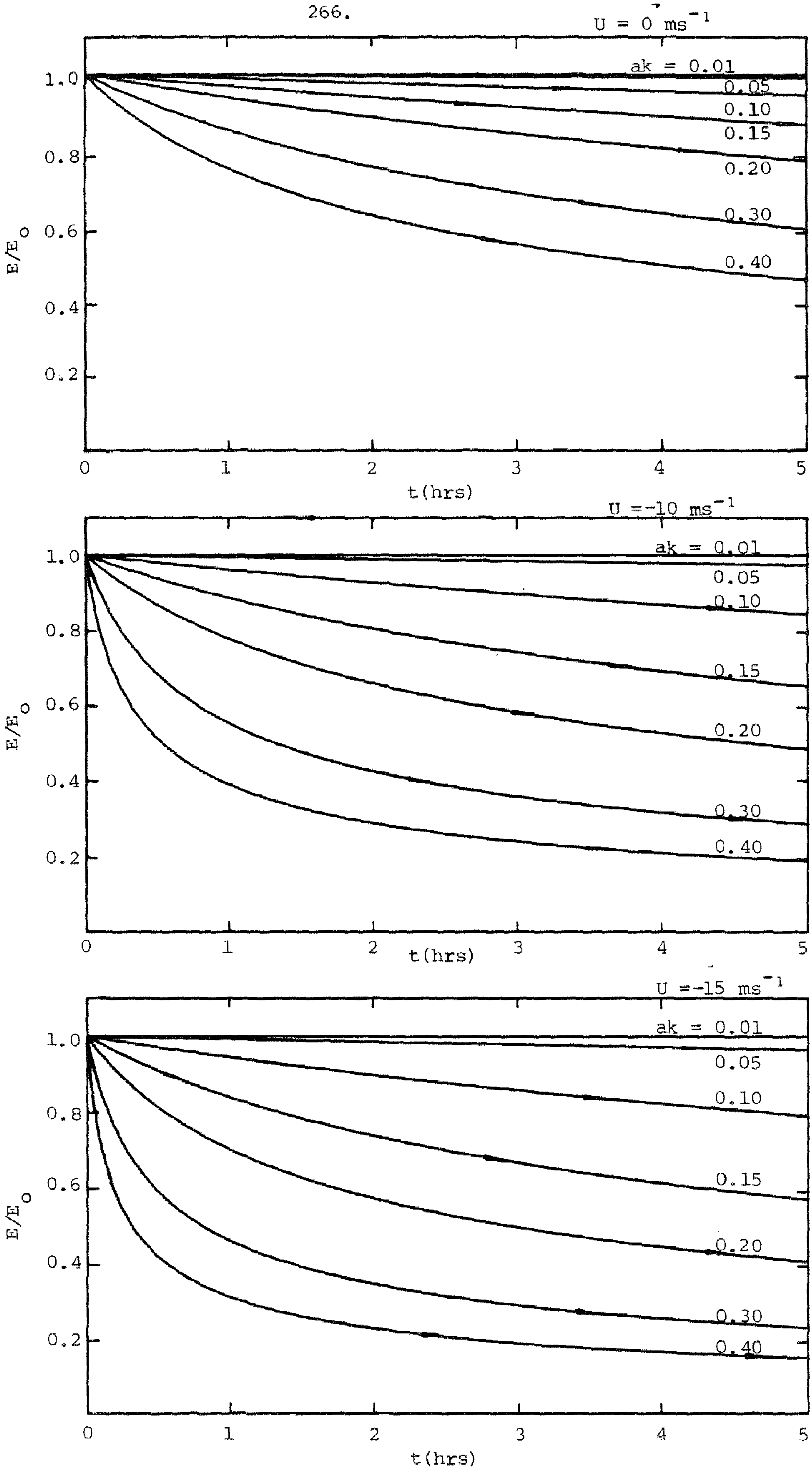

Figure 9.2c Wave decay in an opposing wind as a function of duration.

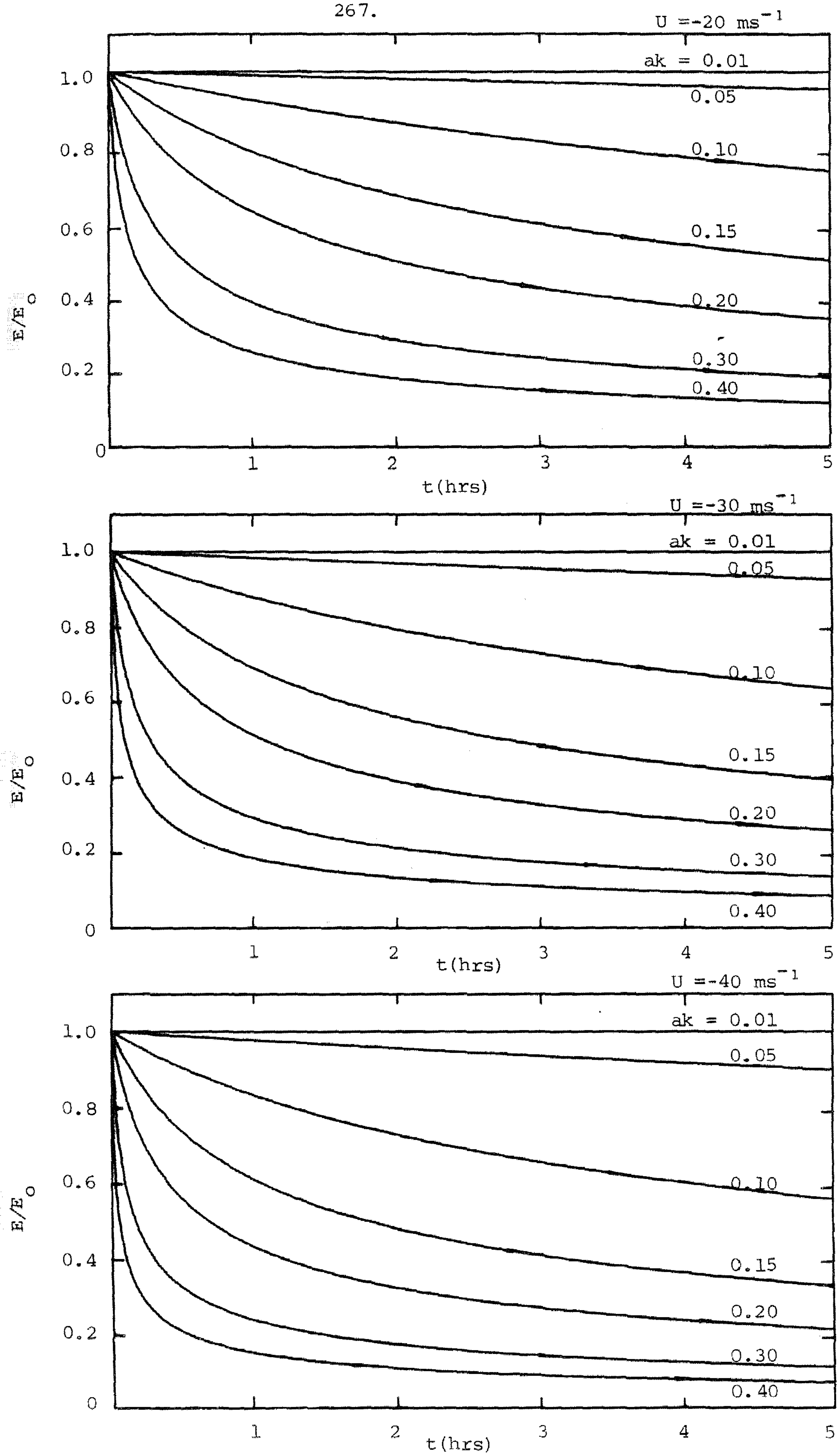

Figure 9.2d Wave decay in an opposing wind as a function of duration.

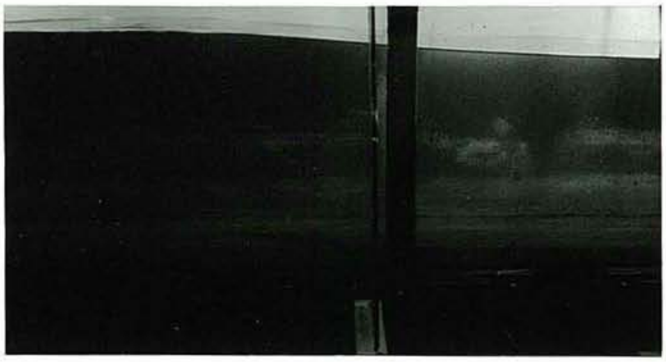

0 rpm

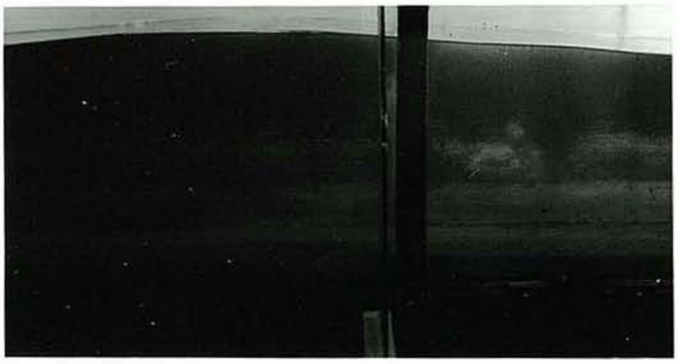

100 rpm

200 rpm

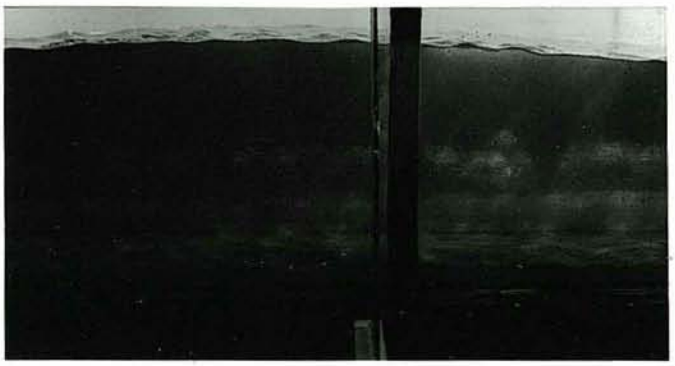

300 rpm

400 rpm

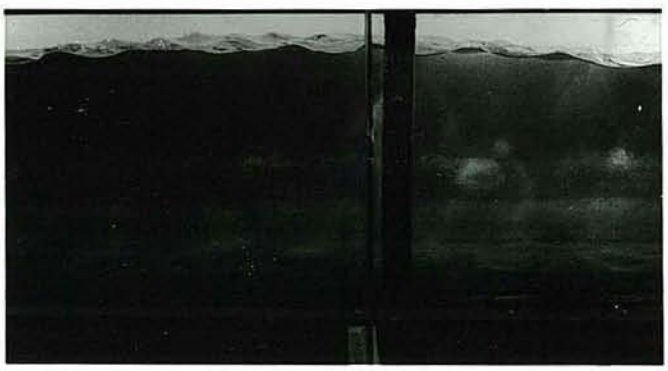

500 rpm

600 rpm

Figure 10.1a The response of f = 0.75 Hz waves to opposing winds.

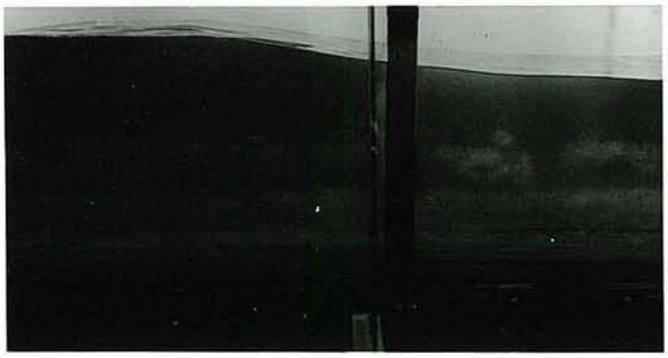

0 rpm

100 rpm

200 rpm

300 rpm

400 rpm

500 rpm

600 rpm

Figure 10.1b The response of f = 1.00 Hz waves to opposing winds.

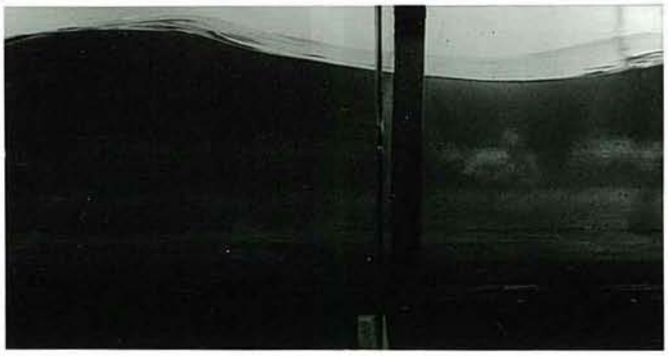

0 rpm

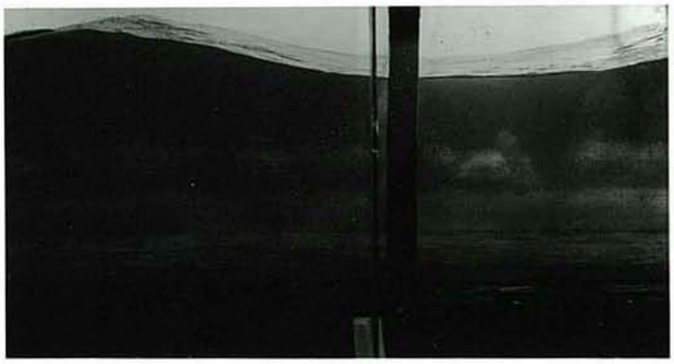

100 rpm

200 rpm

300 rpm

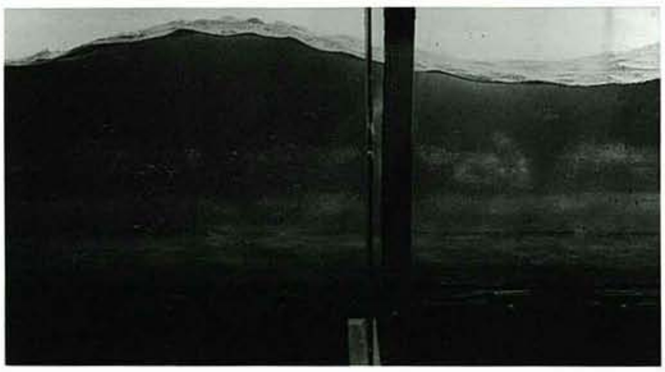

400 rpm

500 rpm

600 rpm

Figure 10.1c The response of f = 1.25 Hz waves to opposing winds.

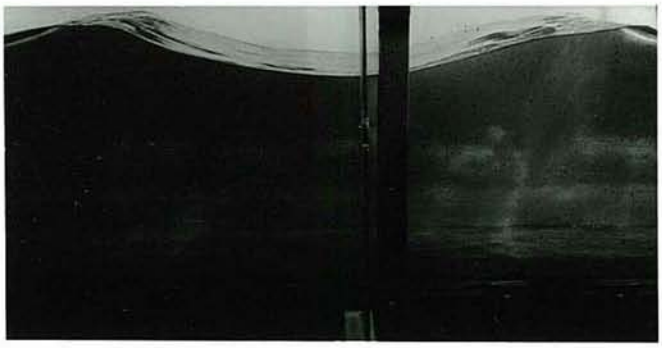

0 rpm

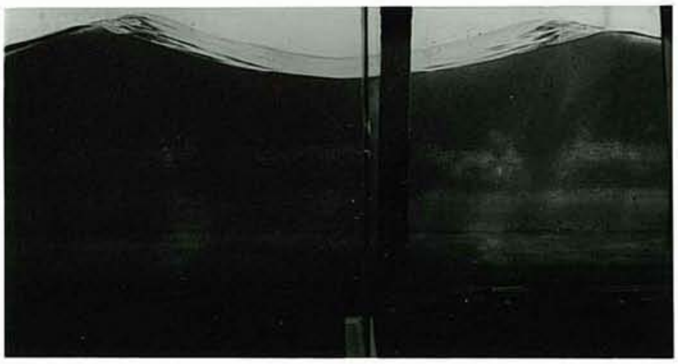

100 rpm

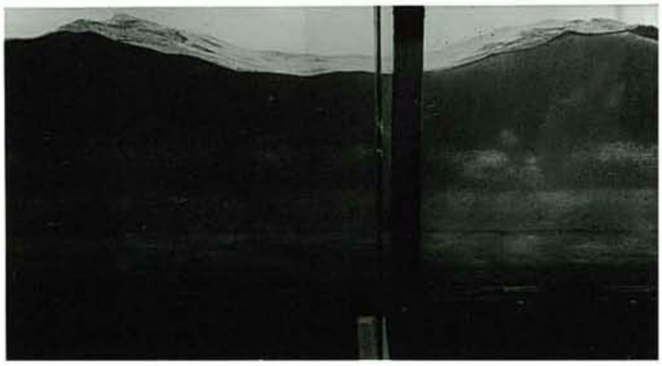

200 rpm

300 rpm

400 rpm

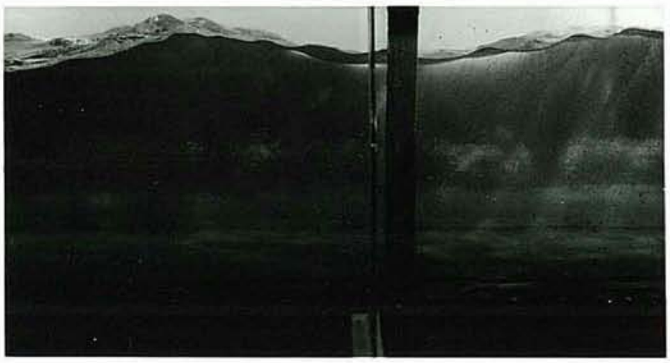

500 rpm

600 rpm

Figure 10.1d The response of f = 1.50 Hz waves to opposing winds.

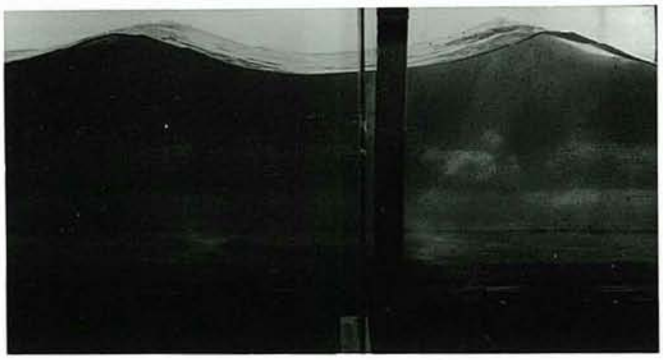

0 rpm

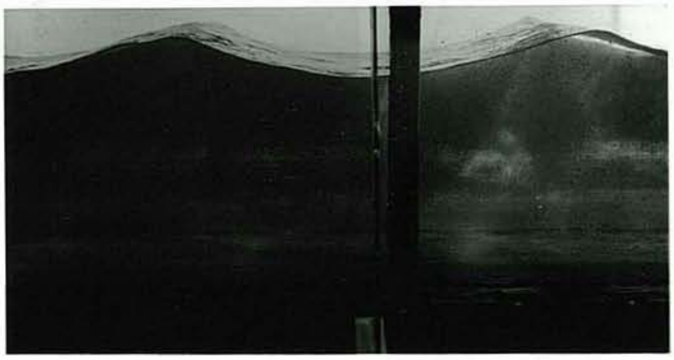

100 rpm

200 rpm

300 rpm

400 rpm

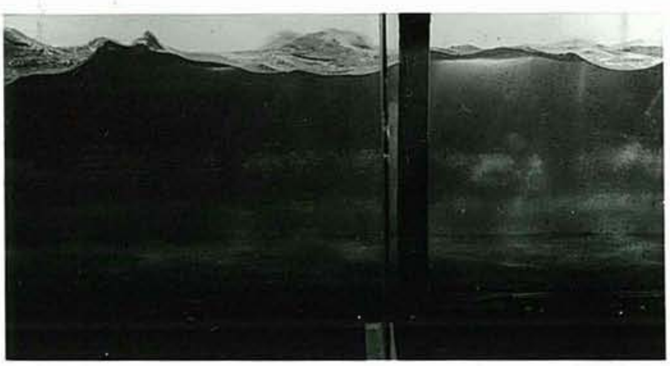

500 rpm

600 rpm

Figure 10.1e The response of $f = 1.75$ Hz waves to opposing winds.

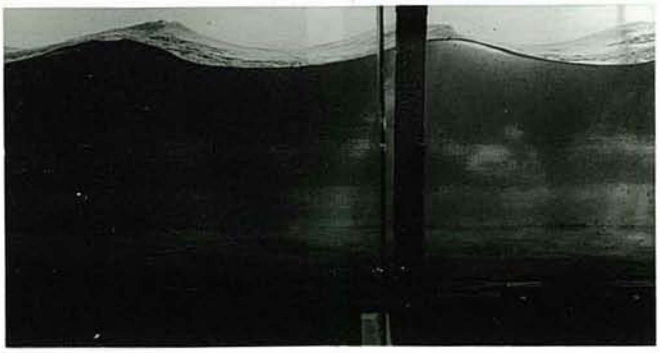

0 rpm

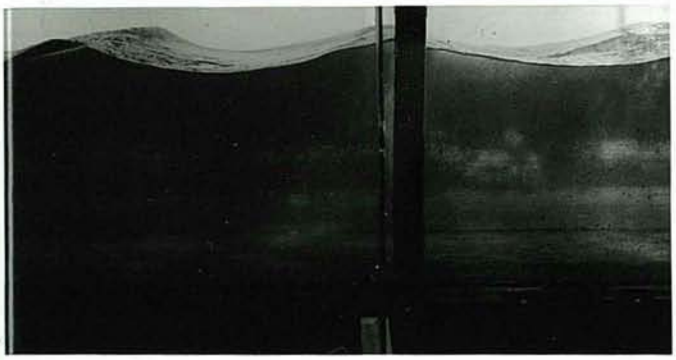

100 rpm

200 rpm

300 rpm

400 rpm

500 rpm

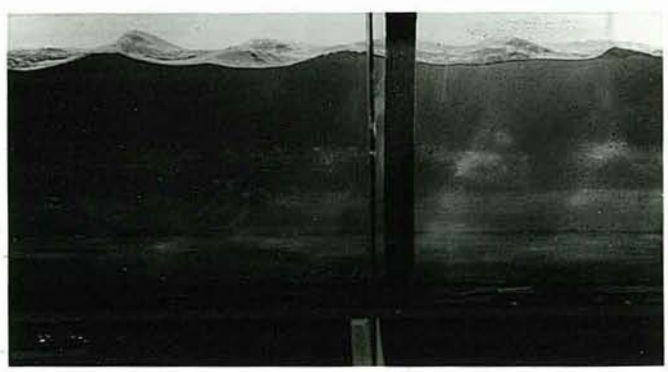

600 rpm

Figure 10.1f The response of f = 2.00 Hz waves to opposing winds.

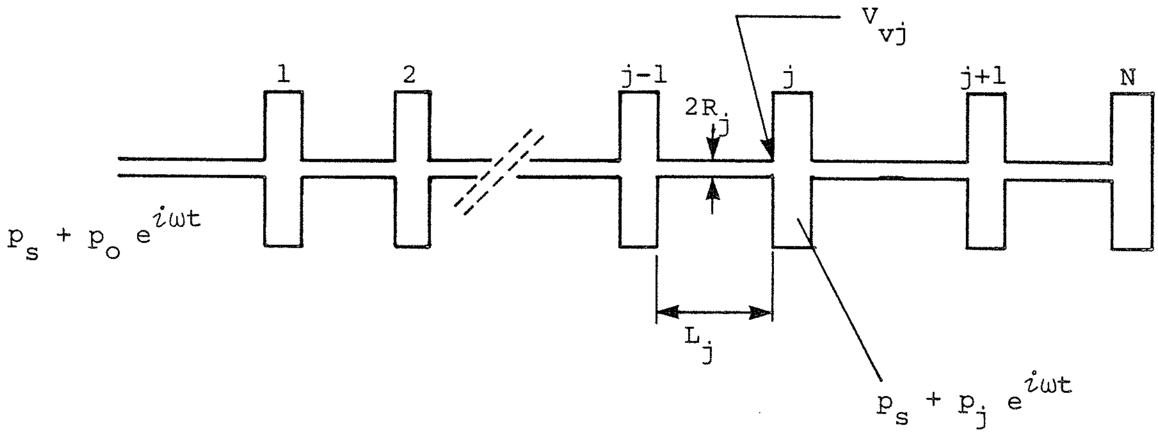

Figure A.1 Schematic diagram of the N tube and N volume system analysed by Bergh and Tijdeman (6).

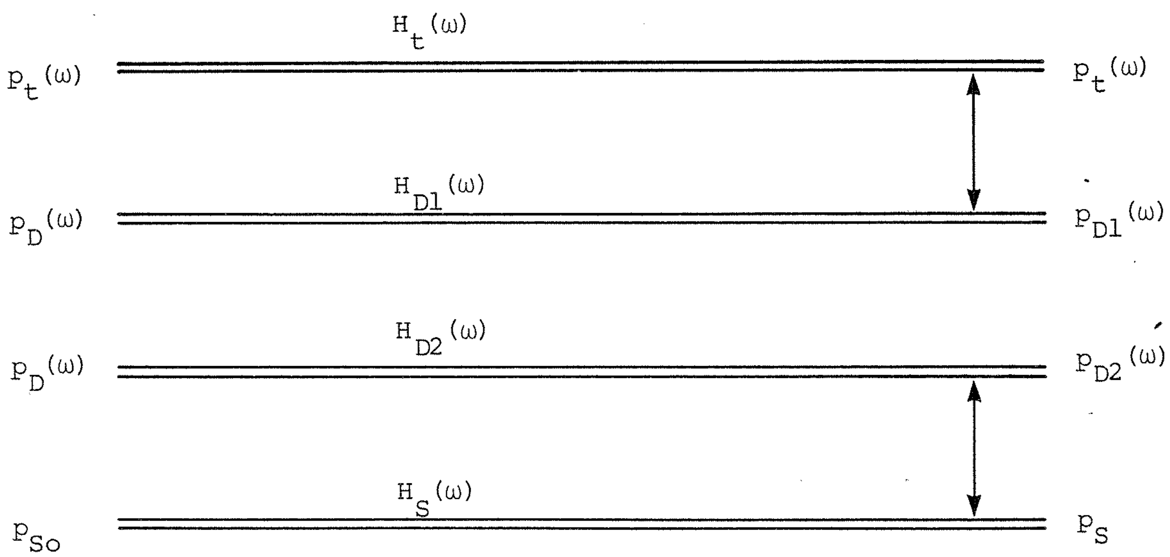

Figure E.2 Applied and measured pressures together with tube transfer functions.

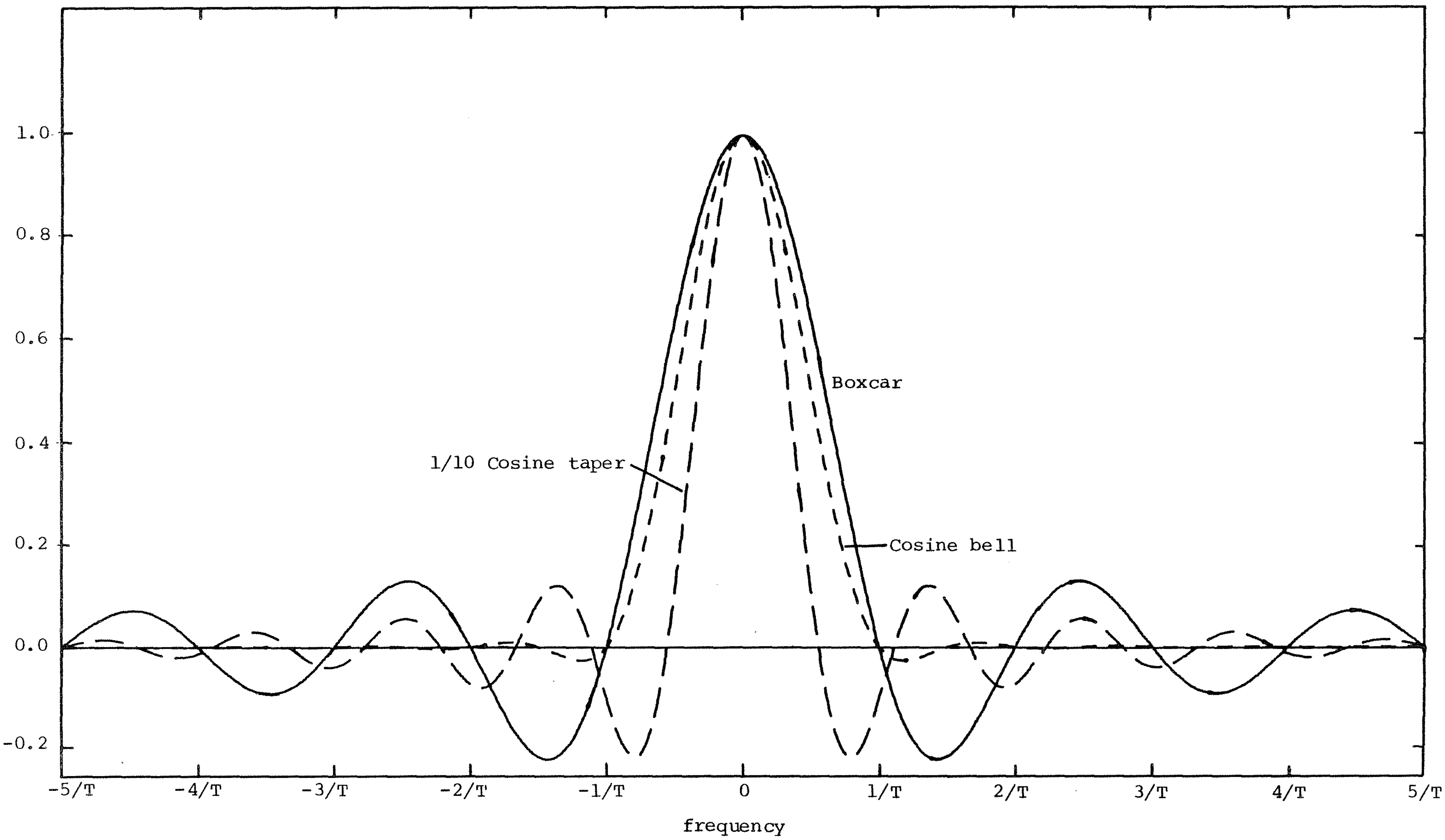

Figure B.1 Fourier transforms of commonly used window functions.

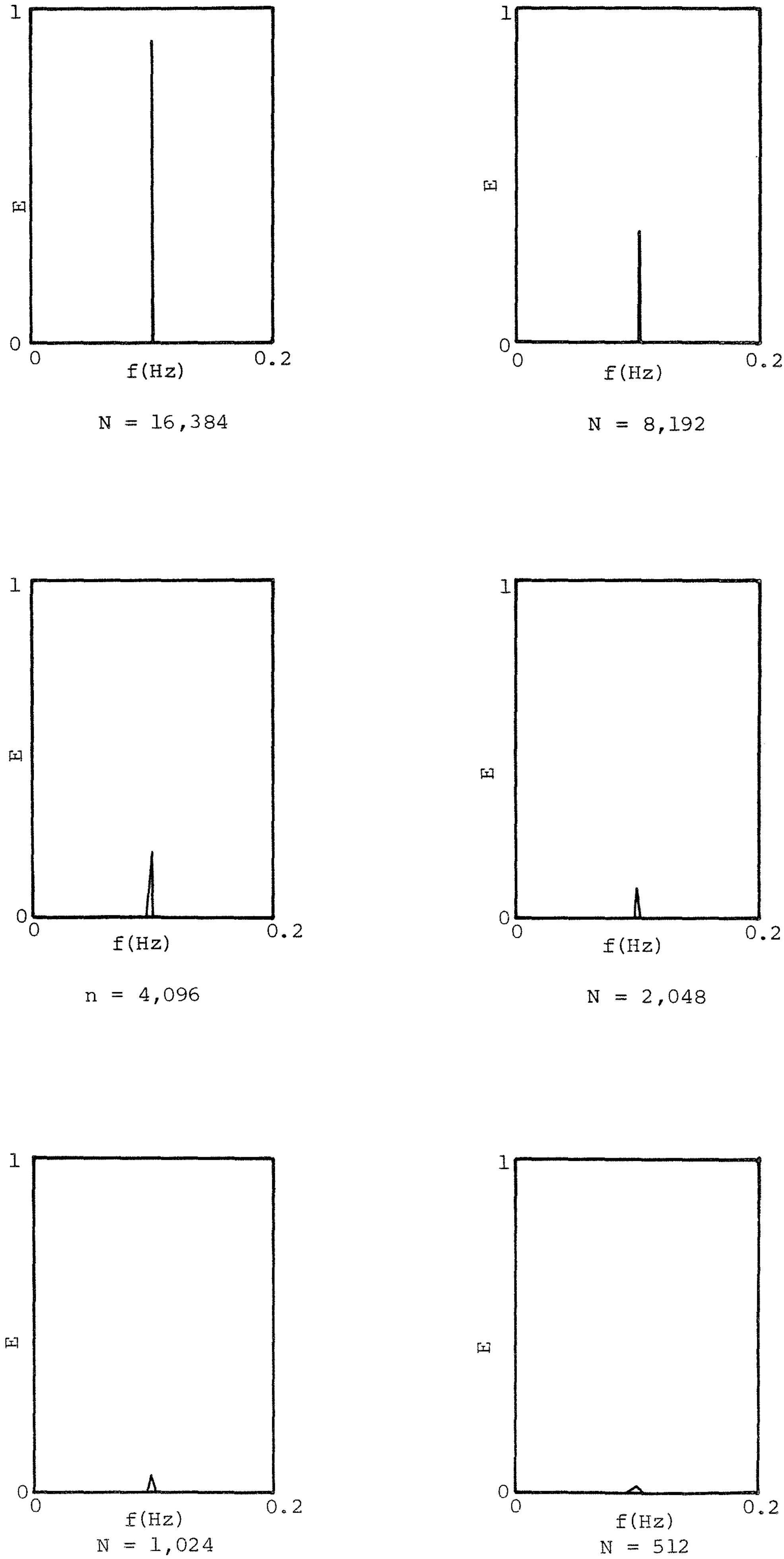

Figure C.1 The effect of changing the record length on the spectrum of a narrow band signal.

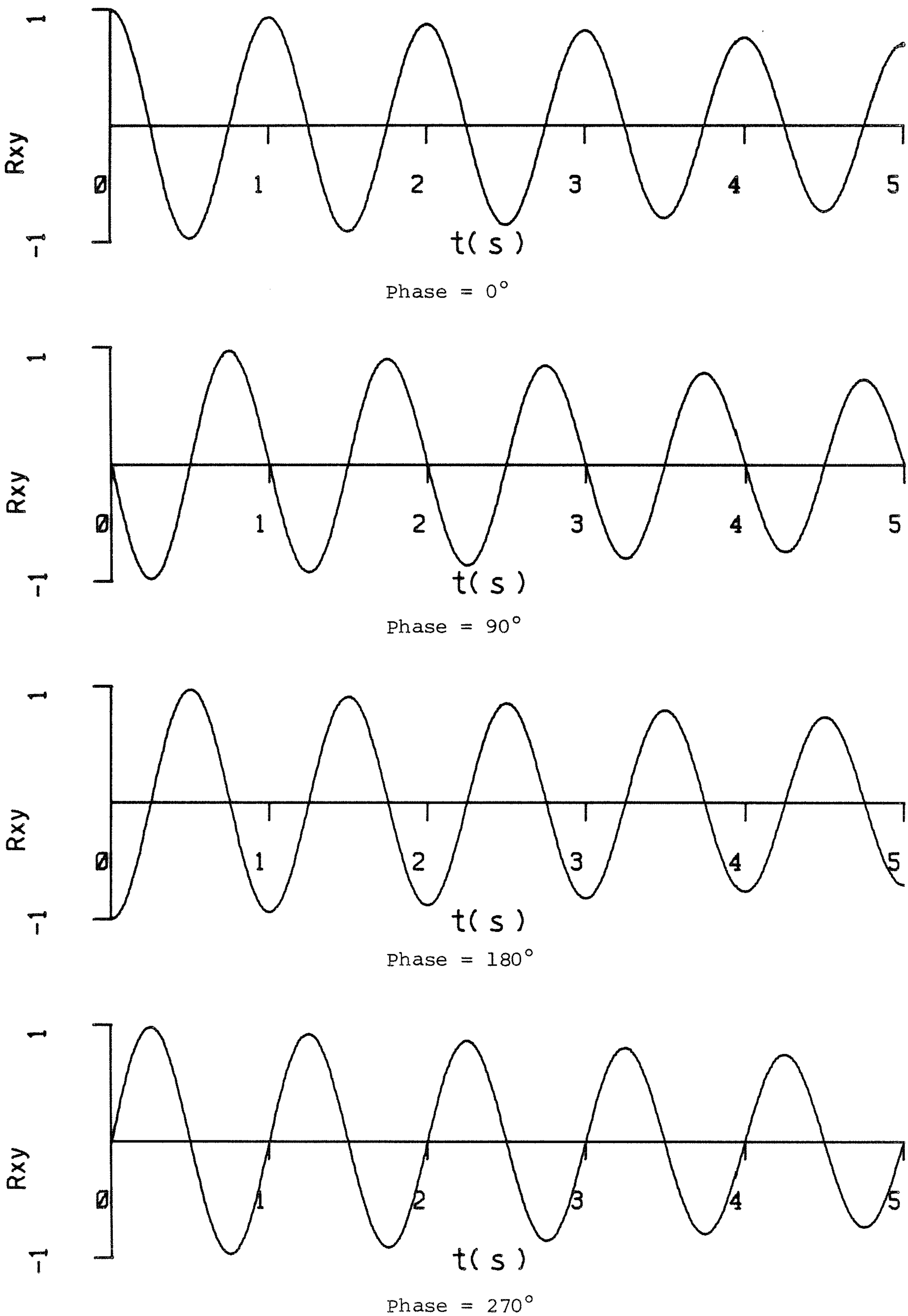

Figure C.2 Crosscorrelograms for signals with various phase differences.

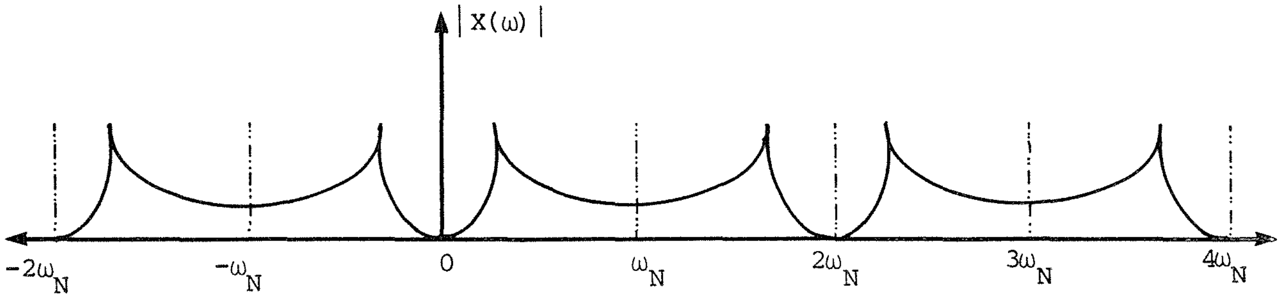

Figure D.1a Folding of the Fourier transform of a finite time series.

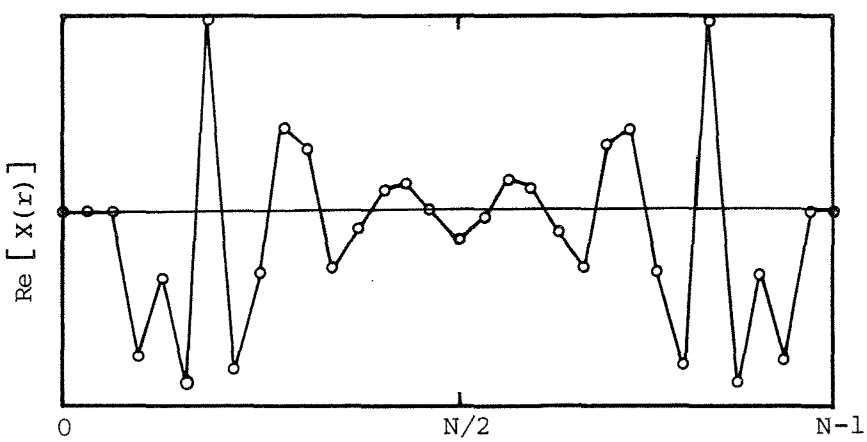

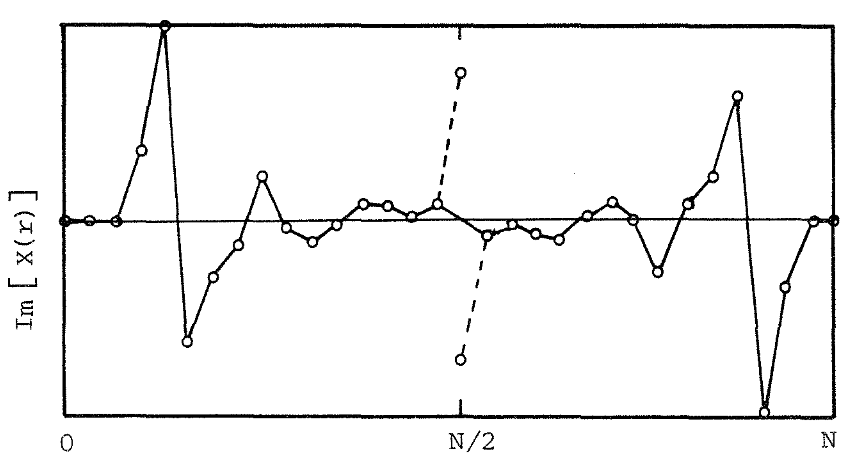

Figure D.1b Folding of real and imaginary parts of the finite discrete Fourier transform.

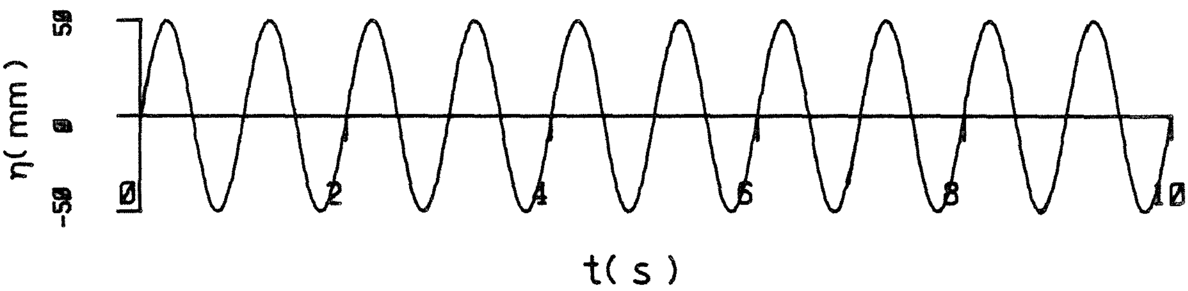

(a) Initial signal

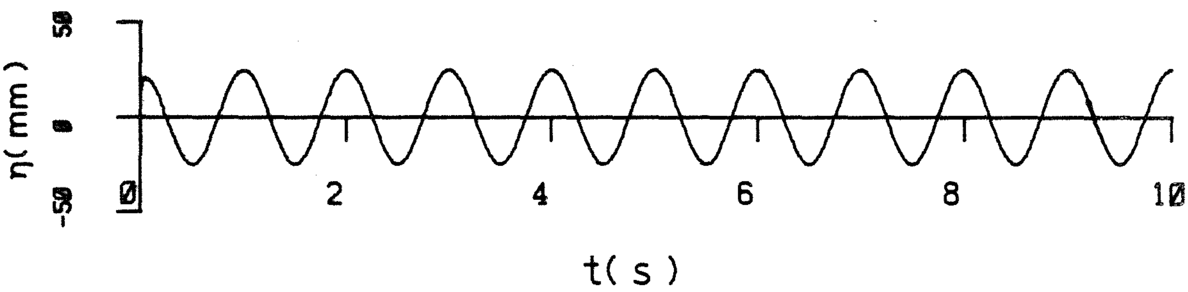

(b) Result after signal (a) is processed in the forward direction.

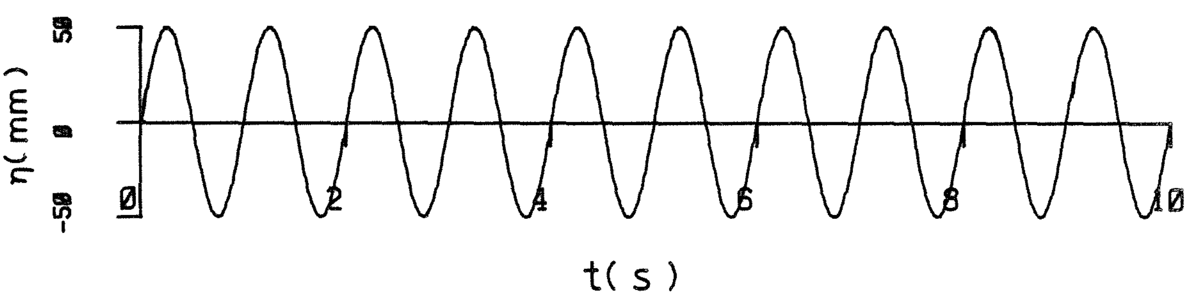

(c) Result after signal (b) is processed in the reverse direction.

Figure D.2 Test of computer program for transfer function correction. Signals (a) and (c) are identical indicating correct operation of program.

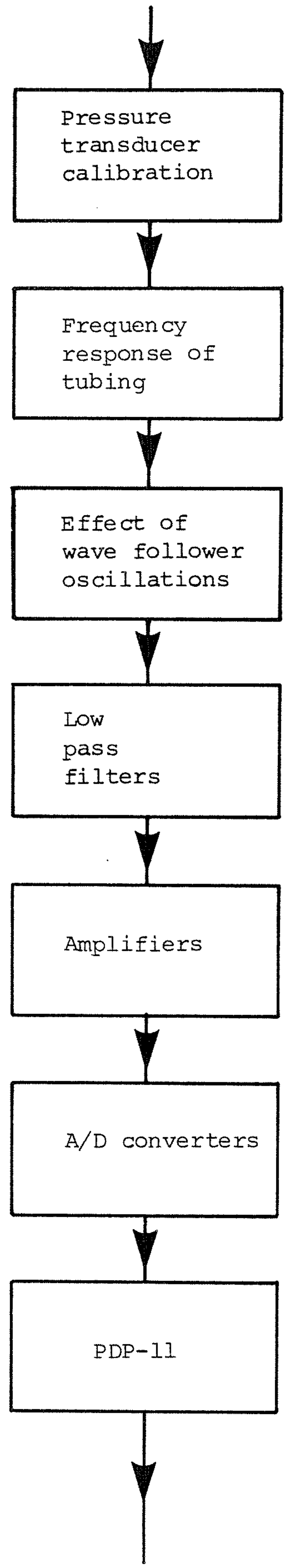

Figure E.1 Schematic diagram of system effects on pressure signal.

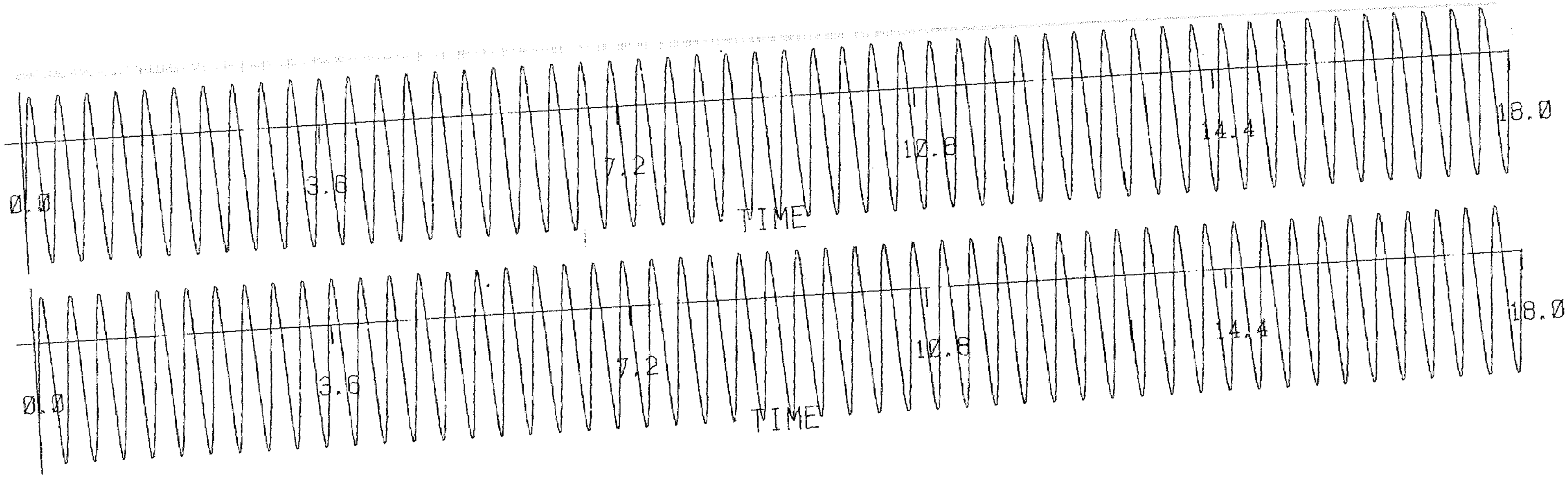

$\Delta p_1(\omega)$ and $[p_D(\omega) - p_t(\omega)]$

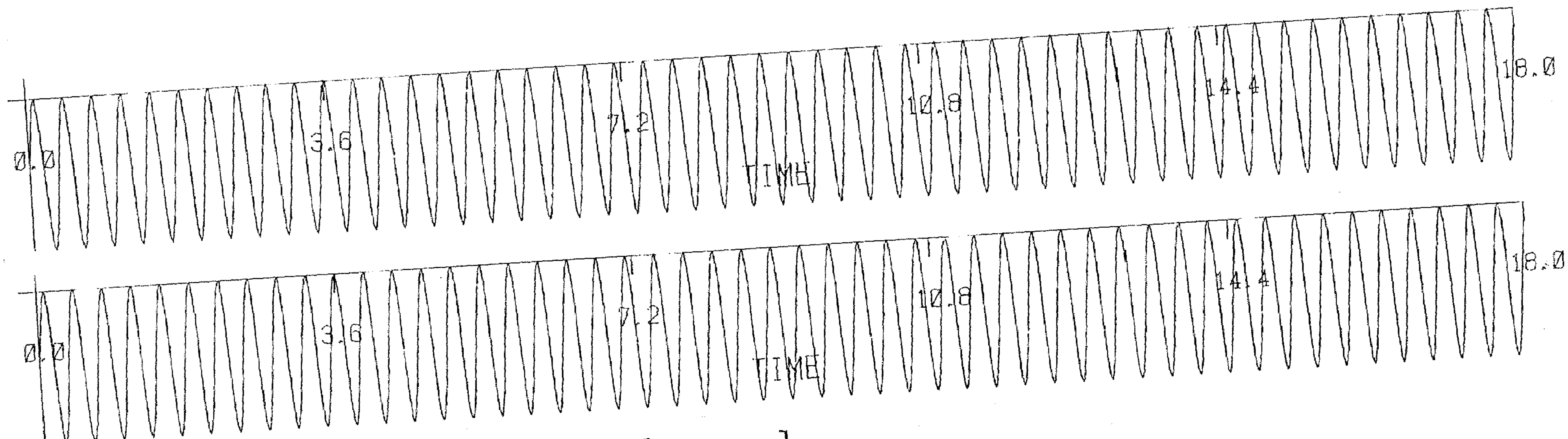

$\Delta p_2(\omega)$ and $[p_D(\omega) - p_s]$

Figure F.1 Initial differential pressure records and regenerated records indicating that TUBTRN.FOR is performing correctly.

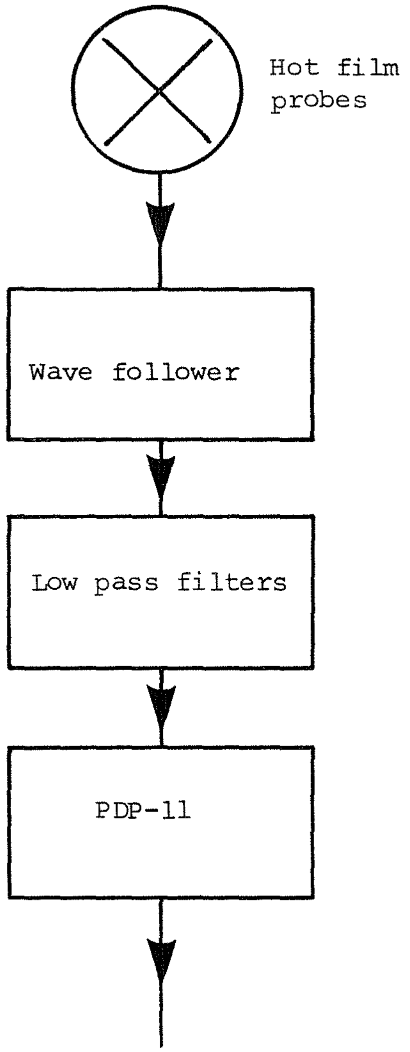

Figure G.1 Schematic diagram of system effects on velocity measurements.

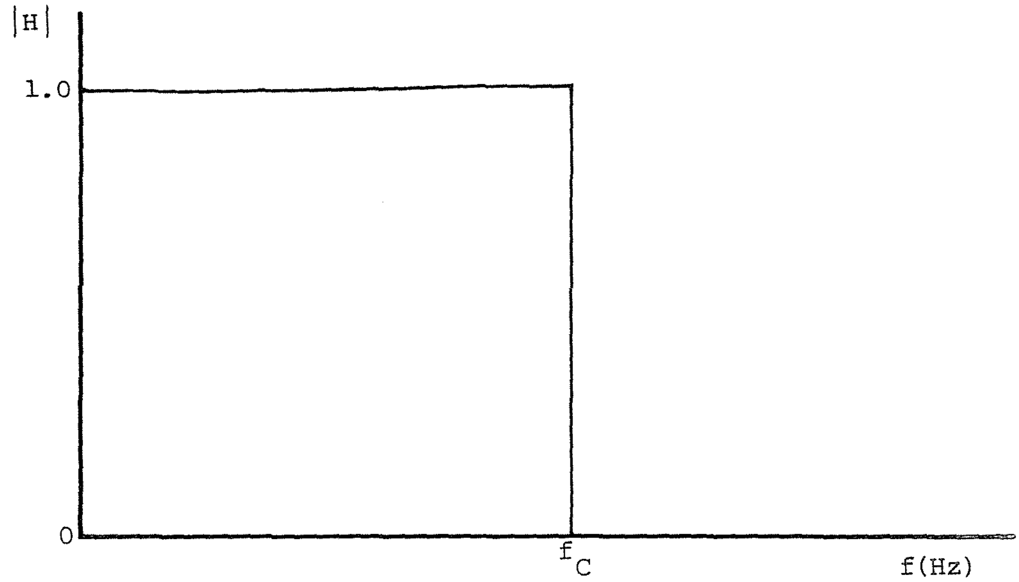

Low pass filter

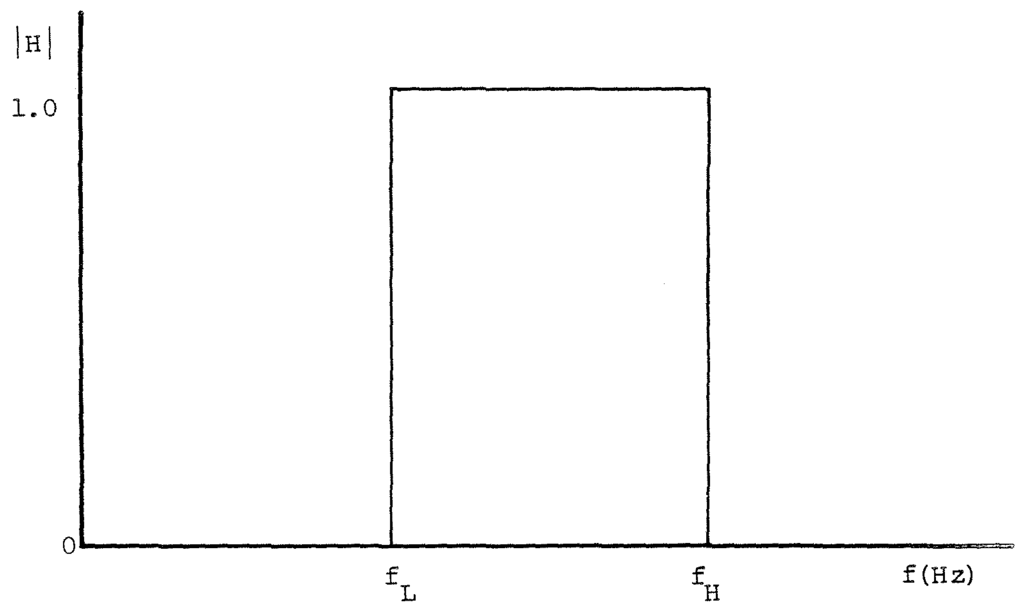

Band pass filter

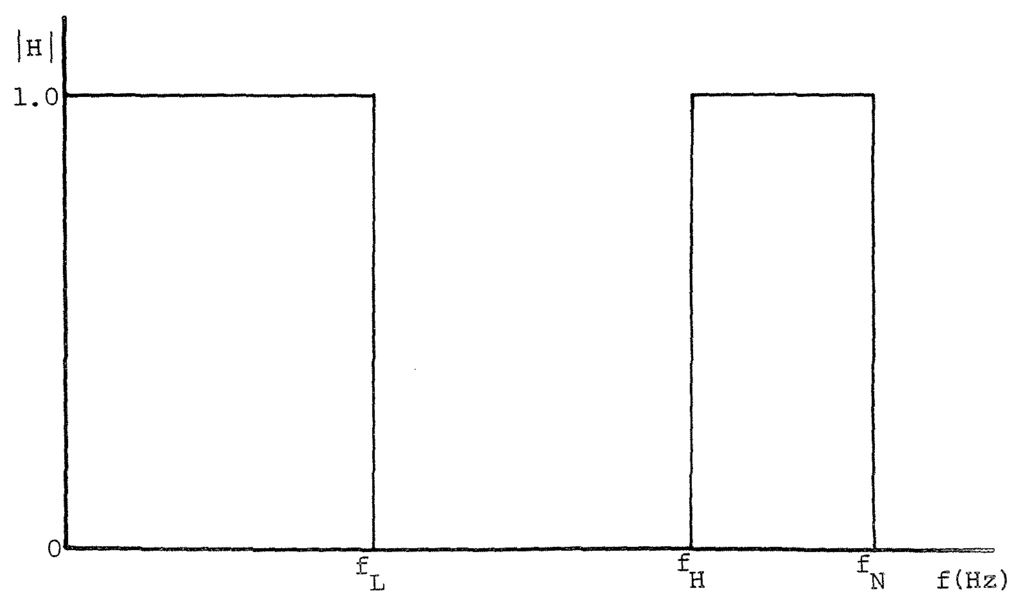

Band reject filter

Figure J.1 Ideal low pass, band pass and band reject filters.

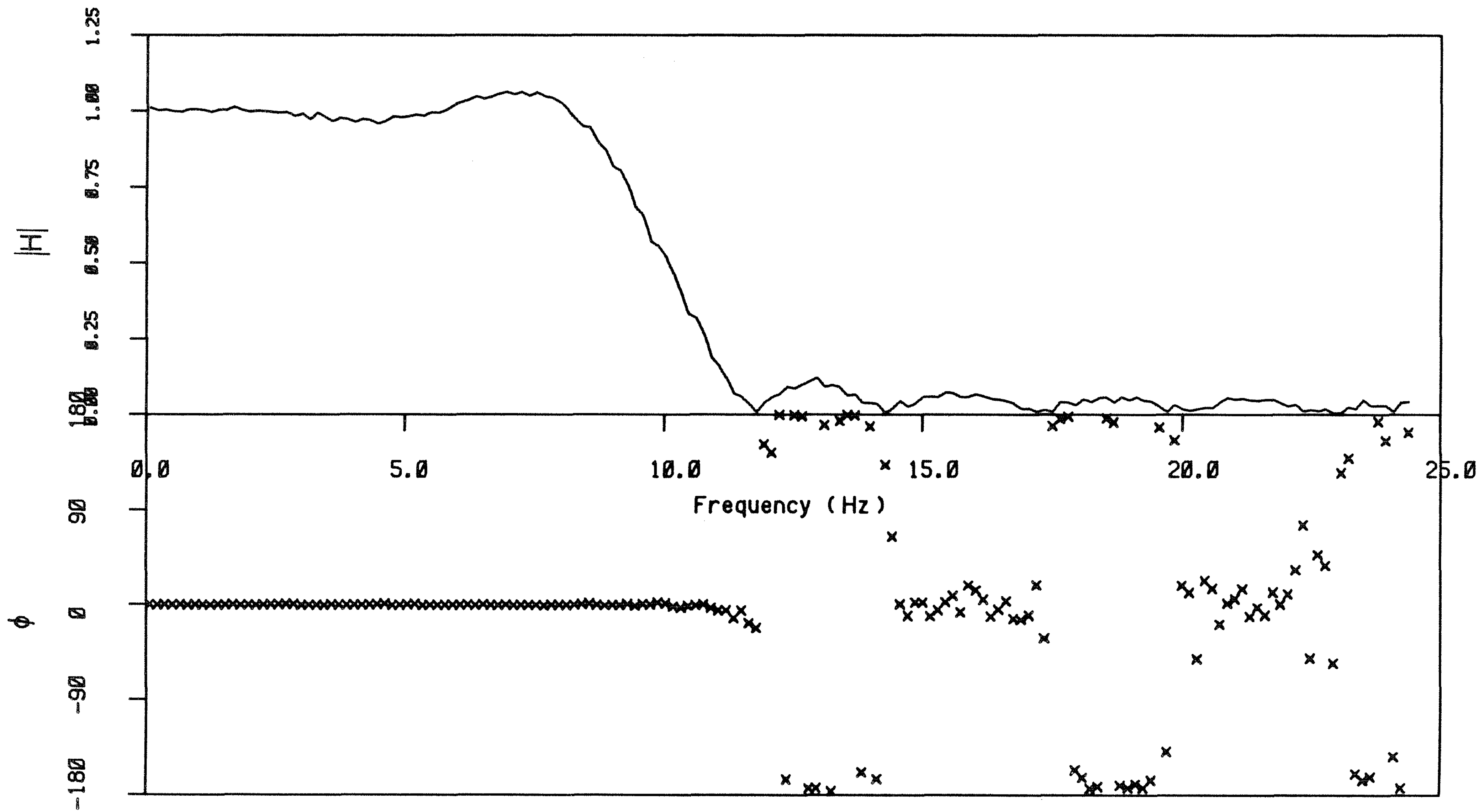

Figure J.2a Transfer function for low pass filter with cut-off frequency of 10 Hz and 10 filter weights.

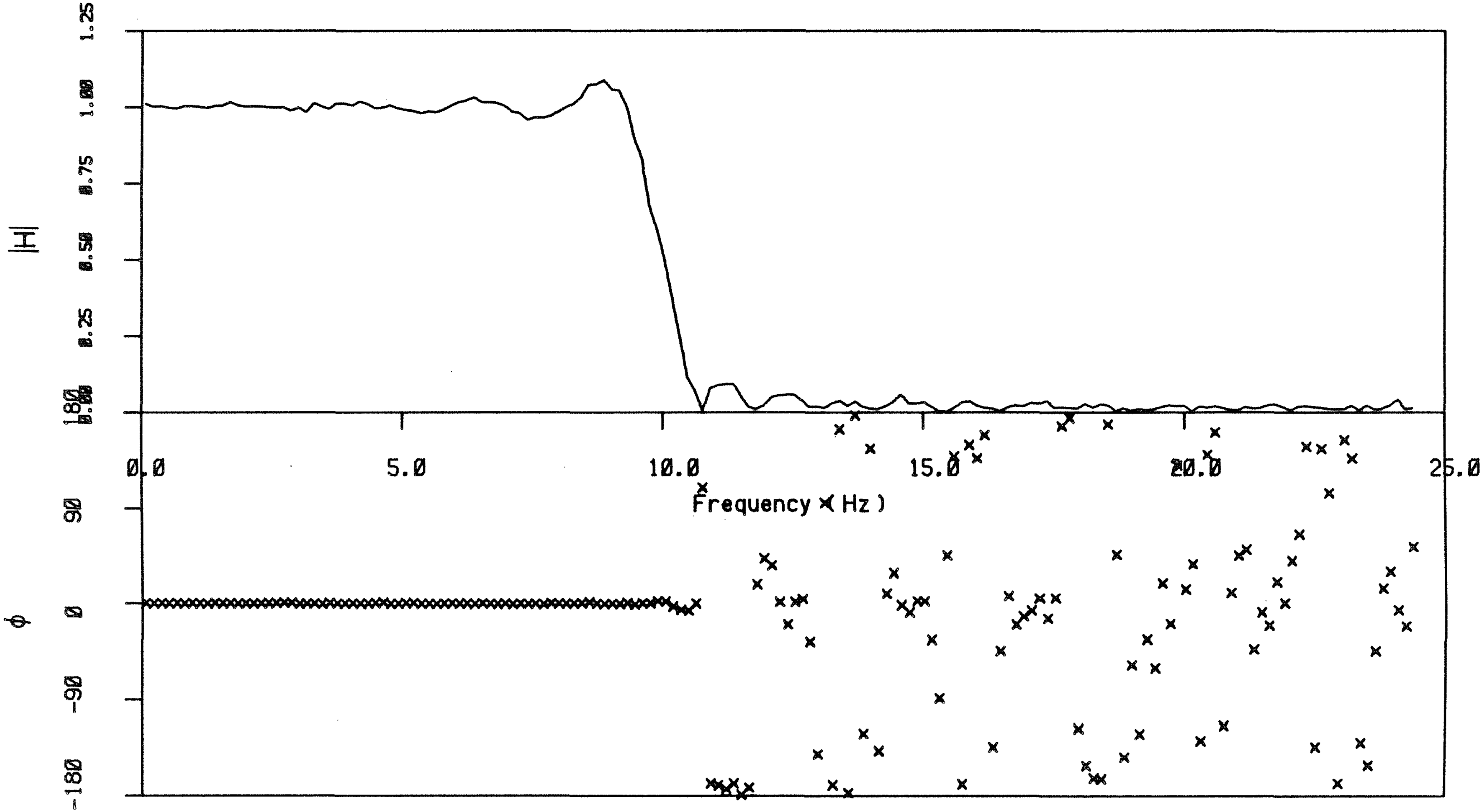

Figure J.2b Transfer function for low pass filter with cut-off frequency of 10Hz and 25 filter weights.

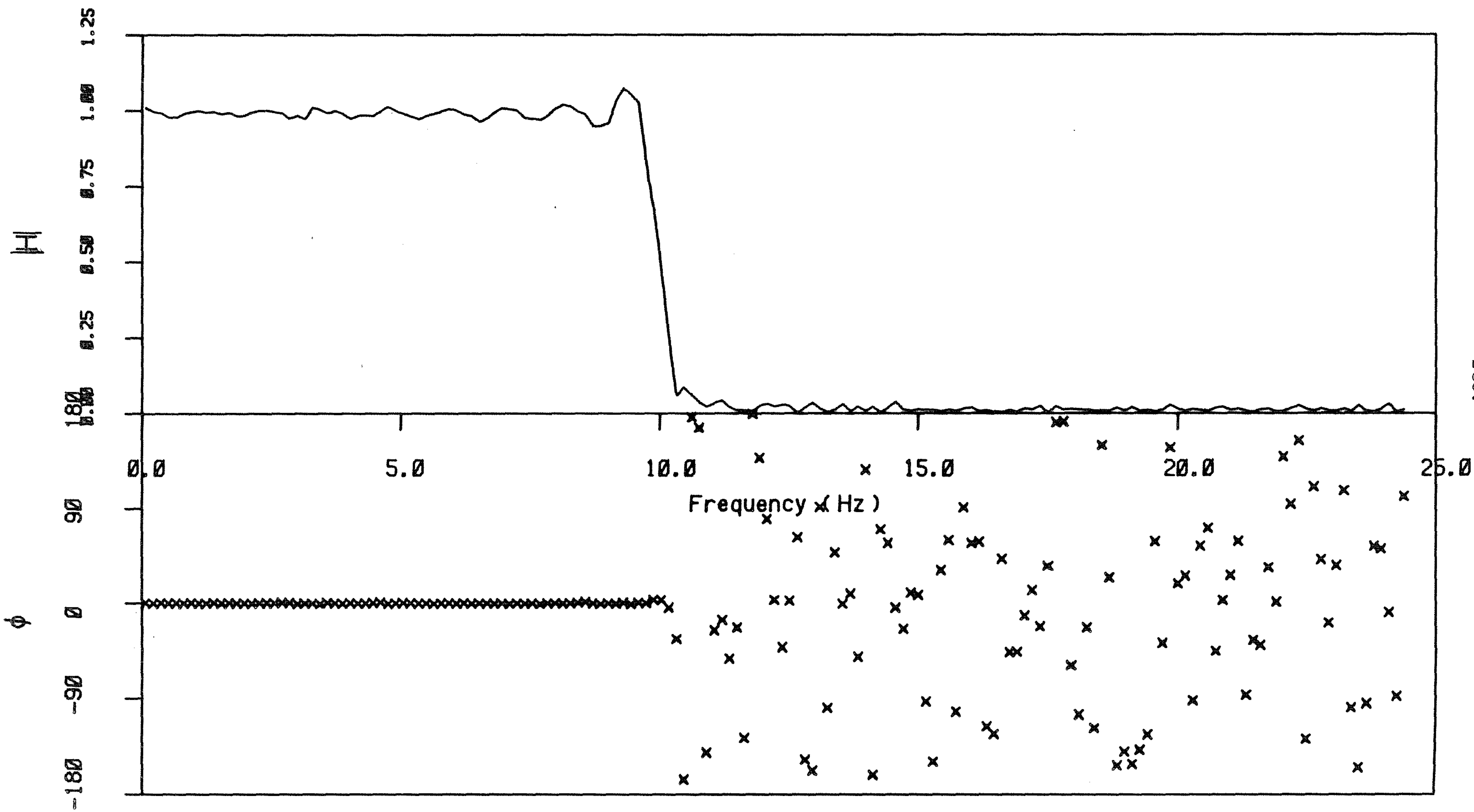

Figure J.2c   Transfer function for low pass filter with cut-off frequency of 10 Hz and 50 filter weights.

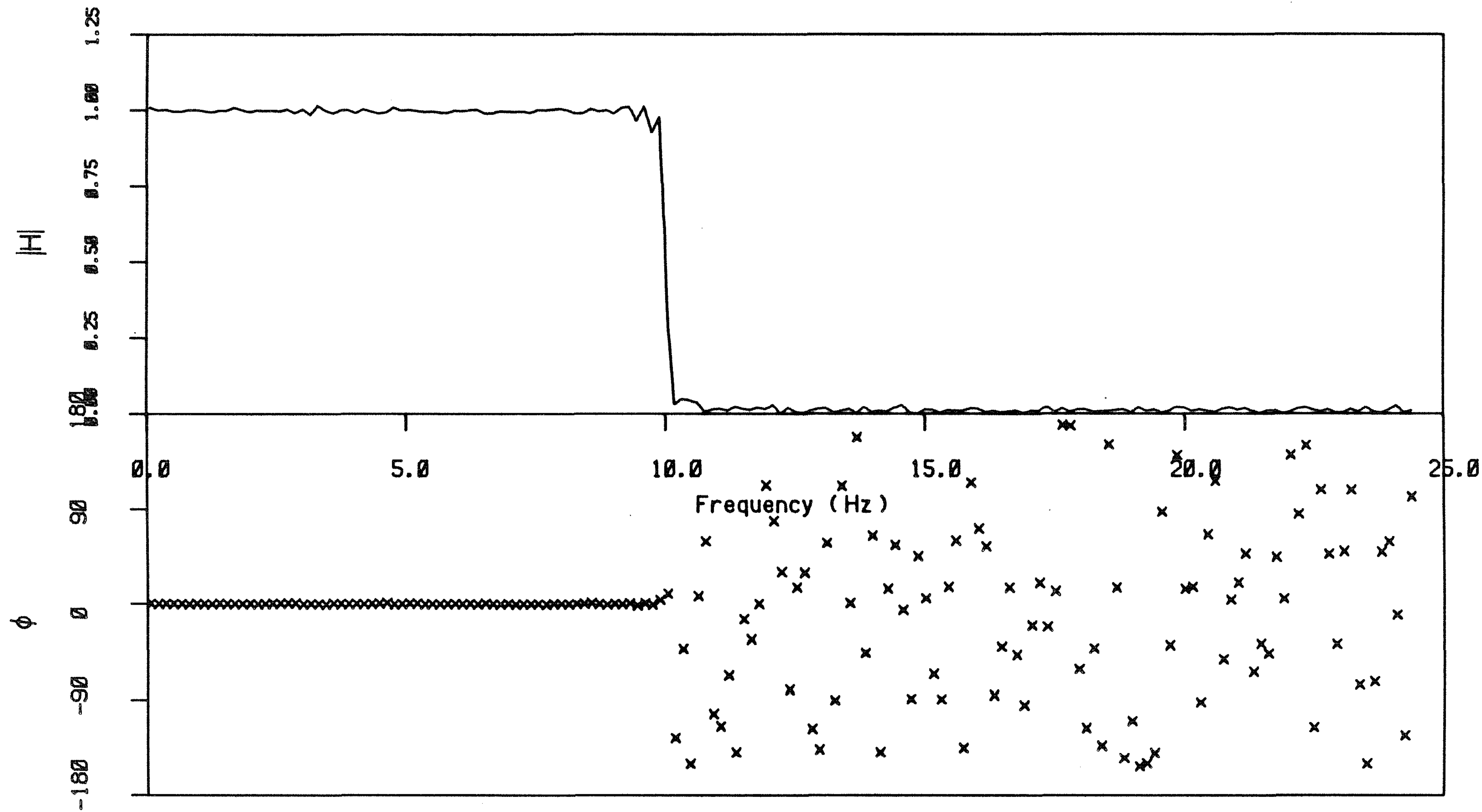

Figure J.2d   Transfer function for low pass filter with a cut-off frequency of 10 Hz and 200 filter weights.

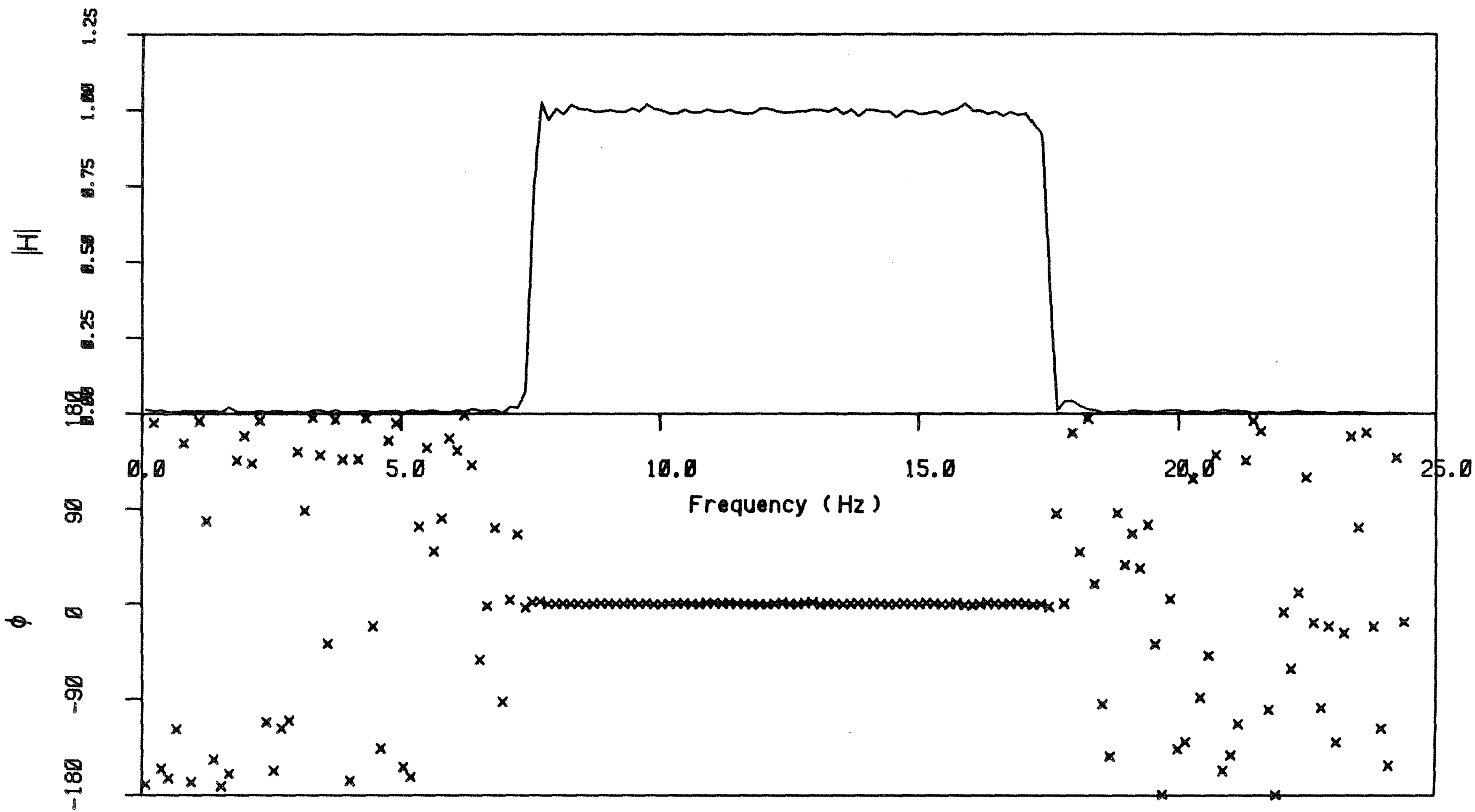

Figure J.3 Transfer function for band pass filter with cut-off frequencies at 7.5 Hz and 17.5 Hz and 200 filter weights.

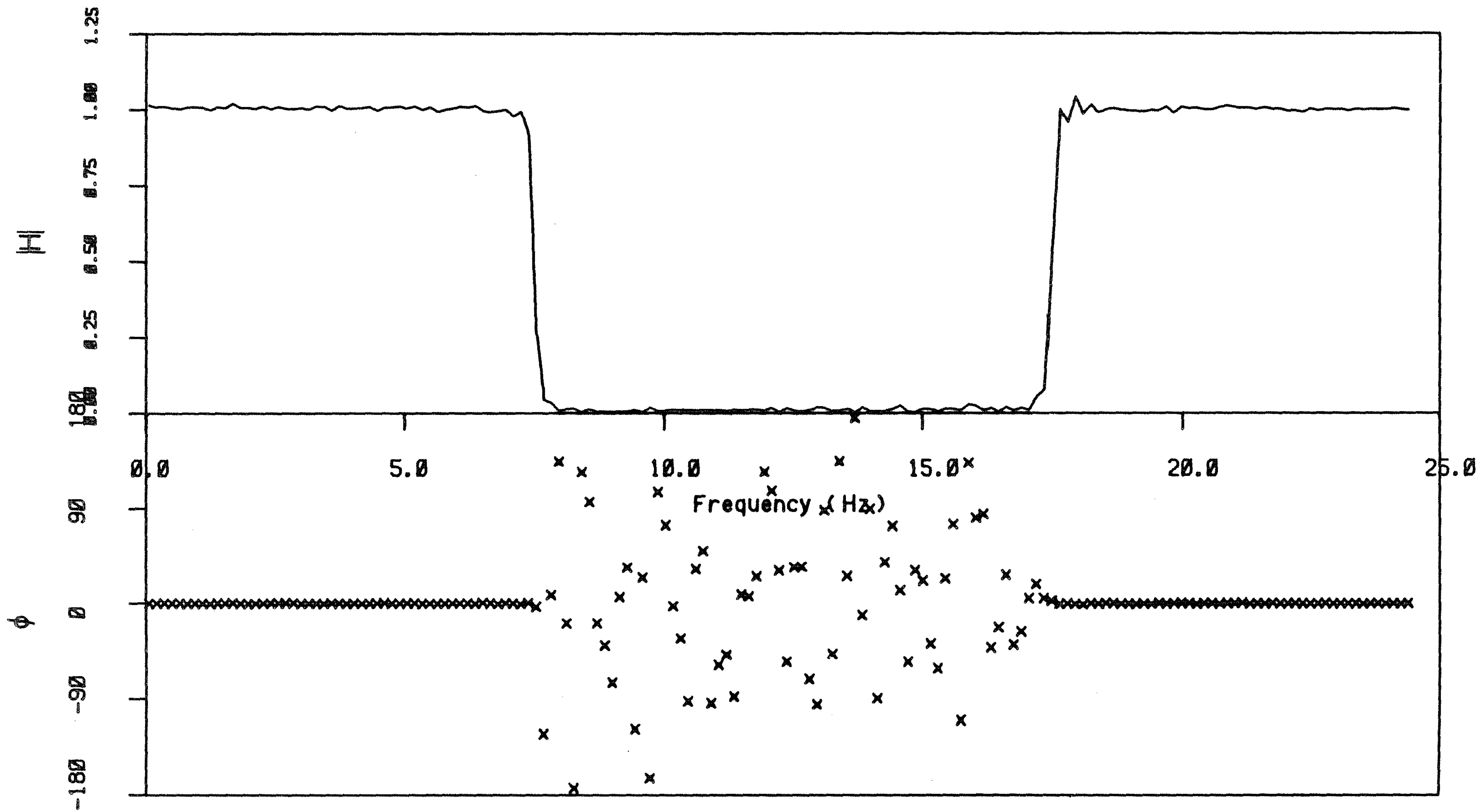

Figure J.4 Transfer function for band reject filter with cut-off frequencies at 7.5 Hz and 17.5 Hz and 200 filter weights.